



University of  
**Salford**  
MANCHESTER

# **Radiation Dose Assessment: Measurement, Estimation and Interpretation**

**Andrew Keith Tootell BSc(Hons) PGCert MSc SFHEA**

Thesis for the Degree of Doctor of Philosophy  
PhD by Published Works

Directorate of Radiography  
School of Health Sciences  
University of Salford  
Greater Manchester  
M6 6PU

2018

# CONTENTS

List of Tables .....	III
List of Figures .....	III
Abstract.....	IV
Acknowledgements.....	V
Declaration of Originality by Postgraduate Candidate .....	VI
Substantiated Author Contributions.....	VII
Preface .....	VIII
1. Introduction .....	1
2. Review of Developed Methods and Analysis of The Data .....	5
2.1 Acquiring Dose Data .....	6
2.1.1 Direct Dose Measurement .....	6
2.1.2 Modelling Radiation Dose .....	14
2.2 The Dosimetry Phantom.....	18
2.3 Radiation dose- Effective dose & Effective Risk .....	25
2.3.1 Effective Dose.....	25
2.3.2 Effective Risk .....	28
2.4 Conveying Risks to Patients .....	32
3. Intellectual Ownership and Contribution .....	36
4. Citation Analysis.....	37
5. Future Direction of Research .....	38
6. Conclusion.....	39
References .....	40
Published Works.....	47
Appendix: Isotope Bone Scan Protocol.....	161

## PUBLISHED WORKS

Paper 1.....	48
Clinical evaluation of the computed tomography attenuation correction map for myocardial perfusion imaging: the potential for incidental pathology detection	
Paper 2.....	57
An overview of measuring and modelling dose and risk from ionising radiation for medical exposures	
Paper 3.....	76
Optimising the number of thermoluminescent dosimeters required for the measurement of effective dose for computed tomography attenuation correction data in SPECT/CT myocardial perfusion imaging	
Paper 4.....	89
Comparison of effective dose and lifetime risk of cancer incidence of CT attenuation correction acquisitions and radiopharmaceutical administration for myocardial perfusion imaging	
Paper 5.....	103
Effect of reconstruction methods and x-ray tube current–time product on nodule detection in an anthropomorphic thorax phantom: A crossed-modality JAFROC observer study	
Paper 6.....	120
A phantom-based JAFROC observer study of two CT reconstruction methods: the search for optimisation of lesion detection and effective dose	
Paper 7.....	128
Effective Dose and Effective Risk From Post–Single Photon Emission Computed Tomography Imaging of the Lumbar Spine	
Paper 8.....	145
Analysis of effective and organ dose estimation in CT when using mA modulation: A single scanner pilot study	

## LIST OF TABLES

Table 1 Comparison of remainder organ and effective dose when salivary glands, extrathoracic and oral mucosa dose were included and excluded.....	19
Table 2 Recorded dose from a simulated CT attenuation correction acquisition of each slice showing where levels were above (grey shaded) and below the 0.05 mGy threshold. ....	21
Table 3 Comparison of methods in calculating organ dose in the colon.....	23
Table 4 ICRP tissue weighting factors from 1977 to present date .....	26
Table 5 Comparison of selected organs and effective dose resulting from administration of radiopharmaceutical compared to CT attenuation correction acquisitions (Tootell et al., 2014b) [Paper 4].....	27
Table 6 Odds of death from Injury as an example of poor comparison for radiation risk (Peck & Samei, 2017) .....	33
Table 7 Typical dose and equivalent amount of background radiation .....	34
Table 8 The four broad risk categories relevant to diagnostic imaging (Wall et al., 2011) .....	34
Table 9 Alternative presentation of the four broad risk categories (Wall et al 2011).....	34
Table 10 Contribution of each author to the papers included in the PhD by published works .....	36
Table 11 Citation analysis of the portfolio of published works (Data collected May 2018).....	37

## LIST OF FIGURES

Figure 1 Process followed in Tootell et al., (2017) [Paper 8] to acquire absorbed organ dose.....	12
Figure 2 The CIRS ATOM dosimetry phantom family models 701-706 (CIRS, Norfolk, Virginia).....	18
Figure 3 Change in absorbed dose along a central column of TLDs in the dosimetry phantom. The decision to exclude above slice 10 and below slice 28 was arbitrary.....	22
Figure 4 Suggested placement of TLDs to assess the range of phantom slices where dosimetry data should be acquired .....	22
Figure 5 Models for extrapolating radiation-induced cancer risk to low doses (dashed line and curves). Linear no-threshold (LNT) model = dashed straight line (Hendee & O'Connor, 2012).....	30
Figure 6 Gantt Chart showing research and writing activities.....	47

## ABSTRACT

New technologies or methods of image acquisition are driven by the need for increased anatomical information to improve diagnostic accuracy or surgical planning. These new technologies are often accompanied with additional radiation dose yet this can be justified through the consideration of the benefit it brings. Examples include the use of CT colonography instead of double contrast barium enemas, CT urography replacing intravenous urography and, in nuclear medicine imaging the increased use of CT imaging as part of single photon emission tomography and positron emission tomography to correct emission data or localise or characterise identified lesions. Manufacturers are quick to promote their systems as “low-dose” but little independent evaluation of this claim existed. In the context of nuclear medicine, the additional imaging raised questions as to the use of the attenuation correction data specifically. The question of should the cross sectional images be reviewed for pathology has been the focus of debate. It was recognised that the quality of these images is poor due to the “low-dose” acquisition.

The research presented in this thesis and portfolio of published work aimed to establish an accurate method of assessing the radiation dose, initially from the CT attenuation correction acquisition, but later in other imaging modalities. In this thesis eight papers are used to illustrate the methods developed in this work, and how they were applied to other fields of medical imaging. Six of these papers were completed as the first author and the remainder as co-author. Initially, the concepts of radiation dose were critically evaluated. Following identification of sub-optimal techniques, steps were taken to improve the accuracy of dose measurement using thermoluminescent dosimeters, digital dosimeters and simulation through software. These techniques have been analysed critically and where appropriate improvements are recommended.

Radiation dose, in particular the associated risk, is a challenging concept to convey to patients and care givers and simply providing a figure of dose does not convey the required information needed to allow consent to be given. Methods by which radiation dose and risk can be interpreted is critiqued with reference to published literature. The thesis concludes with a description of the intellectual contribution illustrating the role played as first author and as a co-author in the works included in the portfolio and a review of impact considering citation metrics and downloads. It was also decided to include citations from within the Diagnostic Imaging Research Programme and PhD theses from The University of Salford to demonstrate how research activities within the portfolio of published works have influenced other methodologies and outputs.

## ACKNOWLEDGEMENTS

Undertaking this PhD has been a significant challenge. It is a challenge that I would not have been able to meet without the help, support and guidance of colleagues, family and friends.

I would like to first say thank you to my supervisors Dr Andrew England and Dr John Thompson for their advice, support and encouragement in the writing up of the thesis.

Many thanks to the co-authors I have worked with in the production of the papers that are included in this thesis. Without their input and advice on data collection and analysis, this portfolio of works would not exist. I would like to single out Prof. Peter Hogg and Ms Katy Szczepura for their support into the papers contained in the portfolio of works. They were there at the start of this project and through their encouragement and expert advice helped me not to lose sight of the finish line.

The work in the thesis would not have been possible without the support of a number of departments in NHS Trusts, namely the Nuclear Medicine Centre of Central Manchester University Hospitals, the Nuclear Medicine and CT departments of Wrexham Maelor Hospital, the nuclear medicine departments of St Helens and Knowsley Teaching Hospitals NHS Trust and my employer, The Directorate of Radiography at University of Salford.

Finally, I would like to thank my family, my wife Karen and my children Grace and Adam for their patience, support and motivation while completing this work.

# DECLARATION OF ORIGINALITY BY POSTGRADUATE CANDIDATE

Name of candidate                      ANDREW TOOTELL

Roll number/Student number:    

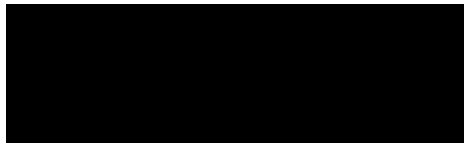
School:                                      HEALTH SCIENCES

Degree: PhD

This is to certify that the copy of my thesis, which I have presented for consideration for my postgraduate degree:

- embodies the results of my own course of study and research
- has been composed by myself
- has been seen by my supervisor before presentation
- has been granted the appropriate level of ethics approval

Signature of candidate



Date: 5<sup>th</sup> June 2018

The candidate's supervisor is asked to declare here that s/he has approved the submission of the thesis. If the supervisor decides to withhold approval, the candidate shall have the right of appeal to the Associate Head/Dean of Research. A candidate may be permitted to submit a thesis despite the Supervisor withholding approval, providing the Associate Dean of Research approves submission

Signature of Supervisors



Date: 5<sup>th</sup> June 2018



Date: 5<sup>th</sup> June 2018

## SUBSTANTIATED AUTHOR CONTRIBUTIONS

The contribution of all those eligible for authorship has been recognised by Andrew Tootell in all the papers included in this PhD by published works thesis.

- No eligible author has been denied authorship of the opportunity to contribute
- No ineligible author has been included on any publication
- Where appropriate, acknowledgements have been made to participants who do not satisfy enough criteria to be considered a co-author
- The contribution and ownership displayed in Table 10 is accurate

I hereby declare that the above statements have been satisfied. I sign to acknowledge the contribution of all authors in accordance with the University Of Salford Code Of Conduct.

Signed



Dr John Thompson,  
University of Salford  
PhD Supervisor and Co-author



Dr Andrew England  
University of Salford  
PhD Supervisor

## PREFACE

This thesis is a critical review of a portfolio of eight papers that were accepted for publication between 2012 and 2017. The aim of this review is to demonstrate the work's fulfilment of the requirements of doctoral degree presented by The Quality Assurance Agency (QAA, 2008).

- *The creation and interpretation of new knowledge, through original research or other advanced scholarship, of a quality to satisfy peer review, extend the forefront of the discipline, and merit publication*
- *Systematic acquisition and understanding of a substantial body of knowledge which is at the forefront of an academic discipline or area of professional practice*
- *The general ability to conceptualise, design and implement a project for the generation of new knowledge, applications or understanding at the forefront of the discipline, and to adjust the project design in the light of unforeseen problems*
- *A detailed understanding of applicable techniques for research and advanced academic enquiry*

The work is structured in chapters discussing critically the aims of the work and a summary of the methods, findings and conclusions. A discussion of the author's contribution to the papers and analysis of the published works' impact is presented. The work concludes with a critical discussion on the advancement of knowledge, limitations and proposal for post-doctoral work.

Due to copyright reasons the portfolio of published work presented in the appendices are versions that are available through the University Of Salford Institutional Repository (USIR) (<https://usir.salford.ac.uk/>) and versions that were accepted for publication.

# 1. INTRODUCTION

The adoption of new technologies and/or methods of image acquisition are often driven from the desire to improve clinical care (Ladapo, Horwitz, Weinstein, Gazelle, & Cutler, 2009). Additional radiation dose can be justified with increased accuracy in diagnoses; for example double contrast barium enema examinations in the UK had a mean radiation dose of 2 mSv compared to a mean of 12 mSv for CT colonography in the corresponding year (2008) (Hart, Wall, Hillier, & Shrimpton, 2010; Public Health England, 2011). The additional radiation dose can be justified due to the additional benefits the technique brings and the new higher radiation dose technique has been adopted into clinical practice (British Society of Gastrointestinal and Abdominal Radiology & The Royal College of Radiologists., 2014). As noted by Shrimpton, Hillier, Meeson, & Golding (2014) there has been an upward trend in the contribution CT brings to the UK annual per caput radiation dose while “conventional” radiographic techniques have declined partly due to the increase in the use of lower dose technology (for example digital radiography (DR)) and partly due to CT replacing imaging techniques for example radiographic projections of the lateral cervical spine, the chest and pelvis referred following major trauma being replaced by the trauma CT protocols (Royal College of Radiologists, 2015). On first glance this could be regarded as concerning but the benefits, such as increased accuracy in diagnoses through quicker acquisitions and sub-millimetre resolution, have been considered during the justification process.

An essential part of any clinical practitioner involved in the imaging of patients using ionising radiation is the need to consider the radiation dose their patients receive. Of the average 2.7 mSv a UK citizen receives per year, 16% can be attributed to medical exposure (the second largest after exposure due to radon and thoron (Public Health England, 2016)). The detrimental effects of ionising radiation are well documented and include carcinogenesis, mutagenesis, teratogenesis and acute toxicity (Nations Scientific Committee on the Effects of Atomic Radiation, 2000). However, at diagnostic levels, the *potential* for developing cancer is the most significant factor that should be considered (Smith, 2011). That is to say, in diagnostic imaging, the aim of radiation protection of patients is to prevent deterministic effects and, as far as reasonably practicable, limit stochastic effects.

The introduction of this review focuses on Paper 1 (Tootell, Vinjamuri, Elias, & Hogg, 2012). This paper questions the use of the non-emission data acquired as part of myocardial perfusion imaging using single photon emission computed tomography and computer tomography (SPECT-CT) hybrid imaging systems and highlights the additional radiation dose and therefore the increased risk the CT

acquisition brings. The need for accurate dose estimation or measurement to quantify risk will be considered.

An issue that proved to be the catalyst for the research included in this portfolio of works follows a similar theme of new technology increasing radiation dose but bringing with it additional benefits. At the time of publication of Tootell et al., (2012) [Paper 1] it was apparent that hybrid imaging technology had brought numerous benefits to nuclear medicine imaging including the correction of emission data, localisation of areas of increased or decreased radiopharmaceutical uptake or characterisation of identified lesions or pathology. Observations at national nuclear medicine conferences and a review of published guidelines evidenced the increase adoption of the technology into common practice. Tootell et al., (2012) (Paper 1) discusses critically the use of the CT data acquired for attenuation correction of myocardial perfusion single photon emission computed tomography (SPECT) studies and made a number of observations. It is noted that;

- the acquisition results in a radiation dose that was greater than the “standard” emission only imaging of myocardial uptake
- axial CT images of the chest will include extracardiac anatomy and there is a possibility that pathology may be identified on these images
- the image quality is low due to the lower tube current and higher slice thickness compared to diagnostic CT imaging of the chest and movement artefacts due to respiration.

However, there is an ethical question regarding the review of data to check actively for extra cardiac pathology. The work fed into the research theme within the Diagnostic Imaging Research Programme at University of Salford and, although not directly cited, stimulated a number of projects that considered the prevalence of incidental findings and viewer’s ability to correctly identify these (Coward et al., 2014, 2015; Thompson, Hogg, Manning, Szczepura, & Chakraborty, 2014). As reported in Tootell et al., (2012) [Paper 1] the quality of CT data is significantly affected by the acquisition parameters used which also impact on the radiation dose the patient receives as part of the acquisition. Many manufacturers promoted the “low-dose” acquisitions of their hybrid systems and quoted effective dose figures that were inarguably lower than diagnostic CT acquisitions of the equivalent area and were quick to demonstrate the additional benefits the acquisitions brought. Literature soon agreed that the ability to fuse emission and transmission data on the same piece of equipment was beneficial in aiding definitive diagnoses (Delbeke, Schöder, Martin, & Wahl, 2009). There was little independent research undertaken to evaluate additional radiation dose and subsequent risk that these acquisitions brought.

Work arising from the Diagnostic imaging Research Programme after the publication of Tootell et al., (2012) [Paper 1] showed that in a population of 1819 patients, 27.3% had a positive extracardiac findings on the CTAC dataset of which 2.8% were potentially clinically significant (Coward et al., 2014). To date no consensus on the use of the CT attenuation correction data has been reached and, while citing the considerations of the moral and legislative obligation of the clinician discussed in Tootell et al., (2012) [Paper 1], Kauling, Post, Rensing, Schaap, & Verzijlbergen (2015) note that this topic remains incompletely discussed by the European Association of Nuclear Medicine and European Society of Cardiology guidelines (Flotats et al., 2011).

To fully appreciate the two sides of risk and benefit in any decision, those involved in the referral process should have adequate information to consider the risk the exposure would bring. The work undertaken in the portfolio of published works as lead author considers the effective dose and subsequent risk the additional CT or conventional X-ray imaging brings. The methods developed in this work were applied to research where contributions were made as a co-author in other contexts to evaluate changes in protocol to include new imaging techniques or technology. For example, in the two co-authored papers (Thompson et al., 2015, and Thompson et al., 2016) [Paper 6, Paper 7], the techniques were used to measure the organ dose and calculate effective dose in CT acquisitions of the chest and used in the optimisation process comparing filtered-back and iterative reconstructions.

The methods developed and data generated has the potential to aid referrers, practitioners and operators in the decisions of referral, justification and optimisation. The Ionising Radiation (Medical Exposure) Regulations 2017 (2018) originates from Council Directive 2013/59/EURATOM (2013) and came into force in the UK in February 2018. It is stated that there is a requirement to strengthen the information provided to patients on the radiation doses and risks from medical procedures. This information should be presented in a manner that is understandable to patients and should allow them to make informed decisions when giving consent to proceed with radiological imaging investigations. This review will consider the recognised limitations with effective dose in translating absorbed organ doses to data that can be understood by referrers and patients and alternative methods, such as calculation of effective risk as proposed by Brenner (2009, 2011, 2012) are utilised in this portfolio of published works (Tootell, McEntee, Szczepura, & Hogg, 2016; Tootell, Szczepura, & Hogg, 2014b, 2017). This approach is novel when compared to published literature and goes beyond the normal approach of reporting of dose by applying organ dose data to specific patient types.

There are a number of methods by which radiation dose can be measured, calculated or estimated and are described and discussed in detail in (Tootell, Szczepura, & Hogg, 2014a) [Paper 2]. For example, measurement using thermoluminescent dosimeters (TLDs), metal-oxide semiconductor field effect transistors (MOSFET), calculation using data supplied by the imaging equipment (dose length product [DLP], CT dose indices [ $CTDI_{vol}$   $CTDI_{100}$ ] or dose area product [DAP]) or estimation through simulation using Monte Carlo modelling.

Papers 2-7 describe the genesis of the project focussing on the development and applications thermoluminescent dosimeters as a means of radiation dosimetry. In this thesis, the methods developed will be analysed critically and where applicable improvements will be identified and evaluated against the current body of knowledge. Tootell et al., (2017) [Paper 8] has been included as a closing paper to illustrate how the research described within the thesis will develop in the future. TLDs or MOSFETS are effective in direct dose measurements in phantom studies. However, in the clinical studies or in patient dose monitoring, direct dose measurement is challenging due to the different patient sizes and body habitussen. The pilot work in Tootell et al., (2017) [Paper 8] demonstrates the start of the development of a method to make dose estimation or simulation more accurate by accounting for differing patient habitussen. Incorporating corrections to dose estimates based on specific patient types has the potential to allow more accurate dosimetry audits to be performed and allow for less generic diagnostic reference level to be developed.

## 2. REVIEW OF DEVELOPED METHODS AND ANALYSIS OF THE DATA

The following section will analyse critically the portfolio of published works in the context of published literature in the field. It is recognised that over the timeline of publications (see Figure 6 Gantt Chart showing research and writing activities page 47) research and technology has progressed but the following chapters aim to reflect the state of literature at the time of writing and to consider recent developments.

As considered in the introduction and in Tootell et al., (2012) [Paper 1], the exposure parameters used to acquire CT data affects the quality of the image. CT acquisitions for attenuation correction are produced using imaging parameters that are much lower than those used in diagnostic CT examinations of the chest (Tootell, Vinjamuri, et al., 2012), yet these are adequate for the purposes for which they are acquired. At the time of writing, four main hybrid systems were in clinical use, two used “low-dose” fixed output CT components, one a full diagnostic capable CT component and one that sat between the two. It was noted that the parameters used in CT attenuation correction acquisitions were different yet were used for the same purpose, to correct emission data. Work was undertaken to compare the effective dose and effective risk from these acquisitions and compared to the effective dose and risk arising from the administration of radiopharmaceuticals only.

The development of this and subsequent publications in the assessment of patient dose from a number of scenarios using “conventional” radiographic imaging and CT, was preceded by the development of accurate, efficient methods for data collection and methods by which the data can be analysed to present meaningful findings and information to health professionals and potentially patients.

## 2.1 ACQUIRING DOSE DATA

Radiation dose assessment can be carried out in a number of ways; through direct measurement, estimation through modelling or calculation. Tootell et al., (2014a) [Paper 2], discusses in detail the definitions of radiation dose and how quantities can be established through the use of analogue or digital dosimeters, calculation or simulation using software. Prior to any comparison between measured and estimated radiation dose, it is essential that the accuracy of any measurement is assured.

Tootell et al., (2014a) [Paper 2], has had a significant impact in the teaching and learning activities associated with dosimetry and dose monitoring of patients i.e. Research Informed Teaching Project Experience (RiTE) in years 1 & 2 and Level 6 Dissertation Module. The paper is a core text within the undergraduate diagnostic radiography programme and provides a single reference point to enable students to develop an understanding of the concepts of radiation dose, its measurement and how the results can be interpreted and used to calculate the risks from exposures.

Within the RiTE 1 and 2 projects, students investigate the effect of changing kilovoltage (kV) and milliampere-seconds (mAs) have on image quality and patient dose. The paper is used to facilitate their understanding of the concept of dose and how the different metrics (for example dose area product (DAP) and entrance surface dose (ESD)) and units (for example mGy and mSv) can be used to report dosimetry data. When combined with image quality measurements it has facilitated the understanding of dose optimisation (Higgins, Hogg, & Robinson, 2013, 2017; Higgins R.N, n.d.). Comments from students in module evaluations and reported in Higgins, Hogg, & Robinson, (2013, 2017) demonstrate that they feel they have an understanding of radiation dose and image quality optimisation. They feel the knowledge they have acquired has influenced their clinical practice by encouraging them to be critical of their selection and manipulation of imaging parameters

### 2.1.1 DIRECT DOSE MEASUREMENT

There are many options available when a direct measurement of radiation dose is to be performed. Analogue or digital dosimeters such as thermoluminescent dosimeters (TLD) or metal-oxide semiconductor field effect transistors (MOSFET) offer advantages and disadvantages and, again, are discussed in Tootell et al., (2014a) [Paper 2]. Radiation dose measurements on live patients were not performed within this portfolio of published works due to ethical considerations and it was also felt that there was a need to establish a robust, valid and reproducible method for data collection before clinical colleagues and patients were included. Instead, phantoms were used in the collection of radiation dose data. While some argue this limits the external validity of research, it is a widely accepted and recognised approach to radiation dose assessment in radiological imaging (White,

1978). The advantage of phantom based studies is that “patient” size was controlled and it allowed the direct measurement of organ doses to be performed which is all but impossible in real patients. The dosimeters were placed inside the phantom in specific locations corresponding to those listed in the International Commission on Radiological Protection’s publication number 103 (ICRP, 2007).

As discussed above and in Tootell et al., (2014a) (Paper 2) researchers conducting direct radiation dose measurement have a choice between analogue (for example TLD) and digital (for example MOSFET) dosimeters. Both measuring devices have advantages and disadvantages and bring with them their own challenges when ensuring accurate data are acquired. Whichever device is used to obtain accurate organ dose data, it is critical that it should provide accurate and reproducible data. As part of this portfolio of works, radiation dose measurement was performed using TLDs (TLD-100 and TLD-100H) or digital dosimeters MOSFET. The following sub-sections provide a discussion on the features of the measuring devices, and the development and considerations made in order to produce quality data.

#### *ANALOGUE DOSIMETERS*

TLDs have a long established pedigree in the measurement of radiation dose in diagnostic radiography. The similar density to tissue, negligible amount of fading (i.e. loss of information from the TLD over time) and the high reproducibility in radiation dose measurement make the material ideal in measuring the quantity of absorbed radiation in biological tissue (Del Sol Fernández et al., 2016). All but one of the empirical papers use TLDs to directly measure radiation dose (Tootell et al., 2013, Tootell et al., 2014b, Thompson et al., 2016, 2015, Tootell et al., 2017) [Paper 3, Paper 4, Paper 5, Paper 6 and Paper 7]. Paper 3 and Paper 4 use Lithium Fluoride doped with Magnesium and Titanium (LiF, Mg, Ti) and are referred to as TLD-100. This type of TLD have a measurement range of 10  $\mu$ Gy to 1 Gy. Another type of TLD material is used in Paper 5, Paper 6 and Paper 7 are Lithium Fluoride doped with Copper and Phosphorus (LiF, Cu, P) and are referred to as TLD-100H. TLD-100H have a measurement range of 1  $\mu$ Gy to 10 Gy (ThermoFisher Scientific, n.d.). TLD-100H have a negligible fade over 3 months where TLD-100 have a fade of less than 20% over 3 months. In the context of the work in the portfolio of publications fading is not a concern as TLDs were read within 24 hours of exposure.

Using TLD-100H in place of TLD-100 addresses the concern of device sensitivity, with the TLD-100H offering greatly increased sensitivity with figures of 15-20 times the sensitivity compared to TLD-100 (Del Sol Fernández et al., 2016). The change to the more sensitive type of TLD material was made in recognition of the small levels of radiation dose being measured; in many cases in the dose

measurements in Tootell et al., (2014b) [Paper 4] were at the lower end and below of the sensitivity of TLD-100. In terms of the data collected in Tootell et al., (2014b) [Paper 4], the reliability of the data could be questioned, however as demonstrated by da Rosa, Regulla, & Fill, (1999), through careful annealing, the pre-heating of the TLD before reading the accuracy of lower radiation doses is possible. It was found that these additional steps did increase the time needed to read the TLDs.

The change to TLD-100H meant that radiation dose below 10  $\mu\text{Gy}$  could be measured accurately. However, the increased sensitivity meant that there was increased potential for contamination by background radiation. When making measurements of small levels of radiation, the background levels recorded by the dosimeters had the potential to be a significant factor in any radiation dose readings. This was of particular concern when the phantom was transported to a nuclear medicine department for the collection of data in Tootell et al., (2016) [Paper 7]. In this environment it is possible that the phantom would be in close enough proximity to unsealed sources and patients attending for examinations using radiopharmaceuticals that they may be influential on the dose measurements made with the TLD-100H. Care was taken to ensure that a selection of TLDs remained with the phantom at all times (except during data acquisition) to ensure radiation dose levels were representative of the imaging and not from environmental sources. In other words, this would allow either a correction of the data, accounting for background radiation, or rule out any influence of the radioactive sources.

On reflection there is a risk that this background correction could over correct the readings from TLDs within the phantom. TLDs within the phantom are surrounded by attenuating material at various thicknesses, for example a TLD in the centre would record less background radiation dose than a TLD near the outside of the phantom and both would receive less than a TLD used for background correction purposes as these would not have any attenuating material surrounding them. On analysis it was decided that this source of error is negligible for a number of reasons; the time spent in the nuclear medicine departments is short (maximum of 1 hour) but more importantly the phantom and TLDs remained no longer than required in a supervised or controlled area therefore the dose rate was below the 7.5  $\mu\text{Gy/h}$  level specified for Controlled Areas (The Ionising Radiations Regulations, 2017). Care was taken to ensure the positioning and scanning of the phantom was performed efficiently to minimise the time taken to acquire the data. As will be discussed later in this chapter, other methods were developed and utilised to ensure the signal from the acquisition was significantly greater than any noise from background.

A second factor that needed consideration was a characteristic of dosimetry using TLDs referred to as residual signal. Residual signal is defined as a carry-over of the TLDs exposure history into current

readings and TLD-100H are more susceptible to this characteristic than TLD-100 (~5% compared to 1.5% for TLD-100H and TLD-100 respectively) (Freire, Calado, Cardoso, Santos, & Alves, 2008). Annealing of the TLDs is a method of preventing historical data from contaminating dosimetry data (Yifrah et al., 2014). To reduce error and the impact of residual energy an annealing phase was built into the TLD reader's cycle. However this cycle is relatively short - 10 seconds at a temperature of 240°C (Thermo Electron Corporation Radiation Measurement & Protection, 2002). Therefore to ensure that as much residual energy was released as reasonably practicable, prior to each use the TLDs were annealed using a temperature controlled annealing oven and tray. The TLDs were heated and held for 10 minutes at 240°C and then cooled rapidly. Incorporating this step into the method ensured that the TLDs were prepared consistently and all were free from stored energy that would contribute to the dosimetry data. It did increase the preparation time and the heating and rapid cooling of the TLDs has the potential to shorten the TLD's useful life but given the reduction in residual energy and the low doses being measured it is a justifiable step.

Noise is unavoidable in the measurement of radiation dose and arises from the TLD reader's components, the TLD or background radiation. Noise arising from the TLD reader is unavoidable but is constant. By exposing the TLD to repeated exposures the radiation dose received by the TLD (and so the signal detected by the reader's photomultiplier tube) will increase, overcoming the constant noise from the reader. For areas within and immediately close to the area of exposure the signal to noise ratio is large but where only scattered radiation is being measured it is small. building up a radiation dose on the TLD would improve the signal and reduce the effect of noise.

A further time saving method was developed and used in Thompson et al., (2015a), Thompson et al., (2016) and Tootell et al., (2016) [Paper 5, Paper 6 and Paper 7]. Instead of replacing a set of TLDs after each exposure a "cumulative dose" approach was utilised. Following annealing and placement of the TLDs within the phantom, the phantom was exposed three times without removing and replacing the TLDs. The TLDs were read and the dose data calculated. This data was corrected for background and then the dose for each TLD divided by three (the number of exposures). A disadvantage of this method is the inability to identify random error or to calculate a standard deviation of the data. An approach that would use both methods i.e. repeated measures and cumulative approach, would give the most reliable data and would allow erroneous results to be identified and a standard deviation to be calculated. However, the time required to change TLDs between measurements is significant and, where research was carried out in the clinical department, was impracticable due to limited access to clinical equipment. Work by Mraity, (2015) based on the developed approach showed that there was no statistically significant difference in the

cumulative and repeated measure method. A practical advantage of this method process was an increase in efficiency and could be used by others when access to resources are an issue.

An observation that was made early in the research was the time needed to complete a full dosimetry measurement using TLDs. The phantom used throughout this work was an ATOM dosimetry phantom model 701C adapted to the 701D configuration (CIRS Tissue simulation and Phantom Technology, Norfolk, Virginia). This phantom contains 268 locations where dosimeters can be located to measure radiation dose. These TLDs required reading using a Harshaw manual TLD reader (Thermo Fisher Scientific, Walton, Massachusetts) meaning a single full-phantom measurement required approximately six hours of reading time. When combined with repeated measures the time required for collation of radiation dose data from TLDs was significant, running into several days depending of the number of variables.

To further improve the accuracy of the radiation dose measurements, an approach to reduce systematic errors arising from the TLDs was developed (Tootell, Lundie, Szczepura, & Hogg, 2012). The method involved grouping together TLDs of similar responses and performing calibrations on these. Manufacturer guidelines suggest a method of calibrating each individual TLD however this would be a very time-consuming exercise and would require an impracticable amount of effort to ensure the ordering of the TLDs remains unchanged during the repeated loading and unloading of the dosimetry phantom. By exposing all the TLDs to the same radiation dose, it was possible to rank and then group together TLDs of a similar response. The coefficient of variation (CV) defined as

$$\frac{\textit{standard deviation}}{\textit{Mean}} * 100\%$$

for a set of 273 TLDs (268 for the phantom and 5 for background correction) was found to be 7.61%. By grouping TLDs of a similar response it was possible to reduce this to ~2%. The more groups, the smaller the CV could be. Given that the manufacturers quote values of around 7% as an acceptable variation it was decided that 2% was acceptable and 5 groups was a practicable compromise between efficiency and accuracy (Tootell, Lundie, et al., 2012). Each group was calibrated and a TLD from each set was used to measure background radiation levels.

The above methods were used in all the empirical publications in this portfolio of works (J. D. Thompson et al., 2015; JD Thompson et al., 2016; Tootell et al., 2013, 2016, 2014b) [Paper 3, Paper 4, Paper 5, Paper 6 and Paper 7] and has been included in PhD work and other research activities (Ali et al., 2017; Ali, England, McEntee, & Hogg, 2015; Ali, 2016; Mraity, 2015; Robinson, Ali, Tootell, & Hogg, 2017).

## *DIGITAL DOSIMETERS*

During the period of time that the portfolio of works was produced, digital dosimeters became available and the dosimetry work in Paper 8 made use of these instead of TLDs (Tootell et al., 2017). Initially these dosimeters were predominantly used in radiotherapy dosimetry which is characterised by higher doses but their use in diagnostic dosimetry has become more popular due to the instant readout of radiation dose data, non-destructive measurement and good linearity (Bower & Hintenlang, 1998; Koivisto, Wolff, Kiljunen, Schulze, & Kortensniemi, 2015). Their function is described in Tootell et al., (2014a) [Paper 2].

It was predicted that the use of digital dosimeters (Metal Oxide Semiconductor Field Effect Transistor (MOSFET)) would increase the efficiency as the measurements could be carried out without having to physically remove the dosimeters to obtain radiation dose data. To some extent this was found to be true as the data collected in Tootell et al., (2017) [Paper 8] took significantly less time to collate compared to data collection using TLDs. However, during the development of the method a number of key lessons were learned with the use of MOSFET and from this a number of novel methods were developed to ensure that the data collected was as accurate as practicable. Since the publication of this paper it has been recognised that further steps can and should be taken to improve the accuracy of the data. The following paragraphs will discuss critically the approaches developed and further steps that could be taken should dosimetry using MOSFET dosimeters be performed.

Dosimetry data using the ATOM dosimetry phantom requires the measurement of radiation dose in 268 locations (CIRS Tissue Simulation and Phantom Technology, 2012). Resources dictated that 20 MOSFET dosimeters were available (4 readers with 5 dosimeters each). A choice existed between distributing the 20 across the 268 locations or repeating acquisitions and repositioning the dosimeters between each repeat so all locations had associated data. The latter approach was chosen to comply with the phantom manufacturer's guidance on radiation dose measurement as the locations had been optimised to allow accurate representation of the radiation dose distribution to and within the organs. A disadvantage of this method was the need to move the dosimeters to acquire data for each location. As can be seen in Figure 1 taken from Tootell et al., (2017) [Paper 8], this process required each scan to be repeated 14 times using 20 dosimeters.

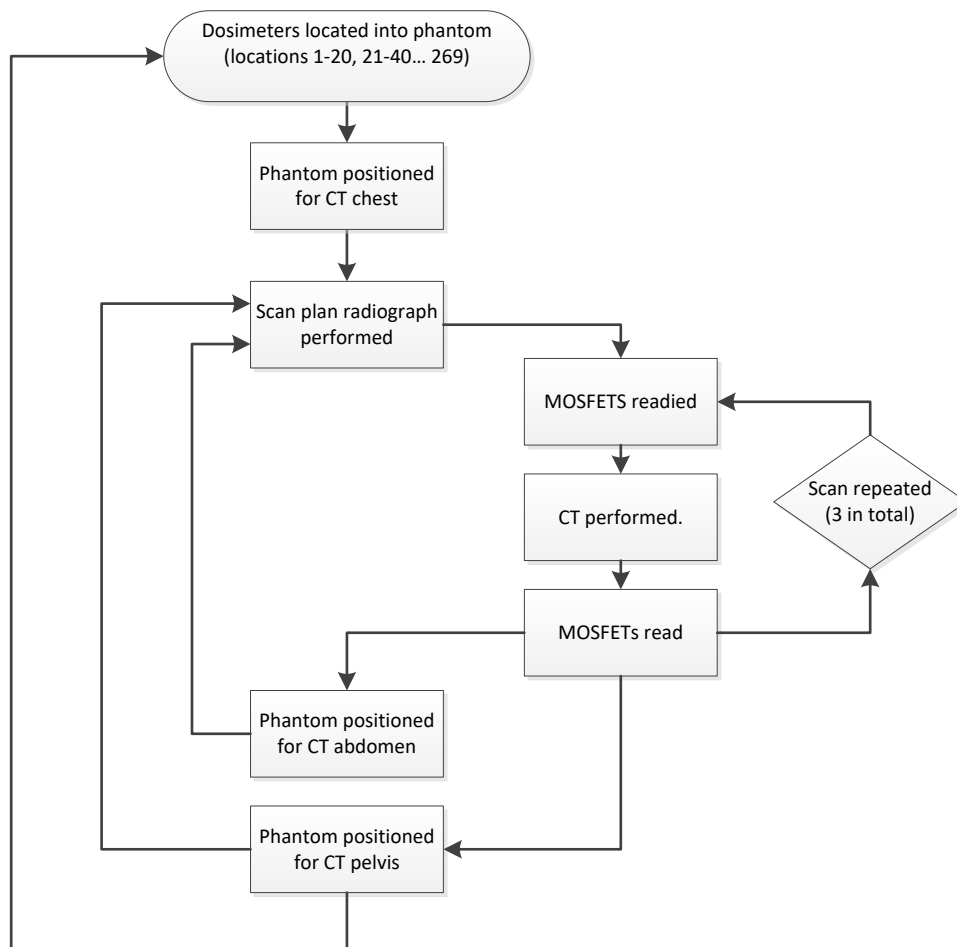


**FIGURE 1 PROCESS FOLLOWED IN TOOTELL ET AL., (2017) [PAPER 8] TO ACQUIRE ABSORBED ORGAN DOSE.**

The challenge was to ensure the same anatomical region was imaged each time, to guarantee the data was consistent. This required special considerations since this study was concerned with automatic tube modulation in CT acquisitions, so a slight change in position could be influential on the output of the x-ray tube. The method developed as part of Paper 4 (Tootell et al., 2014b) was utilised here where small radiopaque markers were attached to the phantom to correspond with the superior and inferior location of the scan range. The median-sagittal plane and mid-axillary line of the phantom were marked in permanent marker to ensure that accurate and reproducible positioning using the CT scanners laser lights was possible. From the result of the development work involved in the development of this portfolio of works, the use of indelible and radiopaque markers has been employed by researchers in their empirical work and by PhD students undertaking dosimetry and image quality research (Ali et al., 2017, 2015; Ali, 2016; Mraity, 2015; Robinson et al., 2017).

During the acquisitions it was noted that the results demonstrated variation especially in low dose regions, i.e. regions where scattered radiation was being measured (below 1.5mGy). There were occasions when a number of additional repeats were necessary due to the apparent randomness of

the readings. Reflecting on this finding it was felt that this statistical error could be addressed better than simply repeating until the results were consistent.

Reviewing literature in this area found that the statistical error using MOSFET dosimeters in low dose research is an issue that has been encountered. Koivisto et al., (2015) in research characterising MOSFET dosimeters for low-radiation dose measurements in maxillofacial anthropomorphic phantoms demonstrated that despite the statistical error at low dose, repeating MOSFET exposures eight times results in a confidence level of 95% in the MOSFET data. This research was carried out at energies of 80kV and used the less sensitive TLD-100 as the “standard” which differs from the energy and TLD type used in Paper 8 of 120kV and the more sensitive TLD-100H (Tootell et al., 2017). Increasing the number of repeats will decrease the uncertainty and the method by Koivisto et al., (2015) should be utilised. However direct dose measurements in patients would be subject to this statistical uncertainty and unavoidable as multiple repeats would be unethical.

Research undertaken in the portfolio of works was undertaken using dosimetry phantoms but post-doctoral research could involve the measurement of radiation doses to patients and/or operators. Ethical reasons would prevent any number of repeated measures being taken using patients so there would be significant lack of evidence on the accuracy of the results and this would need consideration should any data collection be undertaken using patients. In the context of the publication with data acquired using MOSFETS, acquisitions were taken three times and where readings were identified as different, a further repeat performed. On reflection, considering the work undertaken in this portfolio of works and data from published literature, the method described earlier where the cumulative dose approach could have been used to overcome the low-dose (less than 0.3 mGy (Koivisto et al., 2015)) statistical error. This could be further combined with repeated measures as this would be much easier to perform using MOSFET dosimeters compared to TLDs in that the MOSFETs do not need to be removed from the phantom to be read.

The above demonstrates how the method for radiation dosimetry was developed using published literature, manufacturers’ documentation and evolution through simple trial and error. The above development fed directly into work undertaken as part of this portfolio of works and other research projects at undergraduate, postgraduate and doctoral levels ensuring results were as accurate and reproducible as practicable. This review has highlighted where additional steps could be taken to improve further measured dosimetry data.

In summary, to be critical of the empirical works in the portfolio of works that use TLDs and MOSFETS, it is recommended that results should propagate any errors and display these in any results in the way they were shown in Tootell et al., (2017) [Paper 8]. Despite the inability to

calculate standard deviations as repeated measures were not used, each batch of TLDs had an associated error of approximately 2%. This error was not propagated through the calculations for organ or effective dose or carried through into the effective risk calculations. It could be argued that performing this action could have permitted deeper statistical comparisons between the variables. This is an issue with many published dosimetry papers despite the ease in which systematic errors can be identified. A search of literature demonstrates that error propagation is not well represented in diagnostic dosimetry research and the vast majority of papers quote, absorbed, equivalent and effective doses without reference to errors arising from the measuring tool. The same can be said for work where doses have been simulated with software. Software such as PXC MC (STUK, 2012) provide a value for the error in its calculations of organ and effective dose yet published literature does not quote this value on a regular enough basis.

### 2.1.2 MODELLING RADIATION DOSE

Direct dose measurement was used extensively in this portfolio of work despite the noted disadvantages of the time needed to acquire the data and the fixed characteristics of the dosimetry phantoms used. In clinical practice direct dose measurement for patients is challenging with the inability to directly measure organ dose, the ethical reasons preventing repeated measures and the retrospective nature of the data cited (Tootell et al., 2014a, Wall et al., 2011 and Groves et al., 2004). Dose reporting using metrics such as Dose Length Product (DLP), CT Dose Index ( $CTDI_{vol}$ ) or dose area product are adequate in intra-modality dose assessments but as noted in Tootell et al., (2014a) [Paper 2], this is not patient dose per se, just a measurement of the radiation quantity leaving the x-ray tube. Inferences can be made as to patient dose but to compare radiation dose across modalities the figured need to be converted to effective dose.

Dose modelling through simulation or through calculation using exposure parameters and conversion factors is a quicker method and is the most frequently used method in clinical practice. In the time during and since publication there has been a move towards automation of dose assessment using Digital Imaging and Communications in Medicine (DICOM) systems due to the increased accuracy of the data (Boos, Meineke, Bethge, Antoch, & Kröpil, 2016; Noumeir, 2005). NICE, (2017) in their report on radiation dose monitoring software for medical imaging with ionising radiation, quote figures of up to £20 000 per year which may make the purchase and upkeep of such software uneconomical when compared to manual methods. It is recognised that these systems are now becoming more popular in practice but until they are widely available the manual recording of data is required. Tootell et al., (2014a) [Paper 8] aimed to compare the accuracy of these approaches

to the measured organ and subsequent effective dose calculations for CT examinations of the chest, abdomen and pelvis.

The two methods of dose estimation considered; 1) the use of software (specifically ImPACT CTDosimetry v1.0.4 (ImPACT, 2011)) or 2) DLP to effective dose conversion factors in CT examinations of the chest, abdomen and pelvis. Literature reports underestimation of CT doses using computer simulation with magnitudes of 18- 40% (Groves et al., 2004). Conversely though, the results of Tootell et al., (2017) [Paper 8] demonstrated an overestimation of effective dose when compared to calculated effective dose from directly measured organ doses using TLDs or MOSFETS.

At the outset, it was anticipated that the work comparing estimated and calculated effective dose would have been a relatively simple task. However, the initial results demonstrated that there was significant disagreement (an range of of 50.3%, 2%-101%). In response, work was undertaken to identify where the differences could originate from. A number of key findings were noted and are discussed in detail in Tootell et al., (2017). In summary the following was noted, ImPACT CTDosimetry v1.0.4 (ImPACT, 2011) has only one single size virtual phantom available and an incompatibility with automatic tube modulation. The software's guidance documentation recommends that the same scan range is used when estimating the dose from a clinical examination, for example for a CT of the chest the apices to below the diaphragm should be set (ImPACT, 2011). This may differ from the measured scan range used due to the different lengths/height of the patient. In Tootell et al., (2017) a novel approach of scaling the dosimetry phantom to match the taller software's phantom was developed. This allowed for the same scan range to be set. This approach has not been used in published literature and is simple enough to be employed in clinical practice to accurately replicate the clinical scan in the software simulation. The distance between two anatomical landmarks in the patient can be measured from the scan plan radiograph and scaled to allow a scan range to inputted into the software rather than manually selecting a scan range.

The inability to account for automatic tube current modulation was addressed by comparing three methods of inputting an mA value into the software. An average mA, and effective mA were used as single values and a third method involving the calculation of the effective dose per CT slice and the calculating the sum of these. This was done through the creation of a macro-programme in the Excel file of the ImPACT CTDosimetry software. It was found that using average mA or the mA modulated data brought the effective dose closer in agreement yet over estimation was still an issue (27-53% over estimation). Work by Castellano, (2010) demonstrated that effective dose is affected by the mass of the patient with effective dose lower in larger patients for the same imaging parameters. Using the provided ratios for scaling effective dose and the method described in Tootell et al., (2017)

[Paper 8] it was shown that effective dose could be brought into close agreement for CT of the chest and abdomen, yet over estimation persisted for CT of the pelvis. The same improvement was noted when the mass correction was applied to the conversion of dose length product to effective dose using published conversion factors.

A method that is not, and arguably should have been investigated in this research area was the use of size-specific-dose estimation (SSDE) (AAPM Task Group 204, 2011). This method was proposed due to the inability of  $CTDI_{vol}$  to reflect patient size as it is a measurement of tube output and not patient dose (Tootell et al., 2014a [Paper 2], (Brink & Morin, 2012). This method uses the combination of the anterior-posterior (AP) and the lateral (Lat) dimensions. These values are used to estimate the patient size by using either, the AP or Lat dimension only,  $AP + Lat$  or the effective diameter  $\sqrt{AP \cdot Lat}$  (i.e. the diameter of the circle whose area is the same as that of the patient cross section). This figure is then used to multiply the  $CTDI_{vol}$  to provide the size specific dose estimate.

SSDE is able to provide users with an indication of dose to patients giving due consideration to their size. It should not however be used in further calculations to estimate effective dose using the DLP to effective dose calculations. It does not correct for differences in the organ dose distribution and so the resulting figure is for comparative purposes only and would demonstrate that an increasing patient size reflects an increased  $CTDI_{vol}$ . Therefore the unit is regarded as a dose estimate not a calculation (AAPM Task Group 204, 2011). Its use is limited to CT examinations only and so should comparisons between modalities be required, the use of the DLP to effective dose or the use of software remains. The work in Tootell et al., (2017) [Paper 8] has the potential to allow the calculation of effective dose that reflects the patients size, thus allowing inter-modality comparison of radiation dose. As described in (Tootell et al., 2014a) [Paper 2], figures such as DAP, DLP or  $CTDI$  are not patient dose per se, and so when trying to compare imaging with CT to X-ray imaging this method of accurately calculating effective dose will allow comparisons to be made.

It is recognised that further work is required as a number of findings were made and require further exploration. This work is planned as post-doctoral research and will focus on expanding the work undertaken in Tootell et al., (2017) [Paper 8] by considering other CT scanners and the still evident discrepancy in the effective dose estimated and calculated in the pelvis. Patient mass alone is the only one of a number of features that could affect the accuracy of dose estimates. Work by Boos et al., (2015), considered accounting for body mass Index (BMI) in radiation dose assessment in CT examinations of the abdomen. BMI does not provide an estimate for the percentage of body fat compared to muscle, patients of a muscular build have an incorrectly elevated BMI due to the higher

density of muscle over fat. Other metrics, for example the body adiposity index, waist circumference measurement or waist to hip ratio provide an indication of habitus and have the potential to be applied to dose estimations to allow a specific dose estimation for a patient type to be made. This data could be used to create diagnostic reference levels that are more reflective of patient type or build.

## 2.2 THE DOSIMETRY PHANTOM

Measurement of radiation dose was carried out using dosimetry phantoms due to the ethical issues in using patients or volunteers and it offered an element of control of the “patient” size. As will be discussed later, there are methods of assessing radiation dose on “real patients” using calculation and this approach does offer increased external validity. A disadvantage of using physical phantoms is the inability to alter these to reflect different medical conditions or anatomy thus limiting the size of population available to conduct research (Xu & Eckerman, 2010). A range of dosimetry phantoms are available (Figure 2) but resources dictated that in this portfolio of works only the adult male was available (the neonate and one-year phantom were available but research in this portfolio of works focussed on adult dosimetry). Radiation dose measurements and the calculation of effective risk was performed using the adult male phantom only and as can be seen in Figure 2, this phantom is larger than the adult female phantom. This limitation is noted in the published works.

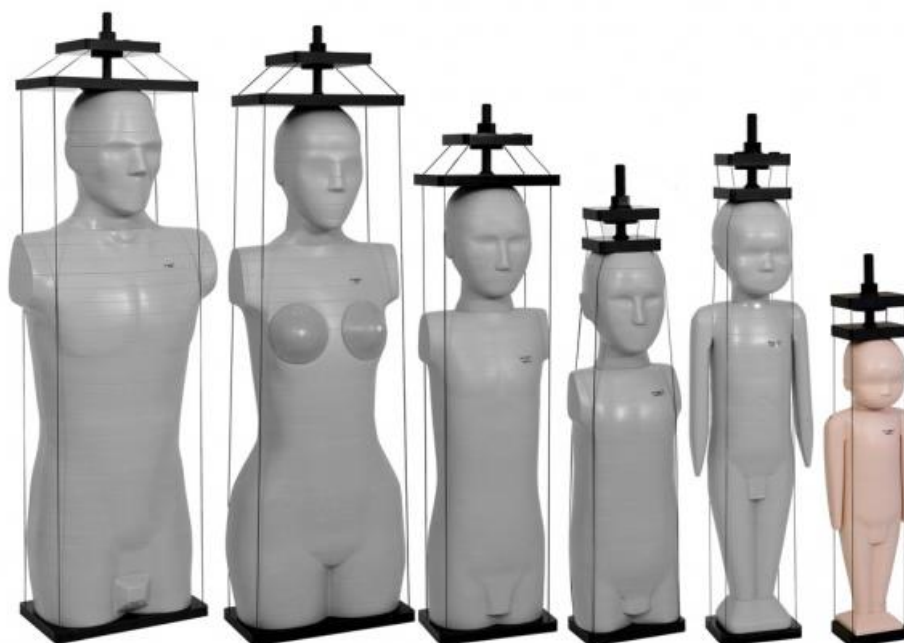


**FIGURE 2 THE CIRS ATOM DOSIMETRY PHANTOM FAMILY MODELS 701-706 (CIRS, NORFOLK, VIRGINIA)**

As described throughout the portfolio of published works, the effective dose is calculated following the measurement of absorbed radiation dose of organs within the phantom. This is done by measuring specific locations in the organs, averaging these to provide a tissue or organ dose, converting absorbed dose to equivalent dose and then multiplying the data by the tissue weighting factors listed in ICRP report 103 before summing the weighted doses (ICRP, 2007). During planning

and pilot work it was discovered that there was a mismatch in the locations and the phantom’s specification and the organs that required dose data to be collected; i.e. the sum of the weighting factors in the phantom data did not add up to unity as anatomical areas and/or structures were identified that did not have corresponding locations for measurement. For example, bone surface, skin and salivary glands and within the remainder category of organs/tissues, the extrathoracic region, lymphatic nodes, muscle, oral mucosa and uterus/cervix (ICRP, 2007). While the recommended method for calculating the equivalent dose for the remainder organs and tissues is to calculate the average dose between the fourteen tissues regardless of how many have data associated with them, it was felt that there was an opportunity to improve the accuracy of the data by examining closely the locations that were already in use within the phantom and reapplying the data to correspond to the required locations. Locations in the anterior aspect of the vertebral body of C2 and the upper oesophagus were used to calculate extra thoracic tissue dose, locations in the left and right lingula of the mandible and to the left and right of the sublingual fossa were used to calculate salivary gland organ dose and locations in the left and right lingula of the mandible were used to calculate oral mucosa organ dose. Skin, muscle and lymph nodes were excluded as it was decided that in the context of this portfolio of work, only a small proportion of the tissue’s total mass was included in the primary field of view and so the total organ/tissue dose would be negligible. This method allowed for more organs/tissues to be included in effective dose calculations meaning that more of the tissues are sampled providing an improved value of the effective dose. The effect of including and excluding dosimetry data of the salivary glands, extrathoracic tissue and oral mucosa in data taken from Tootell et al., (2017) [Paper 8] (CT examinations of the chest, abdomen and pelvis) are shown in Table 1.

Anatomical region	Remainder organ dose (mSv)		effective dose (mSv)	
	Including	Excluding	Including	Excluding
Chest	8.64	6.41	12.07	11.78
Abdomen	9.17	9.14	8.44	8.43
Pelvis	3.21	3.20	4.57	4.57

**TABLE 1 COMPARISON OF REMAINDER ORGAN AND EFFECTIVE DOSE WHEN SALIVARY GLANDS, EXTRATHORACIC AND ORAL MUCOSA DOSE WERE INCLUDED AND EXCLUDED.**

Interestingly, this comparison shows that when analysed using a t-test, the inclusion or exclusion of these data was not statistically significant in both the remainder organ dose and effective dose calculations ( $p > 0.1$ ). Therefore it could be concluded that this extra data is not required. However, from the above data, it is observed that the impact on the CT chest data is greater than the effect on the CT abdomen which in turn is greater than the data for the CT pelvis. If the location of the excluded tissue is considered it can be seen that they are close to the field of view in the chest and become progressively further away from the scan region. The effect of the exclusion of these organs is greater the closer they are to region exposed. For this reason the organs were included in dose calculations in this portfolio of work (Thompson et al., 2015, 2016, Tootell et al., 2016, 2014b, 2017). This method has been used extensively in other research undertaken in dosimetry in the Diagnostic Imaging Research programme (Ali et al., 2017, 2015; Ali, 2016; Mraity, 2015; Robinson et al., 2017).

As stated earlier and in Tootell et al., (2014b, 2016, 2017) [Paper 4, Paper 7 and Paper 8]. The absence of additional breast tissue that would be present in the female phantom would affect the measured dose for that organ. However, as will be discussed, effective dose calculations do not account for male and female breast tissue only the reproductive organs (testes and ovaries) and gender specific organs in the remainder tissues (prostate gland and uterus/cervix). To account for the different locations of the reproductive organs the location of ovaries was established by reviewing cross sectional anatomy texts and locating the equivalent location in the adult male phantom. This is an approach that has been used successfully in publications generated from completed and ongoing PhD and other research activities within the Diagnostic Imaging Research Programme (DIRP) (Ali et al., 2017, 2015; Ali, 2016; Mraity, 2015; Robinson et al., 2017).

Research was undertaken to establish a process to allow the number of TLDs to be reduced without compromising on the accuracy of the dosimetry data. A full detailed description and analysis of this can be found in (Tootell et al., 2013) [Paper 3]. In summary this paper developed a method where TLDs could be sited in locations where they would receive a measurable quantity of radiation. This paper was inspired by methodologies from dental radiography dosimetry where organs and tissue a distance from the exposed area were not included in measurements due to the negligible quantity of radiation they would receive. These areas were identified as regions where the dose readings were below the 50  $\mu\text{Gy}$  limit of the TLDs (Table 1 and Figure 3). On reflection this approach was effective and reduced the required number of TLDs by 82 (268 to 186) saving around 2 hours of reading time per dataset using the manual TLD reader. On further reflection there are limitations in this method. The main one is the way the dose to the phantom's slice was measured. The TLDs were placed in a central column and exposed. Due to attenuation by the surrounding material the central TLD would record less radiation dose than one that situated at the periphery of the phantom therefore there is

the potential for locations to be excluded when a radiation dose of greater than 50  $\mu$ Gy would have been recorded.

Slice number	Mean Dose (mGy)
2	0.00
3	0.00
4	0.00
5	0.02
6	0.00
7	0.01
8	0.00
9	0.02
10	0.03
11	0.07
12	0.20
13	0.32
14	0.67
15	1.34
16	1.88
17	2.57
18	8.66
19	9.83
20	10.01
21	8.11
22	3.68
23	2.10
24	1.44
25	0.68
26	0.51
27	0.37
28	0.10
29	0.02
30	0.00
31	0.00
32	0.07
33	0.05
34	0.00
35	0.01
36	0.01
37	0.02
38	0.02
39	0.01

**TABLE 2 RECORDED DOSE FROM A SIMULATED CT ATTENUATION CORRECTION ACQUISITION OF EACH SLICE SHOWING WHERE LEVELS WERE ABOVE (GREY SHADED) AND BELOW THE 0.05 MGy THRESHOLD.**

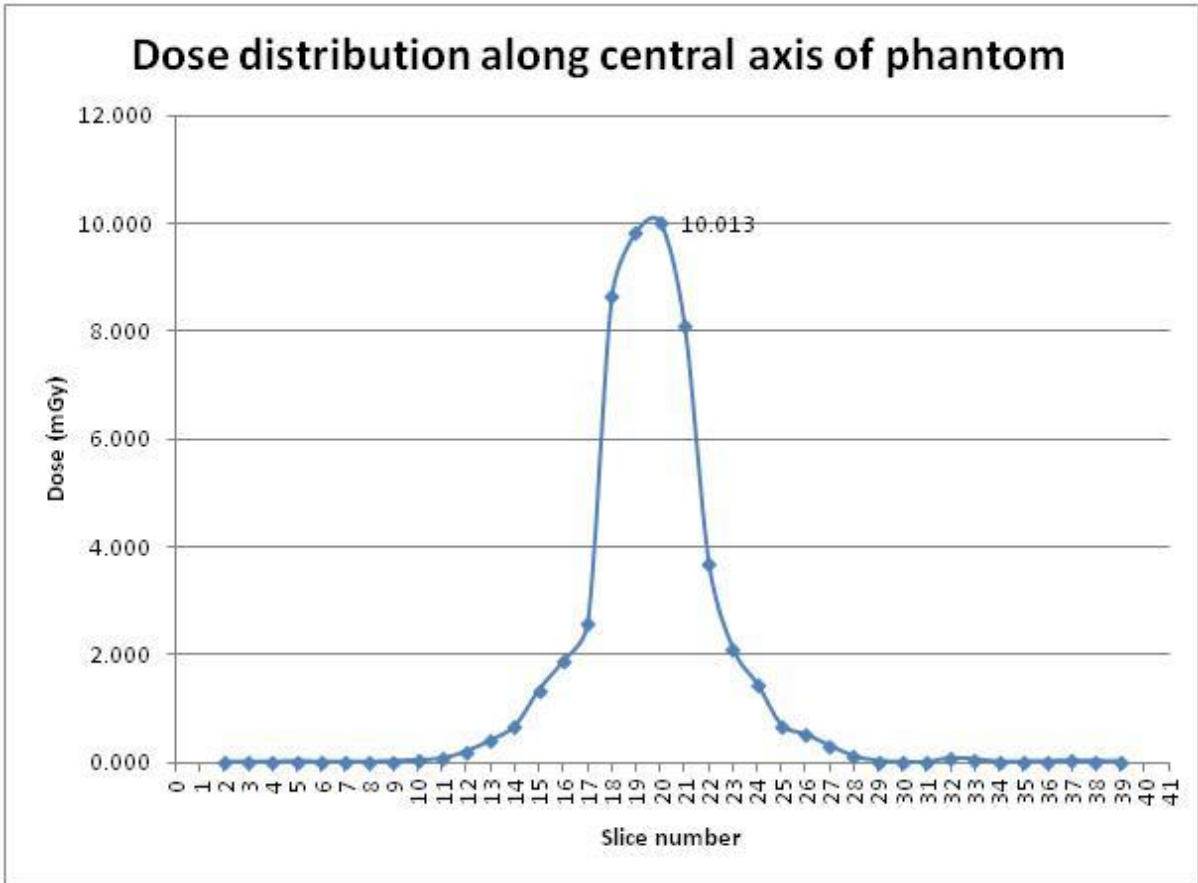


FIGURE 3 CHANGE IN ABSORBED DOSE ALONG A CENTRAL COLUMN OF TLDs IN THE DOSIMETRY PHANTOM. THE DECISION TO EXCLUDE ABOVE SLICE 10 AND BELOW SLICE 28 WAS ARBITRARY.

An alternative approach would have been to place the TLDs in an arrangement illustrated in Figure 4. Measuring radiation dose at the periphery could have expanded the range over which TLDs should have been placed.

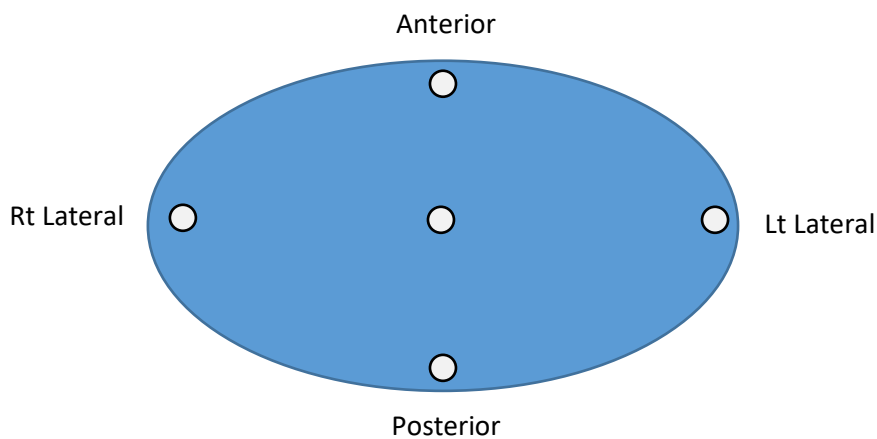


FIGURE 4 SUGGESTED PLACEMENT OF TLDs TO ASSESS THE RANGE OF PHANTOM SLICES WHERE DOSIMETRY DATA SHOULD BE ACQUIRED

Despite the acknowledged limitations and suggested improvements, the paper did prove that, in the context of myocardial perfusion imaging at least, a reduced number of TLDs gives a comparable effective dose readings at only 1.75% lower than if the full set was used. In this paper a number of organs demonstrated a 100% reduction in dose (brain, prostate and testes) yet the impact on the final calculation of effective dose was small due to the small weighting factor that is applied to the organ dose. A 61.4% reduction was noted in the organ dose for the colon due to the exclusion of TLDs located in the caecum, distal ascending and descending colon and the sigmoid colon. This reduction was calculated by calculating the mean dose for all TLD locations, including those at an assumed level of 0. This underestimates the organ dose and arguably a better approach would have been to take the mean of the areas that were measured.

Revisiting the data and comparing the calculated organ dose to the colon using the two above options is illustrated in Table 3. The following data is part of the full dataset from Tootell et al., (2013) [Paper 3]. The calculated organ dose using all locations in the phantom is 0.191mGy. Exclusion of readings below 50 µGy and assuming a dose of 0 results in an organ dose of 0.074 mGy compared to 0.171 mGy if the average of the measured areas is calculated. It is advisable that the whole of the organs with the highest weighting factors (i.e. breast, colon, lungs and stomach) should be included in any measurement. However, as an alternative approach, a mean of the TLDs can be taken and excluded areas should not be assumed as zero dose.

Measured TLD dose (mGy) (n=10)	Exclusion of TLD below 50 µGy *assumed zero dose (n=10)	Exclusion of TLD below 50 µGy (n=6)
0.112	0.112	0.112
0.112	0.112	0.112
0.117	0.117	0.117
0.168	0.168	0.168
0.113	0.113	0.113
0.074	0.074	0.074
0.048	*0.000	-
0.033	*0.000	-
0.000	*0.000	-
0.013	*0.000	-
MEAN = 0.191	=0.074	=0.171
% difference	61.4%	10.5%

TABLE 3 COMPARISON OF METHODS IN CALCULATING ORGAN DOSE IN THE COLON.

This method used in the data collection of Paper 4 (Tootell et al., 2014b) for a number of mainly logistical reasons. Firstly, the data collection took place in clinical departments where access to the imaging equipment was time restricted. Secondly, the method used a repeated measure design whereby the TLDs were removed and replaced after each repeat and, as noted, this is a very time-consuming process and by reducing the number of TLDs required increased the efficiency of the process.

Further dosimetry studies that were conducted involved a larger CT scan range than that used in CT attenuation correction of myocardial perfusion SPECT data. Paper 5, Paper 6, and Paper 7 used a full set of TLD dosimeters and Paper 8 utilised the full set of dosimeter locations with MOSFET dosimeters (Thompson et al., 2015, 2016; Tootell et al., 2017). However, efficiency was increased by using the previously described cumulative method.

The above development work demonstrates the steps taken to optimise and improve the use of the dosimetry phantom in the measurement of radiation dose. It is recognised that there are potential further improvements through the use of the relevant dosimetry phantom but in this portfolio of works, resources dictated otherwise. As before, these methods and development work was used in all of the empirical publications in this portfolio of works (Tootell et al., 2013, 2014b, Thompson et al., 2016, 2015 and Tootell et al., 2016) and has been included in PhD work and other research activities (Ali et al., 2017, 2015; Ali, 2016; Mraity, 2015; Robinson et al., 2017).

## 2.3 RADIATION DOSE- EFFECTIVE DOSE & EFFECTIVE RISK

Effective dose is a relatively new concept introduced by the ICRP in the 1977 Recommendations of the International Commission of Radiological Protection (ICRP, 1977). Initially used in the monitoring and control of radiation exposure in relation to stochastic risks the concept has been extended to members of the public including exposures to embryos and fetuses (ICRP, 1991, 2006, 2007). The method of calculating effective dose and its use in reporting research findings has been heavily criticised and suggestions for alternative approaches have been made. This chapter will review these discussions in the context of the portfolio of works.

### 2.3.1 EFFECTIVE DOSE

Effective dose is a figure that can be used in the comparison between techniques within and across imaging modalities using ionising radiation. The process of effective dose calculation is described in detail in Tootell et al., (2014a) [Paper 2] but in summary it is a three stage process; establishing the absorbed dose to organs and tissues identified in Table 3 in Gray (Gy), converting this to equivalent dose in Sieverts (Sv) through the application of the radiation weighting factor, and finally summing the equivalent dose after the application of the appropriate tissue weighting factor. The weighting factors are an indication of the sensitivity of the tissue or organ to ionising radiation.

In the comparison of techniques, measured dose quantities is the most appropriate method and for this reason dose measurement was used in Thompson et al., (2015, 2016) [Paper 5 and Paper 6]. It could be argued that in these papers, a comparison between the techniques could have been performed using volume averaged computed tomography dose index ( $CTDI_{vol}$ ) and/or dose length product (DLP) as the same anatomical area of the phantom was imaged on the same piece of imaging equipment under different tube current values (Harrison et al., 2016). However, the technology being used in this study was relatively new (volumetric CT) and it was felt that taking the time to acquire measured dosimetry data would be of value as a comparison between techniques. The methods developed and described in 2.1.1 Direct Dose Measurement were used to measure the organ dose and calculate effective dose for the different techniques.

Measurable dose indices are unable to convey meaningful comparisons, for example dose length product cannot be compared to dose area product or techniques that result in different distributions of radiation dose within the body. Effective dose is able to fulfil this requirement (Dietze, Harrison, & Menzel, 2009; Harrison et al., 2016). According to Harrison et al., (2016) there has been confusion in the practical application of effective dose in the communication of information to non-experts in ionising radiation, i.e. referrers and patients. There is a “problematic and growing application to the assessment of risk to individuals”; something that effective dose is not suitable for. Effective dose

does not take into account the age of an individual and only accounts for gender differences in the calculation of the remainder organs (prostate and uterus/cervix).

David J Brenner is director for the Centre for Radiological Research at the Colombia University Medical Centre and is interested in the field of risks and benefits for imaging techniques using ionising radiation in the field of medical imaging. In his publications focussing on the reporting of radiation dose, he notes that there is an increasing number of publications in which effective dose is calculated, and then used to estimate lifetime cancer risks (Brenner, 2012). As presented in Paper 2, (Tootell et al., 2014a), Brenner, (2009, 2011, 2012) is uncompromising in his criticisms of effective dose and its use in published literature. The author goes on to not only criticise the use of effective dose for purposes it was not intended but the method by which it is devised. Issues cited target the ICRP's approach to effective dose citing its calculation being based on tissue weighting factors that are from subjective judgements by a committee and are inflexible in their inability to reflect age and gender differences in radiation sensitivity (Table 3).

Tissue or Organ	Weighting Factor		
	ICRP 26 (1977)	ICRP 60 (1990)	ICRP 103 (2007)
Bone marrow	0.12	0.12	0.12
Breast	0.15	0.05	0.12
Lung	0.12	0.12	0.12
Stomach	-	0.12	0.12
Colon	-	0.12	0.12
Gonads	0.25	0.2	0.08
Thyroid	0.03	0.05	0.04
Bladder	-	0.05	0.04
Liver	-	0.05	0.04
Oesophagus	-	0.05	0.04
Bone surface	0.03	0.01	0.01
Skin	-	0.01	0.01
Salivary Glands	-	-	0.01
Brain	-	-	0.01
Remainder	0.3	0.05	0.12

**TABLE 4 ICRP TISSUE WEIGHTING FACTORS FROM 1977 TO PRESENT DATE**

Since its conception in 1977, these weightings have been reviewed and changed. These changes do make long-term trends in levels of radiation dose challenging to identify yet if the ICRP were to not change these weightings then they would be open to criticism for not responding to new observations or advances in scientific knowledge (Dietze et al., 2009). However, changes in weightings have been made for reasons other than through the discovery of new knowledge, for

example the change in the weighting to the breast from 0.05 in 1991 to 0.12 in 2007 was due to the committee deciding to emphasise cancer incidence rather than mortality (Brenner, 2011).

Considering effective dose in isolation can mask significant changes in radiation dose to specific organs. An example of this is a finding that was made in Tootell et al., (2014b) [Paper 4]. This research compared the additional radiation dose and risk that a CT attenuation correction acquisition would bring compared to the radiation dose and risk from the administration of the radiopharmaceutical alone for a rest and stress myocardial perfusion study. Four commonly used hybrid imaging systems were included in the study and compared to the two most common radiopharmaceuticals. The results demonstrated that the effective dose was increased by 1.8 to 3.0 mSv. However, if individual organs are considered, specifically the radiosensitive organs and tissues such as lung and breast it can be seen that there is a significant increase in radiation dose to these organs. Breast dose in particular was found to increase by 4.1 mSv to 8.2 mSv from 3.7 (121%) for <sup>99m</sup>Tc Tetrafosmin or 5.7 mSv (54.1%) for <sup>99m</sup>Tc Sestamibi.

Organ	Dose (mSv)					
	99mTc Tetrafosmin	99mTc Sestamibi	GE single slice	GE four slice	Siemens Symbia T6	Philips Precedence
Lung	5.1	7.1	3.6	5.4	3.1	5.5
Oesophagus	5.3	6.5	2.5	3.8	2.4	5.6
Colon	28.8	34	0.2	0.2	0.6	0.5
Liver	5.3	16	2.6	4.7	2.7	4.9
Stomach	7.4	10	1.1	2.4	1.7	3.1
Breast	3.7	5.7	7.1	6.6	4.1	8.2
Effective dose (mSv)	11	13.3	1.9	2.5	1.8	3.0

TABLE 5 COMPARISON OF SELECTED ORGANS AND EFFECTIVE DOSE RESULTING FROM ADMINISTRATION OF RADIOPHARMACEUTICAL COMPARED TO CT ATTENUATION CORRECTION ACQUISITIONS (TOOTELL ET AL., 2014B) [PAPER 4]

This paper has successfully highlighted that although the effective dose is low compared to the radiopharmaceutical dose, practitioners and operators should be aware of changes to dose profiles and the individual organs and tissues that could be affected by a change in protocol. This conclusion is supported by the results in Tootell et al., (2016) [Paper 7], in a similar approach to Tootell et al., (2014b) [Paper 4], the effect on radiation dose from supplementary imaging of the lumbar spine following an isotope bone scan is investigated. In this case the changes in effective dose are greater with results showing that the effective dose from lumbar spine imaging using X-ray images was 0.56

mSv ( $\pm 0.09$ ), “low-dose CT” 0.80 mSv ( $\pm 0.12$ ) and diagnostic CT was 3.78 mSv ( $\pm 0.56$ ). The calculated effective dose from the administration of 800 MBq of  $^{99m}\text{Tc}$  labelled phosphate or phosphonate is 4.56 mSv. Thus the additional effective dose from supplementary imaging is 12.3% for X-ray images, 17.5% for low-dose CT and 82.9% for diagnostic CT. Given the small difference in effective dose between x-ray and low-dose CT reported in Tootell et al., (2016) [Paper 7] it can be seen in the appendix (p160) that the findings have influenced clinical practice and has led to a change in protocol at a local nuclear medicine department. The department no longer refers for x-ray imaging of the lumbar spine to characterise lesions as the benefits of fused SPECT-CT images for the now proven small additional amount of radiation dose can be justified

Consideration of individual organ doses reveals that the stomach receives one of the lowest doses from the radiopharmaceutical (0.96 mGy). Following supplementary imaging this figure increased to 10.82 mGy (+1027.35%) for diagnostic CT, 3.10 mGy (+222.95%) for low-dose CT and 2.25 mGy (+134.74%) for X-ray Images. These results are due to the organ being directly in the field of view when imaging the lumbar spine. While these results are specific to lumbar spine imaging they have shown that the supplementary imaging can significantly increase organ dose and subsequent risk to that organ. It is for this reason that accurate organ dose assessment is required supporting the recommendations made in ‘2.2 The Dosimetry Phantom’ stating that the whole of the organ’s dosimetry locations be used or, as stated in this thesis, the mean of the locations used should be calculated without assuming a zero value of excluded locations.

An issue discussed in Tootell et al., (2014a) [Paper 2] and supported by Harrison et al., (2016) is the confusion between dose quantities, specifically equivalent and effective dose. The SI unit for both of these quantities is the Sievert and difficulties in communication have been identified when equivalent dose and effective dose have not been distinguished adequately. Potential confusion could be avoided if specific organ and tissue doses were referred to using the absorbed dose (Gy) (Harrison et al., 2016). This recommendation supports the decision taken in presenting the results in Tootell et al., (2016) [Paper 7] to use absorbed dose (Gy) rather than equivalent dose (Sv).

In conclusion, effective dose is a useful figure in the comparison of techniques where dose distributions are different or the dose indicators do not permit direct comparison, for example DLP and DAP. The identified trend of using the figure to calculate individual risk is of concern as effective dose calculations does not take into account for age and to a lesser extent gender.

### 2.3.2 EFFECTIVE RISK

An alternative to effective dose is proposed by Brenner, (2009, 2011, 2012) and applied in a number of papers in this portfolio of works (Tootell et al., 2016, 2014b, 2017) [Paper 4, Paper 7 and Paper 8].

Referred to as “effective risk”, it provides a statistical figure of risk of cancer induction for a given examination and this figure can reflect age and gender. As described by Brenner, (2009, 2011, 2012) and in Tootell et al., (2014a) [Paper 2], the calculation of effective risk is a similar process to the calculation of effective dose in that the absorbed dose to organs is established, but instead of being applied to tissue weighting factors defined by the ICRP, these values are applied to statistical data produced from epidemiological studies of cancer induction such as National Research Council (U.S.) Committee to Assess Health Risks from Exposure to Low Level of Ionizing Radiation., (2006) and Wall et al., (2011). The approach used by the papers in this portfolio of works has been applied in other publications and PhD work within the Diagnostic Imaging Research Programme (R. M. . Ali et al., 2017, 2015; R. M. K. Ali, 2016).

Effective risk could be used to provide referrers and patients with an easily interpretable value that can be used to inform the imaging pathway or the decision to give consent for the examination. The method used in this portfolio of works and other publications from the Diagnostic Imaging Research Programme could be argued to be relatively simplistic in the approach as they do not follow the full method described by the BEIR VII committee. The development of the method relied heavily on the work undertaken but the Radiation Effect Research Foundation (RERF) who undertook research and documentation of the after effects of the 1945 atomic bombing of Hiroshima and Nagasaki. The adopted philosophy is of a linear non-threshold (LNT) hypothesis involves the scaling of higher radiation doses and recorded effects to low dose scenarios. Other models do exist as illustrated in Figure 5 and with some authors advocating the use of the non-linear threshold model due to the potential significant over estimation of risk in low dose exposure and the assumption that cells respond similarly to high and low-dose exposure (Harvey, Brink, & Frush, 2015; O’Connor, 2017; Siegel et al., 2018). The linear non-threshold model is the “worst case scenario” where any exposure to ionising radiation carries a risk. It could be argued that this is erring too much on the side of caution and could impact on uptake of radiological procedures due to perceived risks.

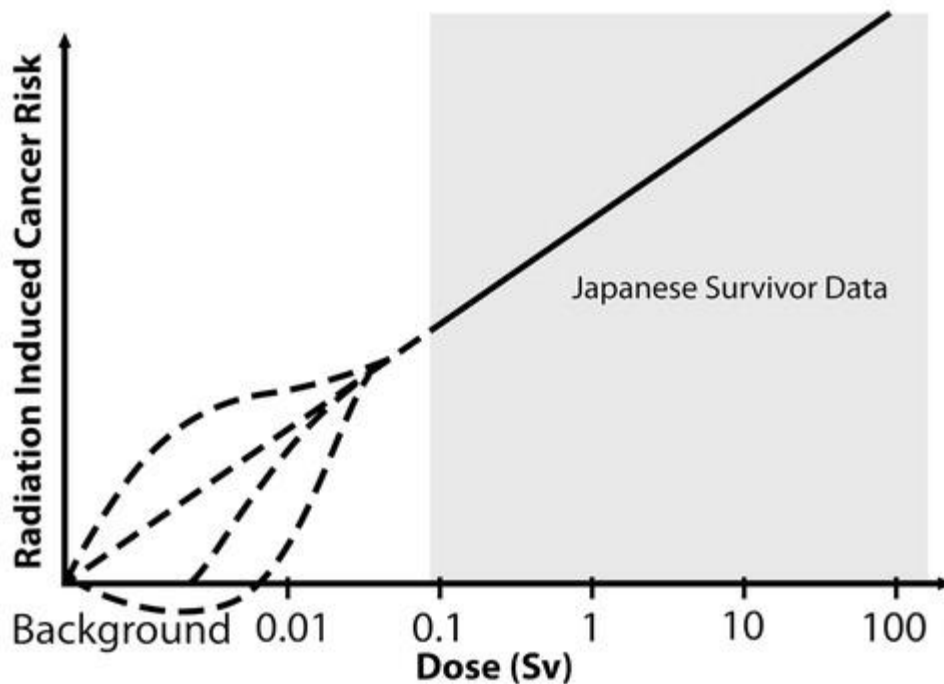


FIGURE 5 MODELS FOR EXTRAPOLATING RADIATION-INDUCED CANCER RISK TO LOW DOSES (DASHED LINE AND CURVES). LINEAR NO-THRESHOLD (LNT) MODEL = DASHED STRAIGHT LINE (HENDEE & O’CONNOR, 2012).

Competing models of risk were developed, the Excess Relative Risk (ERR) and the Excess Absolute Risk (EAR). These are defined in detail by O’Connor, (2017) but in short ERR is the rate of disease in an exposed population divided by the rate of disease in an unexposed population, minus 1.0. This method assumes that there is a proportional relationship between the excess risk of cancer to the baseline cancer incidence, that is to say the ERR is the same for a Japanese and a US or European population. The EAR model is the rate of disease in an exposed population minus the rate of disease in an unexposed population and is more suited if there are significant differences between the reference population and the population under investigation. It is assumed that the baseline cancer incidence does not influence the rate of radiation induced cancers.

These models allow the calculation of the risk of cancer at a specified time post exposure. To allow the calculation of the lifetime risk of cancer, a third method was developed. The Lifetime Attributable risk (LAR) is the sum of ERR and EAR for each year after exposure out to a specified lifespan of approximately 80 years (Nations Scientific Committee on the Effects of Atomic Radiation, 2000). O’Connor, (2017) states that BIER VII committee were confronted with a decision in which method to use to calculate LAR as there was poor correlation between EAR and ERR models and the large discrepancy between risk coefficients from medical studies and the atomic bomb survivor studies. In order to generate a single estimate of LAR the BEIR VII committee created the final risk

model as  $x \cdot ERR + (1 - x) \cdot EAR$  where  $x$  was determined subjectively by the committee.

Subjectivity is one of the arguments Brenner uses against the use of effective dose where the tissue weighting factors are decided by the ICRP committee (Brenner, 2009, 2011, 2012). An alternative approach would be to quote the range of risk quoting both ERR and EAR. This would reflect the error that is inherent in any risk from low-dose radiation exposure.

Data is presented in BEIR VII in easy to interpret tables and the data that is frequently in dose estimations. It could be argued that the degree in error, from the TLD's performance and in the risk estimates are considerable. These are a reflection in the limitations of the epidemiological data which are generated from atomic bomb survivor studies. For future work involving risk analysis it is important that results should be presented with an indication of any uncertainty. Failure to do so could potentially give a misleading impression of statistical precision. For this reason care should be taken when conveying risks to patients and carers as misinterpretation could lead to imaging avoidance leading to greater harm to patients (Siegel et al., 2018).

## 2.4 CONVEYING RISKS TO PATIENTS

Referrers, Practitioners and Operators do have a duty to convey the risks from an examination to their patients in a manner that is understandable (Brenner, 2009, 2011, 2012). This is a requirement as set out in The Ionising Radiation (Medical Exposure) Regulations, (2017) and recommended practice is for communication of the risks through two-way dialogue between Referrer, Practitioners and/or Operators and their patients is at a level that is understandable to each party (Society of Radiographers, 2018). Providing an indication of the level of risk is a better approach than a patient specific risk value is an approach that should be adopted. This supports the opinion of BEIR VII; to quote the report directly specific estimates of LAR should be regarded...

“...with a healthy scepticism, placing more faith in a range of possible values”

(Nations Scientific Committee on the Effects of Atomic Radiation, 2000).

O'Connor, (2017) goes further in recommendations stating that a case can be made for imaging procedures with effective doses below the upper limit of natural background radiation, the practice of associating any risk estimate should be discontinued as scientifically unsound. There is a danger that reporting risks to patients without context could lead to patients withholding consent for radiological examinations (Boutis et al., 2013). There is a history of sensational headlines in the media based on research stating use of ionising radiation causes tens of thousands of cancers every year (Berrington de González et al., 2009; Brenner & Hall, 2007).

The key is contextualising the risks but also considering the current benefits against any future risk. One of the criticisms cited in Tootell et al., (2014a) [Paper 2] about effective dose is that it is meaningless to non-radiology groups, for example telling a patient that the additional CT exposure would increase their dose by 0.8 mSv. Similarly telling the patient that the cancer induction risk from ionising radiation would increase from 143 per million to 154 per million could be a challenging concept to understand. The avoidance of overly technical terminology can lead to confusion and misconceptions in the information. In effect practitioners and operators should be able to communicate the risk to their patients rather than educate them. How this can and should be done is open to debate and work in the field is ongoing. The challenge with statistical figures is in the conveyance of the risk being a population risk not the risk to an individual (Broadbent & Hubbard, 1992; Peck & Samei, 2017).

In any discussion the benefit of the exposure needs to be considered. In the context of this portfolio of works, specifically Paper 4 and Paper 7 (Tootell et al., 2016, 2014b), in the initial discussion about the procedure to the patient, they should be made aware of the radiation risks and that on occasions additional imaging is required (CT for attenuation correction or CT for lesion

localisation/characterisation). Patients could be informed of the benefits of additional imaging and also the risks of not performing the imaging. For example, a false-positive diagnosis of ischaemic heart disease or the misdiagnosis of a lumbar spine lesion identified on a SPECT acquisition.

A simplified method by which risks can be conveyed to patients is to use comparative data. A commonly used method is to compare the risk to odds of accidental death as shown in Table 5. This is poor practice for a number of reasons and can lead to patients perceiving an overestimation of risk as a factor that isn't incorporated into this data is time. The latency factor of cancer occurrence should not be compared to accidental injury and also the above mentioned risk of not performing the procedure carries its own risk. The exposure involves a stochastic risk with very long latency period but not performing the procedure would have another risk, probably much larger with a much shorter time horizon (Peck & Samei, 2017).

Type of incident / Manner of injury	Number of deaths in 2005	Probability of occurrence
All causes of mortality from injuries	176,406	4.5%
Transport accidents	48,441	1.3%
Automobile	14,584	0.4%
Pedestrian	6,074	0.2%
Air travel	590	0.02%
Non-transportation accidents	69,368	1.8%
Falls	19,656	0.5%
Being struck by objects	2,845	0.07%
Intentional self-harm	32,637	0.9%
Assault	18,124	0.5%
Complications from medical care	2,653	0.07%

**TABLE 6 ODDS OF DEATH FROM INJURY AS AN EXAMPLE OF POOR COMPARISON FOR RADIATION RISK (PECK & SAMEI, 2017)**

A recommended method of conveying risks of the radiation alone is to compare the dose to the number of days of background radiation. For example, Table 6, while this method does provide patients with some relative scale to compare the dose against, it does not contextualise the risk. Wall et al., (2011) suggests an approach advocated by (Calman, 1996) that divides risk into four broad risk bands illustrated in Table 7. A criticism that could be made against the table recommended by Wall et al., (2011) is the change in denominator that could cause confusion. Using a common denominator of 1 000 000 would make the change in risks easier to interpret.

X-ray Examinations	Typical Dose (mSv)	Equivalent period of natural background radiation
Limbs or Joints	<0.01	<1.5 days
Teeth	<0.01	<1.5 days
PA Chest	0.02	3 days
Cervical Spine	0.08	2 weeks
Lumbar Spine	1.3	7 months
CT Head	2.5	1 year
CT Chest	8	3.6 years
CT Abdomen and Pelvis	10	4.5 years

TABLE 7 TYPICAL DOSE AND EQUIVALENT AMOUNT OF BACKGROUND RADIATION

Category	Risk		
Negligible	< 1/1,000,000		
Minimal	1 / 1 000 000	to	1 / 100 000
Very Low	1 / 100 000	to	1 / 10 000
Low	1 / 10 000	to	1 / 1 000

TABLE 8 THE FOUR BROAD RISK CATEGORIES RELEVANT TO DIAGNOSTIC IMAGING (WALL ET AL., 2011)

Category	Risk		
Negligible	< 1/1,000,000		
Minimal	1/1 000 000	to	10/1 000 000
Very Low	10 / 1 000 000	to	100 / 1 000 000
Low	100 / 1 000 000	to	1 000 / 1 000 000

TABLE 9 ALTERNATIVE PRESENTATION OF THE FOUR BROAD RISK CATEGORIES (WALL ET AL 2011)

Radiographic x-ray examinations of the knee and foot are seen typically to involve such ‘negligible’ risks for patients of all ages and both genders and the same is likely to be true for all examinations of the distal parts of the arms and legs. Radiographic examinations of the chest and cervical spine also involve ‘negligible’ risks for patients over about 30 years of age, but just creep into the ‘minimal’ risk band for younger patients of either gender, if no account is taken of the fact that the actual doses given to children are likely to be lower than those to adults. When this is taken into account, chest examinations remain in the ‘negligible’ risk band for patients of all ages and both genders, and cervical spine examinations remain in this band for male patients of all ages but could move into the ‘minimal’ risk band for younger females (Wall et al., 2011).

In the context of Tootell et al., (2016, 2014b), myocardial perfusion imaging and bone imaging using radiopharmaceuticals, the additional imaging using CT for attenuation correction or lesion

localisation using low-dose parameters or diagnosis using diagnostic imaging parameters does not affect the categorisation of the examinations as both remain in the low risk category. In conveying this risk to the patient, the information about the additional benefits and the lack of change in the risk classification would provide the patient with adequate and comprehensible information to allow them to consent to the examination.

In conclusion, there is a requirement to provide patients with information about the dose they will receive from an examination using ionising radiation. This information needs to be provided in terms that are understandable and given context to allow patients to give informed consent for the examination. The use of risk statistics as used in Tootell et al., (2016, 2014b) is one such method but the level of uncertainty that is inherent in estimating risk for low radiation doses means that providing patients with absolute risk statistics without an indication of error or range could be misleading. These figures have a value although the range of risk should be used in the conveyance to patients and would provide referrers and practitioners additional data over effective dose alone due to the ability to take into account the gender and age of the patient group. Translating these into a level or category of risk to convey to patients would be a better approach and would provide patients with adequate comprehensible information. Effective dose still has a value in the comparison between modalities or anatomical areas.

### 3. INTELLECTUAL OWNERSHIP AND CONTRIBUTION

The intellectual ownership, type and percentage contribution all co-authors for each paper (1-8) included in this thesis are displayed in Table 8.

The method used is based on a subset of categories for authorship as recommended by the International Committee of Medical Journal Editors (ICMJE, n.d.). All co-authors took the opportunity to review the final submission of manuscripts.

The type of contribution is summarised as:

- a. Concept and Design
- b. Data Collection
- c. Data Analysis
- d. Drafting and Revision
- e. Final Approval

<i>Authors</i>	<i>Papers / Contribution (%) and Type</i>							
	1	2	3	4	5	6	7	8
<i>AKT</i>	60 a.d.e.	70 a.d.e.	70 a.b.c.d.e.	65 a.b.c.d.e.	8 b.d.e.	8 b.d.e.	60 a.b.c.d.e.	65 a.b.c.d.e.
<i>PH</i>	15 d.e.	20 a.d.e.	20 a.d.e.	15 a.d.e.	9 a.d.e.	9 a.d.e.	13 a.d.e.	15 d.e.
<i>KRS</i>		10 d.e.	10 c.e.	20 a.c.d.e.	8 c.e.	8 c.e.	10 c.d.e.	20 b.c.d.e.
<i>MMc</i>							17 c.d.e.	
<i>JT</i>					44 a.b.c.d.e.	44 a.b.c.d.e.		
<i>SV</i>	15 a.d.e.							
<i>ME</i>	10 d.e.							
<i>DJM</i>					11 a.d.e.	11 a.d.e.		
<i>DPC</i>					15 a.c.d.e.	15 a.c.d.e.		
<i>IV</i>					5 b.d.e.	5 b.d.e.		

**TABLE 10 CONTRIBUTION OF EACH AUTHOR TO THE PAPERS INCLUDED IN THE PHD BY PUBLISHED WORKS**

## 4. CITATION ANALYSIS

While the number of citations per article can be regarded as a good indication of the impact published work has had or is having it should not be regarded as the only measure (Meho, 2007; Nightingale & Marshall, 2012). While research in the radiography community has developed, it has yet to fully filter through to the clinical environment and be fully adopted as a core element. The number of research active radiography professionals is relatively small in number. As noted by Seglen, (1997), articles published in niche areas are likely to gain fewer citations than those in general areas. While the majority of the radiography profession will engage with published literature, this is likely to be used in the development of their knowledge and skills for continued professional development (CPD) purposes. For this reason additional measures have been used in Table 11 including number of reads and downloads. The Diagnostic Imaging Research Programme has a number of themes and there is overlap in their activities. As a results there are a number of citations from within the group either in published research or in PhD theses.

<i>Paper</i>	<i>1</i>	<i>2</i>	<i>3</i>	<i>4</i>	<i>5</i>	<i>6</i>	<i>7</i>	<i>8</i>
<i>Year of publication</i>	2012	2014	2013	2014	2016	2015	2016	2017
<i>Journal Impact Factor (present)</i>	1.472	0.289	0.289	2.050	2.617	0.37	0.25	0.289
<i>(at the time of publication)</i>	1.379	0.346	0.232	2.026	2.617	0.37	0.25	0.289
<i>Google Scholar Citations</i>	12	11	10	1	7	2	0	0
<i>Scopus Citations</i>	6	4	5	0	2	1	0	0
<i>ResearchGate Reads</i>	75	74	6	22	-	63	44	-
<i>ResearchGate Citations</i>	9	9	9	0	-	1	0	-
<i>DIRP Citations (Google Scholar)</i>	4	5	10	0	4	1	-	-
<i>PhD Thesis Citations (UoS)</i>	0	4	4	2	2	2	0	0
<i>Self-citations</i>	1	2	3	-	-	1	-	-

**TABLE 11 CITATION ANALYSIS OF THE PORTFOLIO OF PUBLISHED WORKS (DATA COLLECTED MAY 2018)**

## 5. FUTURE DIRECTION OF RESEARCH

Completion of this PhD will provide an ideal time to reflect on the research that has been undertaken over the last six years. The quality of the research has improved and as can be seen through the portfolio of works has evolved. Interestingly during the research, a number of qualitative issues were highlighted.

The ability to calculate risk statistics raises the question of what information should be provided to patients. As discussed in chapter 2.4 (Conveying Risks to Patients) there is a risk that patients could be dissuaded from an investigation or intervention due to their interpretation of the radiation risks. It would be interesting to use the data that has been generated as part of this research to investigate how patients and carers would interpret the risks as part of the decision making process. This would be of particular interest in the research using methods developed in this portfolio of works produced by Ali et al (Ali, England, Tootell, & Hogg, 2016; Ali, England, Tootell, Mercer, & Hogg, 2017; Ali et al., 2017) where the risks from breast screening programmes are investigated.

From this portfolio of works, further empirical research is planned in improving the accuracy of dose estimations compared to dose measurements. Since the completion of this portfolio of works additional dosimetry phantoms from the ATOM dosimetry phantom family have become available, meaning research can be performed using paediatric, adolescent and adult female patients. The research conducted in Paper 8 (Tootell et al., 2017) has shown the potential in the improvement of accuracy in assessing patient dose through the correction due to mass but other metrics can be used to provide information on patient habitus. Work establishing if and how these can be used in the correction of dose estimations is planned.

## 6. CONCLUSION

This portfolio of works and accompanying narrative has demonstrated the development of the research. From Paper 1 that sets the scene for the need to accurately measure radiation dose in light of what was then new technology, through to a review of how radiation dose can be measured or estimated and how this data can be interpreted to provide referrers, practitioners, operators and patients and their carers with understandable information about the potential risks an exposure could bring and finally the application of the methods developed.

The commentary provides an appraisal of the methods and then manner in which they have been presented and interpreted. Where applicable, the limitations of the chosen methods have been identified and recommendations for improvements made.

In summary, this thesis and accompanying portfolio of works has demonstrated the ability to conceptualise and develop original research resulting in the creation and interpretation of new knowledge. This has been supported by developing a detailed understanding of the applicable techniques through critically reviewing the current body of knowledge.

The impact of the work has been demonstrated, not only through the number of citations, but the number of reads and downloads the published works has had. The impact in the Diagnostic Imaging Research Programme has been illustrated showing the cohesion of the group where research activities are complimentary.

The direction of future work is anticipated to continue in dosimetry with research planned to improve the accuracy of dose measurements, calculation or simulations to aid referrers, practitioners and operators in the conveyance of risks to patients and carers and also in the development of less generic diagnostic reference levels. A qualitative evaluation of what patients and carers want to know would allow the integration of the dosimetry research finding with clinical practice.

## REFERENCES

- AAPM Task Group 204. (2011). *Size-Specific Dose Estimates (SSDE) in Pediatric and Adult Body CT Examinations*. Retrieved from [https://www.aapm.org/pubs/reports/RPT\\_204.pdf](https://www.aapm.org/pubs/reports/RPT_204.pdf)
- Ali, R., England, A., Tootell, A., & Hogg, P. (2016). Radiation risk from screening mammography B-0307. *Insights into Imaging, ECR 2016 Book of Abstracts - B - Scientific Sessions and Clinical Trials in Radiology*, 7(Suppl 1), 162–465. <https://doi.org/10.1007/s13244-016-0475-8>
- Ali, R., England, A., Tootell, A., Mercer, C., & Hogg, P. (2017). The effect of mean glandular dose variations on effective risk from full-field digital mammography in screening. In *European Congress of Radiology* (p. B-0667).
- Ali, R. M. ., England, A., McEntee, M. F., & Hogg, P. (2015). A method for calculating effective lifetime risk of radiation-induced cancer from screening mammography. *Radiography*, 21(4), 298–303. <https://doi.org/10.1016/j.radi.2015.07.008>
- Ali, R. M. ., England, A., Mercer, C., Tootell, A., Walton, L., Schaake, W., & Hogg, P. (2017). Mathematical modelling of radiation-induced cancer risk from breast screening by mammography. *European Journal of Radiology*, 96, 98–103. Retrieved from <http://www.sciencedirect.com/science/article/pii/S0720048X17303868>
- Ali, R. M. K. (2016). *Risk of radiation-induced cancer from screening mammography*. University of Salford. Retrieved from <http://usir.salford.ac.uk/41581/>
- Berrington de González, A., Mahesh, M., Kim, K.-P., Bhargavan, M., Lewis, R., Mettler, F., & Land, C. (2009). Projected Cancer Risks From Computed Tomographic Scans Performed in the United States in 2007. *Archives of Internal Medicine*, 169(22), 2071. <https://doi.org/10.1001/archinternmed.2009.440>
- Boos, J., Lanzman, R. S., Meineke, A., Heusch, P., Sawicki, L. M., Antoch, G., & Kröpil, P. (2015). Dose monitoring using the DICOM structured report: assessment of the relationship between cumulative radiation exposure and BMI in abdominal CT. *Clinical Radiology*, 70(2), 176–182. <https://doi.org/10.1016/j.crad.2014.11.002>
- Boos, J., Meineke, A., Bethge, O., Antoch, G., & Kröpil, P. (2016). Dose Monitoring in Radiology Departments: Status Quo and Future Perspectives. *RöFo - Fortschritte Auf Dem Gebiet Der Röntgenstrahlen Und Der Bildgebenden Verfahren*, 188(05), 443–450. <https://doi.org/10.1055/s-0041-109514>
- Boutis, K., Cogollo, W., Fischer, J., Freedman, S. B., Ben David, G., & Thomas, K. E. (2013). Parental knowledge of potential cancer risks from exposure to computed tomography. *Pediatrics*, 132(2), 305–311. <https://doi.org/10.1542/peds.2013-0378>
- Bower, M. W., & Hintenlang, D. E. (1998). The characterization of a commercial MOSFET dosimeter system for use in diagnostic x ray. *Health Physics*, 75(2), 197–204. <https://doi.org/10.1097/00004032-199808000-00013>
- Brenner, D. J. (2011). Effective dose - A flawed concept that could and should be replaced. *International Commission on Radiological Protection*, 25(3), 488–490. <https://doi.org/10.1007/978-3-642-03902-7-139>

- Brenner, D. J. (2012). We can do better than effective dose for estimating or comparing low-dose radiation risks. *Annals of the ICRP*, 41(3–4), 124–128. <https://doi.org/10.1016/j.icrp.2012.07.001>
- Brenner, D. J., & Hall, E. J. (2007). Computed Tomography — An Increasing Source of Radiation Exposure. *New England Journal of Medicine*, 357(22), 2277–2284. <https://doi.org/10.1056/NEJMra072149>
- Brink, J. A., & Morin, R. L. (2012). Size-specific Dose Estimation for CT: How Should It Be Used and What Does It Mean? *Radiology*, 265(3), 666–668. <https://doi.org/10.1148/radiol.12121919>
- British Society of Gastrointestinal and Abdominal Radiology, & The Royal College of Radiologists. (2014). Guidance on the use of CT colonography for suspected colorectal cancer. BSGAR, RCR. Retrieved from [https://www.rcr.ac.uk/system/files/publication/field\\_publication\\_files/BFCR\(14\)9\\_COLON.pdf](https://www.rcr.ac.uk/system/files/publication/field_publication_files/BFCR(14)9_COLON.pdf)
- Broadbent, M. V, & Hubbard, L. B. (1992). Science and perception of radiation risk. *RadioGraphics*, 12(2), 381–392. <https://doi.org/10.1148/radiographics.12.2.1561427>
- Calman, K. C. (1996). Cancer: science and society and the communication of risk. *BMJ (Clinical Research Ed.)*, 313(7060), 799–802. Retrieved from <http://www.ncbi.nlm.nih.gov/pubmed/8842078>
- Castellano, E. (2010). Dose calculations for individual patients - what you should know. In *12th CT users group, London*.
- CIRS Tissue Simulation and Phantom Technology. (2012). Dosimetry Verification Phantoms Model 701-706 Data Sheet. Retrieved April 16, 2018, from [http://www.cirsinc.com/file/Products/701\\_706/701\\_706\\_DS.pdf](http://www.cirsinc.com/file/Products/701_706/701_706_DS.pdf)
- Council Directive 2013/59/EURATOM. Laying down basic safety standards for protection against the dangers arising from exposure to ionising radiation, and repealing Directives 89/618/Euratom, 90/641/Euratom, 96/29/Euratom, 97/43/Euratom and 2003/122/Euratom (2013).
- Coward, J., Lawson, R., Kane, T., Elias, M., Howes, A., Birchall, J., & Hogg, P. (2014). Multi-centre analysis of incidental findings on low-resolution CT attenuation correction images. *The British Journal of Radiology*, 87(1042), 20130701. <https://doi.org/10.1259/bjr.20130701>
- Coward, J., Lawson, R., Kane, T., Elias, M., Howes, A., Birchall, J., & Hogg, P. (2015). Multicentre analysis of incidental findings on low-resolution CT attenuation correction images: an extended study. *The British Journal of Radiology*, 88(1056), 20150555. <https://doi.org/10.1259/bjr.20150555>
- da Rosa, L. A. R., Regulla, D. F., & Fill, U. A. (1999). Precision for Low Dose Assessment Using TLD-100 Chips and Computerised Glow Curve Analysis. *Radiation Protection Dosimetry*, 85(1), 175–178. <https://doi.org/10.1093/oxfordjournals.rpd.a032829>
- Del Sol Fernández, S., García-Salcedo, R., Mendoza, J. G., Sánchez-Guzmán, D., Rodríguez, G. R., Gaona, E., & Montalvo, T. R. (2016). Thermoluminescent characteristics of LiF:Mg, Cu, P and CaSO<sub>4</sub>:Dy for low dose measurement. *Applied Radiation and Isotopes*, 111, 50–55. <https://doi.org/10.1016/J.APRADISO.2016.02.011>
- Delbeke, D., Schöder, H., Martin, W. H., & Wahl, R. L. (2009). Hybrid Imaging (SPECT/CT and PET/CT): Improving Therapeutic Decisions. *Seminars in Nuclear Medicine*, 39(5), 308–340. <https://doi.org/10.1053/J.SEMNUCLMED.2009.03.002>

- Dietze, G., Harrison, J. D., & Menzel, H. G. (2009). Effective dose: a flawed concept that could and should be replaced. Comments on a paper by D J Brenner (Br J Radiol 2008;81:521–3). *The British Journal of Radiology*, 82(976), 348–351. <https://doi.org/10.1259/bjr/91937653>
- Flotats, A., Knuuti, J., Gutberlet, M., Marcassa, C., Bengel, F. M., Kaufmann, P. A., ... Cardiovascular Committee of the EANM, the ESCR and the ECNC. (2011). Hybrid cardiac imaging: SPECT/CT and PET/CT. A joint position statement by the European Association of Nuclear Medicine (EANM), the European Society of Cardiac Radiology (ESCR) and the European Council of Nuclear Cardiology (ECNC). *European Journal of Nuclear Medicine and Molecular Imaging*, 38(1), 201–212. <https://doi.org/10.1007/s00259-010-1586-y>
- Freire, L., Calado, A., Cardoso, J. V., Santos, L. M., & Alves, J. G. (2008). Comparison of LiF (TLD-100 and TLD-100H) detectors for extremity monitoring. *Radiation Measurements*, 43(2–6), 646–650. <https://doi.org/10.1016/J.RADMEAS.2007.12.013>
- Groves, A. M., Owen, K. E., Courtney, H. M., Yates, S. J., Goldstone, K. E., Blake, G. M., & Dixon, A. K. (2004). 16-detector multislice CT: dosimetry estimation by TLD measurement compared with Monte Carlo simulation. *The British Journal of Radiology*, 77(920), 662–665. <https://doi.org/10.1259/bjr/48307881>
- Harrison, J. D., Balonov, M., Martin, C. J., Ortiz Lopez, P., Menzel, H.-G., Simmonds, J. R., ... Wakeford, R. (2016). Use of effective dose. *Annals of the ICRP*, 45(1\_suppl), 215–224. <https://doi.org/10.1177/0146645316634566>
- Hart, D., Wall, B. F., Hillier, M. C., & Shrimpton, P. C. (2010). HPA-CRCE-012 Frequency and Collective Dose for Medical and Dental X-ray Examinations in the UK, 2008. Retrieved from [https://www.gov.uk/government/uploads/system/uploads/attachment\\_data/file/340154/HPA-CRCE-012\\_for\\_website.pdf](https://www.gov.uk/government/uploads/system/uploads/attachment_data/file/340154/HPA-CRCE-012_for_website.pdf)
- Harvey, H. B., Brink, J. A., & Frush, D. P. (2015). Informed Consent for Radiation Risk from CT Is Unjustified Based on the Current Scientific Evidence. *Radiology*, 275(2), 321–325. <https://doi.org/10.1148/radiol.2015142859>
- Higgins, R., Hogg, P., & Robinson, L. (2013). Integrating research-informed teaching within an undergraduate level 4 (year 1) diagnostic radiography curriculum: a pilot study. *Journal of Vocational Education & Training*, 65(3), 351–368. <https://doi.org/10.1080/13636820.2013.819562>
- Higgins, R., Hogg, P., & Robinson, L. (2017). Research Informed Teaching Experience in Diagnostic Radiography: The Perspectives of Academic Tutors and Clinical Placement Educators. *Journal of Medical Imaging and Radiation Sciences*, 48(3), 226–232. <https://doi.org/10.1016/J.JMIR.2017.06.002>
- Higgins R.N. (n.d.). Research-informed Teaching experience (RiT) in BSc Diagnostic Radiography curriculum | Council of Deans of Health. Retrieved July 25, 2018, from <https://councilofdeans.org.uk/case-study/research-informed-teaching-experience-rite-in-bsc-diagnostic-radiography-curriculum/>
- ICMJE. (n.d.). ICMJE | Recommendations | Defining the Role of Authors and Contributors. Retrieved May 9, 2018, from <http://www.icmje.org/recommendations/browse/roles-and-responsibilities/defining-the-role-of-authors-and-contributors.html>
- ICRP. (1977). *Recommendations of the International Commission on Radiological Protection. ICRP Publication 26. Ann. ICRP 1(3)*.

- ICRP. (1991). *1990 Recommendations of the International Commission on Radiological Protection. ICRP Publication 60 Ann. ICRP 21 (1-3).*
- ICRP. (2006). *Assessing Dose of the Representative Person for the Purpose of the Radiation Protection of the Public ICRP Publication 101a Ann. ICRP 36 (3) Title.*
- ICRP. (2007). *The 2007 Recommendations of the International Commission on Radiological Protection. ICRP Publication 103. Ann ICRP 37 (2-4). Annals of the ICRP.*  
<https://doi.org/10.1007/s13398-014-0173-7.2>
- ImPACT. (2011). ImPACT CTDosimetry. Retrieved from <http://www.impactscan.org/ctdosimetry.htm>
- Kauling, R. M., Post, M. C., Rensing, B. J. W. M., Schaap, J., & Verzijlbergen, J. F. (2015). Is Attenuation Correction for Myocardial Perfusion Imaging Underutilized? *Current Cardiovascular Imaging Reports*, 8(8), 31. <https://doi.org/10.1007/s12410-015-9346-9>
- Koivisto, J. H., Wolff, J. E., Kiljunen, T., Schulze, D., & Kortensniemi, M. (2015). Characterization of MOSFET dosimeters for low-dose measurements in maxillofacial anthropomorphic phantoms; Characterization of MOSFET dosimeters for low-dose measurements in maxillofacial anthropomorphic phantoms. *JOURNAL OF APPLIED CLINICAL MEDICAL PHYSICS*, 16(4).  
<https://doi.org/10.1120/jacmp.v16i4.5433>
- Ladapo, J. A., Horwitz, J. R., Weinstein, M. C., Gazelle, G. S., & Cutler, D. M. (2009). Adoption and spread of new imaging technology: a case study. *Health Affairs (Project Hope)*, 28(6), w1122-32. <https://doi.org/10.1377/hlthaff.28.6.w1122>
- Meho, L. I. (2007). The rise and rise of citation analysis. *Physics World*, 20(1), 32–36.  
<https://doi.org/10.1088/2058-7058/20/1/33>
- Mraity, H. Optimisation of radiation dose and image quality for AP pelvis radiographic examination (2015). Retrieved from <http://usir.salford.ac.uk/36914/>
- National Research Council (U.S.). Committee to Assess Health Risks from Exposure to Low Level of Ionizing Radiation. (2006). *Health risks from exposure to low levels of ionizing radiation : BEIR VII, Phase 2.* National Academies Press. Retrieved from  
[https://books.google.co.uk/books/about/Health\\_Risks\\_from\\_Exposure\\_to\\_Low\\_Levels.html?id=H4J3Ns\\_3lUIC&source=kp\\_cover&redir\\_esc=y](https://books.google.co.uk/books/about/Health_Risks_from_Exposure_to_Low_Levels.html?id=H4J3Ns_3lUIC&source=kp_cover&redir_esc=y)
- Nations Scientific Committee on the Effects of Atomic Radiation, U. (2000). *Sources and Effects of Ionizing Radiation- United Nations Scientific Committee on the Effects of Atomic Radiation UNSCEAR 2000 Report to the General Assembly, with Scientific Annexes.* New York. Retrieved from [http://www.unscear.org/docs/publications/2000/UNSCEAR\\_2000\\_Report\\_Vol.I.pdf](http://www.unscear.org/docs/publications/2000/UNSCEAR_2000_Report_Vol.I.pdf)
- NICE. (2017). Radiation dose monitoring software for medical Radiation dose monitoring software for medical imaging with ionising r imaging with ionising radiation adiation Medtech innovation briefing. Retrieved from <https://www.nice.org.uk/advice/mib127/resources/radiation-dose-monitoring-software-for-medical-imaging-with-ionising-radiation-pdf-2285963340271045>
- Nightingale, J. M., & Marshall, G. (2012). Citation analysis as a measure of article quality, journal influence and individual researcher performance. *Radiography*, 18(2), 60–67.  
<https://doi.org/10.1016/J.RADI.2011.10.044>
- Noumeir, R. (2005). Benefits of the DICOM modality performed procedure step. *Journal of Digital Imaging*, 18(4), 260–269. <https://doi.org/10.1007/s10278-005-6702-3>

- O'Connor, M. K. (2017). Risk of low-dose radiation and the BEIR VII report: A critical review of what it does and doesn't say. *Physica Medica*, 43, 153–158.  
<https://doi.org/10.1016/J.EJMP.2017.07.016>
- Peck, D., & Samei, E. (2017). How to Understand and Communicate Radiation Risk. Retrieved from <https://www.imagewisely.org/-/media/ImageWisely-Files/Medical-Physicist-Articles/IW-Peck-Samei-Radiation-Risk.pdf>
- Public Health England. (2011). Doses from Computed Tomography (CT) Examinations in the UK – 2011 Review. Retrieved from [https://www.gov.uk/government/uploads/system/uploads/attachment\\_data/file/349188/PHE\\_CRCE\\_013.pdf](https://www.gov.uk/government/uploads/system/uploads/attachment_data/file/349188/PHE_CRCE_013.pdf)
- Public Health England. (2016). *PHE-CRCE-026 Ionising Radiation Exposure of the UK Population : 2010 Review About Public Health England*. Retrieved from [https://www.gov.uk/government/uploads/system/uploads/attachment\\_data/file/518487/PHE-CRCE-026\\_-\\_V1-1.pdf](https://www.gov.uk/government/uploads/system/uploads/attachment_data/file/518487/PHE-CRCE-026_-_V1-1.pdf)
- QAA. (2008). The framework for higher education qualifications in England, Wales and Northern Ireland. *The Framework for Higher Education in England, Wales and Northern Ireland*. Gloucester: QAA. Retrieved from <http://www.qaa.ac.uk/en/Publications/Documents/Framework-Higher-Education-Qualifications-08.pdf>
- Robinson, J. B. B., Ali, R. M. M., Tootell, A. K., & Hogg, P. (2017). Does collimation affect patient dose in antero-posterior thoraco-lumbar spine? *Radiography*, 23(3), 211–215.  
<https://doi.org/10.1016/j.radi.2017.03.012>
- Royal College of Radiologists. (2015). Standards of practice and guidance for trauma radiology in severely injured patients. Retrieved from [https://www.rcr.ac.uk/sites/default/files/docs/radiology/pdf/BFCR\(11\)3\\_trauma.pdf](https://www.rcr.ac.uk/sites/default/files/docs/radiology/pdf/BFCR(11)3_trauma.pdf)
- Seglen, P. O. (1997). Why the impact factor of journals should not be used for evaluating research. *BMJ*, 314(7079), 497–497. <https://doi.org/10.1136/bmj.314.7079.497>
- Shrimpton, P., Hillier, M., Meeson, S., & Golding, S. (2014). *Public Health England - Doses from Computed Tomography ( CT ) Examinations in the UK – 2011 Review*. Retrieved from [https://www.gov.uk/government/uploads/system/uploads/attachment\\_data/file/349188/PHE\\_CRCE\\_013.pdf](https://www.gov.uk/government/uploads/system/uploads/attachment_data/file/349188/PHE_CRCE_013.pdf)
- Siegel, J. A., Greenspan, B. S., Maurer, A. H., Taylor, A. T., Phillips, W. T., Van Nostrand, D., ... Silberstein, E. B. (2018). The BEIR VII Estimates of Low-Dose Radiation Health Risks Are Based on Faulty Assumptions and Data Analyses: A Call for Reassessment. *Journal of Nuclear Medicine : Official Publication, Society of Nuclear Medicine*, jnumed.117.206219.  
<https://doi.org/10.2967/jnumed.117.206219>
- Smith, K. P. (2011). Overview of Radiological Dose and Risk Assessment. Retrieved from [https://www.iaea.org/OurWork/ST/NE/NEFW/documents/IDN/ANL\\_Course/Day\\_5/RiskOverview\\_revised.pdf](https://www.iaea.org/OurWork/ST/NE/NEFW/documents/IDN/ANL_Course/Day_5/RiskOverview_revised.pdf)
- Society of Radiographers. (2018). Obtaining consent: a clinical guideline for the diagnostic imaging and radiotherapy workforce Executive Summary. Retrieved from [https://www.sor.org/sites/default/files/document-versions/obtaining\\_consent\\_170118.pdf](https://www.sor.org/sites/default/files/document-versions/obtaining_consent_170118.pdf)
- STUK. (2012). PCXMC. Helsinki. Retrieved from <http://www.stuk.fi/palvelut/pcxmc-a-monte-carlo-program-for-calculating-patient-doses-in-medical-x-ray-examinations>

- The Ionising Radiation (Medical Exposure) Regulations (2017). Queen's Printer of Acts of Parliament. Retrieved from <http://www.legislation.gov.uk/uksi/2017/1322/contents/made>
- The Ionising Radiations Regulations (2017). Queen's Printer of Acts of Parliament. Retrieved from <http://www.legislation.gov.uk/uksi/2017/1075/contents/made>
- Thermo Electron Corporation Radiation Measurement & Protection. (2002). Harshaw Standard TTP Recommendations. *Technical Notice No.DOSM-0-N-1202-001*. Thermo Electron Corporation. Retrieved from DOSM-0-N-1202-001
- ThermoFisher Scientific. (n.d.). TLD-100™ Thermoluminescent Dosimetry Material. Retrieved March 29, 2018, from <https://www.thermofisher.com/order/catalog/product/SNO10106>
- Thompson, J., Chakraborty, D. D. P., Szczepura, K., Vamvakas, I., Tootell, A., Manning, D. D. J., & Hogg, P. (2015). A phantom-based JAFROC observer study of two CT reconstruction methods: The search for optimisation of lesion detection and effective dose. In C. R. Mello-Thoms & M. A. Kupinski (Eds.), *Medical Imaging 2015: Image Perception, Observer Performance, and Technology Assessment* (Vol. 9416, p. 94160B). Orlando, Florida: International Society for Optics and Photonics. <https://doi.org/10.1117/12.2081632>
- Thompson, J., Chakraborty, D. P., Szczepura, K., Tootell, A. K., Vamvakas, I., Manning, D. J., & Hogg, P. (2016). Effect of reconstruction methods and x-ray tube current-time product on nodule detection in an anthropomorphic thorax phantom: A crossed-modality JAFROC observer study. *Medical Physics*, *43*(3). <https://doi.org/10.1118/1.4941017>
- Thompson, J., Chakraborty, D., Szczepura, K., Tootell, A. K., Vamvakas, I., Manning, D. J., & Hogg, P. (2016). Effect of reconstruction methods and x-ray tube current – time product on nodule detection in an anthropomorphic thorax phantom : A crossed-modality JAFROC observer study Effect of reconstruction methods and x-ray tube current – time product on nodule det. *Medical Physics*, *43*(12625), 1265–1274. <https://doi.org/10.1118/1.4941017>
- Thompson, J. D., Chakraborty, D. P., Szczepura, K., Vamvakas, I., Tootell, A., Manning, D. J., & Hogg, P. (2015). A phantom-based JAFROC observer study of two CT reconstruction methods: The search for optimisation of lesion detection and effective dose. In *Progress in Biomedical Optics and Imaging - Proceedings of SPIE* (Vol. 9416). <https://doi.org/10.1117/12.2081632>
- Thompson, J., Hogg, P., Manning, D., Szczepura, K., & Chakraborty, D. P. (2014). A Free-response Evaluation Determining Value in the Computed Tomography Attenuation Correction Image for Revealing Pulmonary Incidental Findings: A Phantom Study. *Academic Radiology*, *21*(4), 538–545. <https://doi.org/10.1016/J.ACRA.2014.01.003>
- Tootell, A., Lundie, M., Szczepura, K., & Hogg, P. (2012). Reducing error in TLD dose radiation measurements. *United Kingdom Radiological Congress*. Manchester.
- Tootell, A., McEntee, M., Szczepura, K., & Hogg, P. (2016). Effective Dose and Effective Risk from Post-Single Photon Emission Computed Tomography Imaging of the Lumbar Spine. *Journal of Medical Imaging and Radiation Sciences*, *47*(3), 267–275. <https://doi.org/10.1016/j.jmir.2016.04.012>
- Tootell, A., Szczepura, K., & Hogg, P. (2014a). An overview of measuring and modelling dose and risk from ionising radiation for medical exposures. *Radiography*, *20*(4), 323–332. <https://doi.org/10.1016/j.radi.2014.05.002>

- Tootell, A., Szczepura, K., & Hogg, P. (2014b). Comparison of effective dose and lifetime risk of cancer incidence of CT attenuation correction acquisitions and radiopharmaceutical administration for myocardial perfusion imaging. *British Journal of Radiology*, *87*(1041), 20140110. <https://doi.org/10.1259/bjr.20140110>
- Tootell, A., Szczepura, K., & Hogg, P. (2017). Analysis of effective and organ dose estimation in CT when using mA modulation: A single scanner pilot study. *Radiography*, *37*(2), 842–847. <https://doi.org/10.1016/j.radi.2017.02.006>
- Tootell, A., Szczepura, K. R. K. R., Hogg, P., Vogl, T. J., Maentele, W., Bauer, R. W., & Al., E. (2013). Optimising the number of thermoluminescent dosimeters required for the measurement of effective dose for computed tomography attenuation correction data in SPECT/CT myocardial perfusion imaging. *Radiography*, *19*(1), 42–47. <https://doi.org/10.1016/j.radi.2012.11.001>
- Tootell, A., Vinjamuri, S., Elias, M., & Hogg, P. (2012). Clinical evaluation of the computed tomography attenuation correction map for myocardial perfusion imaging: the potential for incidental pathology detection. *Nuclear Medicine Communications*, *33*(11), 1122–1126. <https://doi.org/10.1097/MNM.0b013e3283571b35>
- Wall, B. F., Haylock, R., Jansen, J. T. M., Hillier, M. C., Hart, D., & Shrimpton, P. C. (2011). *Radiation Risks from Medical X-ray Examinations as a Function of the Age and Sex of the Patient*. Health Protection Agency Centre for Radiation, Chemical and Environmental Hazards. Retrieved from [https://www.gov.uk/government/uploads/system/uploads/attachment\\_data/file/340147/HPA-CRCE-028\\_for\\_website.pdf](https://www.gov.uk/government/uploads/system/uploads/attachment_data/file/340147/HPA-CRCE-028_for_website.pdf)
- White, D. R. (1978). Tissue substitutes in experimental radiation physics. *Medical Physics*, *5*(6), 467–479. <https://doi.org/10.1118/1.594456>
- Xu, X. G., & Eckerman, K. F. (2010). *Handbook of anatomical models for radiation dosimetry*. Florida, USA: CRC Press/Taylor & Francis Group.
- Yifrah, T., Abraham, A., Weinstein, M., Pelled, O., German, U., & Mintz, M. (2014, February 1). About Background Correction for LiF:Mg,Ti readout. Retrieved from [https://inis.iaea.org/search/search.aspx?orig\\_q=RN:45114767](https://inis.iaea.org/search/search.aspx?orig_q=RN:45114767)

## PUBLISHED WORKS

The following papers make of the portfolio of published works cited within this thesis. Figure 6 illustrates the activities the research and writing. The papers are presented in an order to illustrate the development of knowledge, skills and methods rather than chronologically.

Paper 1: Clinical evaluation of the computed tomography attenuation correction map for myocardial perfusion imaging: the potential for incidental pathology detection

Paper 2: An overview of measuring and modelling dose and risk from ionising radiation for medical exposures

Paper 3: Optimising the number of thermoluminescent dosimeters required for the measurement of effective dose for computed tomography attenuation correction data in SPECT/CT myocardial perfusion imaging.

Paper 4: Comparison of effective dose and lifetime risk of cancer incidence of CT attenuation correction acquisitions and radiopharmaceutical administration for myocardial perfusion imaging

Paper 5: Effect of reconstruction methods and x-ray tube current–time product on nodule detection in an anthropomorphic thorax phantom: A crossed-modality JAFROC observer study

Paper 6: A phantom-based JAFROC observer study of two CT reconstruction methods: the search for optimisation of lesion detection and effective dose

Paper 7: Effective Dose and Effective Risk from Post–Single Photon Emission Computed Tomography Imaging of the Lumbar Spine

Paper 8: Analysis of effective and organ dose estimation in CT when using mA modulation: A single scanner pilot study

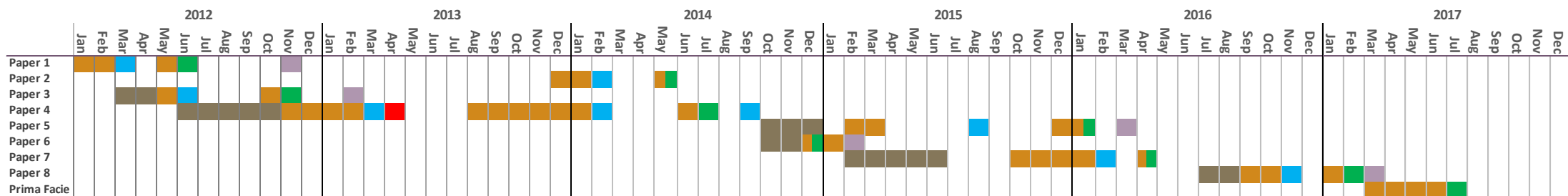
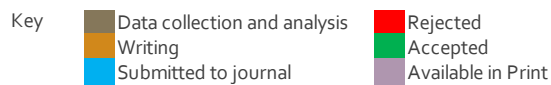


FIGURE 6 GANTT CHART SHOWING RESEARCH AND WRITING ACTIVITIES

## PAPER 1

### CLINICAL EVALUATION OF THE COMPUTED TOMOGRAPHY ATTENUATION CORRECTION MAP FOR MYOCARDIAL PERFUSION IMAGING: THE POTENTIAL FOR INCIDENTAL PATHOLOGY DETECTION

Tootell AK, Vinjamuri S, Elias M and Hogg P (2012). Nucl Med Commun, 33(11), 1122-1126. doi: <http://10.1097/MNM.0b013e3283571b35>

#### **Introduction**

Since the origins of hybrid imaging in nuclear medicine many papers have established the diagnostic benefits that computed tomography (CT) can bring to the emission data. Initially CT was shown to have value for attenuation correction (AC); more recently its role in lesion localisation and characterisation has been demonstrated [1-3] The benefits of hybrid systems have been so well illustrated that it has become virtually impossible to purchase a PET scanner without integral CT; also the availability of SPECT/CT systems has increased tremendously [4]. Contemporary SPECT/CT and PET/CT systems can now have state-of-the-art CT technology such that the CT component could have the same specification and capability to that of standalone multi-detector diagnostic scanners.

This paper focuses on SPECT/CT in the context of myocardial perfusion imaging (MPI); it addresses the question '*should the low resolution CT images for AC in SPECT be interpreted for the detection of incidental extra-cardiac disease?*' Recently, debate has raised questions on whether additional clinical information might be gained from CTAC image data - particularly to determine whether incidental extra-cardiac pathology might be detected [5, 6]. Surprisingly, guidelines jointly issued by the European Association of Nuclear Medicine (EANM) and European Society of Cardiology (ESC) [7] give no mention to the clinical evaluation of the CTAC data for detection of incidental pathology.

The aim of this paper is not to provide a definitive answer to whether the CTAC (MPI) image should be interpreted; rather the intention is to initiate discussion and suggest a way forward. This paper will consider a number of issues that have been raised by clinicians from within and outside nuclear medicine, it will draw parallels to other imaging modalities that have similar quandaries, and it will consider pertinent regulatory matters.

#### **Incidental findings**

Literature highlights that incidental findings are an acknowledged phenomena within medical imaging and many discussions are documented about whether evaluation of *all available data* should take place. Discussions similar to this paper have and still are taking place in modalities outside the nuclear medicine field with many authors considering how the additional data that is acquired as part of cardiac CT, CT urography and CT colonography might be used [8-10]. Similarly, in medical research, there is a growing opinion that acquired data may contain information that could have significant health implications for the patient. It may be possible to make decisions regarding nature and significance, and whether further investigation is warranted [6, 11].

A question worth considering is 'how often are incidental findings detected'? The Royal College of Radiologists suggest that they are relatively common, quoting figures of up to 30% in radiological examinations of the abdomen and chest imaging (depending of the population being studied) [11]. There is surprisingly little published on incidental findings on the CTAC image of MPI acquisitions;

however figures indicate that 8.1% to 18% of CTAC images may demonstrate some abnormality [5, 12, 13].

The study carried out by Pandey et al [5] involved the review of CTAC for MPI images from 494 cases over a 20 month period acquired on a Philips Precedence 16-slice hybrid system. Forty cases (8.1%) were found to have extra-cardiac pathology with four of these diagnosed with lung cancer following further investigations. Similarly the work of Kane [5] found that of 1001 cases 217 (18%) demonstrated abnormalities. Of these 217 (10.6%) had minor findings deemed unlikely to affect management, 67 (5.5%) had minor findings with possible cardiac significance (eg coronary artery calcification), 17 (1.4%) had possible clinically significant pathology, with four (0.3%) having significant pathology. These findings demonstrate that the incidence of clinically important pathology is small but cases that have significant bearing on immediate and long term health of a patient can be identified.

It is difficult, if not impossible, to indicate the false negative rate - that is to say in how many cases significant pathology are missed without a long term follow up of normal and abnormal CTAC for MPI acquisitions. This does make the specificity and accuracy difficult to calculate. It is reasonable to say that the image quality of CTAC for MPI images is low making it difficult if not impossible for reporters to detect smaller lesions.

#### **Quality of the CTAC Image for MPI**

Thompson et al [14] found that in a Free Response Receiver Operating Characteristic (FROC) anthropomorphic chest phantom study there was no deterioration in lesion pick up rates in CT acquisitions using lower mA values but the false positive rate did increase. This study suggests that review of the CTAC for MPI image could lead to unnecessary investigations. However the images generated in this study were acquired on a standalone "diagnostic quality" system with higher rotation speeds and images were not subject to breathing artefact which plays a major role in degrading the quality of CTAC for MPI images. A comparative phantom-based FROC study on a range of SPECT/CT systems demonstrated that lesion pick up varied significantly between the different image qualities, with the early generation SPECT/CT systems performing much worse than the newer multi-slice alternatives [15]. The decision to review CTAC for MPI images should bear in mind the CT system's capabilities.

The relatively poor image quality and the limited volume of the chest imaged during CTAC for MPI are possibly the main arguments for not reporting. Generally speaking the CTAC images are acquired using a low mA, no breath hold and slow gantry rotation speed (together incurring motion artefact) and, in lower specification CT systems, a slice thicknesses of up to 10mm. (See Fig 1)

**Fig1** Examples of CTAC for MPI images acquired on different specification hybrid gamma cameras. (a) 16 slice scanner, 4mm slice 0.3s/slice, (b) 6 slice scanner, 5mm slice, 0.8s/slice, (c) 4 slice scanner, 5mm slice, 15s/slice, (d) single slice scanner, 10mm slice, 15s/slice

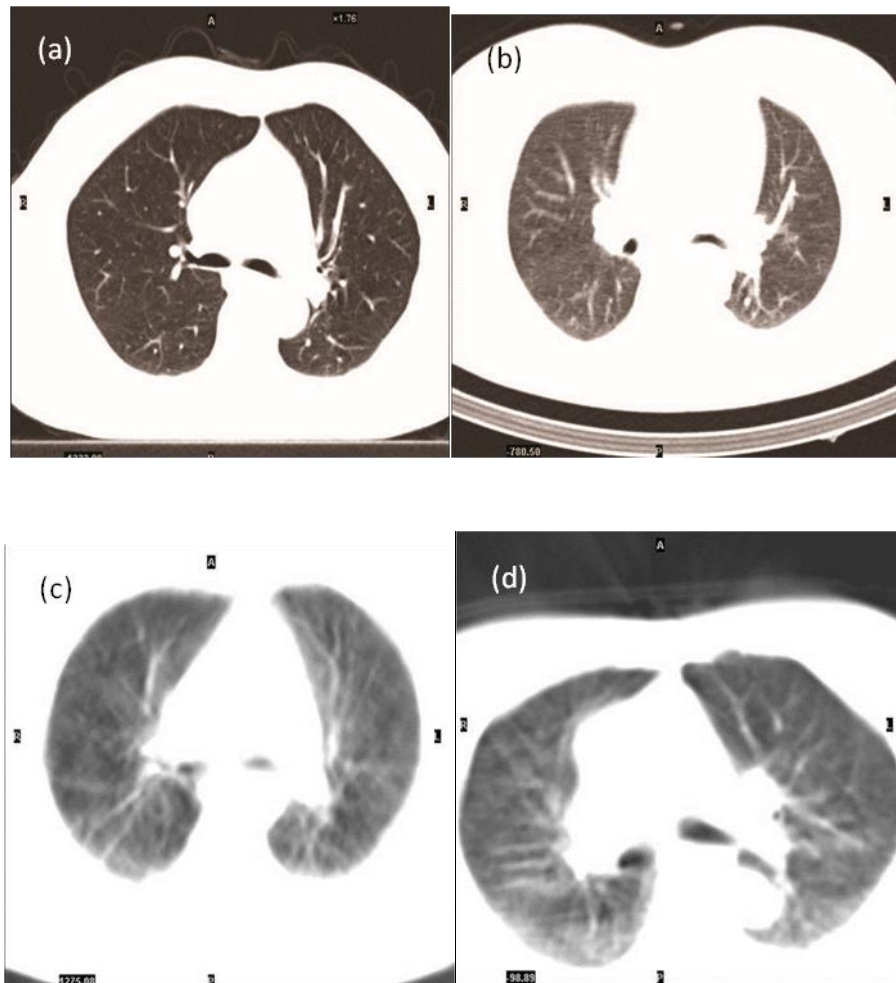


Fig 1a shows an attenuation correction image for MPI that was acquired on a higher specification 16 slice-CT scanner using non-breath hold technique. Comparing this to the other types of CT equipment using in hybrid systems there is a clear decrease in quality through Figures 1b to 1d. Fig 1d is a CTAC for MPI image acquired on the lowest specification CT scanner using a very slow rotation time of 15 seconds and a 10mm slice thickness.

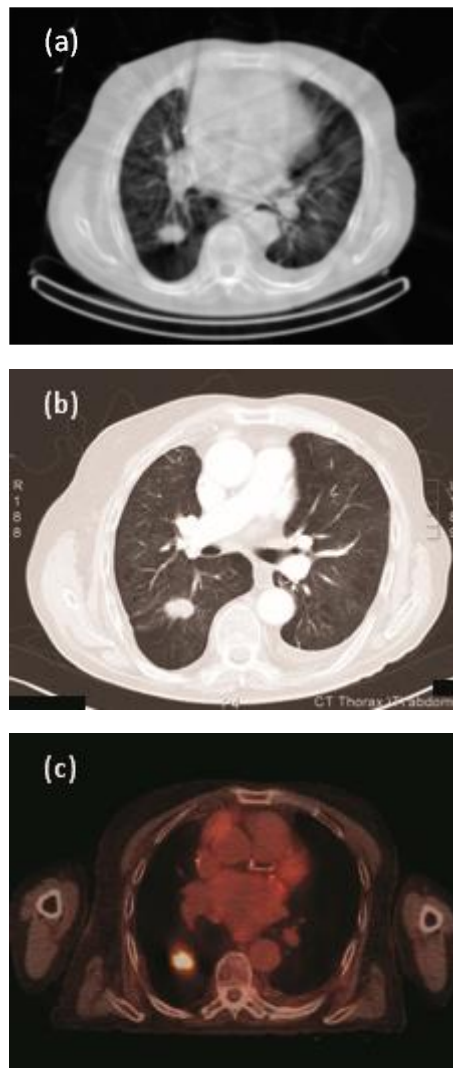
Perhaps an interesting parallel that can be drawn is to screening for lung cancer using low dose CT. As can be seen in table 1, screening protocols use exposure factors that are lower than typical diagnostic acquisitions; these are likely to exhibit lower image qualities. Nevertheless, studies by Jett [17] and Swensen et al [18] found that lung nodules and other pathologies are detectable on images acquired using low dose acquisition parameters. It is also recognised that a definitive diagnosis was not always possible yet it was feasible to identify cases that would benefit from further investigation. The work of Thompson et al [15] found that there is large disparity in the CT systems' ability to demonstrate simulated lesions in an anthropomorphic phantom. This disparity is likely due to the aforementioned specifications of the CT component of the different hybrid systems. However as noted by Kane [5],

and as seen in Fig 2, lesions can be identified, if not characterised, within CTAC for MPI images and followed up for definitive diagnosis.

**Table 1** Comparison of typical CTAC and Diagnostic CT parameters [5, 16, 17]

Characteristic	Typical CT AC	Screening CT	“Diagnostic” CT
Tube current	2.5	80/auto	80/auto
Tube voltage	140	120	120
Slice thickness	5-10mm	3mm	3mm
Field Of View	Left ventricle  (ascending aorta to apex)	Entire thorax	Entire thorax
Scan Time	5min	5-10 seconds	5-10 seconds
Axial resolution (mm)	10	0.5	0.5
Breath-hold	No	Yes	Yes
Intravenous Contrast	No	No	Yes
Radiation dose	<1mSv	<2mSv	5-6mSv

**Fig 2** Example of significant pathology found on CTAC for MPI acquisition. (a) Significant breathing artefact is evident but lesion in the right lung can be clearly seen. (b) Diagnostic CT scan of the same area. (c) PET-CT of the same area showing uptake of FDG in the lesion. A previously unknown malignant lung lesion was diagnosed [5].



### **Ethical and Legal Considerations**

The fact that in some cases a lesion can be identified raises the ethical question of whether the CTAC for MPI image should be examined for incidental extra-cardiac pathology. This question is one that has been considered previously in other areas of imaging [6, 11]. However, the counterpoint to the ethical question is the risk of over investigating clinically insignificant pathology and the potential for unnecessarily increasing patient anxiety. Budoff and Gopal [19] presented an argument that a reporting physician should not actively look for extracardiac pathology on CT angiography for this very reason. They argue that although it is possible to reconstruct a larger field of view to include the lung fields, soft tissue and bony structures, this “over reading” should not be done as it will lead to additional costs, liability and patient anxiety without proven benefit. The pragmatic and perhaps questionable approach this paper suggests is that to prevent the reporter from missing an incidental lesion is simply to not look for them. This appears to conflict with guidance issued by professional bodies and statements in UK legislation where it is stated that the review of images may reveal

incidental findings unrelated to the initial request and that clinical evaluation of the outcome of each medical exposure should be recorded [11, 20-22]. Whilst it could be argued that the outcome of the CT exposure does occur as evaluation of the corrected and non-corrected emission data is recommended in the EANM/ESC guidelines [7], it could be said that the acquired data is not being used to its full potential and clinical review of the CTAC for MPI images should take place.

### **Financial**

The economic impact of investigating incidental pathology is a topic that is raised quite frequently in literature [8-10, 12, 19, 23, 24]. With rising economic pressures on health service delivery there is a need to make best use of resources. Liu et al [9] found that the impact on costs of investigating extraordinary findings in CT urography was an increase of \$3257 and \$10974 for clinically moderate and clinically significant findings respectively. The study used a relatively small sample (n=259) but it was found that a protocol of following up moderate and significant incidental findings added \$41.37 per patient. Similarly Gluecker et al [25] found that in a larger sample (n=681) undergoing CT colonography investigation found that further investigation and, where required, intervention added \$34.33 per CT colonography investigation. In UK MPI examinations cost around £600, investigation of incidental findings using chest radiography would add around £50 where investigation with contrast enhanced CT chest would add an additional £600. Applying this to the findings of Kane [5], investigating with CT the 17 patients with probable significant pathology and the 4 diagnosed with lung cancers would add just £12.59 to each of the 1001 patients in the study. This figure, however only takes into consideration a follow-up diagnostic chest CT and costs of biopsy, intervention and/or therapy would need a longer term study to be undertaken.

Rumberger [26] considers that arguments around the economics of diagnosing incidental findings are weak as many consider a single case and follow this through to the worst case scenario whereby a patient undergoes invasive tests such as biopsy on a benign, clinically insignificant lesion. It is argued that there are evidence based guidelines on the management of pulmonary nodules that are identified on CT that allow the clinicians and practitioners to proceed in the most economical, legal and moral manner thus preventing unnecessary imaging and testing [27, 28].

### **Expertise of the Reporter**

The focus should not be purely on the technicalities of the imaging process and quantitative data concerning lesion detection. Consideration should be given to the knowledge and skill of the reporting clinician/healthcare professional [21, 24]. There are many instances when MPI studies are reported by non-radiological professionals and there are examples of non-nuclear medicine professionals (such as cardiologists) and non-medically qualified professionals (physicists, radiographers, and technologists) undertaking reporting of nuclear medicine studies. Whoever reports the examination including the CTAC dataset should be appropriately trained should operate within the boundaries of their knowledge and expertise.

In a discussion regarding the interpretation of extracardiac findings in CT angiography it is suggested that it is the reporting clinician (in the case of CT angiography, cardiologists) should be able to interpret extra-cardiac findings but to do so may require additional training. Conversely it is argued that there are radiologists with this expertise in reporting CT chest images and so why not make use of this knowledge and experience and issue a two-part report [23]. Guidelines on non-medical reporting state that any reporter should be able to at least offer an opinion on whether the appearances are normal, abnormal or normal variant and, if indicated, recommend further imaging or investigations for

correlation [21]. A comment on the appearance of the CTAC for MPI image (with or without possible diagnosis) may adhere to these guidelines.

### **Summary**

How the above issues manifest themselves into a protocol that includes evaluation of the CTAC for MPI image and how this is communicated to the Referrer would be a matter for individual departments to address. Any issued report should not only note the clinical findings but should provide a summary of how the examination was performed and any information that may impact on the diagnostic accuracy of the procedure [20]. Reporters who are not competent in the clinical evaluation of CT chest examinations should consider not undertaking the task of reviewing the CTAC for MPI image. Instead a multi-disciplinary approach might be taken to involve radiology input into the final report. A standard caveat regarding the CTAC for MPI image could be included in the MPI report that conveys the technical details and limitations of the CT acquisition. For example: "a limited CT scan through the lungs has been performed as part of the imaging protocol. This has not been performed as a diagnostic scan of the chest, and the whole thorax has not been imaged." Following this statement there could be a brief report on any normal or abnormal appearances in the image.

Controversy exists on whether or not the CTAC for MPI image should be reported. For certain specifications of CT in SPECT the image quality is undeniably poor suggesting that lesion identification and definitive diagnoses would be difficult, if not impossible. Legislation suggests that all data should be clinically evaluated, and therefore used to its full potential. However Thompson et al [15] suggests that there may be a "threshold specification" below which the hybrid camera may produce genuinely non-diagnostic CT chest images. Adopting this stance would be in line with evidence based practice.

Perhaps the strongest pro-argument is based on ethical and moral grounds as, despite the poor image quality, it has been shown that pathology can be detected. There are likely to be instances when over investigation will occur or significant pathology missed. Equally there will be instances when significant pathology will be detected, investigated further and managed. The outcome of current research projects concerning the prevalence of incidental pathology, the clinical impact of the evaluation of the CTAC for MPI images and empirical work on lesion perception and detection on low dose/non-diagnostic systems is awaited to clarify the usefulness or otherwise of the CTAC for MPI image.

1. Even-Sapir, E, Keidar, Z, Bar-Shalom, R, Hybrid Imaging (SPECT/CT and PET/CT)—Improving the Diagnostic Accuracy of Functional/Metabolic and Anatomic Imaging. *Semin Nucl Med*, 2009. **39**(4): p. 264-275.
2. Schillaci, O., Hybrid SPECT/CT: A New Era for SPECT Imaging? *European Journal of Medical Molecular Imaging*, 2005. **32**(5): p. 521-524.
3. Schillaci, O, Danieli, R, Manni, C, Simonetti, G. Is SPECT/CT with a Hybrid Camera Useful to Improve Scintigraphic Imaging Interpretation. *Nucl Med Commun*, 2004. **25**(7): p. 705-710.
4. Griffiths, M, Thompson, J, Tootell, AK, Sil, J, Kane, TP, Mountain, V, et al., SPECT-CT and its roles in Imaging and Oncology. *Imaging and Oncology: The Society of Radiographers.*, 2009.
5. Kane, TP, The Clinical Value of the CT Image Produced for Attenuation Correction, in *Annual Congress of the European Association of Nuclear Medicine 2011*: Birmingham.
6. Wolf, SM, Paradise, J, Caga-anan, C. The Law of Incidental Findings in Human Subjects Research: Establishing Researchers' Duties. *J Law Med Ethics*, 2008. **36**(2): p. 361-383.
7. Hesse, B, Lindhardt, TB, Anampa, W, Anagnostopoulos, C, Ballinger, J Bax, JJ. et al EANM/ESC Guidelins for Radionuclide Imaging of Cardiac Function. *European Journal of Medical Molecular Imaging*, 2008. **35**(4): p. 851-885.
8. Bartoletti, S, Perna, F, Santangeli, P, Casella, M, A Closer Look at Incidental Findings on Cardiac Computed Tomography. *J Am Coll Cardiol*, 2010. **55**(7): p. 702-a-703.
9. Liu, W, Morteale, KJ, Silverman, SG. Incidental Extraordinary Findings at MDCT Urography in Patients with Hematuria: Prevalence and Impact on Imaging Costs. *Americal Journal of Radiology*, 2004. **185**(4): p. 1051-1056.
10. Siddiki, H, Fletcher, JG, McFarland, B, Dajani, N, Orme, N, Koenig, B, et al Incidental Findings in CT Colonography: Literature Review and Survey of Current Research Practice. *J Law Med Ethics*, 2008. **36**: : p. 320-331.
11. The Royal College of Radiologists, *Management of Incidental Findings Detected During Research Imaging*, 2011, The Royal College of Radiologists,: London.
12. Goetze, S, Pannu, HK, Wahl, RL, Clinically Significant Abnormal Findings on the "Nondiagnostic" CT portion of Low-Amperage-CT Attenuation-Corrected Myocardial Perfusion SPECT/CT Studies. *The Journal of Nuclear Medicine*, 2006. **47**(8): p. 1312-1318.
13. Pandya, A, Pissay, P, Gopala, R, Elias M. *Should Myocardial Perfusion Attenuation Correction Datasets Be Reviewed?*, 2009, British Nuclear Cardiology Society.
14. Thompson J, Szczepura, K, Tootell, AK, Driver, J, Manning, D, Hogg, P. *Determination of optimal CT exposure factors for lung lesions using an anthropomorphic chest phantom for SPECT-CT.* in European Association of Nuclear Medicine Annual Conference. 2010. Vienna, Austria: EANM.
15. Thompson, J, Manning, D, Hogg, P. *Lesion Detection in the CT Attenuation Correction Image Of Five Different Low Resolution SPECT/CT Systems: A Multi-centre Study*, in *British Nuclear Medicine Society Spring Meeting 2012*: Harrogate.
16. James, J, *Does The Low Dose Attenuation Correction CT Have Clinical Value*, 2009, The University of Salford.
17. Jett, JR. Limitation of Screening for Lung Cancer with Low-Dose Spiral Computed Tomography. *Clin Cancer Res*, 2005. **11**(13 Supplement): p. 4988s-4993s.
18. Swensen, S.J., et al., *Screening for Lung Cancer with Low-Dose Spiral Computed Tomography*. *Am. J. Respir. Crit. Care Med.*, 2002. **165**(4): p. 508-513.
19. Budoff, M.J. and A. Gopal, *Incidental Findings on Cardiac Computed Tomography. Should we look?* *Journal of Cardiocascular Tomography*, 2007. **1**: p. 97-105.
20. The Royal College of Radiologists, *Standards for the Reporting and Interpretation of Imaging Investigations 2006*, London: The Royal College of Radiologists.
21. British Nuclear Medicine Society. *Guidelines for the Issue of Reports by Non-Medical Staff*. 2005 [cited 2011 30th October]; Available from: [http://www.bnms.org.uk/~bnms/images/stories/downloads/documents/non\\_medics\\_reporting\\_final\\_march\\_05.pdf](http://www.bnms.org.uk/~bnms/images/stories/downloads/documents/non_medics_reporting_final_march_05.pdf).

22. *Council Directive 97/43/Euratom On Health Protection of Individuals Against the Dangers of Ionizing Radiation in Relation to Medical Exposure, and Repealing Directive 84/466/Euratom, in Council Directive 97/43/EURATOM1997.*
23. Xiong, T, McEvoy, K, Morton, DG, Halligan, S, Lilford, RJ. Resources and costs associated with incidental extracolonic findings from CT colonography: a study in a symptomatic population. *Br J Radiol*, 2006. **79**(948): p. 948-961.
24. Douglas, PS, Cerqueria, M, Rubin, GD, Shu-Lei, C, A Extracardiac Findings: What Is a Cardiologist to Do? *J Am Coll Cardiol*, 2010. **1**(5): p. 682-687.
25. Gluecker, TM, Johnson, C, Wilson, D, MacCarty, LA, Welch, RL, Vanness, TJ, David J. et al. Extracolonic findings at CT colonography: Evaluation of prevalence and cost in a screening population. *Gastroenterology*, 2003. **124**(4): p. 911-916.
26. Rumberger, JA. Noncardiac Abnormalities on Diagnostic Cardiac Computed Tomography: Within Normal Limits or We Never Looked! *J Am Coll Cardiol*, 2010. **48**(2): p. 407-408.
27. National Institute for Clinical Excellence, *Lung Cancer: The Diagnosis and Treatment of Lung Cancer*, 2005: London.
28. MacMahon, H, Austin, JH, Gamsu, G, Herold, CJ, Jett, JR, Naidich, DP, et al. Guidelines for Management for Management of Small Pulmonary Nodules Detected on CT Scans: A Statement from the Fleischner Society. *Radiology*, 2005. **237**: p. 395-400.

## PAPER 2

### AN OVERVIEW OF MEASURING AND MODELLING DOSE AND RISK FROM IONISING RADIATION FOR MEDICAL EXPOSURES

Tootell AK, Szczepura K and Hogg P, 2014, *Radiography*, 20(4), 323-332. doi: <http://dx.doi.org/10.1016/j.radi.2014.05.002>

#### Abstract

**PURPOSE:** This paper gives an overview of the methods that are used to calculate dose and risk from exposure to ionizing radiation as a support to other papers in this special issue.

**BACKGROUND:** The optimization of radiation dose is a legal requirement in medical exposures. This review paper aims to provide the reader with knowledge of dose by providing definitions and concepts of absorbed, effective and equivalent dose. Criticisms of the use of effective dose to infer the risk of an exposure to an individual will be discussed and an alternative approach considering the lifetime risks of cancer incidence will be considered.

Prior to any dose or risk calculation, data concerning the dose absorbed by the patient needs to be collected. This paper will describe and discuss the main concepts and methods that can be utilised by a researcher in dose assessments. Concepts behind figures generated by imaging equipment such as dose-area-product, computed tomography dose index, dose length product and their use in effective dose calculations will be discussed. Processes, advantages and disadvantages in the simulation of exposures using the Monte Carlo method and direct measurement using digital dosimeters or thermoluminescent dosimeters will be considered.

Beyond this special issue it is proposed that this paper could serve as a teaching or CPD tool for personnel working or studying medical imaging.

## Introduction

Within this special issue of Radiography several articles use Monte Carlo mathematical methods to estimate radiation dose to humans. It is appreciated that readers may have a limited knowledge of these methods, or indeed measurement methods which are used to estimate dose. For readers with limited knowledge in dose estimation this article explains a range of approaches which might be used. This article also outlines concepts and defines terms associated with dose and it discusses how data can be used to provide an indication of risk to an individual.

Ionising radiation is made up of sub-atomic particles or, in the case of X and gamma rays, it comprises electromagnetic waves from the high energy part of the electromagnetic spectrum. At energies associated with medical imaging, these particles and waves have sufficient energy to ionise an atom and liberate an electron. This process may lead to tissue damage which can result in cell mutation or apoptosis. The higher the dose of radiation, the greater chance that tissue damage will occur [1]. This probability model of biological damage is referred to as the stochastic effect. It suggests that no dose of radiation is safe. It is this worst case scenario that radiation protection is based on, in that Operators should aim to minimise the probability of tissue damage by using the least practicable amount of ionising radiation [2].

In medical imaging a range of professionals are responsible for ensuring doses are As Low As Reasonably Practicable (ALARP). The Operator performing the exposure is required to have an understanding of the steps that they can take to optimise dose thus minimising the chance of stochastic affects.

### *Absorbed Dose*

Interactions of ionising radiation with matter can result in a proportion of radiation energy being deposited. The amount of energy deposited per unit mass is the absorbed dose (represented by the letter  $D$ ) and is defined as joules per kilogram ( $\text{Jkg}^{-1}$ ). The SI unit of absorbed is the Gray (Gy). Quantities of absorbed dose are usually quoted as milli-Gray (mGy, 1/1 000 of a Gray) or a micro-Gray ( $\mu\text{Gy}$ , 1/1 000 000 of a Gray).

### *Equivalent Dose*

The chance of tissue damage occurring does not just depend on the absorbed dose but also the type and energy of the radiation. Equivalent dose (represented by the symbol  $H$ ) takes these factors into consideration and is obtained by applying a radiation weighting factor ( $W$ ) to the absorbed dose. Radiation weighting factors are published by The International Commission On Radiation Protection (ICRP) [1]; they reflect the biological damage potential of different radiation types (Table 1). It can be considered a less fundamental quantity than absorbed dose but it is useful for indicating the health risk of radiation exposure. Equivalent dose is still defined as joules per kilogram, but is assigned the SI unit Sievert (Sv). Figures are often quoted as milli-Sieverts (mSv) or micro-Sieverts ( $\mu\text{Sv}$ ).

The equation for equivalent dose is defined in Figure 1.

**TABLE 1 RECOMMENDED RADIATION WEIGHTING FACTORS FROM ICRP 103[1]**

<b>Radiation Type</b>	<b>Radiation weighting factor</b>
<b>Photons (X-ray and gamma ray)</b>	1
<b>Electrons</b>	1
<b>Alpha particles</b>	20
<b>Protons</b>	2

**FIGURE 1 EQUATION FOR CALCULATING EQUIVALENT DOSE FROM ABSORBED DOSE. [1]**

$$H_T = W_R \cdot D_{T,R}$$

Where  $H_T$  is the equivalent dose

$W_R$  is the radiation weighting factor obtained from

$D_{T,R}$  is the absorbed dose in tissue ( $T$ ) by radiation type ( $R$ ).

Ionising radiation that forms part of the electromagnetic spectrum (e.g. X and gamma radiation) ionise atoms through the photoelectric absorption and the Compton Effect. Both these interactions will eject an electron from an atom; this electron may ionise many more atoms. Since most of the affected atoms are ionised indirectly by the secondary electrons, photons are considered to be indirectly ionising.

Using the data in Table 1 it can be seen that an absorbed dose of 1 mGy of X-ray photons results in an equivalent dose of 1 mSv, i.e. 1 mGy x 1 (radiation weighting factor for X-ray photons), where 1 mGy of alpha particles results in an equivalent dose of 20 mSv i.e. 1 mGy x 20 (radiation weighting factor for alpha particles). In other words alpha particles have a higher risk to biological tissue.

### *Effective Dose*

Effective dose (represented by the symbol  $E$ ) takes into account the type and amount of exposed tissue. Different tissues within the body have different sensitivities to radiation meaning a dose applied to one area of the body can carry a higher risk than the same dose applied to another. Effective dose takes the equivalent doses of a number of organs and through the application of a tissue weighting factor, the sum of these aims to provide a single number that is proportional to the detriment from a particular exposure. It allows comparisons of the risks associated with different imaging techniques or modalities.

The tissue weighting factors (Table 2) represent the sensitivity of their respective tissue, for example bone marrow is highly sensitive to radiation and so has a weighting factor of 0.12 where the brain is less sensitive and so has a weighting factor of 0.01. The sum of the tissue weighting factors is 1 and so the sum of the weighted equivalent doses would provide a whole body effective dose. Performing this process for different techniques allows for a comparison of doses and an indication of the detriment of these.

**TABLE 2 TISSUE WEIGHING FACTORS FROM ICRP 103 [1]**

<b>Organ</b>	<b>Tissue Weighting Factor</b>
<b>Gonads</b>	0.08
<b>Bone marrow</b>	0.12
<b>Colon</b>	0.12
<b>Lung</b>	0.12
<b>Stomach</b>	0.12
<b>Breast</b>	0.12
<b>Bladder</b>	0.04
<b>Liver</b>	0.04
<b>Oesophagus</b>	0.04
<b>Thyroid</b>	0.04
<b>Skin</b>	0.01
<b>Bone (surface)</b>	0.01
<b>Salivary Glands</b>	0.01
<b>Brain</b>	0.01
<b>Remainder*</b>	0.12
<b>TOTAL</b>	<b>1.00</b>
*Remainder tissues: Adrenals, Extrathoracic (ET) region, Gall bladder, Heart, Kidneys, Lymphatic nodes, Muscle, Oral mucosa, Pancreas, Prostate (♂), Small intestine, Spleen, Thymus, Uterus/cervix (♀)	

Effective dose is still defined as joules per kilogram and also has the same SI unit as equivalent dose, Sievert (Sv, with figures quoted as milli-Sieverts (mSv) or micro-Sieverts (μSv)). The equation for calculating effective dose is shown in Figure 2.

**Figure 8 Equation for the calculation of effective dose. [1]**

$$E = \sum_T W_T \cdot H_T$$

Where  $E$  is the effective dose to the entire body

$W_T$  is the tissue weighting factor of tissue ( $T$ ) defined by ICRP 103

$H_T$  is the equivalent dose absorbed by tissue ( $T$ )

### *Controversies with Effective dose*

Effective dose is commonly used in medical imaging to compare the risks from different modalities (for example, CT of the cervical spine versus conventional radiographic imaging of the same anatomical area) or examinations that have differing dose distributions (for example, comparison of effective dose from an antero-posterior hip to that from an antero-posterior shoulder). The application of the tissue weighting factors to the equivalent doses of the organs provides the whole

body effective dose from that exposure. The application of effective dose is useful in these situations as it provides Referrers, Practitioners and Operators with data that allows them to make decisions during the referral, justification and optimisation of medical imaging procedures [2, 3]. When used for this purpose effective dose is a useful figure to use, however a number of publications use this figure to calculate the risk of the exposure to an individual. As noted by a number of authors, and the ICRP themselves, the effective dose concept is not intended to be used this way as a number of factors are not taken into consideration [3-8].

The tissue weighting factors are averaged over all ages and both genders in the general population and so it cannot be applied to an individual patient [9]. For example a measurement of organ doses and effective dose calculations from a chest radiograph could be the same in a 15 year old and a 35 year old female. Using data published by Wall et al [9] the lifetime risk of cancer incidence for breast tissue in 10-19 year olds of 3.34% per Gray and 30-39 year olds of 1.44% per Gray it can be seen that the risk to female breast in 10-19 year old is higher. This difference in sensitivity due to age and gender is not captured within conventional effective dose calculations.

The tissue weighting factors published by the ICRP are derived using data that is assessed and analysed by The United Nations Scientific Committee on the Effects of Atomic Radiation (UNSCEAR) on cancer risks from follow-up studies of the Japanese atomic bomb survivors [10]. As a result of these ongoing long term studies the tissue weighting factors have undergone a number of revisions as new data on cancer incidence has been collected [11]. The effect of these revisions can be seen in Table 3.

**TABLE 3 COMPARISON OF THE TISSUE WEIGHTING FACTORS FORM ICRP PUBLICATIONS 26, 60 AND 103 [1, 12, 13]**

Organs	Tissue Weighting factors		
	ICRP 26 (1977) [12]	ICRP 60 (1990) [13]	ICRP 103 (2007) [1]
<b>Gonads</b>	0.25	0.20	0.08
<b>Red Bone Marrow</b>	0.12	0.12	0.12
<b>Colon</b>	-	0.12	0.12
<b>Lung</b>	0.12	0.12	0.12
<b>Stomach</b>	-	0.12	0.12
<b>Breasts</b>	0.15	0.05	0.12
<b>Bladder</b>	-	0.05	0.04
<b>Liver</b>	-	0.05	0.04
<b>Thyroid</b>	0.03	0.05	0.04
<b>Skin</b>	-	0.01	0.01
<b>Bone Surface</b>	0.03	0.01	0.01
<b>Salivary Glands</b>	-	-	0.01
<b>Brain</b>	-	-	0.01
<b>Remainder</b>	0.03	0.05	0.12
<b>TOTAL</b>	1.00	1.00	1.00

From Table 3 it can be seen that weightings assigned to the gonads have undergone significant changes over the three publications, from 0.25 in ICRP 26 to 0.08 in ICRP 103 that is a reflection of the understanding of heritable risk and the change in breast tissue changed from 0.05 in 1990 to 0.12 in 2007 due to a decision by the ICRP committee to put more emphasis on cancer incidence rather than mortality [4-6]. Brenner, in a number of publications, suggests that these tissue weighting factors

represent a subjective balance between the different stochastic endpoints of cancer incidence, cancer mortality, life shortening and hereditary risk. This subjectivity is an example of the “flaws in the science” behind the derivation of these factors [4-6]. However Dietze [11] argues that this revision was in response to the publication of more reliable cancer incidence data published by UNSCEAR [10] rather than a change in the committee’s emphasis. Whatever the reason, it is clear that these revisions do have an impact on effective dose calculations making comparisons to older data difficult.

#### *Lifetime Risk of Cancer Induction*

It is with these criticisms in mind that Brenner proposes an alternative to effective dose that can be applied to individual patients - this is referred to by Brenner as “effective risk”. Effective risk considers the life time risk of cancer induction from an absorbed dose of radiation and the equation for this is shown in Figure 3 [4].

**FIGURE 2 EQUATION FOR CALCULATING EFFECTIVE RISK [2-4]**

$$R = \sum_T r_T H_T$$

Where  $R$  = Effective risk

$r_T$  = lifetime radiation-attributable tissue-specific cancer risks  
(per unit equivalent dose to tissue T)

$H_T$  = is the equivalent dose absorbed by tissue (T)

This equation is very similar to that used to calculate effective dose. It is proposed that the tissue weighting factors are replaced with organ-specific radiation-induced cancer risk, such as those published by The Nuclear and Radiation Studies board ([14] or more recently by Wall [9] (a selection of data is shown in Table 4).

**TABLE 4 LIFE TIME RISKS OF CANCER INCIDENCE FOR MALES AND FEMALES BY ORGAN AND AGE FOR A EURO-AMERICAN POPULATION (% PER Gy)**

Organ (Male)	Age at exposure (y)						
	0-9	10-19	20-29	30-39	40-49	50-59	60-69
Lung	0.65	0.69	0.73	0.78	0.80	0.76	0.61
Stomach	0.93	0.73	0.57	0.43	0.31	0.20	0.12
Colon	1.49	1.22	0.98	0.79	0.60	0.43	0.25
Red Bone Marrow	1.06	1.05	0.77	0.76	0.78	0.65	0.49
Bladder	0.89	0.76	0.65	0.55	0.46	0.35	0.23
Liver	0.56	0.44	0.34	0.26	0.18	0.12	0.07
Thyroid	0.18	0.10	0.05	0.03	0.01	0.01	0.00
Oesophagus	0.12	0.11	0.11	0.11	0.12	0.14	0.15

Organ (Female)	Age at exposure (y)						
	0-9	10-19	20-29	30-39	40-49	50-59	60-69
Breast	4.92	3.34	2.21	1.44	0.84	0.45	0.21
Lung	1.36	1.46	1.58	1.70	1.78	1.72	1.39
Stomach	1.45	1.14	0.88	0.67	0.48	0.33	0.20
Colon	0.73	0.59	0.48	0.38	0.29	0.21	0.14
Red Bone Marrow	0.48	0.48	0.50	0.45	0.77	0.49	0.29
Bladder	0.70	0.61	0.52	0.45	0.39	0.32	0.24
Liver	0.24	0.19	0.15	0.11	0.08	0.06	0.03
Thyroid	0.92	0.52	0.26	0.13	0.06	0.02	0.01
Oesophagus	0.10	0.09	0.10	0.12	0.15	0.21	0.28

The lifetime risk figures (Table 4) are calculated from stronger data as they are based directly on epidemiological studies and not decided by committee [10, 14]. . The organ-specific radiation-induced risk data reflects current knowledge in the biological effects of radiation. The results would be easier to interpret (for example x per 1 000 000) for medical imaging professionals and non-medical imaging professionals too. The lifetime risk can be used to provide risk to different genders and age groups

Conveying risk to patients is arguably one of the more challenging aspects the radiography profession has to contend with. To this end Wall suggests using a category based approach to convey the risk from the radiological examination (Table 5) [9].

**TABLE 5 FOUR BROAD RISK BANDS FOR THE TYPICAL TOTAL LIFETIME CANCER RISK FOR PATIENTS [9]**

<b>Category</b>	<b>Total lifetime cancer risk</b>
<b>Negligible risk</b>	Less than 1 in a million
<b>Minimal Risk</b>	1 in a million To 1 in 100,000
<b>Very Low Risk</b>	1 in 100,000 To 1 in 10,000
<b>Low Risk</b>	1 in 10,000 To 1 in 1,000

Prior to any analysis of risk, dose data has to be collected. Dose data can be measured or estimated. In medical imaging either method can be used to determine dose data in most situations, although there could be occasions where only one method is suitable.

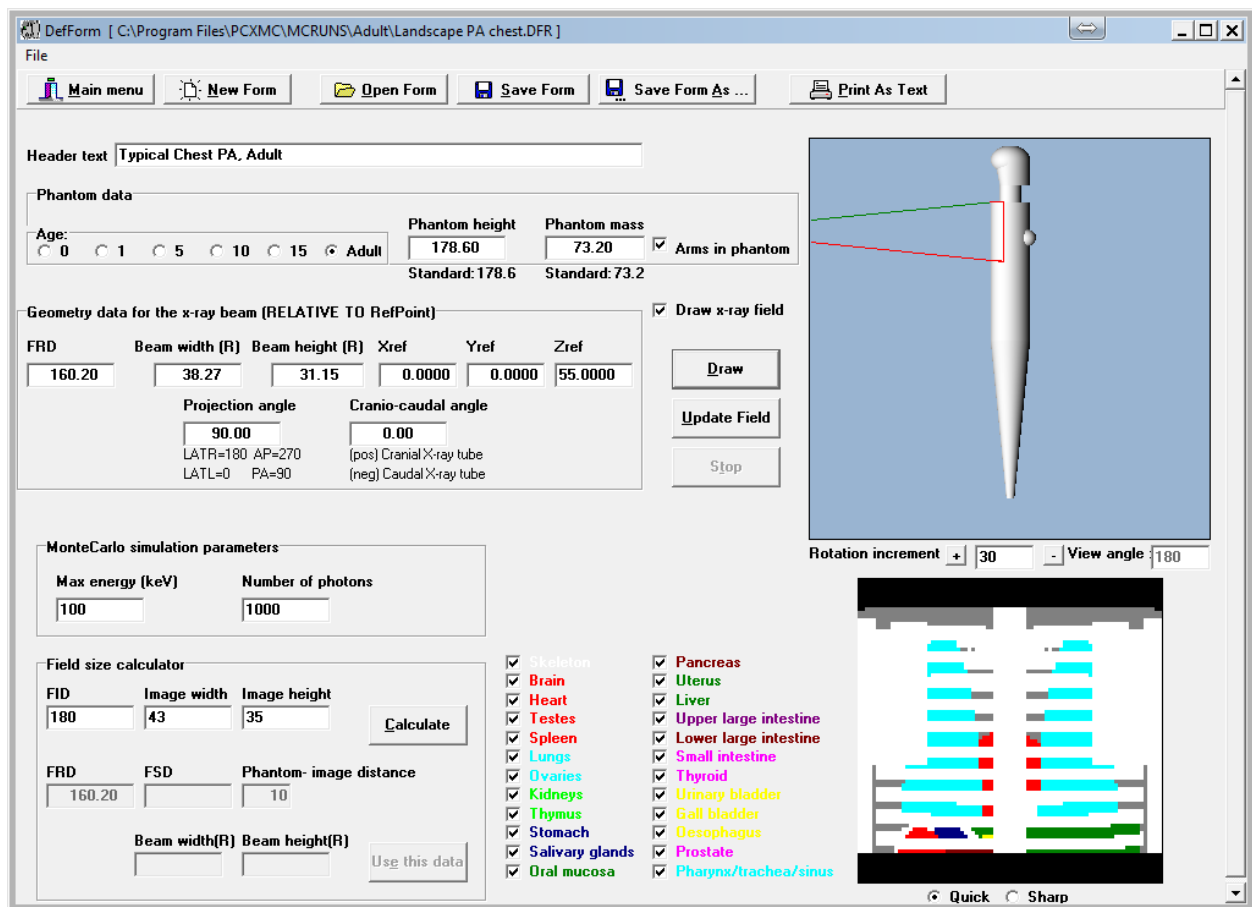
#### *Modelling Dose*

Mathematical modelling of dose using commercially available software is relatively quick and easy. Software is available that allows for organ and effective dose values for conventional radiographic techniques and CT imaging to be estimated. The software employs Monte Carlo modelling which is a mathematical technique that simulates as closely as possible the real interactions suffered by photons.

The process involves the computer simulation of an anthropomorphic phantom being exposed to a large number of photons of varying energies emitted from a point source. The path of each photon is followed through a sequence of interaction points and subsequent energy losses and outgoing directions (through coherent scattering or Compton scattering). This chain of interactions forms a so-called photon history. At each interaction point the energy deposited to the organ is calculated and used in the dose calculation. A large number of independent random photon histories are generated and estimates of the mean values of the energy depositions in the various organs are used for calculating the dose in these organs. Eventually the photon loses sufficient energy to allow photoelectric absorption to occur [15, 16].

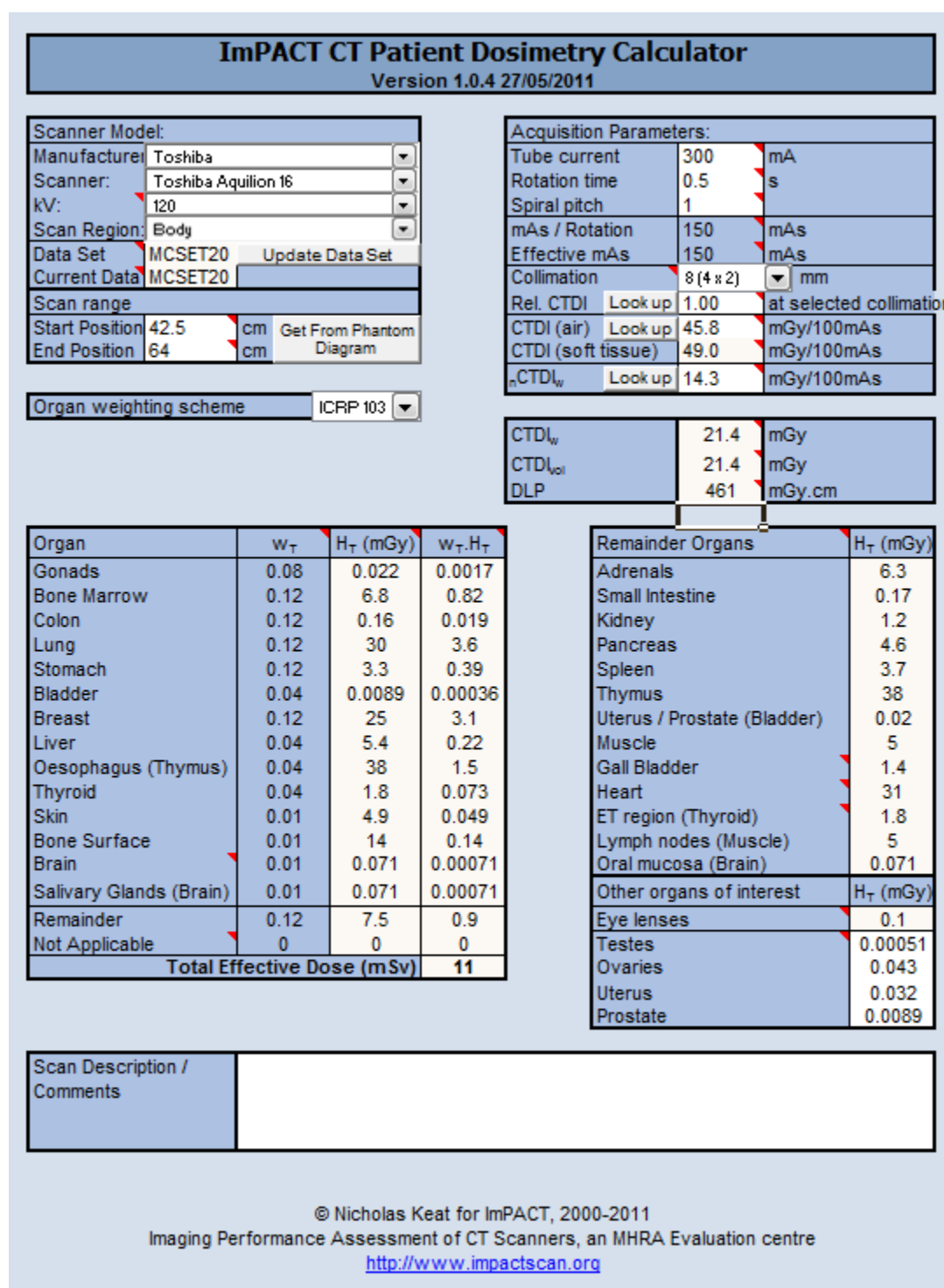
PCXMC (STUUK, Helsinki, Finland [16, 17]) is one such programme that allows for organ and effective dose to be estimated in many conventional radiographic techniques. Figure 4 illustrates the positioning of a PA chest with landscape orientation of the image receptor. Other parameters can be manipulated in the software including X-ray anode angle, tube filtration material and thickness to obtain final dose estimates.

**FIGURE 4 EXAMPLE OF DATA ENTRY PAGE OF PCXMC FOR THE CALCULATION OF ORGAN AND EFFECTIVE DOSE FROM A PA CHEST RADIOGRAPH**



Dose modelling software is also available for CT dose estimations. For example, ImPact's CT Dosimetry Tool (ImPact, London [18, 19]) software simulation allows for quick and easy calculation of organ and effective dose through the use of Monte Carlo data for normalised organ doses. However, as can be seen in Figure 5, results are dependent on selecting the imaging parameters and CT model as calculations take into account specific features of each CT unit (e.g. radiation quality and field geometry) [20]. Selection of the correct scanner may not always be possible as new technology and systems are constantly being introduced. These systems are currently not included in dose simulation software meaning that dose simulation has to rely on "best fitting" the attributes of these scanners to those of a similar design. As noted by Groves et al [21], this introduces the potential for significant error in the estimated doses. Automatic mA manipulation by the scanners can also lead to error as the software only allows a single value to be used.

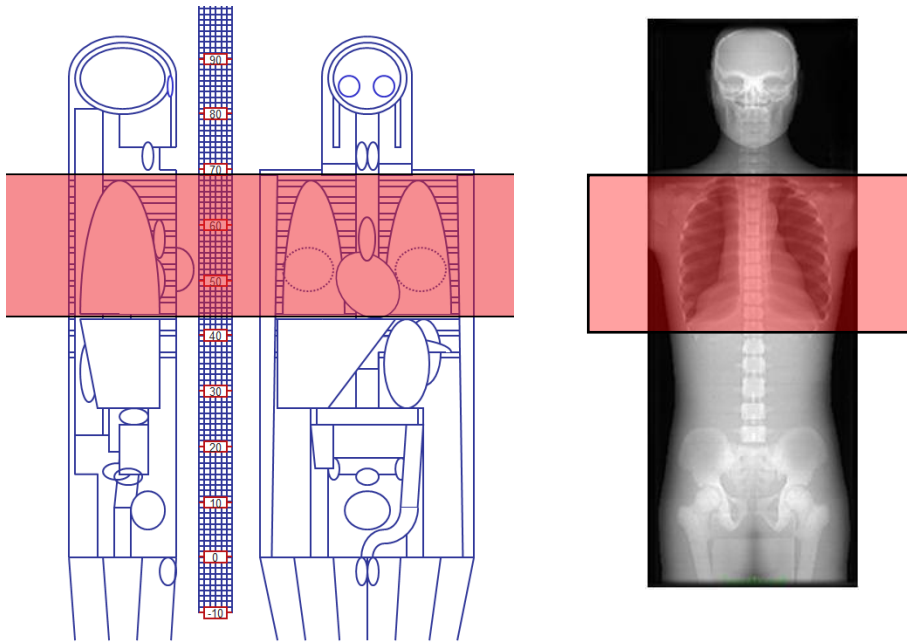
FIGURE 5 EXAMPLE OF THE DOSE REPORT GENERATED BY IMPACT CT DOSIMETRY SOFTWARE



Underestimation of CT doses using computer simulation is frequently reported with magnitudes between 18 and 40% [5, 12, 13]. Reasons for these underestimations have been explained by the differences in the physical dosimetry phantoms and the virtual phantoms used by dose modelling software. Close examination of this highlights the simplified geometric shapes of the organs. Subsequently, as can be seen in Figure 6, in CT examinations of the chest the CT virtual phantom

suggests that the liver is not exposed to primary X-ray beam and thus the calculated liver dose would be low. In reality a significant volume of this organ is included in the scan and so will contribute to the effective dose calculations.

**FIGURE 3 COMPARISON OF THE VIRTUAL PHANTOM IN IMPACT CT DOSIMETRY SOFTWARE AND ATOM DOSIMETRY PHANTOM**



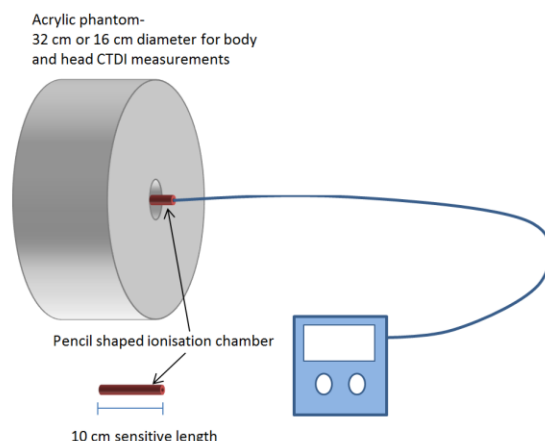
However, accuracy of CT dose modelling can be improved by careful selection of the scan range to match the fractions of organs irradiated and to include overbeaming and overranging that is a feature of helical scanning. The use of an average mAs for the scan parameters will further improve the accuracy of the dose calculations [22].

#### *Measuring dose*

There are many tools which may be used to measure the dose absorbed during a radiographic procedure that will allow dose to be calculated. The one that most Operators will be familiar with is the Dose Area Product (DAP) meter. DAP combines two quantities- as its name suggests absorbed dose in air and the field size giving the unit Gray centimetre squared  $\text{Gycm}^2$  (or  $\text{cGycm}^2$  or  $\text{mGycm}^2$ ) (NB not Gray *per* square centimetre). DAP meters are mounted onto the X-ray tube in front of the collimators making readings easy to acquire, however it is important to note that DAP is not patient dose *per se* [23]. It is independent of the distance between the source and the patient meaning that if this figure is to be used to estimate patient dose the source to patient distance, the field size and the location of the area exposed are required [24].

CT acquisitions have similar values that are often used as a reference for patient dose; the computed tomography dose index (CTDI) and dose length product (DLP). The CTDI measurement was based on an axial CT scanner and was defined as the dose from the primary beam plus scatter from surrounding slices from a single slice in an acrylic phantom (Figure 7). Phantoms come in two diameters, 16cm and 32cm, to represent the head and body respectively [25].

**FIGURE 4 TYPICAL ARRANGEMENT OF THE PHANTOM AND PENCIL BEAM IONISATION CHAMBER USED TO COLLECT CTDI**



Developments in technology and the advent of multislice CT equipment lead to variations in CTDI.  $CTDI_{100}$  reflects the dose contribution from a 100mm range (50mm either side of the reference slice). The weighted CTDI ( $CTDI_w$ ) reflects the weighted sum of two thirds the peripheral dose and one third the central dose in a 100mm range. The most commonly quoted CTDI value in modern CT technology is the volume CTDI ( $CTDI_{vol}$ ). This value is obtained by dividing  $CTDI_w$  by the beam pitch factor [22, 26]. As before CTDI in any form is not patient dose but a quantification of the radiation output of the CT system so does not take into account differing patient sizes and area of the body that is being imaged [27].

A derivative of CTDI is Dose length product (DLP). This figure takes into account the length of the scan and is calculated by multiplying the  $CTDI_{vol}$  by the length of the scan. In a similar way to CTDI and  $CTDI_{vol}$ , DLP is not patient dose as it does not take into account what part of the body is being exposed, the size of the patient, or the patient's age.

Conversion of DLP to patient dose is possible using a conversion coefficient ( $k$ ) shown in (Table 6). This conversion factor is defined as the effective dose per dose-length product and has the unit mSv / mGy cm. Multiplying the DLP by the relevant conversion factor gives a value for effective dose.

**TABLE 6 NORMALISED VALUES OF EFFECTIVE DOSE PER DOSE-LENGTH PRODUCT (DLP) OVER VARIOUS BODY REGIONS**

Region of the body	Normalised effective dose (E/DLP) (mSv/mGy cm)
Head	0.0023
Neck	0.0054
Chest	0.017
Abdomen	0.015
Pelvis	0.019

Criticisms of  $k$  state that the factors are based on old technology and old data; they are based on several scanners that were in use circa 1990 and the tissue weighting factors used in their calculation are from ICRP 60 [13, 26, 28]. There are also a number of assumptions made that would increase the error in the calculated effective dose. For example, the patient is assumed to be standard, and as noted by McCollough et al [27], this standard patient is a little thin by today's standards (nominal body

mass of 70 kg). Variation in the way CT scanners report  $CTDI_{vol}$  for paediatric patients can make comparison difficult. Some use the 16cm phantom while others use the 32cm phantom. For example Siemens, Philips dose reports are based on a 32cm phantom, Toshiba reports are based on 16 cm phantom and GE reports use the 16cm or 32 cm depending on the scan field of view.  $CTDI_{vol}$  can differ by a factor of approximately 2.5 between the two diameter phantoms [27].

True measurement of dose using digital or analogue dosimeters such as metal oxide semi-conductor field effect transistor (MOSFET) or thermoluminescent dosimeters (TLDs) (described later) can be done in a number of ways. In the experimental setting it is possible to measure organ dose by placing dosimeters in a specially designed anthropomorphic phantom. These phantoms are available in a range of patient types; male and female and paediatric, adolescent and adult (Figure 8). They are made up of contiguous slices with different tissues represented by different densities of epoxy resin. The resin has attenuation properties that are equivalent to real tissue. Within the slices are locations for placing dosimeters that will provide data of organ dose (Figure 9). Using these phantoms allows the researcher to carry out experimentation on different techniques, exposure factors or positioning to optimise dose without the involvement of real patients.

**FIGURE 8 THE CIRS ATOM DOSIMETRY PHANTOM FAMILY MODELS 701-706 (CIRS, NORFOLK, VIRGINIA) [29]**

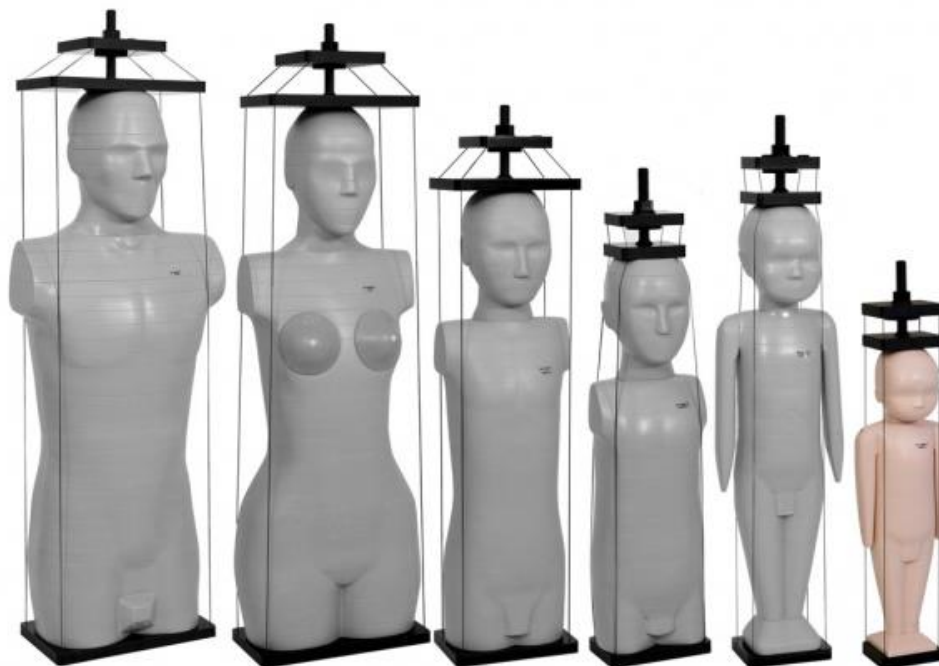
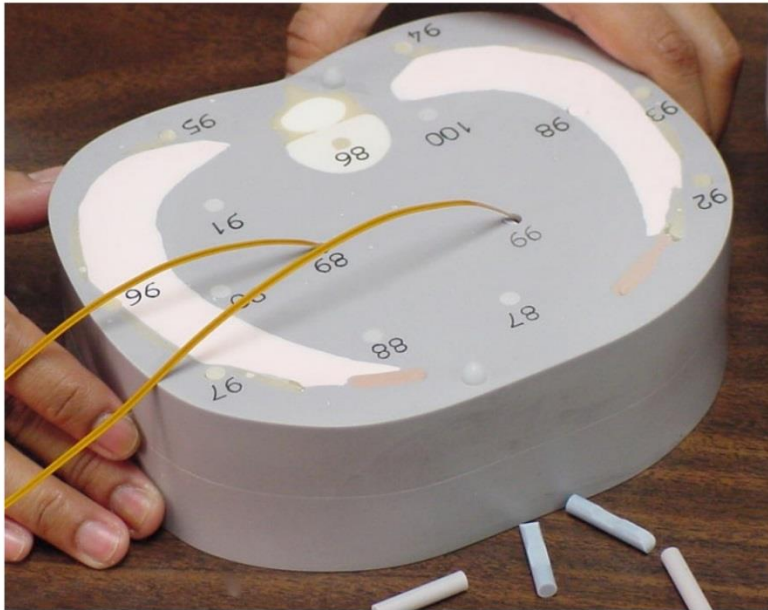


**FIGURE 9 LOWER THORACIC SLICES OF A PAEDIATRIC PHANTOM SHOWING DIFFERENT DENSITY RESIN FOR THE LUNG, SOFT TISSUE AND BONE WITH LOCATIONS FOR DOSIMETERS. THESE DOSIMETERS CAN BE ELECTRONIC (SHOWN HERE BY THE TWO WIRES INSERTED INTO THE PHANTOM) OR ANALOGUE SUCH AS THERMOLUMINESCENT DOSIMETERS [29].**



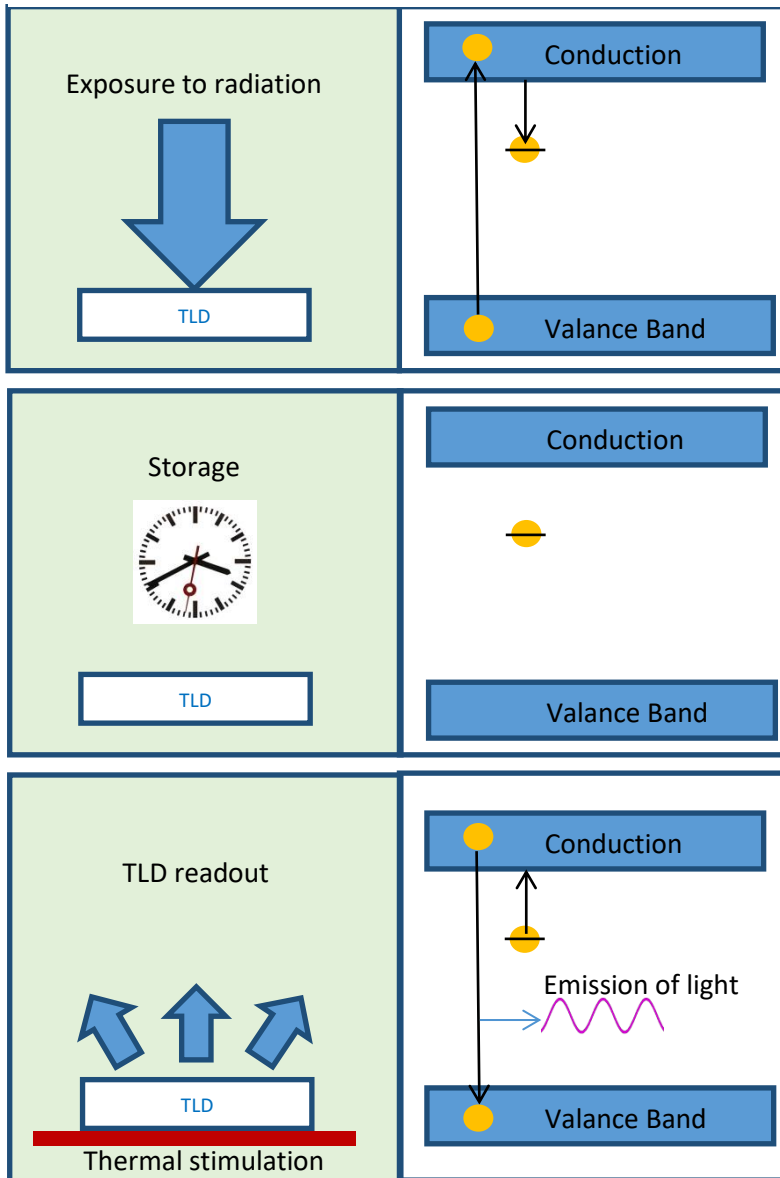
It is obviously impossible to directly measure organ dose in the clinical setting, so the entrance surface dose (ESD) can be used. ESD is defined as the absorbed dose in the skin at a given location on the patient and also includes backscattered radiation from the patient. As a measurement it can be combined with DAP to allow calculations of patient dose to be made.

### **Dosimeters**

ESD and organ dose in the anthropomorphic phantom can be measured using a digital dosimeter or using thermoluminescent dosimeters (TLD). Most medical imaging personnel will be familiar with TLDs in the context of radiation protection as they are frequently used in personal dosimeter badges. TLDs are available in a variety of forms, from powder to square or circular chips, rods, cubes and in a range of materials.

Thermoluminescence (illustrated in Figure 11) uses the atomic model of two energy bands; the valence band and conduction band. Within the valence band electrons are bound to individual atoms as opposed to the conduction band where electrons can move freely within the atomic lattice. Separating these two bands is an area that is referred to as the forbidden gap in which no electron state can exist. The impurities mentioned above create electron traps within this gap. Exposure to ionising radiation excites electrons allowing them to move up to the conduction band leaving holes within the valence band. Electrons can travel amongst the crystal lattice until either the electron can cross back towards the valence band and recombine with a hole or, if near a defect, it can fall into the energy trap. The electron is now prevented from filling a hole within the valence band until it can gain enough energy to once again reach the conduction band before moving back to the valence band. This stimulation is in this context accomplished by introducing heat [30]. The movement of the electron back to the valence band requires the electron to lose energy. This energy is released in the form of visible light and this light is detected by a photomultiplier tube. The charge (measured in Coulombs [C]) generated from this component is measured.

**FIGURE 5 ILLUSTRATION OF THE PROCESS INVOLVED IN TLD DOSIMETRY**



The choice of material depends on the nature of radiation; in diagnostic and therapeutic energies the chemical composition of the dosimeters is either lithium fluoride with magnesium and titanium impurities added or lithium fluoride with magnesium, copper and phosphorus impurities added [31]. The difference in the materials affects their sensitivity and the measurement range the TLD is capable of. For example TLDs made from Calcium Fluoride Dyprosium are suitable for environmental monitoring and as capable of detecting doses of between 0.1 pGy to 1 Gy [32]. Lithium Fluoride with magnesium and titanium are suitable for medical physics dosimetry applications and operate at doses between 10 pGy to 10 Gy [33].

Conversion from charge to dose involves a calibration process. The TLD or batches of TLDs plus scattering material and a digital dosimeter are exposed to a range of exposures at energy (kV) consistent with the experiment that will be performed. The charge generated from the reading process and the doses recorded by digital dosimeter are used to establish the calibration factor through linear regression. An example of calibration data using is shown Figure 11.

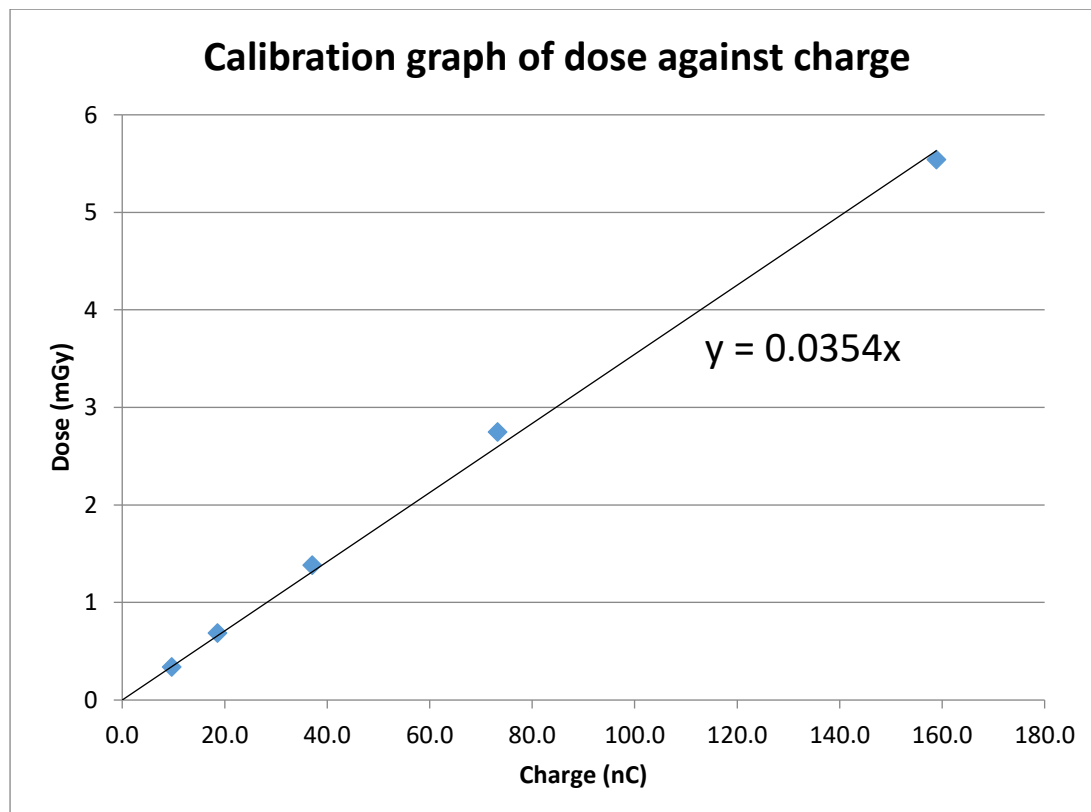
General radiographic equipment can be used in this process although some TLD readers will perform calibration using sealed sources of gamma emitting isotopes such as Strontium-90 or Yttrium-90. Such systems will calibrate each TLD individually rather than in batches increasing the accuracy of the final readings. The response of the TLDs is energy dependent therefore calibration should be performed at the energy that will be used in the research or measurements. If this cannot be done then energy conversion factors can be used but this can introduce error [34].

**Figure 11** Example of calibration data for TLDs at 80kV. Plotting data from table (a) results in graph (b) and shows the linear relationship between the charge generated from reading the TLD to dose. The gradient of this line is the calibration factor.

(a)

kV	mAs	Digital Dose reading (mGy)	Background corrected charge (nC)
80	10	0.338	9.7
80	20	0.685	18.6
80	40	1.382	37.1
80	80	2.749	73.2
80	160	5.542	158.9

(b)



One of the disadvantages of the TLD is the time needed to prepare and setup and process them. A typical whole body adult phantom measurement for calculation of effective dose involves the use of 268 individual TLDs. Reading this number using a manual TLD reader equates to approximately 6 hours of work [35]. Research has been undertaken to follow the dental radiography dosimetry process to reduce the number of TLD required for effective dose measurement however, if comparison of organ dose and risk is to be carried out it has been shown that a measurement organ dose is required for all critical organs [35].

An alternative to TLDs is the digital dosimeter. An example of this is the metal oxide semi-conductor field effect transistor (MOSFET) (Best Medical Canada, Ontario, Canada) (Figure 12).

**FIGURE 12 A MOSFET DOSIMETER WITH AN ARRAY OF FIVE DOSIMETERS CONNECTED TO THE MODULE [36]**



Exposure of the digital dosimeter results in a voltage shift between the components of the dosimeter. This difference is measured and is proportional to the dose absorbed by the detector. However, it is unlikely that the total number of digital dosimeters would be available to allow measurement of all critical organs in one exposure due to expense of the dosimeters. Therefore a number of repeated measurements with the dosimeter relocated between each would be required. As with TLDs, MOSFET dosimeters require calibration and their response is energy dependent meaning separate calibrations are required if a significant difference in beam energies is to be used in any research [37]

Measurements using TLD or digital dosimeters have their advantages and disadvantages relating to preparation time, acquisition time processing following exposure, and cost. These have to be considered when planning research that involves the direct measurement of dose from exposure to ionising radiation [21, 35, 38].

## Summary

This article has given insight into terms and concepts associated with dose measurement and modelling, as well as risk estimation. Some limitations and values of dose estimation and measurement methods have been considered. As support for this *special issue* the reader should have gained enough background and insight into Monte Carlo mathematical dose modelling to be able to appreciate some of the empirical articles. Beyond the *special issue* we anticipate that the article could serve as a teaching or CPD aid for personnel working in medical imaging.

1. ICRP, *The 2007 Recommendations of the ICRP*, in *ICRP Publication 103*. 2007, Ann. ICRP. p. 2-4.
2. *The Ionising Radiation (Medical Exposure) Regulations*. 2000: United Kingdom.
3. Oritz, P., *The use of Effective Dose in Medicine* in *The 2nd International Symposium on the System of Radiological Protection*. 2013, ICRP: United Arab Emirates.
4. Brenner, D.J., *Effective dose: a flawed concept that could and should be replaced*. *British Journal of Radiology*, 2008. **81**(967): p. 521-523.
5. Brenner, D.J., *Effective Dose- A Flawed Concept that Could and Should be Replaced*, in *International Commission on Radiological Protection*. 2011: Washington DC.
6. Brenner, D.J., *We can do better than effective dose for estimating or comparing low-dose radiation risks*. *Annals of the ICRP*, 2012. **41**(3-4): p. 124-128.
7. Harrison, J., *The use of Effective Dose*, in *The 2nd International Symposium on the System of Radiological Protection*. 2013, ICRP: United Arab Emirates.
8. Martin, C.J., *Effective dose: how should it be applied to medical exposures?* *British Journal of Radiology*, 2007. **80**(956): p. 639-647.
9. Wall, B.F., et al., *Radiation Risks from Medical X-ray Examinations as a Function of the Age and Sex of the Patient. Report HPA-CRCE-028*. 2011, Health Protection Agency: Chilton.
10. United Nations. Scientific Committee on the Effects of Atomic Radiation, *Effects of Ionizing Radiation: United Nations Scientific Committee on the Effects of Atomic Radiation - UNSCEAR 2006 Report, Volume II - Report to the General Assembly, with Scientific Annexes C, D, and E*. 2009: UN.
11. Dietze, G., J.D. Harrison, and H.G. Menzel, *Effective dose: a flawed concept that could and should be replaced. Comments on a paper by D J Brenner (Br J Radiol 2008;81:521-3)*. *British Journal of Radiology*, 2009. **82**(976): p. 348-351.
12. ICRP, *Recommendations of the ICRP*, in *ICRP Publication 26*. 1977, Ann. ICRP. p. 3.
13. ICRP, *1990 Recommendations of the ICRP*, in *ICRP Publication 60*. 1991, Ann. ICRP. p. 1-3.
14. Committee to Assess Health Risks from Exposure to Low Levels of Ionizing Radiation, Nuclear and Radiation Studies Board Division on Earth and Life Studies, and National Research Council of the National Academies, *Health Risks From Exposure to Low Levels of Ionizing Radiation: BEIR VII Phase 2*. 2006: Washington, DC.
15. Baker, C., *Physicist toolbox- Basics of Monte Carlo simulation of radiation transport*, in *United Kingdom Radiological Congress*. 2013: Liverpool.
16. Tapiovaara, M. and T. Siiskonen, *PCXMC: A Monte Carlo Program for Calculating Patient Doses in Medical X-Ray Examinations*. 2nd Edition ed. 2008, Helsinki, Finland: STUK.
17. Tapiovaara, M., Lakkisto, M., Servomaa, A., *PCXMC 2.0 Rotation Dose Calculations*. 2012, STUK: Helsinki, Finland.
18. ImPACT. *Imaging Performance Assessment of CT Scanners*. [cited 2012 22nd April]; Available from: <http://www.impactscan.org>.
19. ImPACT, *CT Patient Dosimetry Calculator*. 2003, Medical Devices Agency: London.
20. Hashemi-Malayeri, B.J. and J.R. Williams. *A practical approach for the assessment of patient doses from CT Examinations*. 2003 [cited 2012 10th January]; Available from: [www.dundee.ac.uk/medphys/documents/hashemi.pdf](http://www.dundee.ac.uk/medphys/documents/hashemi.pdf).
21. Groves, A.M., et al., *16-detector multislice CT: dosimetry estimation by TLD measurement compared with Monte Carlo simulation*. *Br J Radiol*, 2004. **77**(920): p. 662-5.
22. Castellano, E., *CT Dose calculations for individual patients - what you should know*, in *12th CT Users Group*. 2010: London.
23. Conference of Radiation Control Program Directors Committee on Quality Assurance in Diagnostic X-ray, *Dose-Area Product (DAP)*, in *Q.A. Collectible*. 2001, reviewed and republished 2008: Frankfurt.
24. Moores, B.M., *Radiation dose measurement and optimization*. *British Journal of Radiology*, 2005. **78**(933): p. 866-868.

25. Coursey, C. and D. Frush, *CT and radiation: What radiologists should know*. Applied Radiology, 2008. **37**(3): p. 22-29.
26. McNitt-Gray, M., *Assessing Radiation Dose: How to Do It Right*, in *2011 AAPM CT Dose Summit*. 2011: Denver.
27. McCollough, C.H., et al., *CT Dose Index and Patient Dose: They Are Not the Same Thing*. Radiology, 2011. **259**(2): p. 311-316.
28. European Commission and EUR 16262 EN, *European guidelines for quality criteria for computed tomography*. 1999, European Commission: Luxembourg.
29. CIRS Tissue Simulation and Phantom Technology. *Dosimetry Verification Phantoms Model 701-706 Data Sheet*. 2012 [cited 2012 19th January]; Available from: [http://www.cirsinc.com/file/Products/701\\_706/701\\_706\\_DS.pdf](http://www.cirsinc.com/file/Products/701_706/701_706_DS.pdf).
30. Stabin, M.G., *Radiation Protection and Dosimetry: An Introduction to Health Physics*. 2007: Springer.
31. Bilski , P., *Lithium Fluoride: From LiF:Mg,Ti to LiF:Mg,Cu,P*. Radiation Protection Dosimetry, 2002. **100**(1-4): p. 199-205.
32. ThermoScientific. *TLD-200™ Thermoluminescent Dosimetry Material*. 2014 [cited 2014 29th April]; Available from: <http://www.thermoscientific.com/en/product/tld-200-thermoluminescent-dosimetry-material.html>.
33. ThermoScientific. *TLD-100™ Thermoluminescent Dosimetry Material*. 2014 [cited 2014 29th April]; Available from: <http://www.thermoscientific.com/en/product/tld-100-thermoluminescent-dosimetry-material.html>.
34. Podgoršak, E.B. and International Atomic Energy Agency, *Radiation oncology physics: a handbook for teachers and students*. 2005: International Atomic Energy Agency.
35. Tootell, A.K., K.R. Szczepura, and P. Hogg, *Optimising the number of thermoluminescent dosimeters required for the measurement of effective dose for computed tomography attenuation correction data in SPECT/CT myocardial perfusion imaging*. Radiography, 2013. **19**(1): p. 42-47.
36. Best Medical Canada. *MOSFET Dosimetry, Patient Dose Verification*. [cited 2013 19th Nov]; Available from: [http://www.bestmedicalcanada.com/MOS\\_PDFs/mobilemosfet.pdf](http://www.bestmedicalcanada.com/MOS_PDFs/mobilemosfet.pdf).
37. Brady, S.L. and R.A. Kaufman, *Establishing a standard calibration methodology for MOSFET detectors in computed tomography dosimetry*. Med Phys, 2012. **39**(6): p. 3031-40.
38. Geleijns, J., et al., *Comparison of two methods for assessing patient dose from computed tomography*. Br J Radiol, 1994. **67**(796): p. 360-5.

## PAPER 3

OPTIMISING THE NUMBER OF THERMOLUMINESCENT DOSIMETERS REQUIRED FOR THE MEASUREMENT OF EFFECTIVE DOSE FOR COMPUTED TOMOGRAPHY ATTENUATION CORRECTION DATA IN SPECT/CT MYOCARDIAL PERFUSION IMAGING.

Tootell, A., Szczepura, K., & Hogg, P. (2013). *Radiography*, 19(1), 42-47. doi: <http://dx.doi.org/10.1016/j.radi.2012.11.001>

### **Abstract:**

The use of thermoluminescent dosimeters (TLDs) is regarded as time consuming and laborious. As part of our dosimetry research it was necessary to optimise the use of our resources, both physical and time. Experimental work was carried out to develop a method that allowed for a reduction in the number of TLDs needed for accurate effective dose measurement. For this work specific reference to computed tomography attenuation correction (CTAC) for myocardial perfusion imaging (MPI) acquisitions is made although it is proposed that the developed method could be applied to dose assessments using TLDs.

Research to measure and compare the effective dose from CTAC for MPI was to be carried out using an ATOM 701 dosimetry phantom, Harshaw 3500 manual TLD reader and TLD-100s.

Method: To establish the areas of the phantom where dose measurements should be carried out, a batch calibrated TLD-100 dosimeters were placed along the centre of the phantom. A simulated CTAC for MPI was performed. After reading the distribution of the dose was recorded and areas where dose levels were below the sensitivity threshold dose of 50 $\mu$ Gy were noted. To test the effect of excluding dose measurement for some areas on the final calculation of effective dose and the time taken to acquire the data a repeat acquisition was performed with the full complement of TLDs placed in the phantom in organ locations recommended by the manufacturer. The time taken for loading, unloading and reading was recorded. Effective dose and organ doses were calculated. The calculation was repeated with TLDs outside the established range excluded and the potential time saved calculated.

Results: Excluding TLDs from areas where doses were below the 50 $\mu$ Gy threshold resulted in 82 fewer TLDs being used (268 to 186) leading to a time saving of around 2 hours per batch. The results of the experiment showed that effective dose measurements were 1.75% lower with the reduced chipset and organ dose measurements were not significantly different ( $p>0.10$ ).

Conclusion: It is proposed that this methodology could be applied to TLD dosimetry work to establish the areas that should be included in the measurements. In some cases significant savings in time could be made.

### **Keywords:**

Thermoluminescent Dosimetry; SPECT/CT; Nuclear Medicine; Myocardial Perfusion Imaging

## Introduction:

The addition of computed tomography (CT) to single photon emission computed tomography (SPECT) has been shown not only to provide additional information to correct the emission data for attenuation and scatter artefact but also to more accurately localise pathology and aid characterisation of lesions [1]. Since the introduction of the first commercial SPECT/CT system in 1999 the modality's availability and its use has grown rapidly. Early SPECT/CT systems consisted of low dose fixed output CT components, with newer CT systems offering capabilities similar to stand-alone diagnostic systems [2]. When used for attenuation correction (AC), CT tube output, and dose, is kept comparatively low. However a comparison between three manufacturer's exposure parameters suggests dose differences could exist (See table 1). To determine whether dose differences do exist and to establish their magnitude two approaches can be adopted – dose modelling and dose measuring.

**Table 1: Comparison of imaging parameters for the four systems involved in the study. (GE Healthcare, Buc, Paris,), (Siemens Healthcare, Erlangen, Germany), (Philips Healthcare, Veenpluis, The Netherlands)**

Scanner	Scout view	Axial/Helical	kV	mA	Rotation	Slice thickness	Pitch	Automatic exposure/dose modulation
GE Infinia Hawkeye (1)	No	Axial	140	2.5	30second per rotation (214° exposure)	10mm	NA	NA
GE Infinia Hawkeye 4	No	Helical	140	2.5	30second per rotation (214° exposure)	5mm	1.9	NA
Siemens Symbia T6	Yes	Helical	130	20	0.6s	3mm	0.938	AEC and DOM
Philips Presedence 16	Yes	Helical	120	30	1.5s	5mm	0.938	No

This paper focuses on the preparatory research into dose measurement using thermoluminescent dosimeters (TLDs) and the development of a methodology which would allow the efficient collection of data for the calculation of effective dose from four SPECT/CT systems in common use. It is proposed that the methodology this paper describes could be applied to any dose measurements using TLDs.

## Measuring and modelling dose in CT AC for SPECT/CT

Effective dose (E) is a reflection on the risk of a non-uniform dose distribution in terms of a uniform, or whole-body, exposure [3]. The aim of E is to provide a dose quantity that is related to the probability

of health detriment due to stochastic effects [4]. Calculation of E involves the weighted sum of doses to tissues/organs that are known to be sensitive to radiation [3, 5, 6]. The use of E is not without its critics and, as noted by Martin [4] and Brenner [7], over reliance is often placed on effective dose values and the associated risk estimates based upon it. However as Dietze et al [8] note, E applies to a reference person and is not intended to provide a measure of risk to individuals. Therefore the use of E was deemed appropriate to allow comparison of dose from the different manufacturer's and different systems' approaches to CTAC for MPI acquisitions.

Dose analysis for diagnostic CT can be carried out using mathematical simulations (e.g. Monte Carlo modelling) by commercially available software such as that developed by ImPactscan [9-11] or by using direct measurements [5, 12]. The latter would involve using dosimeters, such as thermoluminescent detectors (TLDs) or digital Mosfet dosimeters, placed within a suitable phantom [13, 14].

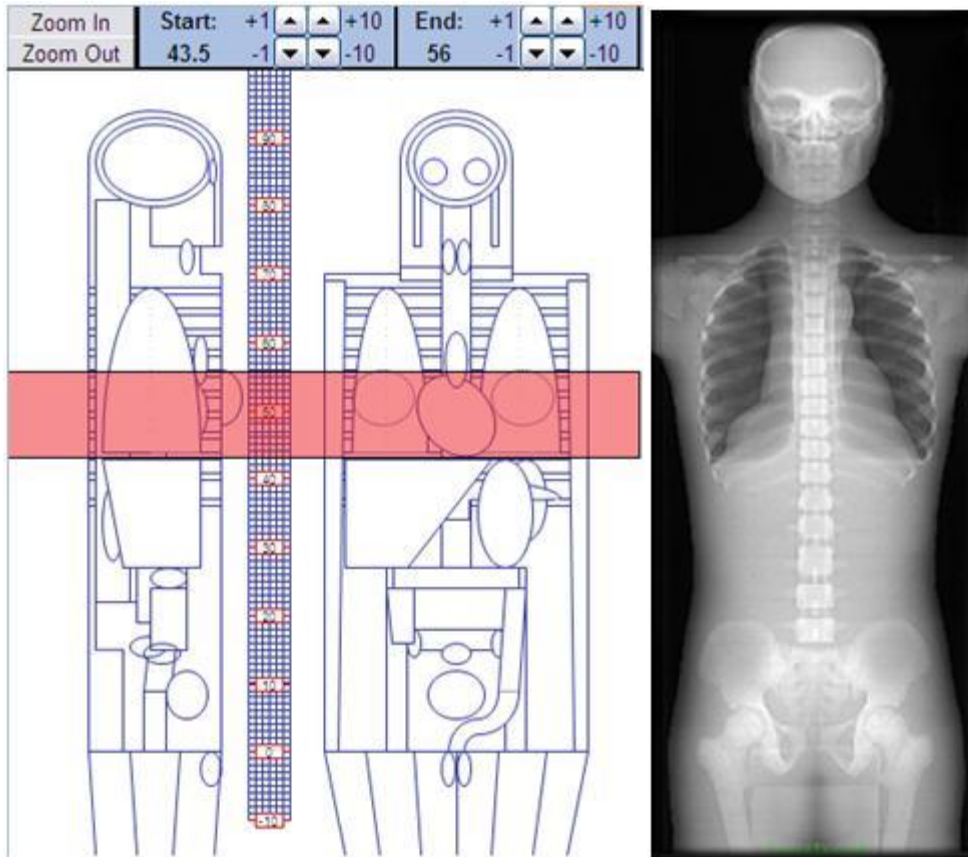
Software simulation allows for quick and easy calculation of effective dose [9, 13], however accurate results are dependent on selecting the correct CT unit within the software as calculations take into account specific features of each CT unit (e.g. radiation quality and field geometry). Selection of the correct scanner and parameters for some SPECT/CT systems is possible as some manufacturers have combined CT systems into their hybrid gamma cameras that are identical to their standalone systems. However, some manufacturers have developed new technology (often termed low-dose CT) specifically for attenuation correction of SPECT image data. These systems, and some of the more recent multi-slice CT scanners, are currently not included in dose simulation software, this means that dose simulation has to rely on "best fitting" the attributes of these scanners to those of a similar design [5, 9, 12, 13]. As noted by Groves et al [13] this introduces the potential for significant error in the estimated doses.

Underestimation using computer simulation is frequently reported with magnitudes between 18 and 40% [5, 12, 13]. Reasons for these underestimations have been explained by the differences in the physical dosimetry phantom characteristics and the Medical Internal Radiation Dose (MIRD) mathematical phantom that is utilised in the ImPact software [5, 9, 12, 13, 15-17]. Close examination of this highlights the simplified geometric shapes of the organs. Subsequently, as can be seen in fig 1, in CT examinations of the mid-thorax, the MIRD phantom suggests that the liver is not exposed in the primary X-ray beam and thus the calculated liver dose would be low. In reality a significant volume of this organ is included in the scan and so will contribute to the E calculations [6]. Consequently, for (SPECT/CT) CT dose analyses, when accurate estimations of E are required, simulations cannot be used and a direct measurement approach has to be adopted.

Figure 1

(a) Image from the Impact SR250 software

(b) CT scout view of the ATOM 701



Despite the reported advantages of direct measurement the process of using TLDs to measure organ dose is regarded as laborious and time consuming [5]. For our research this is particularly true because we use a manual TLD reader (Harshaw 3500). Timings carried out by the research team showed that it took around 90 seconds to read one TLD-100 - meaning a full set of TLDs (n=268 [16, 18]) would require around 6 hours to complete. Any reduction in the number of TLDs would obviously lead to a reduction in the time needed to read the data. Resources available dictated that there was a need to reduce the chipset from the recommended 268 [15] to a number that would allow data collection to be carried out in a timely manner yet would not adversely affect data quality.

A number of papers describe the process of dose measurement from a range of CT examinations and each utilise a different number of TLDs (ranging from 66-268) [16, 18] yet little explanation of how these figures were arrived it is available. Tailoring the number of TLDs to the examination type is common place in dose measurements in dental radiography with many papers crediting Ludlow and Ivanovic [19] with devising the number and locations of TLDs for measurement of effective dose from cone beam CT examinations. Within this paper the authors argue that it is not necessary to

measure all the organs cited as critical in ICRP publication 103 [6] as some are not directly exposed as part of their protocol. Although some will be exposed to scattered radiation, more distal organs would receive less exposure due to their distance from the source and attenuation by tissues in the path of the scatter [19]. Excluding dose measurement of these organs, that is to say assuming a dose of zero, is likely to lead to an underestimation the final value of effective dose. However, organs at the extremes of the phantom (i.e. the brain and the male gonads), have very small tissue weighting factors (brain 0.01 and gonads 0.08 [6]). Application of these factors to any measured equivalent dose suggests that their contribution to effective dose calculations for this examination type would be very small and their exclusion would have negligible effect on the final calculation.

The aim of our work was to take determine if it was possible to take a similar approach to Ludlow and Ivanovich [19] and produce a reduced yet reliable TLD chipset for the ATOM 701-D dosimetry phantom. For the purpose of this work specific emphasis was placed CT attenuation correction (CTAC) for myocardial perfusion imaging however the developed method could be applied to other dose measurements using TLDs.

#### **Method:**

To reduce the number of TLDs required to produce a measurement of effective dose from CTAC for MPI the characteristics of TLD performance and the anatomical region of interest was considered. According to published literature and manufacturer's documentation the lower limit of dose measurement of TLD-100 is 50 $\mu$ Gy [20-22]. Any area that had an absorbed dose less than this figure could be excluded from any measurement. As discussed by Ludlow and Ivanovich [19] TLDs in the z-axis receive decreasing levels of radiation with increasing distance from the exposed area and at some point this level would fall below 50 $\mu$ Gy.

To compare the results of excluding these areas an anthropomorphic dosimetry phantom was loaded with the recommended 268 TLDs in the critical locations identified by the phantom manufacturer [15] and a CT acquisition using the CTAC for MPI parameters performed. To establish the amount of time saved by any reduction in the TLDs, the time taken to load, unload and read 268 chips was recorded and compared to the reduced chipset. A statistical comparison of the organ dose and the effective whole body dose was carried out between the full and reduced datasets. The main purpose of this exercise was to optimise the time taken to collect data while maintaining valid and reliable results.

#### Equipment

Dosimetry measurements were to be carried out using TLD-100 (Thermo-fisher) and a CIRS ATOM dosimetry adult male phantom model 701-B [15, 16]. This version of the phantom consists of 39 contiguous sections of differing density epoxy resin (representing bone, lung and soft tissue) that when put together make up the head and torso. The 701-B is supplied with 5mm pre-drilled holes spaced in a 30x30mm matrix that are filled with tissue equivalent plugs.

#### Preparation of the TLDs

Prior to use, the TLDs underwent a process of cleaning and annealing to improve batch consistency [23] and this preparation adhered to manufacturer's instructions by annealing at 400°C for 1 hour followed by 2 hours at 100°C. Quality control checks on the consistency of TLD performance was carried out by irradiating all the TLDs to a uniform X-ray field using a Wolverson general X-ray unit at 130kV and 20mAs. The TLDs were treated to a post irradiation, pre-read heating cycle of 10minutes

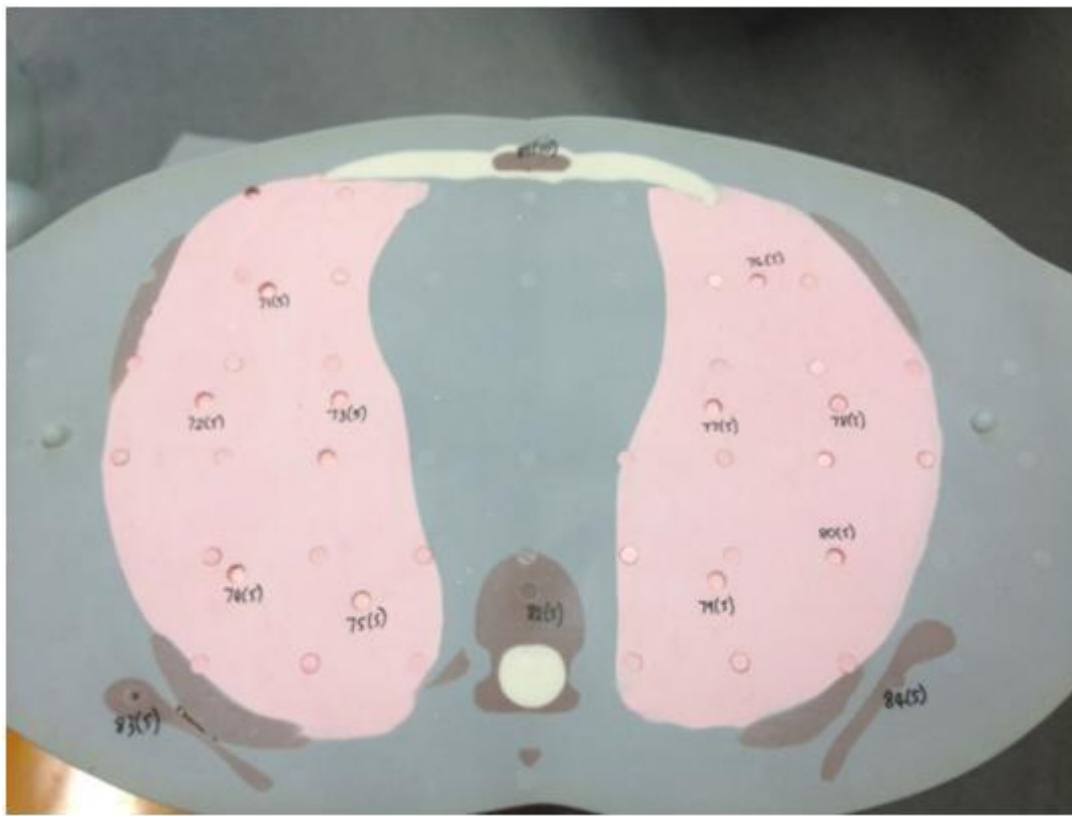
at 100°C as per manufacturer’s recommendations; they were read using a Harshaw 3500 manual TLD reader and WinRems software [20]. The TLDs were again exposed to 130kV 20mAs and read. The TLDs were then grouped into batches of 20 with similar responses.

Calibration was performed on each batch using the same general X-ray unit described above and 100mm of Perspex scattering material and a calibrated Unfors 401 QC meter. Although individual calibration is possible the process is very time consuming and only small improvements to accuracy are noted [24]. The calibration process involved exposure of batches of 5 TLDs using exposure factors of 4, 8, 16, 32 and 64mAs at 130kV. Calibration factors were derived by performing linear regression forced through zero.

#### Preparation of the Phantom

On comparison to the organ map that is available and supplied with the “-D” configuration of the ATOM 701 phantom, it was found that the 30x30mm grid did not align with the detector locations that are optimised for precise dosimetry of specific internal organs [15]. To ensure accurate TLD placement for organ dose measurement the phantom was corrected by drilling additional 5mm holes in the appropriate locations (Fig 2). Whole body effective dose measurement using the ATOM 701-D configuration utilises a total of 268 TLDs over 22 organs.

**Fig 2 ATOM 701-B with additional detector locations as recommended in 701-D organ map [13]**



The focus of the dosimetry work that was being carried out was concerning attenuation correction using CT for myocardial perfusion imaging. This process involves imaging a region of the thorax that includes the left ventricle. To allow for accurate positioning of the phantom and to ensure the same region of the thorax was scanned for each repeat the midline of the anterior and lateral aspects of the phantom were marked using permanent marker. A CT chest examination was carried out on the phantom and using the scout view and axial images the region of the left ventricle was established.

This region was marked on the phantom using permanent marker. Using the laser positioning lights it was possible to ensure that the same region of the phantom would be scanned each time (Fig 3).

**Fig 3 Marking the phantom to ensure accurate and reproducible positioning of the phantom.**



### **Data collection**

The research team had unlimited access to a non-clinically based CT unit and this was used to collect data due to limited access to hybrid SPECT/CT equipment based in clinical practice. It is recognised that this may affect the external validity of the results.

To determine the dose distribution along the z-axis of the phantom TLDs were placed in each slice along the central column of the ATOM dosimetry phantom. A review of the manufacturer's parameters for CTAC for MPI acquisitions suggests that those used by the Philips Presedence system would give the highest dose and would represent "the worst case scenario" in terms of patient dose.

A 16-slice Toshiba CT scanner (Aquillion 16) (Toshiba Medical Systems, Zoetermeer, Netherlands) set up to emulate these acquisition parameters and the phantom was exposed. Following exposure the TLDs were removed from the phantom and treated to a post-irradiation, pre-read heat cycle. Five TLDs remained with the phantom at all times except during acquisition, these were read for background correction and the mean of their readings subtracted from the exposed TLDs.

The process was repeated three times in total to allow for a mean dose to be calculated. The relevant calibration factors established earlier were applied to the TLD readings and the mean dose for the slice number obtained.

### Results

Data was tabulated and a dose profile curve was plotted. The slice numbers where dose fell below the manufacturer's stated threshold were noted. Fig 4 illustrates the distribution of the dose from head to toe within the phantom. Slices 17-21 were exposed to primary beam radiation with scattered radiation being detected above and below this range. As expected, the dose detected decreased as the distance between the region exposed and the TLD increased. Table 2 details the dose for the TLDs in each slice of the phantom (slice one has no location for TLD placement). It can be seen that from slices two to ten and twenty-nine to thirty-nine dose readings are below the 50µGy threshold for TLD-100.

Fig 4 Distribution of dose through the phantom.

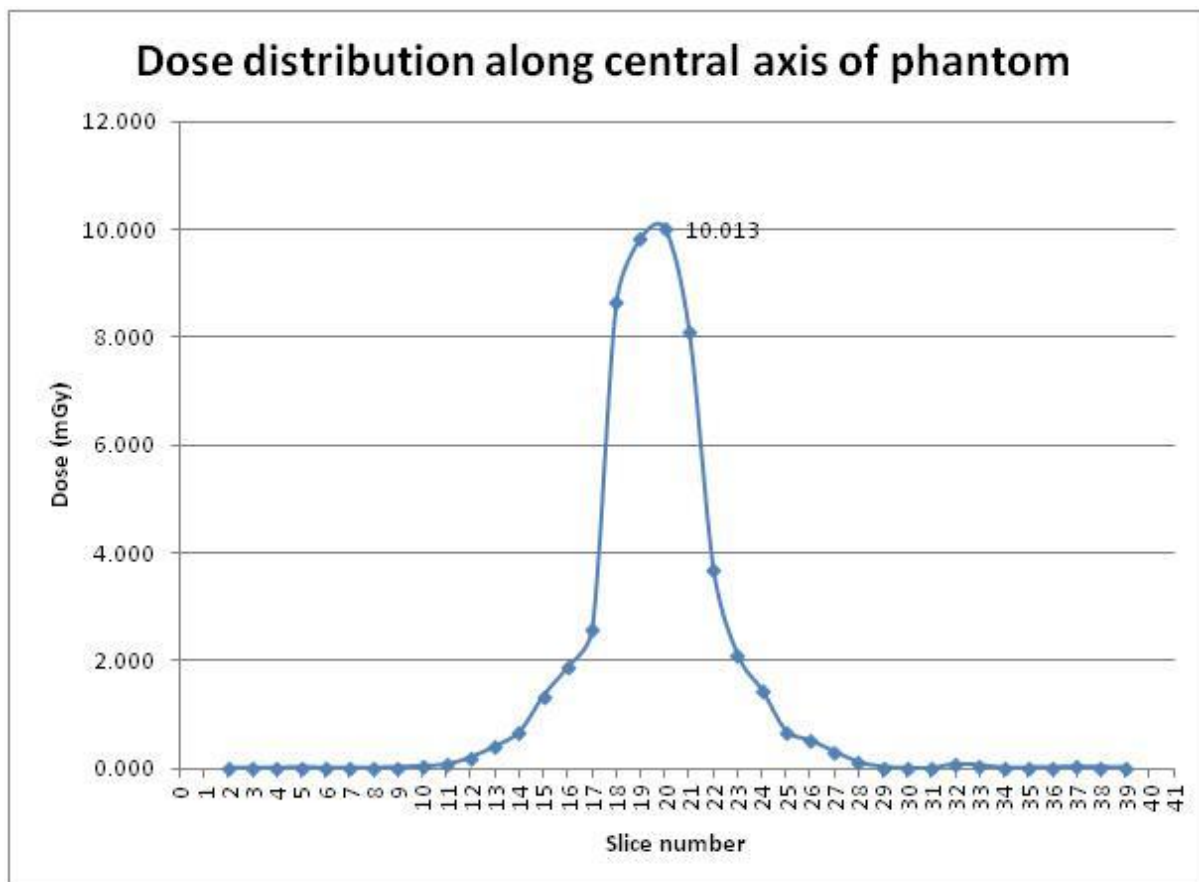


**Table 2 recorded dose of each slice showing where levels were below the 50 $\mu$ Gy threshold.**

Slice number	Mean Dose (mGy)
2	0.00
3	0.00
4	0.00
5	0.02
6	0.00
7	0.01
8	0.00
9	0.02
10	0.03
11	0.07
12	0.20
13	0.32
14	0.67
15	1.34
16	1.88
17	2.57
18	8.66
19	9.83
20	10.01
21	8.11
22	3.68
23	2.10
24	1.44
25	0.68
26	0.51
27	0.37
28	0.10
29	0.02
30	0.00
31	0.00
32	0.07
33	0.05
34	0.00
35	0.01
36	0.01
37	0.02
38	0.02
39	0.01

Comparison of organ and effective dose calculations using the full and reduced data set produced results shown in Table 3. The “weighted organ dose” is the figure produced when the measured organ dose is multiplied by the weighting factor set out in ICRP publication 103 [6]. The data is set out so that an easy comparison can be made between the full and reduced chipsets.

Table 3

Organ	Weighting	Full Chipset		Reduced Chipset	
		Mean Organ dose (mSv)	Mean Weighted dose (mSV)	Organ dose (mSv)	Weighted dose (mSV)
Brain	0.01	0.016	0.000	0.000	0.000
Active bone marrow	0.12	0.868	0.104	0.833	0.100
Adrenals* (Remainder)	0.12*	1.950	0.023	1.950	0.023
Bladder	0.04	0.088	0.004	0.000	0.000
Breast	0.12	3.987	0.478	3.987	0.478
Colon	0.12	0.135	0.016	0.051	0.006
Gall Bladder* (Remainder)	0.12*	0.520	0.006	0.520	0.006
Heart*(Remainder)	0.12*	3.699	0.044	3.699	0.044
Kidneys* (Remainder)	0.12*	0.802	0.009	0.802	0.009
Liver	0.04	2.318	0.093	2.318	0.093
Lungs	0.12	2.652	0.318	2.652	0.318
Oesophagus	0.04	2.175	0.087	2.175	0.087
Pancreas* (Remainder)	0.12*	0.808	0.010	0.808	0.010
Prostate* (Remainder)	0.12*	0.045	0.001	0.000	0.000
Small Intestine* (Remainder)	0.12*	0.144	0.002	0.000	0.000
Spleen* (Remainder)	0.12*	2.163	0.026	2.163	0.026
Stomach	0.12	1.415	0.170	1.415	0.170
Testes	0.08	0.045	0.004	0.000	0.000
Thymus* (Remainder)	0.12*	0.835	0.010	0.835	0.010
Thyroid	0.04	0.255	0.010	0.232	0.009
<b>TOTAL EFFECTIVE DOSE (mSv)</b>			<b>1.413</b>		<b>1.389</b>
<b>% difference</b>			<b>1.75</b>		
Excluded remaining organs: extrathoracic (ET) region, lymphatic nodes, muscle, and oral mucosa.		*Weighting to "remainder organs" averaged across those measured.			

Comparison of the percentage difference in effective dose using a full and reduced chipset indicates a reduction of 1.75% using the reduced dataset. Excluding the organs that would have a dose recorded of 0mSv (Brain, Bladder, Prostate, Small intestine and Testes) a related two way student T-test indicates that there is no statistical difference between the full and reduced data sets ( $p > 0.10$ ).

## **Discussion**

From the results it is suggested that this optimisation process and the arguments behind it could be applied to other areas of radiography. Exclusion of organs where dose is small will lead to underestimation of E but this under estimation is considered to be negligible [19] and in the case of our work it resulted in a reduction of E of 1.75%, which demonstrated no statistical difference.

In our research a number of organs demonstrated a 100% reduction in dose (brain, prostate and testes) yet the impact on the final calculation of E is small due to the small weighting factor that is applied to the organ dose. A 62% reduction is noted in the organ dose for the colon due to the exclusion of TLDs located in the caecum, distal ascending and descending colon and the sigmoid colon. If comparison of organ dose is to be made then it is advisable that the whole of the organs with the highest weighting factors (i.e. breast, colon, lungs and stomach) should be included in any measurement. However, as stated in the context of our research the exclusion of the low dose regions and organs had an insignificant effect on effective dose calculations.

Our empirical work was carried out on a standalone CT system however the parameters used simulated those that would be used by a similar system that is part of the Philips Presedence hybrid system. These exposure factors would suggest that this system and these factors would result in the highest patient dose. However to ensure external validity the process will be carried out on the range of systems that form part of the main study.

It is recognised that the dose profile could be unique to each acquisition protocol, i.e. it will be affected by kV, mA, slice thickness/pitch, and in some cases it may be necessary to use the full complement of TLDs to measure E if larger regions are to be imaged (such as CT examination of the abdomen and pelvis). Similarly the type of TLD used will affect the shape of the profile curve with the more sensitive TLD-100H likely to produce a wider dose profile.

Our experiment to establish the dose distribution has led to a reduced number of TLDs required and to give an accurate measure of effective dose for CTAC for MPI. This method has made the process of dose measurement more efficient and a less laborious task. In the case of this experiment there was a 30.6% reduction in the required number of TLDs (268 to 186 per scan). This equates to approximately 6 ½ hours less reading time per measurement (three repeats per scan) using the manual TLD reader.

## **Conclusion**

The use of TLDs for effective dose measurement is a time consuming process. By producing a dose profile of the ATOM 701-D we have established that it is possible to reduce the total number of TLDs needed by excluding the regions where the detected dose is below a recordable level. Further work is planned using the more sensitive TLD-100H and repeated exposure of the same TLD to establish if the profile differs and more TLDs are required to give an accurate measurement of effective dose.

1. Bybel, B., et al., SPECT/CT Imaging: Clinical Utility of an Emerging Technology<sup>1</sup>. *RadioGraphics*, 2008. 28(4): p. 1097-1113.
2. International Atomic Energy Agency, *Clinical Applications of SPECT/CT: New Hybrid Nuclear Medicine Imaging System 2008*, Vienna: International Atomic Energy Agency.
3. McCollough, C.H., J.A. Christner, and J.M. Kofler, How Effective Is Effective Dose as a Predictor of Radiation Risk? *American Journal of Roentgenology*, 2010. 194(4): p. 890-896.
4. Martin, C.J., Effective dose: how should it be applied to medical exposures? *British Journal of Radiology*, 2007. 80(956): p. 639-647.
5. Hashemi-Malayeri, B.J. and J.R. Williams. A practical approach for the assessment of patient doses from CT Examinations. 2003 [cited 2012 Retrieved 10th January]; Available from: [www.dundee.ac.uk/medphys/documents/hashemi.pdf](http://www.dundee.ac.uk/medphys/documents/hashemi.pdf).
6. International Commission On Radiological Protection, *The 2007 Recommendations of the International Commission on Radiological Protection*. ICRP Publication 103. Ann, 2007. 37(2-4).
7. Brenner, D.J., Effective dose: a flawed concept that could and should be replaced. *British Journal of Radiology*, 2008. 81(967): p. 521-523.
8. Dietze, G., J.D. Harrison, and H.G. Menzel, Effective dose: a flawed concept that could and should be replaced. Comments on a paper by D J Brenner (*Br J Radiol* 2008;81:521–3). *British Journal of Radiology*, 2009. 82(976): p. 348-351.
9. *ImPACT, CT Patient Dosimetry Calculator*, 2003, Medical Devices Agency: London.
10. Jones, D.G. and P.C. Shrimpton, *Normalised Organ Doses for X-Ray Computed Tomography Calculated Using Monte Carlo Techniques*. NRPB-SR250, 1993.
11. *ImPACT. Imaging Performance Assessment of CT Scanners*. [cited 2012 22nd April]; Available from: <http://www.impactscan.org>.
12. Geleijns, J., et al., Comparison of two methods for assessing patient dose from computed tomography. *British Journal of Radiology*, 1994. 67(796): p. 360-365.
13. Groves, A.M., et al., 16-detector multislice CT: dosimetry estimation by TLD measurement compared with Monte Carlo simulation. *British Journal of Radiology*, 2004. 77(920): p. 662-665.
14. Hintenlang, D. TH-C-301-03: Utilization of MOSFET Dosimeters for Clinical Measurements in Radiology. 2011. AAPM.
15. *CIRS Tissue Simulation and Phantom Technology, Adult Male Phantom Model Number 701-D Appendix 5*, 2010, CIRS, Inc: Virginia, USA.
16. *CIRS Tissue Simulation and Phantom Technology. Dosimetry Verification Phantoms Model 701-706 Data Sheet*. 2012 [cited 2012 19th January]; Available from: [http://www.cirsinc.com/file/Products/701\\_706/701\\_706\\_DS.pdf](http://www.cirsinc.com/file/Products/701_706/701_706_DS.pdf).
17. The Phantom Laboratory. *The RANDO Phantom, RAN100 and RAN11 technical data sheets*. n.d. [cited 2012 19th January]; Available from: [http://www.phantomlab.com/library/pdf/rando\\_datasheet.pdf](http://www.phantomlab.com/library/pdf/rando_datasheet.pdf).
18. Paul, J., et al., Estimation and comparison of effective dose (E) in standard chest CT by organ dose measurements and dose-length-product methods and assessment of the influence of CT tube potential (energy dependency) on effective dose in a dual-source CT. *European Journal of Radiology*, 2012. 81(4): p. e507-e512.
19. Ludlow, J.B. and M. Ivanovic, Comparative dosimetry of dental CBCT devices and 64-slice CT for oral and maxillofacial radiology. *Oral Surgery, Oral Medicine, Oral Pathology, Oral Radiology, and Endodontology*, 2008. 106(1): p. 106-114.
20. Thermo Scientific. *Product Overview: Materials and Assemblies for Thermoluminescence Dosimetry*. 2007 [cited 2012 7th March]; Available from: <https://fscimage.thermoscientific.com/images/D10472~.pdf>.
21. Kron, T., *Thermoluminescence dosimetry and its applications in medicine -part 1: Physics, Materials and Equipment*. *Australasian Physical & Engineering Sciences in Medicine* 1994. . 17: p. 175-199.

22. Mueller, J., In-vivo CT Dosimetry During Virtual Colonoscopy, 2011, The University of Texas: UT GSBS Dissertations and Theses.
23. Tootell, A., et al., Reducing error in TLD dose radiation measurements, in United Kingdom Radiological Congress2012: Manchester.
24. Burke, K. and D. Sutton, Optimization and deconvolution of lithium fluoride TLD-100 in diagnostic radiology. British Journal of Radiology, 1997. 70(831): p. 261-71.

## PAPER 4

### COMPARISON OF EFFECTIVE DOSE AND LIFETIME RISK OF CANCER INCIDENCE OF CT ATTENUATION CORRECTION ACQUISITIONS AND RADIOPHARMACEUTICAL ADMINISTRATION FOR MYOCARDIAL PERFUSION IMAGING

Tootell, A., Szczepura, K., & Hogg, P. (2014). The British journal of radiology, 87(1041), 20140110. doi: <http://dx.doi.org/10.1259/bjr.20140110>

#### **Abstract**

**Objectives:** To measure the organ dose and calculate effective dose from CTAC acquisitions from four commonly used gamma camera SPECT/CT systems.

**Method:** CTAC dosimetry data was collected using thermoluminescent dosimeters on GE's Infinia Hawkeye four and single slice systems, Siemen's Symbia T6 and the Philips Precedence. Organ and effective dose from the administration of  $^{99m}\text{Tc}$ -tetrofosmin and  $^{99m}\text{Tc}$ -sestamibi were calculated using ICRP reports 80 and 106. Using this data the lifetime biological risk was calculated.

**Results:** The Siemens Symbia gave the lowest CTAC dose (1.8 mSv) followed by the GE Infinia Hawkeye single-slice (1.9 mSv), GE Infinia Hawkeye four-slice (2.5 mSv) and Philips Precedence (3.0). Doses were significantly lower than the calculated doses from radiopharmaceutical administration (11 mSv and 14 mSv for  $^{99m}\text{Tc}$ -Tetrofosmin and  $^{99m}\text{Tc}$ -Sestamibi respectively). Overall lifetime biological risks were lower suggesting that using CTAC data posed minimal to the risk to the patient. Comparison of data for breast tissue demonstrated a higher risk than that from the radiopharmaceutical.

**Conclusions:** CTAC doses were confirmed to be much lower than from radiopharmaceutical administration. The localised nature of the CTAC exposure compared to the radiopharmaceutical biological distribution indicated dose and risk to the breast to be higher.

**Advances in knowledge:** This research proved that CTAC is a comparatively low dose acquisition. However, it has been shown that there is increased risk to breast tissue especially in the younger patient. As per legislation justification is required and CTAC should only be used in situations that demonstrate sufficient net benefit.

#### **Introduction**

SPECT/CT has become common place in clinical imaging and a major role for CT is for the attenuation correction (AC) of SPECT data in myocardial perfusion imaging (MPI) [1, 2]. The benefits of CTAC in MPI are well known and many national and international professional organisations recommend its use to improve SPECT MPI diagnostic accuracy [3, 4]. Associated with the CT acquisition is an additional radiation dose which is often considered to be low yet very few papers quantify the dose and the associated risk.

Effective dose is a useful figure that allows for a comparison between different techniques and protocols to be made. However it is widely recognised that the tissue weighting factors are averaged over both genders and all ages and so assessment and comparison of risk for an individual patient or patient group is not advised [5-8]. Lifetime risk of cancer incidence, sometimes referred to as lifetime biological risk is a concept that has been suggested by a number of authors as an alternative to effective dose ( $E$ ) to allow a comparison of risk from non-uniform dose distributions [5-7, 9]. Brenner [5-7] is arguably the strongest advocate for a move to what he terms "effective risk" as it is argued

that  $E$  is based on “questionable science” as the tissue-specific weighting factors used, although based on research, are established by committee decisions and do not take into account differing age and gender dependencies. Wall et al [10] similarly states that  $E$  can and should play a role in radiation protection of radiation workers and members of the public and for the optimisation of techniques involving changes in radiation quality.

The quality of the images generated by CTAC and the clinical evaluation of these to identify incidental extracardiac findings has been discussed in literature [11-13]. Using phantom and human studies it has been shown that CTAC data has the potential to allow a reporter to identify extracardiac pathology. The accuracy and confidence has been shown to vary with the protocols used. This paper measured the organ dose and calculated the  $E$  from CTAC acquisitions from four different protocols. The protocols selected were those pre-set by manufacturers in four commonly used SPECT-CT scanners and were considered to be suitable to produce data of adequate quality to allow attenuation and scatter correction. The aim was to establish what differences in dose exist from the different protocols when the data produced is used for the same purpose. Using this data the lifetime biological risk was calculated with a specific emphasis on the female breast. To contextualise these figures organ,  $E$  and lifetime biological risks from the administration of radiopharmaceuticals ( $^{99m}\text{Tc}$  Tetrofosmin and  $^{99m}\text{Tc}$  Sestamibi) were calculated from data contained in ICRP reports 80 and 106 [14, 15]. Comparisons were also made to estimated doses using the dose length product (DLP) and published normalised values of effective dose per DLP [16].

## Materials and Methods

Organ dose ( $H_T$ ) was measured using thermoluminescent dosimeters (TLD-100 [LiF], Thermofisher Scientific Massachusetts), and  $E$  was calculated from these values using the ICRP 103 weighting factors [17]. TLDs were placed within critical organs in an adult CIRS ATOM dosimetry phantom (model no 701B, CIRS, Virginia, USA). Four SPECT/CT systems were selected due to the variations in the CTAC protocols. The systems included: GE Infinia Hawkeye (single slice), GE Infinia Hawkeye (4 slice) (GE Healthcare, Buckinghamshire UK), Siemens Symbia T6 (Siemens Healthcare Erlangen, Germany) and Philips Precedence (Philips Healthcare, Amsterdam, Netherlands).

The CIRS ATOM dosimetry verification phantom is made up of the head and torso of an adult male. There are thirty-nine contiguous slices containing differing density epoxy resin (representing bone, lung and soft tissue). The 701B is supplied with 5mm pre-drilled holes spaced in a 30 x 30 mm matrix that are filled with tissue equivalent plugs. Hole configuration had to be modified so that they aligned to specific internal organs. The modification was carried out by drilling additional holes as indicated in the phantom manufacturer’s documentation for organ dosimetry [18].

The location and range to be scanned was established by performing CT scan of the phantom thorax and the upper and lower limit of the left ventricle identified. The scan range was measured and found to be 12 cm. The upper and lower borders of the scan range were marked on the phantom using permanent ink. Radiopaque markers were attached to the phantom to allow localisation on the scan projection radiograph (SPR) on the Siemens and Philips systems. The GE systems do not acquire an SPR as the operator uses the emission data to plan the CTAC range. Using a zero refresh rate on these scanners’ positioning monitors a cobalt-57 source was placed on the marks for no more than five seconds to allow the scan range to be established. Using the reference activity of 3.7 MBq for the Cobalt source, the dose from this in 5 seconds at a distance of 1 cm in air would be  $6.53 \times 10^{-4}$  mGy. This value was considered to be negligible when calculating the dose from the TLDs in the phantom from the CTAC acquisitions.

Thermo-luminescent dosimeters (TLD-100) (Thermo Scientific, Erlangen, Germany) were cleaned and prepared in accordance with Tootell et al [19]. TLDs were organised into batches that ensured that the percentage variation of each batch was between 1.8 and 2.2 %. This was done by annealing and exposing all the TLDs to a uniform exposure of 120kV and 20mAs using a standard X-ray unit (Wolverson Arcoma, Willenhall, UK). The TLDs were ranked in order of response and organised into five batches. Each batch was calibrated using the same general X-ray unit at beam energies equivalent to the CTAC protocols using a calibrated Unfors Mult-O-Meter (Unfors RaySafe, Billdal, Sweden).

The TLDs were placed in a bespoke shielded case for transportation to the nuclear medicine departments involved in the study to prevent exposure to background radiation and any sources of radiation in the nuclear medicine departments. These TLDs were placed in the phantom in critical organs identified in ICRP 103 and the manufacturer user guide of the phantom to allow organ dose to be measured [17, 18, 20] (Table 1)

**TABLE 1 NUMBER OF TLDs USED IN CRITICAL ORGANS**

Organ	Number of TLD
Adrenals	2
Bladder	16
Brain	11
Breast	2
Active bone Marrow	85 Clavicle 20, Cranium 4 Cervical Spine <sup>†</sup> 2 Femora 4 Mandible <sup>◇×</sup> 6 Pelvis 18, Ribs 18 Sternum 4 Thoraco-lumbar Spine 9
Eyes*	2
Gall Bladder	5
Heart	2
Intestine (Small and large)	16 Colon 11 Small intestine 5
Kidneys	16
Liver	30
Lungs	36
Oesophagus	3
Pancreas	5
Prostate	3
Spleen	14
Stomach	11
Testes	2
Thyroid	10
<p>* Not included in effective dose calculations  <sup>†</sup> TLDs located in the anterior of C2 and upper oesophagus were used to calculate extra thoracic organ dose  <sup>◇</sup> TLDs located in the left and right lingula of the mandible and to the left and right of the sublingual fossa were used to calculate salivary gland organ dose  <sup>×</sup> TLDs located in the left and right lingula of the mandible were used to calculate oral mucosa organ dose</p>	

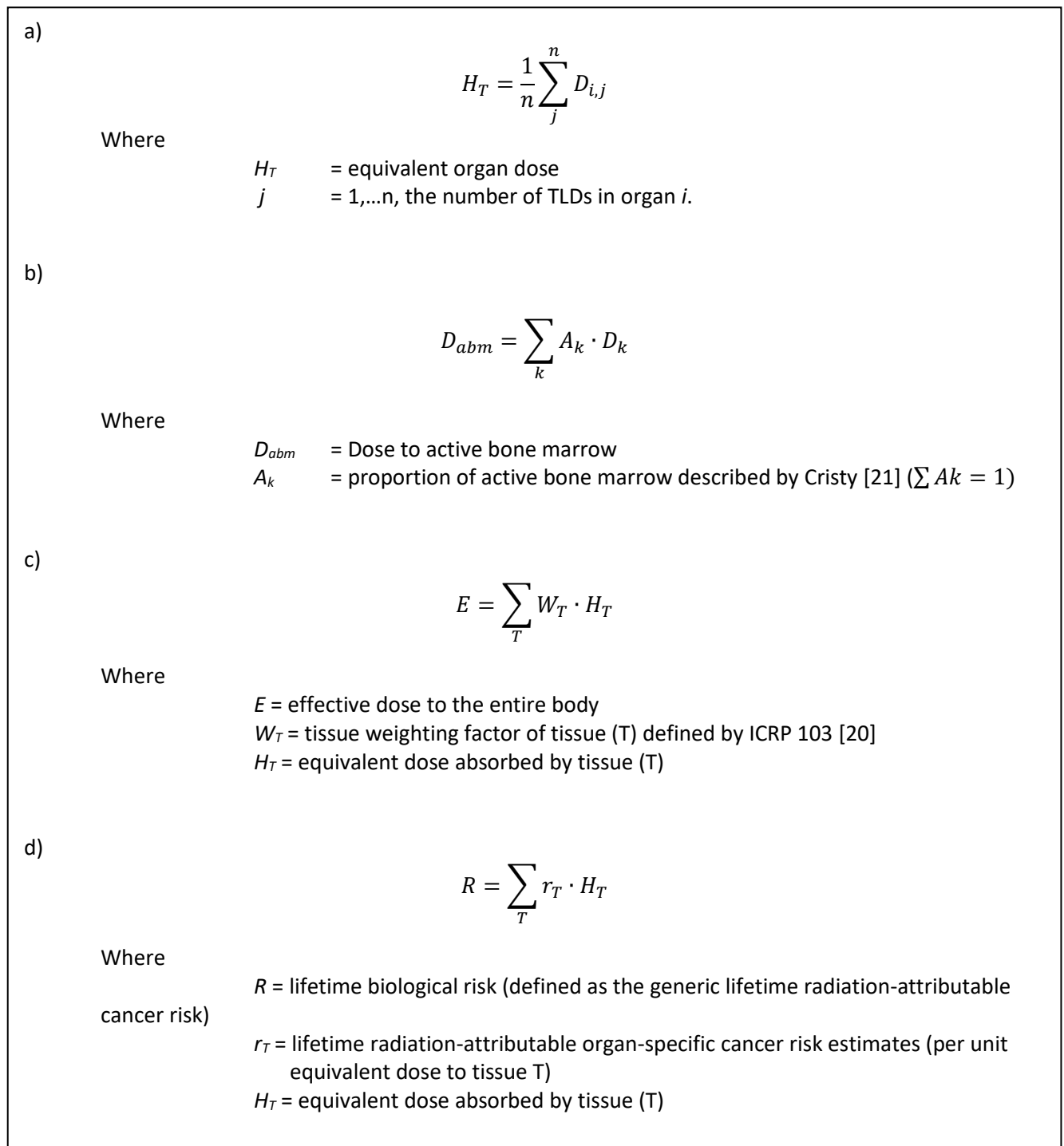
A total of five TLDs remained with the phantom except during imaging for background radiation correction. CTAC imaging was performed using the standard manufacturer protocols for MPI attenuation correction (Table 2).

**TABLE 2 PROTOCOLS USED FOR ATTENUATION CORRECTION FOR MYOCARDIAL PERFUSION IMAGING.**

Scanner	Scout view	Axial/ Helical	kV	mA	Rotation	Slice thickness	Pitch	Automatic exposure/ dose modulation
GE Infinia Hawkeye (1 slice)	No	Axial	140	2.5	30 second per rotation (214° exposure)	10mm	N/A	N/A
GE Infinia Hawkeye (4 slice)	No	Helical	140	2.5	30 second per rotation (214° exposure)	5mm	1.9mm per rotation	N/A
Siemens Symbia T6	Yes	Helical	130	20	0.6s	3mm	0.938	AEC and DOM
Philips Precedence 16	Yes	Helical	120	30	1.5s	5mm	0.938	N/A

Three CTAC exposures were performed on each SPECT-CT system to allow a cumulative dose on the TLDs to be acquired.  $CTDI_{vol}$  and dose length product data was recorded to be used for dose calculation and comparison to measured doses. Reading of the TLDs was carried out using a Harshaw 3500 manual TLD reader (Thermo Electron Corporation, Reading, UK) and WinRems software (Saint-Gobain Crystals & Detectors, Wermelskirchen, Germany). TLD readings were corrected for background and an average value for each TLD calculated. Organ doses were calculated and then used to calculate  $E$  and lifetime biological risk using the equations shown in Figure 1. The conversion coefficient for CT chest imaging was applied to the DLP readings and the resulting dosimetry compared to the measured readings [16].

**FIGURE 1 EQUATIONS FOR (A) ORGAN DOSE, (B) ACTIVE BONE MARROW DOSE, (C) EFFECTIVE DOSE AND (D) LIFETIME BIOLOGICAL RISK [18].**



Active bone marrow dose was calculated using data on bone marrow distribution from Christy [21]. According to statistics, ischaemic heart disease affects a larger proportion of the population of men over 55 and women over 65 [22]. The maximum age considered by Christy is 40 therefore this data

was used in the equation for calculating the equivalent dose to active bone marrow.

Values for  $r_T$  used in this study are tabulated in the Health Protection Agency report HPA-CRCE-028 for 11 cancers of high risk organs over age ranges 0-9, 10-19, 20-29 etc. up to 90-99 [10]. Cancers of other radiosensitive organs share a collective risk estimate. This study followed the method described by Li et al [9] by applying this value to a weighted average dose of other radiosensitive organs (Figure 2).

**FIGURE 2 EQUIVALENT DOSE TO OTHER ORGANS DEFINED IN ICRP 103[17]**

$$H_{other} = \frac{\sum_{other\ organs} w_T \cdot H_T}{\sum_{other\ organs} w_T}$$

Other organs included the salivary glands, brain, heart, kidney, gallbladder, spleen, pancreas, adrenal glands, thymus, small intestine, extrathoracic region and oral mucosa. Data collection using TLDs for lymph nodes, muscle, bone surface and skin was not performed as they are large organs/systems and it was deemed these would contribute very little to the overall  $E$  and lifetime biological risk calculations as only a small proportion of the tissue would be exposed during the imaging process and their exclusion would have negligible effect. The weighting for the remaining organs was averaged over those organs where dose was measured [23].

Organ and  $E$  for the radiopharmaceutical administration were calculated using data provided in ICRP report 80, report 106, diagnostic reference levels (DRL) indicated in the Administration of Radioactive Substances Advisory Committee's publication and guidance published by the British Nuclear Medicine Society and adopted by the British Cardiac Society and the British Nuclear Cardiology Society [15, 24-26]. The total dose and risks for a stress and rest procedure using a total 1600MBq of  $^{99m}\text{Tc}$ -tetrofosmin and  $^{99m}\text{Tc}$ -sestamibi were compared to the additional dose and risk from the CTAC acquisitions performed using parameters described in Table 2. Data for lifetime biological risk incidence was obtained from Wall et al [10].

## Results

Table 3 shows the dose effective dose for a single CTAC acquisition of the four protocols used in the study.

**TABLE 3 ORGAN AND EFFECTIVE DOSES FOR A SINGLE CTAC ACQUISITION MEASURED USING TLDs.**

<u>Organ</u>	Dose (mSv)			
	<u>GE Infinia Hawkeye 1</u>	<u>GE Infinia Hawkeye 4</u>	<u>Siemens Symbia T6</u>	<u>Philips Precedence</u>
Brain	0.0	0.0	0.1	0.1
Salivary glands	0.0	0.0	0.1	0.2
Thyroid	0.1	0.3	0.8	0.4
Oesophagus	1.3	1.9	1.2	2.3
Lungs	1.8	2.7	1.5	2.8
Breast	3.5	3.3	2.0	4.1
Liver	1.3	2.4	1.3	2.4
Stomach	0.5	1.2	0.9	1.5
Colon	0.0	0.1	0.2	0.2
Bladder	0.0	0.0	0.2	0.2
Testes	0.0	0.0	0.1	0.2
Active (red) bone marrow	0.6	0.6	0.9	0.9
Remainder	0.1	0.1	0.1	0.1
Effective Dose	1.0	1.2	0.9	1.5

Table 4 shows the comparison in E measured using TLD and E calculated using the DLP.

**TABLE 4 EFFECTIVE DOSE USING  $DLP \cdot K$  (CONVERSION COEFFICIENT (mSv/mGy\*cm) WHERE  $K=0.017$  [16])**

System protocol	CTDI <sub>vol</sub> (mGy)	DLP (mGy*cm)	Calculated Effective Dose ( $E_{DLP}$ ) (mSv)	Measured Effective Dose ( $E_{TLD}$ ) (mSv)	Percentage difference (%)
GE single slice	4.11	49	0.83	1.0	13.5
GE four slice	3.9	46	0.78	1.2	46.3
Siemens Symbia T6	1.75	21	0.36	0.9	85.7
Philips Precedence	3.5	42	0.71	1.5	71.5

$E$  and organ dose for the lung, oesophagus, colon, liver and stomach from the administration of  $^{99m}\text{Tc}$  Tetrofosmin and  $^{99m}\text{Tc}$  Sestamibi are shown in Table 4 and two CTAC acquisitions (performed for both rest and stress protocol) are shown in Table 5.

**TABLE 5 EQUIVALENT AND EFFECTIVE DOSES FOLLOWING ADMINISTRATION OF RADIOPHARMACEUTICALS FOR A REST/STRESS PROCEDURE AND TWO CTAC ACQUISITIONS.**

Organ	Dose (mSv)					
	$^{99m}\text{Tc}$ Tetrofosmin	$^{99m}\text{Tc}$ Sestamibi	GE single slice	GE four slice	Siemens Symbia T6	Philips Precedence
Lung	5.1	7.1	3.6	5.4	3.1	5.5
Oesophagus	5.3	6.5	2.5	3.8	2.4	5.6
Colon	28.8	34	0.2	0.2	0.6	0.5
Liver	5.3	16	2.6	4.7	2.7	4.9
Stomach	7.4	10	1.1	2.4	1.7	3.1
Breast	3.7	5.7	7.1	6.6	4.1	8.2
$E$ (mSv)	11	13.3	1.9	2.5	1.8	3.0

Following the method described by Wall et al [10] conversion to lifetime cancer risk per million ( $10^6$ ) was performed and are shown in Table 6.

**TABLE 6 TOTAL RISK (PER MILLION) FROM RADIOPHARMACEUTICAL AND CTAC ACQUISITIONS USING DIAGNOSTIC REFERENCE LEVELS AND MANUFACTURER PROTOCOLS**

Examination	Risk (per $10^6$ )			
	Age at exposure			
	40-49	50-59	60-69	70-79
$^{99m}\text{Tc}$ Tetrofosmin	525	386	244	130
$^{99m}\text{Tc}$ Sestamibi	608	447	284	152
CTAC GE single slice	63	52	39	24
CTAC GE four slice	101	83	61	37
CTAC Siemens Sybmia T6	80	63	45	27
CTAC Philips Precedence	103	86	64	40

Consideration was given to the risk to the breast from radiopharmaceutical administration and CTAC acquisition. The phantom used in the study was male and no additional breast tissue was added however, the acquired data allowed for a comparison of the risks within the context of this study.

**TABLE 7 RISK TO BREAST (PER MILLION) FROM RADIOPHARMACEUTICAL AND CTAC ACQUISITIONS USING DIAGNOSTIC REFERENCE LEVELS AND MANUFACTURER PROTOCOLS**

Examination	Risk (per 10 <sup>6</sup> )			
	Age at exposure			
	40-49	50-59	60-69	70-79
<sup>99m</sup> Tc Tetrofosmin	31	31	8	3
<sup>99m</sup> Tc Sestamibi	48	48	12	5
CTAC GE single slice	60	60	15	6
CTAC GE four slice	55	55	14	5
CTAC Siemens Sybmia T6	34	34	9	3
CTAC Philips Precedence	69	69	17	6

## Discussion

Comparison of  $E_{DLP}$  and  $E_{TLD}$  showed significant differences in the two values with  $E_{DLP}$  being consistently lower. This agrees with published literature [27-29]. However, the average percentage difference between the two is 54.2% which far exceeds figures quoted by Groves et al [27] of 18% and Hurwitz et al [29] of 25%. Criticisms of  $k$  state that the factors are based on old technology and old data; they are based on several scanners that were in use circa 1990 and the tissue weighting factors used in their calculation are from ICRP 60 [16, 30, 31]. There are also a number of assumptions made that would increase the error in the calculated effective dose. For example, the patient is assumed to be standard and, as noted by McCollough et al [32], this standard patient is a little thin by today's standards (nominal body mass of 70 kg). Possible sources of error were considered and additional quality checks performed on the TLDs. The batches were checked for uniformity and were found to be within the 2% level established before the experiment commenced at higher and lower doses of X-radiation. The images acquired as part of the CTAC exposure were also compared and it was clear that the same region of the phantom was exposed each time. Whether the cited criticisms of  $k$  are the main contribution to these differences is unclear from this research.

Comparing  $E$  of the CTAC acquisitions to those from the administration of the radiopharmaceuticals it can be seen that these figures are smaller but acquisition of AC data using CT does contribute additional dose to the patient. From this research this is in the magnitude of 7.3% to 27.3%. Comparison of CTAC to the "typical effective dose" for a CT chest of 6.6 mSv supports the popular opinion that CTAC is a low-dose CT procedure [10].

Consideration of risk again highlights large differences between the radiopharmaceutical and CTAC acquisition. When considered with the reported benefits of CTAC in improving the sensitivity and specificity it can be said that the reported benefits of attenuation and scatter correction using CT benefits do outweigh the risks [33-35].

A comparison of doses from the CTAC acquisitions showed some interesting findings. The protocol from the Siemens Symbia T6 gave the lowest  $E$ , this was significantly different to the protocols from the Philips Precedence and GE Hawkeye 4 slice systems (paired T Test,  $p < 0.05$ ). However statistical comparison of the protocols from the Symbia T6 to the GE Infinia Hawkeye single slice showed no statistical difference (paired T Test  $p = 0.37$ ). The Siemens Symbia T6 CT component is a higher specification system that has been shown to produce diagnostic quality CT images so it would be expected that  $E$  would be higher [12]. Close examination of the imaging parameters in Table 2 does highlight two interesting features, including the use of automatic exposure control (AEC) and dose modulation (DOM) during the acquisition. This technology (referred to as CARE Dose4D) manipulates the tube current in two ways. Firstly the tube current is varied based on the attenuation data acquired as part of the SPR. Secondly, attenuation in the patient is measured in real-time during the helical acquisition, where the mA is modulated to equalise the photon flux reaching the detectors during the scan. The aim of both these techniques is to keep noise levels consistent throughout the scan to allow for anatomical variations in attenuation, hence optimising image quality and patient dose.

The GE systems have a low specification CT component with many of the exposure parameters being fixed. On first glance it could be assumed that with a tube current of 2.5 mA, the dose from CTAC acquisitions would be significantly lower than the Siemens which has a mA of 20. However, taking the rotation time into account the effective mAs of each slice is much higher. Calculations using the mA and rotation time and angle of rotation illustrate that an effective mAs of 44.6 is used for each slice in these acquisitions. Performing a T-test between the two GE systems together illustrates a statistically significant difference in dose ( $p = 0.0002$ ), with the four slice system giving the higher dose. Reasons for this could be due to the method of acquisition as the four-slice system acquires data helically rather than axially.

The protocol used by the Phillips Precedence gave the highest  $E$  of the four systems. The Phillips Precedence is a 16 slice "full diagnostic" system but as can be seen in Table 2, parameters used are significantly lower than those that would be used in diagnostic CT imaging. The opportunity for further dose reduction should be recognised by the Operator and options for dose optimisation on an individual patient basis utilised. The authors recognise that the imaging parameters used are set by the manufacturer and a departmental process of optimisation may have the potential to further reduce  $E$ . Manipulation of parameters such as mA, rotation time, pitch and/or acquisition method (helical or axial) have the potential to reduce dose while ensuring adequate data quality.

The phantom used in this study is representative of an adult male phantom and so risk and calculations of  $E$  are specific to this gender. Dose to breast and risk calculations were carried out and are shown in Table 7 however It is recognised that the risk to the female breast is likely to be different to the quoted figures due to the absence of additional breast tissue that would be present in the female phantom but as a comparison within the context of this study, some interesting results were found. This comparison highlights that although the overall lifetime biological risks associated with the CTAC exposure are much lower, organ specific risks may be comparable or higher. For example the addition of a CTAC using the Philips Precedence protocol to a  $^{99m}\text{Tc}$  Tetrofosmin stress and rest study in a 40-49 year old increases the risk to the breast from 31 per million to 100 per million.

## Conclusion

The authors recognise that local optimisation of administered radioactivity and CT imaging parameters should be performed and actual values for  $E$  and risk will vary accordingly. However, as a comparison exercise this paper provides the information on the associated risks of performing CTAC. On comparison to doses and risks from the administration of radiopharmaceutical, the CTAC poses a small increase to risk especially to the older population. However, it has been shown that consideration should be given to risks to individual organs and in this case Practitioners should be aware of the increased risk to breast tissue especially in the younger patient. As per legislation justification is required and CTAC should only be used in situations that demonstrate sufficient net benefit to the patient.

1. Hendel RC, Corbett JR, Cullom SJ, DePuey EG, Garcia EV, and Bateman TM, *The Value and Practice of Attenuation Correction for Myocardial Perfusion SPECT Imaging: A Joint Position Statement from the American Society of Nuclear Cardiology and the Society of Nuclear Medicine*. Journal of Nuclear Medicine, 2002. **43**(2): p. 273-280.
2. Hesse B, Lindhardt TB, Anampa W, Anagnostopoulos C, Ballinger J, Bax JJ, et al., *EANM/ESC Guidelines for Radionuclide Imaging of Cardiac Function*. European Journal of Medical Molecular Imaging, 2008. **35**(4): p. 851-885.
3. Garcia TB, *Introduction to 12-Lead ECG: The Art of Interpretation*. 2011: Jones & Bartlett Learning.
4. Heller GV, Links J, Bateman TM, Ziffer JA, Ficaro E, Cohen MC, et al., *American Society of Nuclear Cardiology and Society of Nuclear Medicine joint position statement: attenuation correction of myocardial perfusion SPECT scintigraphy*. J Nucl Cardiol, 2004. **11**(2): p. 229-30.
5. Brenner DJ, *Effective dose: a flawed concept that could and should be replaced*. British Journal of Radiology, 2008. **81**(967): p. 521-523.
6. Brenner DJ, *Effective Dose- A Flawed Concept that Could and Should be Replaced*, in *International Commission on Radiological Protection*. 2011: Washington DC.
7. Brenner DJ, *We can do better than effective dose for estimating or comparing low-dose radiation risks*. Annals of the ICRP, 2012. **41**(3-4): p. 124-128.
8. Ortiz P, *The use of Effective Dose in Medicine in The 2nd International Symposium on the System of Radiological Protection*. 2013, ICRP: United Arab Emirates.
9. Li X, Samei E, Segars WP, Sturgeon GM, Colsher JG, and Frush DP, *Patient-specific Radiation Dose and Cancer Risk for Pediatric Chest CT*. Radiology, 2011. **259**(3): p. 862-874.
10. Wall BF, Haylock R, Jansen JTM, Hillier MC, Hart D, and Shrimpton PC, *Radiation Risks from Medical X-ray Examinations as a Function of the Age and Sex of the Patient. Report HPA-CRCE-028*. 2011, Health Protection Agency: Chilton.
11. Thompson J, Hogg P, Higham S, and Manning D, *Accurate localization of incidental findings on the computed tomography attenuation correction image: the influence of tube current variation*. Nucl Med Commun, 2013. **34**(2): p. 180-4.
12. Thompson JD, Hogg P, Manning DJ, Szczepura K, and Chakraborty DP, *A Free-response Evaluation Determining Value in the Computed Tomography Attenuation Correction Image for Revealing Pulmonary Incidental Findings: A Phantom Study*. Academic radiology, 2014. **21**(4): p. 538-545.
13. Tootell A, Vinjamuri S, Elias M, and Hogg P, *Clinical evaluation of the computed tomography attenuation correction map for myocardial perfusion imaging: the potential for incidental pathology detection*. Nucl Med Commun, 2012. **33**(11): p. 1122-6.
14. ICRP, *Radiation Dose to Patients from Radiopharmaceuticals (Addendum to ICRP Publication 53)*, in *ICRP Publication 80*. 1998, ICRP.
15. ICRP, *Radiation Dose to Patients from Radiopharmaceuticals (Addendum 3 to ICRP Publication 53)*, in *ICRP Publication 106*. 2008, ICRP.
16. European Commission and EUR 16262 EN, *European guidelines for quality criteria for computed tomography*. 1999, European Commission: Luxembourg.
17. ICRP, *The 2007 Recommendations of the ICRP*, in *ICRP Publication 103*. 2007, Ann. ICRP. p. 2-4.
18. CIRS Tissue Simulation and Phantom Technology, *Adult Male Phantom Model Number 701-D Appendix 5*. 2010, CIRS, Inc: Virginia, USA.
19. Tootell A, Szczepura K, and Hogg P, *Optimising the number of thermoluminescent dosimeters required for the measurement of effective dose for computed tomography attenuation correction data in SPECT/CT myocardial perfusion imaging*. Radiography, 2013. **19**(1): p. 42-47.
20. CIRS Tissue Simulation and Phantom Technology. *Dosimetry Verification Phantoms Model 701-706 Data Sheet*. 2012 [cited 2012 19th January]; Available from: [http://www.cirsinc.com/file/Products/701\\_706/701\\_706\\_DS.pdf](http://www.cirsinc.com/file/Products/701_706/701_706_DS.pdf).

21. Cristy M, *Active bone marrow distribution as a function of age in humans*. Phys Med Biol, 1981. **26**(3): p. 389-400.
22. Townsend N WK, Bhatnagar P, Smolina K, Nichols M, Leal J, Luengo-Fernandez R, Rayner M,, *Coronary heart disease statistics 2012 edition*. 2012, British Heart Foundation: London.
23. Brady Z, Ramanauskas F, Cain TM, and Johnston PN, *Assessment of paediatric CT dose indicators for the purpose of optimisation*. British Journal of Radiology, 2012. **85**(1019): p. 1488-1498.
24. ARSAC, *Notes for Guidance on the Clinical Administration of Radiopharmaceuticals and Use of Sealed Radioactive Sources 2006*, Health Protection Agency for the Administration of Radioactive Substances Advisory Committee: Oxford, UK.
25. Arumugam PH, M. Reyes, E. Sabharwal, N. Tonge, C. Underwood, SR. *Procedure Guidelines for Radionuclide Myocardial Perfusion Imaging with Single-Photon Emission Computed Tomography (SPECT)*. 2012 [cited 2013 13th November ]; Adopted by the British Cardiac Society, the British Nuclear Cardiology Society, and the British Nuclear Medicine Society]. Available from:  
[http://www.bnms.org.uk/images/stories/Procedures\\_and\\_Guidelines/MPS\\_procedure\\_guidelines\\_Final\\_12.pdf](http://www.bnms.org.uk/images/stories/Procedures_and_Guidelines/MPS_procedure_guidelines_Final_12.pdf).
26. ICRP, *Diagnostic reference levels in medical imaging: review and additional advice*. Ann ICRP, 2001. **31**(4): p. 33-52.
27. Groves AM, Owen KE, Courtney HM, Yates SJ, Goldstone KE, Blake GM, et al., *16-detector multislice CT: dosimetry estimation by TLD measurement compared with Monte Carlo simulation*. Br J Radiol, 2004. **77**(920): p. 662-5.
28. Hashemi-Malayeri BJ and Williams JR. *A practical approach for the assessment of patient doses from CT Examinations*. 2003 [cited 2012 10th January]; Available from:  
[www.dundee.ac.uk/medphys/documents/hashemi.pdf](http://www.dundee.ac.uk/medphys/documents/hashemi.pdf).
29. Hurwitz LM, Reiman RE, Yoshizumi TT, Goodman PC, Toncheva G, Nguyen G, et al., *Radiation Dose from Contemporary Cardiothoracic Multidetector CT Protocols with an Anthropomorphic Female Phantom: Implications for Cancer Induction*. Radiology, 2007. **245**(3): p. 742-750.
30. ICRP, *1990 Recommendations of the ICRP*, in *ICRP Publication 60*. 1991, Ann. ICRP. p. 1-3.
31. McNitt-Gray M, *Assessing Radiation Dose: How to Do It Right*, in *2011 AAPM CT Dose Summit*. 2011: Denver.
32. McCollough CH, Leng S, Yu L, Cody DD, Boone JM, and McNitt-Gray MF, *CT Dose Index and Patient Dose: They Are Not the Same Thing*. Radiology, 2011. **259**(2): p. 311-316.
33. Dorbala S, Di Carli MF, Delbeke D, Abbara S, DePuey EG, Dilsizian V, et al., *SNMMI/ASNC/SCCT Guideline for Cardiac SPECT/CT and PET/CT 1.0*. Journal of Nuclear Medicine, 2013. **54**(8): p. 1485-1507.
34. Giubbini RM, Gabanelli S, Lucchini S, Merli G, Puta E, Rodella C, et al., *The value of attenuation correction by hybrid SPECT/CT imaging on infarct size quantification in male patients with previous inferior myocardial infarct*. Nucl Med Commun, 2011. **32**(11): p. 1026-32.
35. Ou X, Jiang L, Huang R, Li F, Zhao Z, and Li L, *Computed tomography attenuation correction improves the risk stratification accuracy of myocardial perfusion imaging*. Nucl Med Commun, 2013. **34**(5): p. 495-500

## PAPER 5

### EFFECT OF RECONSTRUCTION METHODS AND X-RAY TUBE CURRENT–TIME PRODUCT ON NODULE DETECTION IN AN ANTHROPOMORPHIC THORAX PHANTOM: A CROSSED-MODALITY JAFROC OBSERVER STUDY

Thompson, J. D., Chakraborty, D. P., Szczepura, K., Tootell, A. K., Vamvakas, I., Manning, D. J., & Hogg, P. (2016). *Medical Physics*, 43(3), 1265-1274. doi: <http://dx.doi.org/10.1118/1.4941017>

#### Introduction

Radiation dose in computed tomography (CT) is a highly topical concern in medical imaging and there is a recognition of increased dose with the use of multi-detector CT (MDCT).[1-5] However, radiation dose risk needs to be balanced with benefits, and MDCT has been a significant development in acute medicine[6-9] where a quick and accurate diagnosis is important for patient outcome.

Low noise and high spatial resolution are important considerations for accurate radiological CT reports. Until recently, filtered back projection (FBP) had been the image reconstruction method of choice. Unfortunately, data non-linearity and image reconstruction artefacts are prevalent with FBP and a loss of spatial resolution is an unwanted trade-off when attempting to reduce image noise. [10-12]<sup>10-12</sup> Improved computer processing capability currently allows the use of iterative reconstruction (IR) in CT as an alternative to FBP. Incorporating physical models into the algorithm allows image quality to be maintained at lower dose and lower noise levels [13] and dose reductions ~ 23-79% have been reported when using IR in place of FBP [14-17].

Adaptive iterative dose reduction 3D (AIDR<sup>3D</sup>, *Toshiba Medical Systems, Minato-ku, Japan*) is a recently developed iterative reconstruction (IR) algorithm for CT data, where it has been suggested that using AIDR<sup>3D</sup> in place of FBP could allow dose saving ~ 75% [18]. A detailed explanation of how AIDR<sup>3D</sup> works in the projection and reconstruction domains has been published [19].<sup>19</sup>

Several studies [19-21] have assessed this new algorithm using objective and subjective measures. Common to all is an objective evaluation of image noise, evaluating either the standard deviation of pixels values in regions of interest in various quasi-uniform anatomical regions [19-20] or the noise power spectrum (NPS) in a phantom model [21]. All studies report reductions in image noise. Spatial resolution was assessed objectively using the modulation transfer function<sup>21</sup> and subjectively using a 5-point scale to assess the pulmonary vessels [20]; both of these methods suggested that spatial resolution (or sharpness) was reduced with AIDR<sup>3D</sup> in comparison to FBP [20-21]. Subjective evaluations of images, using 5-point visual scoring systems, were used to assess diagnostic acceptability [19-21], artefacts [20-21], and pathology [19]. With one exception subjective image quality was stated as being better with AIDR<sup>3D</sup> [20]. Despite the inconsistencies listed above, all studies suggested that AIDR<sup>3D</sup> could offer a large dose reduction in the thorax: by a factor of 6 from 150 mAs down to 25 mAs, [19] when using a low dose acquisition in place of a standard dose acquisition, [20] or as an average of 36% over a range of tube current-time product settings (comparing FBP and AIDR<sup>3D</sup> directly) [21]. Ohno et al [19] and Yamada et al [20] both used the computed tomography dose index (CTDI) to assess radiation dose, when in fact it is only a measure of absorbed dose to a standardized phantom and does not account for patient size and potential cancer risk [22]. The above studies are further limited by a the lack of an ROC type analysis and low case numbers: e.g., 37, and 50 patients respectively [19-20].

We are aware of only one paper that assesses the value of IR in the thorax with observer performance methods. A study by Katsura et al [23] assessed the value of using a model-based IR algorithm (MBIR) against adaptive statistical IR (ASIR; *GE Healthcare, Waukesha, WI*). An ultralow-dose MBIR acquisition with a fixed tube current was compared to a low-dose acquisitions using ASIR and automatic tube current modulation. The study used 59 patients and 2 observers, with 84 nodules present in 41 patients, with the remaining 18 patients having no lung nodules. Nodule detection rates were similar between the two acquisitions ( $p=0.57$ ), and the authors reported dose saving of more than a factor of 4, from a DLP of 66mGy-cm to 14.5mGycm. However, it is not possible to claim that nodule detection rates were equivalent without performing an equivalence study [24,25]. Stated simply, not being able to reject the null hypothesis of equal performance does not imply the two modalities have equal performances. The work of Katsura et al differs from previous work and this study in that they compared two IR algorithms and not FBP. In this work we make methodological improvements on previous studies to evaluate the performance of AIDR<sup>3D</sup> and FBP for nodule detection over a range of tube current-time product. Initial results questioning the advantages of IR over FBP in an anthropomorphic chest phantom were presented as a conference paper in early 2015 [26].

## Method

A free-response study was conducted using an anthropomorphic chest phantom to determine nodule detection performance for images constructed using FBP and IR over a range of mAs values. This was combined with an accurate assessment of radiation dose using a separate phantom.

## Phantoms

An anthropomorphic chest phantom (*Lungman N1 Multipurpose Chest Phantom, Kyoto Kagaku Company, Japan*) representing a 70Kg male was loaded with simulated nodules measuring 5, 8, 10 and 12mm in spherical diameter and +100, -630 and -800 Hounsfield Units (HU) densities. The higher electron density (+100HU) nodules are composed of polyurethane, hydroxyapatite and a urethane resin; the lower electron density (-630 and -800HU) nodules are composed of urethane.

An ATOM 701D (*ATOM 701; CIRS, Norfolk, VA*) whole-body dosimetry verification phantom was used to measure organ doses. Prior to data collection the median-sagittal and mid-coronal planes, and the scan range that covered the lung apices and costo-diaphragmatic recesses, were marked on the dosimetry phantom using an indelible marker. This allowed accurate and reproducible positioning and scanning of the dosimetry phantom.

## Image Acquisitions

All image acquisitions were completed on a Toshiba Aquilion One 320-slice MDCT scanner (*Toshiba Medical Systems, Minato-ku, Japan*) in volume mode. Each volume covered 160mm in the transaxial (z-axis) plane, where the volume is also the collimation size in this instance, and three volumes were required to provide complete coverage of the anthropomorphic chest phantom. A tube current-time product range (10, 20, 30 and 40 mAs) was investigated for both reconstruction algorithms (FBP and IR) while all other CT acquisition parameters remained constant (120kVp, 0.5 second rotation time, pitch 1, 64x0.5 mm detector configuration, 1mm slice reconstruction, 512x512 matrix size, 320 mm scan and reconstruction field of view, 0.625mm pixel size, a medium bowtie filter, appropriate for the 320mm field of view). The images were reconstructed with FBP and AIDR<sup>3D</sup>, Figure 1.

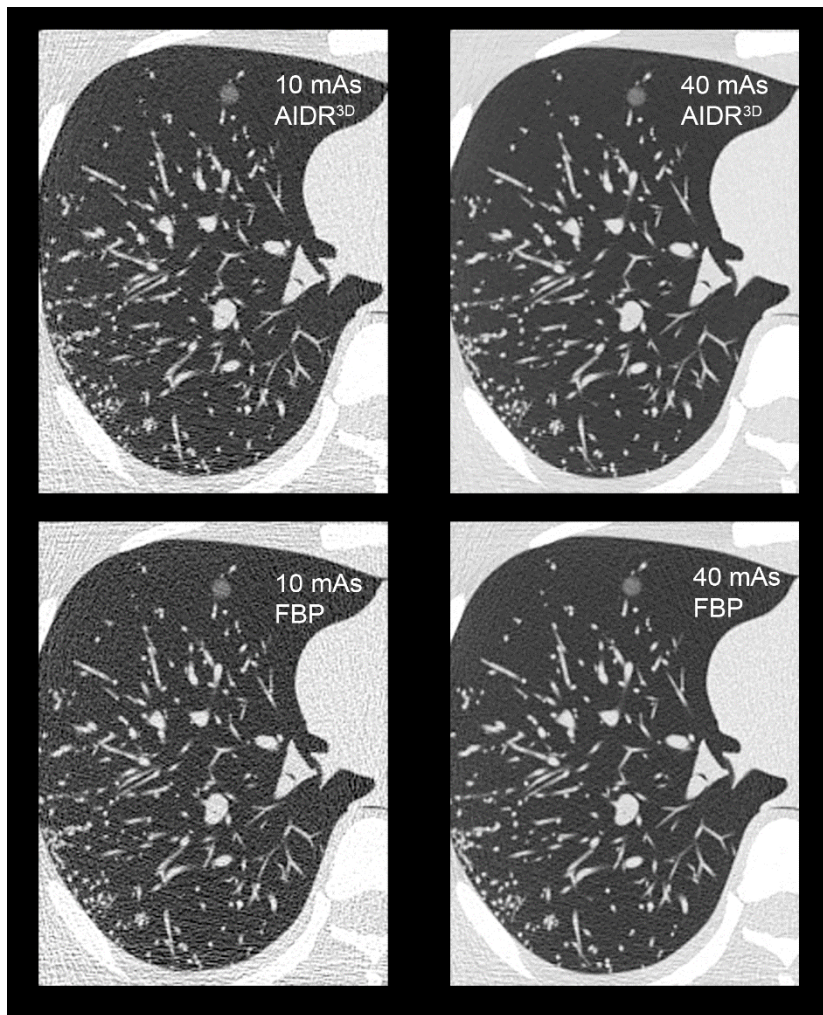


**Figure 1: Sample images to demonstrate the effect of tube current-time product (horizontally) and reconstruction method (vertically). A simulated nodule measuring 10mm and -630HU is visualised in the antero-medial aspect of the simulated lung.**

The anthropomorphic chest phantom was loaded with three different nodule configurations. Nodules were distributed as described in Table 1, with nodules considered peripheral if they were in close proximity to the chest wall. For each tube current-time product and image reconstruction, 34 abnormal transaxial image slices (containing 1-3 nodules, mean  $1.35 \pm 0.54$ ) and 34 normal transaxial image slices corresponding to the same anatomical position for each modality were chosen for the observer study. Nodule positions were recorded at the time of insertion, and confirmed on the lowest noise images (40 mAs, reconstructed with AIDR<sup>3D</sup>) to act as the truth (gold standard) for the observer study.

Zone	Anterior		Posterior		Central		Peripheral	
	Right	Left	Right	Left	Right	Left	Right	Left
Upper	-	3	3	1	-	1	-	2
Mid	2	1	9	7	3	4	2	5
Lower	2	-	3	2	3	2	4	5

## Dosimetry

TLDs (*TLD100H LiF:Mg,Cu,P, Thermo Scientific, Waltham, MA*) (n=271 plus n=5 for background correction) were grouped into batches of similar response (intra batch variation  $\leq 2\%$ ). Processing of the TLDs was carried out using Harshaw 3500 manual TLD reader (*Thermo Scientific, Waltham, MA*). Each batch of TLDs was calibrated. Annealed TLDs were positioned within the dosimetry phantom at locations corresponding to 23 of the critical organs identified in ICRP report 103<sup>27</sup> for each of the four imaging conditions. Effective dose was calculated from the organ doses by applying radiation and tissue-weighting factors specified in the same publication [27].

Effective risk was calculated using PCXMC software (*STUK, Helsinki, Finland*), a Monte Carlo program for estimating patient doses. The software estimates the patient risk of death due to radiation-induced cancer, according to the risk model of the BEIR VII committee [28,29].

This CT system acquires data in volume mode. The volume of 160mm is not fully contained within the dimensions of a typical CT dose phantom and standard pencil CT ionization chamber [30]. This CT scanner reports CTDI<sub>vol</sub> values that are adjusted for wide beam CT when acquiring data in volume mode.

## Observer Study

Six radiologists (12.2±9.1 years reporting experience) and five radiographers trained to perform CT examination (18±5.3 years CT imaging experience) completed the observer study. For each combination of tube current-time product and reconstruction method, each observer interpreted 68 cases (i.e., single transaxial CT images) using the FROC paradigm. The interpretations were performed in two sessions, each lasting approximately 1 hour. Each observer viewed the cases in a different randomised order. They were unaware of the tube current-time product and reconstruction methods used to generate each image, but were informed that half of the images contained 1-3 simulated nodules of varying size and contrasts and the remaining contained none. All observers completed a training exercise prior to the main study. Ten non-identifiable images containing nodules and ten not containing any nodules, which were cases not used in the main study, were used to demonstrate the appearance of the anthropomorphic chest phantom and simulated nodules, while also giving the opportunity to learn how to localise nodules and use the rating scale and familiarize themselves with the user interface. The same monitor (PG21HQX, Wide, 20", LCD, Wide Corporation, Korea) (1536x2080 pixels, 3.2 megapixel resolution) was used for all observers and evaluations under the same controlled viewing conditions.

The free-response receiver operating characteristic (FROC) method was used to acquire the observer data. Observers were instructed to mark the centre of each simulated nodule using a single mouse click; this would cause a "pop-up" a slider bar rating scale to appear by which they could rate confidence on a 1-10 integer scale. Using a 20-pixel acceptance radius, marks were classified as

nodule localisation (LL) if they were within the acceptance radius of the nearest nodule, or non-nodule localisation (NL). Image display and FROC study functionality was managed by ROCView display and data acquisition software [31]. Images were viewed on a fixed lung window (1500, -500) to maximise nodule visibility and reduce observer variability.

### Statistical Analysis

In this study the equally weighted JAFROC figure of merit was used, denoted by  $\theta$  [32]. The JAFROC figure of merit is the weighted empirical probability that a nodule rating is higher than any rating on a normal case [32]. In this study all nodules on a case were assigned the same weight. The weighting gives equal importance to each case, independent of the number of true nodules in it. To check for consistency, inferred-ROC analysis was also performed. To do this we used the highest rating on a case to define the inferred-ROC rating for that case.

In this study there were two *factors* (in the statistical sense) that would ultimately influence the performance of the observer – tube current-time product and image reconstruction method. In a typical analysis of multi-modality multiple reader multiple case, typically termed an MRMC ROC/FROC study, modality is considered as a single factor with  $I$  levels, where  $I$  is usually small, but greater than 2. For example, if comparing two image reconstruction methods,  $I = 2$ . The measure of performance or figure of merit for modality  $i$  ( $i = 1, 2, \dots, I$ ) and reader  $j$  ( $j = 1, 2, \dots, J$ ), where  $J$  is the number of readers, is denoted  $\theta_{ij}$ . Current MRMC ROC/FROC analysis compares the observed difference in reader-averaged figures of merit between modalities  $i$  and  $i'$  ( $i \neq i'$ ) to the estimated variability of the difference. For example, the reader-averaged difference in figures of merit is  $\theta_{i\cdot} - \theta_{i'\cdot}$ , where the dot symbol represents an average of the corresponding index, specifically, the reader index. The variability of the difference is estimated using the Hillis-modified Obuchowski-Rockette (ORH) method [33], with resampling (i.e., jackknifing) used to determine the two covariances needed for the ORH method. With  $I$  levels, the number of possible  $i$  versus  $i'$  comparisons is  $I(I - 1)/2$ . If the current study were analysed in this manner, where  $I = 8$  (4 levels of tube current-time product and two image reconstruction methods) then this would imply 28 comparisons. The large number of comparisons is sub-optimal in terms of statistical power and does not inform us of the main points of interest: whether performance depends on (i) tube current-time product and/or (ii) reconstruction method.

Unlike conventional ROC type studies, the images in this study are defined by two factors. The first factor, tube current-time product, had four levels: 10, 20, 30 and 40 mAs. The second factor, reconstruction method, had two levels: FBP and AIDR<sup>3D</sup>. Each factor is combined with the other, so they are *fully-crossed factors* (in the statistical sense). The figure of merit is represented by  $\theta_{i_1 i_2 j}$  where  $i_1$  ( $i_1 = 1, 2, \dots, I_1$ ) represents the levels of the first factor (mAs),  $I_1 = 4$  and  $i_2$  ( $i_2 = 1, 2, \dots, I_2$ ) represents the levels of the second factor (reconstruction method),  $I_2 = 2$ . This called for two sequential analyses to be performed: the first was *mAs analysis*, where the figure of merit was averaged over the  $i_2$  or the reconstruction index; the second was *reconstruction analysis*, where the figure of merit was averaged over the  $i_1$  or the mAs index. For example, the *mAs analysis* figure of merit difference is  $\theta_{i_1 \cdot \cdot} - \theta_{i_1' \cdot \cdot}$ , where the first dot represents the average over the *reconstruction* index and the second dot represents an average over readers. In either analysis the figure of merit is dependent on only a single factor, and therefore the standard ORH method applies.

The *mAs analysis* determines whether there is a tube current-time product effect and in this analysis the number of possible comparisons is six. The *reconstruction analysis* determines whether AIDR<sup>3D</sup> offers any advantage over FBP and in this analysis the number of possible comparisons is one.

Multiple testing on the same dataset increases the probability of Type I error, therefore a Bonferroni correction (Appendix A) was applied by setting the threshold for declaring significance at 0.025; this is expected to conservatively maintain the overall probability of a Type I error at  $\alpha = 0.05$ . We use the term *crossed-modality* analysis to describe this type of analysis of ROC/FROC data.

Since the phantom is unique, and conclusions are only possible that are specific to this one phantom, the case (or image) factor was regarded as fixed. For this reason only results of random-reader fixed-case analyses are reported. Software for *crossed-modality* modified JAFROC analysis was implemented in the R programming language [34], and is downloadable from the <https://cran.r-project.org/web/packages/RJafroc/index.html>.

A Welch’s independent sample t-test was performed to assess any difference in performance between radiologists (n=6) and radiographers (n=5); the null hypothesis of no difference was tested at an alpha of 0.05.

#### Contrast-to-Noise Ratio of Nodules

The contrast-to-noise ratio (CNR) of all nodules was measured using ImageJ [35] software. The CNR is a measure of image quality based on contrast (in this instance between nodule and background), rather than the raw signal [36]. Nodule measurements were made on images viewed by the observer. A region of interest (ROI) was placed just within the outer edge of each nodule and the mean pixel value was recorded. A background ROI was placed within a portion of the lung field containing no nodule or vascular markings, and the mean pixel value and standard deviation were recorded. A linear least squares analysis was performed to determine the impact of tube current-time product and image reconstruction method on the CNR of all nodules. Test alpha was set at 0.05 for detecting significant differences in CNR between images reconstructed with FBP and AIDR<sup>3D</sup>.

#### Results

A Welch’s unpaired t-test of observer averaged figures of merit revealed no significant difference in nodule detection performance between radiologists and CT trained radiographers ( $p = 0.1124$ , mean difference 0.051 (95% CI -0.015, 0.117)). Based on this all observers were included in the subsequent analysis.

Averaged over index	Reconstruction Method & Tube Current-Time Product	Crossed-Modality JAFROC FOM (95% CI)	Inferred ROC FOM (95% CI)
<i>i1</i>	FBP	0.867 (0.832,0.903)	0.918 (0.894,0.941)
	AIDR3D	0.869 (0.833,0.904)	0.915 (0.891,0.938)
<i>i2</i>	10mAs	0.835 (0.769,0.875)	0.892 (0.865,0.919)
	20mAs	0.867 (0.827,0.908)	0.910 (0.884,0.937)
	30mAs	0.878 (0.864,0.910)	0.925 (0.904,0.945)
	40mAs	0.891 (0.858,0.925)	0.938 (0.916,0.960)

**Table 2: Figures of merit and 95% confidence intervals (CI) for crossed-modality JAFROC analysis and highest-rating inferred ROC analysis. Analysis *i1* is averaged over tube current-time product (mAs) and analysis *i2* is averaged over reconstruction method (FBP or AIDR3D).**

For a statistically significant difference to be declared the p-value of the treatment pair t-test and that of the overall F-test must both be significant (Appendix B). For the first of the sequential *crossed-modality* JAFROC analyses, the *mAs analysis*, where the figure of merit is averaged over the  $i_2$  or the reconstruction index, significant differences were revealed between multiple pairs of tube current-time product settings ( $F(3,30) = 15.96, p < 0.001$ ). For the second of the sequential analyses, the reconstruction analysis, where the figure of merit was averaged over the  $i_1$  or the mAs index, there was no statistically significant difference in nodule detection performance between FBP and AIDR<sup>3D</sup> ( $F(1,10) = 0.08, p = 0.789$ ). Individual figures-of-merit are displayed in Table 2 and Figure 2; inter-treatment differences are presented in Figure 3. The Inter-treatment differences for inferred ROC analysis are presented in Figure 4. These yielded similar results; *mAs analysis* ( $F(3,30) = 15.18, p < 0.001$ ) and *reconstruction analysis* ( $F(1,10) = 0.27, p = 0.615$ ), i.e., consistent with *crossed-modality* JAFROC analysis. The important outcome is that no statistical difference was demonstrated between images reconstructed with FBP and AIDR<sup>3D</sup>. A statistically strong effect ( $p < 0.001$ ) was seen with tube current-time product. Figure 3 shows weighted JAFROC FOM differences and 95% confidence intervals for all 6 pairings of tube current-time product. A difference is significantly different from zero if the corresponding confidence interval does not include zero. Figure 3 shows that except for the 20-30 mAs and 30-40 mAs comparisons, the rest were all statistically significant. Figure 4 shows corresponding results using the inferred ROC FOM: the results are consistent with those shown in Figure 3. As expected, the inferred ROC differences are smaller in magnitude than the corresponding JAFROC FOM differences (the ROC FOM ranges from 0.5 to 1, while the JAFROC FOM ranges from 0 to 1).

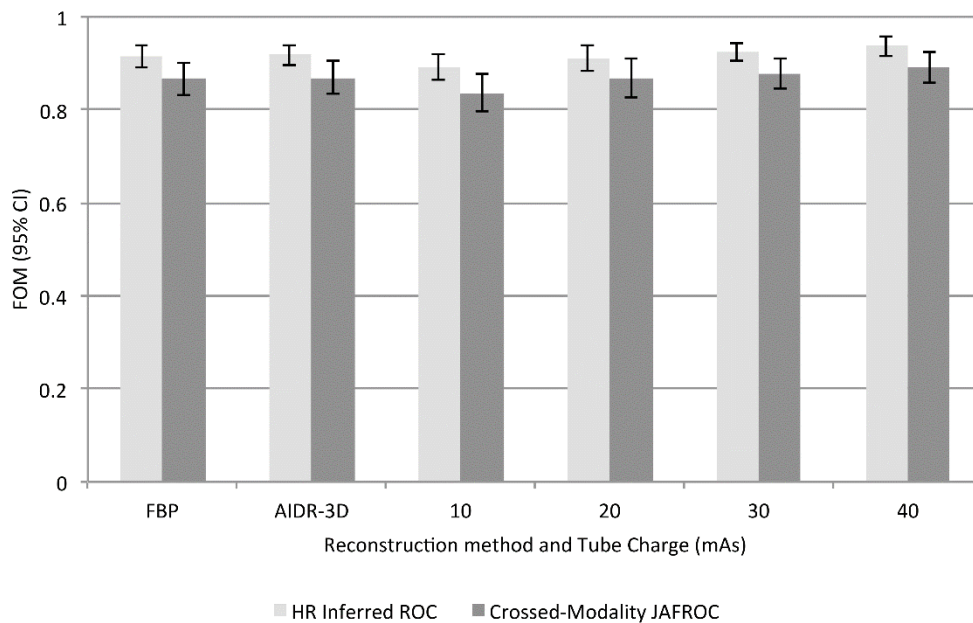
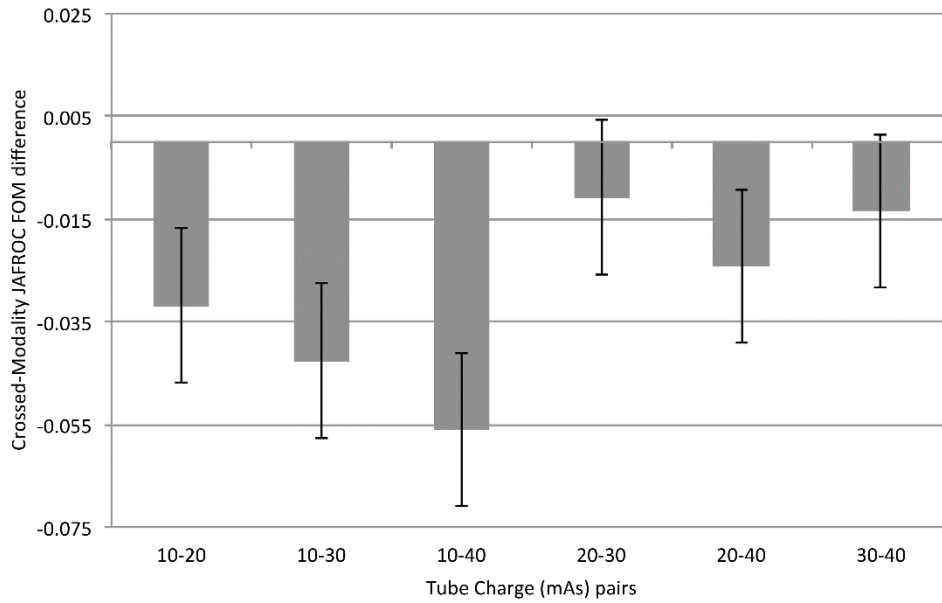
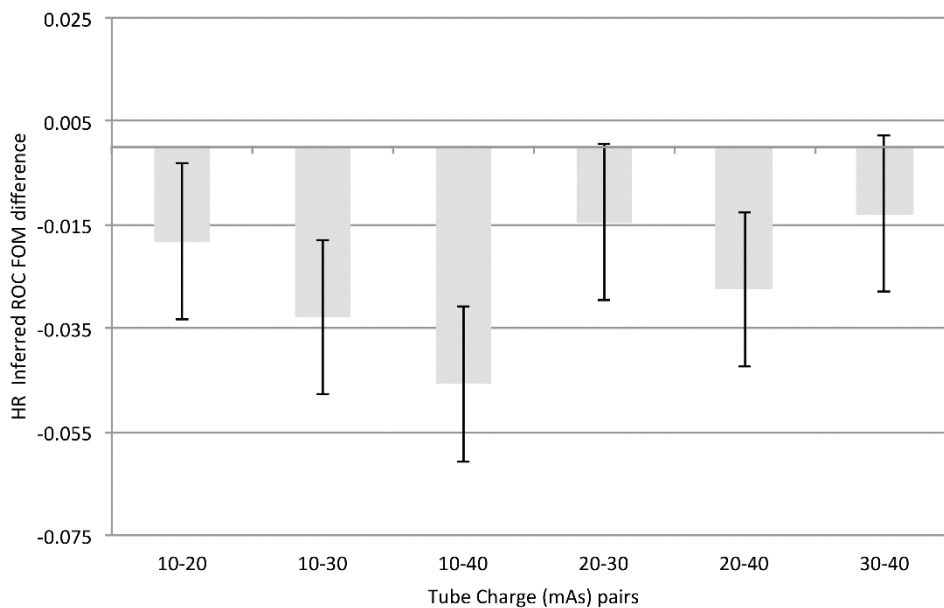


Figure 2: Figures of merit and 95% CI for crossed-modality JAFROC analysis (top) and highest-rating inferred ROC analysis (bottom).<sup>1</sup>

<sup>1</sup> The error bars indicate the 95% confidence level.



**Figure 3: Inter-treatment differences for crossed-modality modified JAFROC analysis. A difference is considered significant if the 95% confidence interval does not include zero and the p-value of the overall F test is less than 0.025. Statistical differences are seen between 10-20, 10-30, 10-40 and 20-40 mAs<sup>2</sup>.**



**Figure 4: Inter-treatment differences for the inferred ROC analysis. Statistical differences are observed for the same treatment pairs, as with JAFROC FOM in Figure 3, with slight variation in the magnitudes of the differences (as expected the inferred ROC differences are smaller in magnitude than the corresponding JAFROC FOM differences).<sup>2</sup>**

<sup>2</sup> The error bars indicate the 95% confidence level.

Statistically significant differences in nodule detection performance were observed between multiple pairs of tube current-time product settings when the p-value of the overall F-test was  $p < 0.001$ ; significant pairs were 10 mAs and 20 mAs ( $p < 0.001$ ), 10 mAs and 30 mAs ( $p < 0.001$ ), 10 mAs and 40 mAs ( $p < 0.001$ ), and 10 mAs and 20 mAs ( $p = 0.008$ ); no difference was found between 20 mAs and 30 mAs or between 30 mAs and 40 mAs ( $p > 0.025$ ).

The results of effective dose and effective risk are summarized in Table 3. The observations are consistent with the expected strict linear dependence of dose on tube current-time product. The  $CTDI_{vol}$  values for each tube current-time product setting are also reported.

Tube current-time product (mAs)	10	20	30	40
$CTDI_{vol}$ (mGycm <sup>2</sup> )	0.7	1.4	2.1	2.6
Effective Dose (mSv)	0.49	0.97	1.64	2.11
Effective Risk (%)	1 in 714 (0.0014)	1 in 345 (0.0029)	1 in 208 (0.0048)	1 in 167 (0.0060)

**Table 3: Effective dose and effective risk for the tube current-time product range investigated in this study. An approximately linear increase in dose and risk is observed.**

Results for CNR are summarised in Table 4. Analysis by least squares revealed that measures of CNR were statistically higher for the simulated nodules on images reconstructed with  $AIDR^{3D}$  ( $p < 0.001$ ). The reconstruction method did not impact on the contrast between nodule and background ( $p = 0.223$ ), but the image noise was statistically higher on images reconstructed with FBP ( $p < 0.001$ ). This is to be expected as the HU of the nodules and background should not change when using different reconstruction method, and therefore the only variable element within the CNR is the image noise. The relationship between image noise and tube current-time product for each image reconstruction method is demonstrated in Figure 5. Mean noise is lower at all tube current-time product settings for images reconstructed with  $AIDR^{3D}$  in place of FBP. At 40 mAs, the noise level is very consistent when images are reconstructed with  $AIDR^{3D}$ , demonstrated by the small standard deviation.

		Mean values and standard deviation			
Tube Current-Time Product (mAs)		10	20	30	40
Nodule CNR	FBP	2.58±2.42	3.36±3.43	4.13±4.46	4.90±4.65
	AIDR3D	4.52±4.30	6.85±7.15	9.17±9.27	11.5±9.16
Contrast	FBP	423±316	412±324	443±337	419±407
	AIDR3D	410±315	471±318	441±336	417±311
Noise	FBP	190±63.6	137.53±71.1	110±51.41	104±58.5
	AIDR3D	117±70.0	74.7±57.4	67.6±63.4	40.9±19.7

**Table 4: A summary of the mean contrast-to-noise ratio of all simulated nodules, mean contrast between nodule and background and the mean noise levels on all images containing nodules for both reconstruction methods and over the range of tube current-time product investigated in this study.**

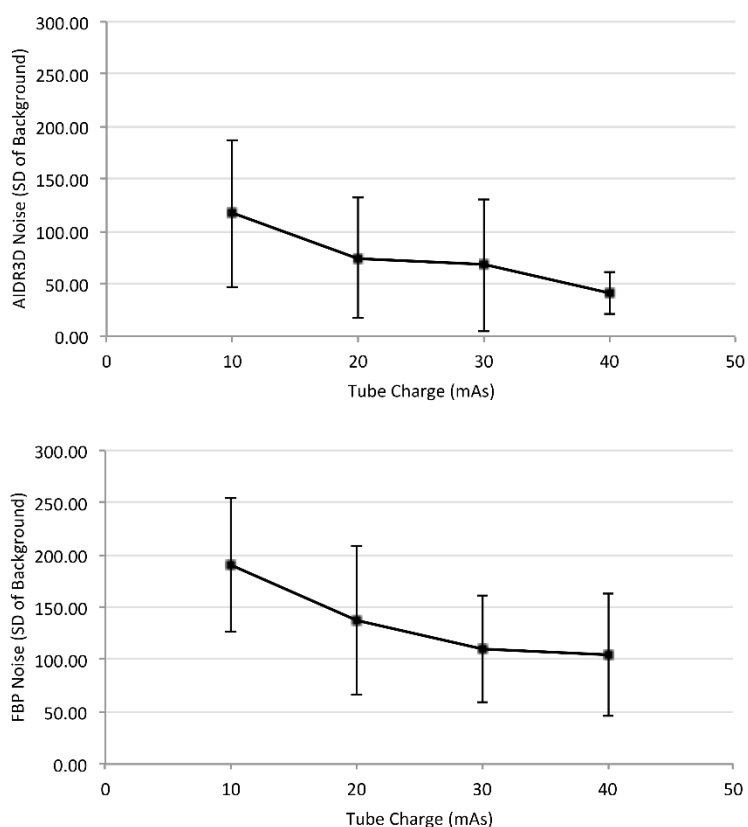


**Figure 5: The mean noise and standard deviation as calculated from all images containing nodules for AIDR3D (top) and FBP (bottom) respectively over the tube current-time product range investigated in this study. The difference in image noise between reconstruction methods was significant ( $p < 0.001$ ) according to a least squares analysis.**

## Discussion

This study has evaluated nodule detection in CT images reconstructed with AIDR<sup>3D</sup> and FBP over a range of tube current-time product. We found no statistically significant difference in nodule detection when images were reconstructed with either FBP or AIDR<sup>3D</sup>. However, we did find that the level of image noise was statistically higher in images reconstructed with FBP. This disparity, consistent with earlier studies, between image noise, a physical measure, and nodule detection, an observer performance measure, is an important finding given the steps taken to improve statistical power in this study. We removed case variability through the use of a phantom and the large number of readers (n=11) used minimized reader variability, the *crossed-modality* methodology averaged the data over all tube current-time product settings for a more stable measure, and taking location into account, i.e., FROC study, increases statistical power compared to the ROC method. The other important finding of this work, evident in Fig. 2, is that tube current-time product was found to have a significant effect on nodule detection, with detection compromised below 20 mAs as compared to 40 mAs. However, the fact that the 95% CI for the 20-30 comparison, includes zero, does not imply that the two are equivalent. A different type of statistical procedure is needed to infer equivalence between the two tube current-time product settings [24]. Software for this type of testing is not readily available.

Many previous studies [19-21, 37,38] have found a similar result to the present study when assessing image noise, be in by measuring CNR, NPS or signal-to-noise ratio (SNR): they all find that the physical metrics improve as a result of reduced image noise with the IR algorithm. Our study is consistent with previous results: significant effect on physical measures between processing algorithms but insignificant effect in objective observer performance. We believe the difference is due to the fact that an objective FROC observer performance measure, such as used in this study, takes the combined effect of all factors affecting nodule detectability into account, including visual search, while physical measure focus on a few individual measures in isolation and do not account for visual search. Moreover, the physical measures considered in this manuscript do not represent state-of-the-art because they do not account for spatial corrections in the images. Newer model observer methods account for some of these correlations [39-41], and they are just beginning to account for visual search [42]. However, observer performance studies suffer from much larger sources of variability than physical measures, so more careful statistical analysis is needed. As noted by the late Dr. Robert F. Wagner, finding physical measures, or combinations of physical measures, that correlate with the more time-consuming observer measures is one of the "holy-grails" of medical imaging [43].

Diagnostic acceptability must be maintained when looking to optimise the dose delivered to the patient. Many studies have suggested that IR algorithms can be used to optimise dose with a range of percentage reductions previously quoted (36-75 %) [18-20]. This requires the pre-optimisation start point to be reasonable and it is the post-optimisation dose that should be given the greatest consideration.

For true optimisation, the risk to the patient must also be understood. Patient dose is frequently reported using sub-optimal estimation methods (CTDI, DLP, body part specific conversion factors) and the lifetime risk associated with X-ray exposures is rarely reported. The method used in the current work is considered a reliable method to accurately represent dose and risk and we would encourage future studies of IR algorithms to adopt this technique.

Lee et al [44] quote a mean effective dose of  $1.84 \pm 1.05$  mSv in a study of paediatrics, where the purpose of the examination was to evaluate lung metastases. The mean weight of the patients was

41.4 kg, somewhat lighter than the estimated 70Kg patient size in our study. When using ASIR-FBP blending and FBP alone, Qi et al [45] showed that radiation dose to the patient could be optimised at an average effective dose of 4.25 mSv (range 2.6-6.3 mSv) with ASIR-FBP blending compared to an average of 8.65mSv (range 7.9-9.5 mSv) with FBP alone. This finding is supported by Chen et al [46], but their post-optimisation dose was much lower at 0.74 mSv. Both studies investigated ASIR in a patient population, and both proposed ASIR blending at 50% as being optimal. The large difference in estimated effective dose in these studies is likely due to the amount of noise permitted in the images by the automatic exposure control (AEC) and image quality paradigm. The noise index, in the GE systems of the above papers, is referenced to the standard deviation of pixel values in a water phantom, compared to patient attenuation measured in the CT planning image, in order to maintain a constant level of image noise [47]. Qi et al chose a noise index of 15, while Chen et al chose a noise index of 30, where a higher noise index provides a greater reduction in tube current. Neither observer performance evaluation nor equivalency study was performed in either of these works, and further assessment is required before dose optimisation can be claimed with IR algorithms.

Previous optimistic claims of dose reduction with IR algorithms are mainly based on physical measures. While our methods were sensitive enough to find statistical differences in nodule detection performance attributed to tube current-time product, we were unable to detect any statistical difference in nodule detection on the basis of image reconstruction algorithm. It is not surprising that pixel-variance is a poor predictor of lesion detectability; for example it can be reduced almost arbitrary, by smoothing the image. The inadequacy of pixel variance as a predictor of lesion detectability was noted in 1999 by Burgess, but this work is not well appreciated [48]. IR algorithms require further investigation, with observer performance and equivalency testing playing a more prominent role.

## Conclusion

We have successfully demonstrated the use of a *crossed-modality* JAFROC analysis that allows us to take co-existing factors into account in order to determine the dependence of nodule detection on each factor. We believe this is a useful methodological improvement, since system performance is usually dependent on more than just a single factor. No significant difference in nodule detection performance was demonstrated between images reconstructed with FBP and AIDR<sup>3D</sup>. Tube current-time product was found to influence nodule detection, but further work is required for dose optimization.

## Conflict of Interest

No author has any conflict of interest or relationship to any of the aforementioned manufacturers. DPC was supported by NIH grant R01-EB005243.

## Acknowledgement

We wish to thank the University of Cumbria for the kind loan of the Lungman phantom and the Radiology Department at Wrexham Maelor Hospital for their cooperation in the data collection phase of this study. We also acknowledge the contribution of Xuetong Zhai M.S. at the University of Pittsburgh for assisting with the development of the modified JAFROC software.

- 1 W. Kalender, "Dose in x-ray computed tomography," *Phys. Med. Biol.* 59, R129–R150 (2014).
- 2 M.L.D. Gunn and J.R. Kohr, State of the art: Technologies for computed tomography dose reduction, *Emerg. Radiol.* 17, 209–218 (2010).
- 3 D.J. Brenner and E.J. Hall, "Computed tomography--an increasing source of radiation exposure," *N. Engl. J. Med.* 357, 2277–2284 (2007).
- 4 R. Smith-Bindman, J. Lipson, R. Marcus, K.-P. Kim, M. Mahesh, R. Gould, A. Berrington de González, and D.L. Miglioretti, "Radiation dose associated with common computed tomography examinations and the associated lifetime attributable risk of cancer," *Arch. Intern. Med.* 169, 2078–2086 (2009).
- 5 M.S. May, W. Wüst, M. Brand, C. Stahl, T. Allmendinger, B. Schmidt, M. Uder, and M.M. Lell, Dose Reduction in Abdominal Computed Tomography, *Invest. Radiol.* 46, 465–470 (2011).
- 6 N.E. Manghat, G.J. Morgan-Hughes, and C.A. Roobottom, Multi-detector row computed tomography: Imaging in acute aortic syndrome, *Clin. Radiol.* 60, 1256–1267 (2005).
- 7 S. Leschka, H. Alkadhi, S. Wildermuth, and B. Marincek, "Multi-detector computed tomography of acute abdomen," *Eur. Radiol.* 15, 2435–2447 (2005).
- 8 M. Scaglione, A. Pinto, I. Pedrosa, A. Sparano, and L. Romano, "Multi-detector row computed tomography and blunt chest trauma," *Eur. J. Radiol.* 65, 377–388 (2008).
- 9 S. Brunot, O. Corneloup, V. Latrabe, M. Montaudon, and F. Laurent, "Reproducibility of multi-detector spiral computed tomography in detection of sub-segmental acute pulmonary embolism," *Eur. Radiol.* 15, 2057–2063 (2005).
- 10 J.D. Evans, D.G. Politte, B.R. Whiting, J.A. O'Sullivan, and J.F. Williamson, "Noise-resolution tradeoffs in x-ray CT imaging: a comparison of penalized alternating minimization and filtered backprojection algorithms," *Med. Phys.* 38, 1444–1458 (2011).
- 11 A.K. Hara, R.G. Paden, A.C. Silva, J.L. Kujak, H.J. Lawder, and W. Pavlicek, "Iterative reconstruction technique for reducing body radiation dose at CT: feasibility study," *AJR. Am. J. Roentgenol.* 193, 764–771 (2009).
- 12 A. Korn, M. Fenchel, B. Bender, S. Danz, T.K. Hauser, D. Ketelsen, T.G. Flohr, C.D. Claussen, M. Heuschmid, and U. Ernemann, "Iterative Reconstruction in Head CT : Image Quality of Routine and Low-Dose Protocols in," *Am. J. Neuroradiol.* 33, 218–224 (2012).
- 13 C. Ghetti, F. Palleri, G. Serreli, O. Ortenzia, and L. Ruffini, "Physical characterization of a new CT iterative reconstruction method operating in sinogram space," *J. Appl. Clin. Med. Phys.* 14, 4347 (2013).
- 14 M.J. Willeminck, T. Leiner, P. a de Jong, L.M. de Heer, R. a J. Nievelstein, A.M.R. Schilham, and R.P.J. Budde, "Iterative reconstruction techniques for computed tomography part 2: initial results in dose reduction and image quality," *Eur. Radiol.* 23, 1632–42 (2013).
- 15 F. Pontana, A. Duhamel, J. Pagniez, T. Flohr, J.B. Faivre, A.L. Hachulla, J. Remy, and M. Remy-Jardin, "Chest computed tomography using iterative reconstruction vs filtered back projection (Part 2): Image quality of low-dose CT examinations in 80 patients," *Eur. Radiol.* 21, 636–643 (2011).
- 16 M. Katsura, I. Matsuda, M. Akahane, J. Sato, H. Akai, K. Yasaka, A. Kunimatsu, and K. Ohtomo, "Model-based iterative reconstruction technique for radiation dose reduction in chest CT:

- Comparison with the adaptive statistical iterative reconstruction technique," *Eur. Radiol.* 22, 1613–1623 (2012).
- 17 S. Singh, M.K. Kalra, M.D. Gilman, J. Hsieh, H.H. Pien, S.R. Digumarthy, and J.-A.O. Shepard, "Adaptive statistical iterative reconstruction technique for radiation dose reduction in chest CT: a pilot study," *Radiology* 259, 565–573 (2011).
- 18 R. Irwan, S. Nakanishi, and A. Blum, "AIDR 3D - Reduces Dose and Simultaneously Improves Image Quality," *Toshiba Med. Syst.* <https://www.toshiba-medical.eu/eu/wp-content/uploa> (2011).
- 19 Y. Ohno, D. Takenaka, T. Kanda, T. Yoshikawa, S. Matsumoto, N. Sugihara, and K. Sugimura, "Adaptive Iterative Dose Reduction Using 3D Processing for Reduced- and Low-Dose Pulmonary CT: Comparison With Standard-Dose CT for Image Noise Reduction and Radiological Findings," *Am. J. Roentgenol.* 199, W477–W485 (2012).
- 20 Y. Yamada, M. Jinzaki, T. Hosokawa, Y. Tanami, H. Sugiura, T. Abe, and S. Kuribayashi, "Dose reduction in chest CT: Comparison of the adaptive iterative dose reduction 3D, adaptive iterative dose reduction, and filtered back projection reconstruction techniques," *Eur. J. Radiol.* 81, 4185–4195 (2012).
- 21 R.M.S. Joemai, W.J.H. Veldkamp, L.J.M. Kroft, I. Hernandez-Giron, and J. Geleijns, "Adaptive iterative dose reduction 3d versus filtered back projection in CT: Evaluation of image quality," *Am. J. Roentgenol.* 201, 1291–1297 (2013).
- 22 C.H. McCollough, S. Leng, L. Yu, D.D. Cody, J.M. Boone, and M.F. McNitt-Gray, "CT Dose Index and Patient Dose: They Are Not the Same Thing," *Radiology* 259, 311–316 (2011).
- 23 M. Katsura, I. Matsuda, M. Akahane, K. Yasaka, H. Shohei, H. Akai, J. Sato, A. Kunimatsu, and K. Ohtomo, "Model-Based Iterative Reconstruction Technique for Ultralow-Dose Chest CT Comparison of Pulmonary Nodule Detectability With the Adaptive Statistical Iterative Reconstruction Technique," *Invest. Radiol.* 48, 206–212 (2013).
- 24 N.A. Obuchowski, "Testing for equivalence of diagnostic tests," *Am. J. Roentgenol.* 168, 13–17 (1997).
- 25 W. Chen, N.A. Petrick, and B. Sahiner, "Hypothesis Testing in Noninferiority and Equivalence MRMROC Studies," *Acad. Radiol.* 19, 1158–1165 (2012).
- 26 J.D. Thompson, D.P. Chakraborty, K. Szczepura, I. Vamvakas, A. Tootell, D.J. Manning, and P. Hogg, "A phantom-based JAFROC observer study of two CT reconstruction methods: the search for optimisation of lesion detection and effective dose," *SPIE Proc. Med. Imaging* 9416, 94160B (2015).
- 27 J. Valentin, "The 2007 Recommendations of the International Commission on Radiological Protection. ICRP publication 103," *Ann. ICRP* 37, 1–332 (2007).
- 28 X. Li, E. Samei, W.P. Segars, G.M. Sturgeon, J.G. Colsher, and D.P. Frush, "Patient-specific radiation dose and cancer risk for pediatric chest CT," *Radiology* 259, 862–874 (2011).
- 29 N.R. Council, *Health Risks from Exposure to Low Levels of Ionizing Radiation: BEIR VII Phase 2* (The National Academies Press, Washington, DC, 2006).
- 30 J. Geleijns, M. Salvadó Artells, P.W. de Bruin, R. Matter, Y. Muramatsu, and M.F. McNitt-Gray, "Computed tomography dose assessment for a 160 mm wide, 320 detector row, cone beam CT scanner.," *Phys. Med. Biol.* 54, 3141–3159 (2009).

- 31 J.D. Thompson, P. Hogg, S. Thompson, D.J. Manning, and K. Szczepura, "ROCView: prototype software for data collection in jackknife alternative free-response receiver operating characteristic analysis," *Br. J. Radiol.* 85, 1320–6 (2012).
- 32 D.P. Chakraborty and K.S. Berbaum, "Observer studies involving detection and localization: Modeling, analysis, and validation," *Med. Phys.* 31, 2313–2330 (2004).
- 33 N.A. Obuchowski and H.E. Rockette, Hypothesis testing of diagnostic accuracy for multiple readers and multiple tests an anova approach with dependent observations, *Commun. Stat. Simul. Comput.* 24, 285–308 (1995).
- 34 R Core Team, R: A language and environment for statistical computing, <http://www.r-project.org/> (2015).
- 35 W. Rasband, "ImageJ U. S. National Institutes of Health, Bethesda, Maryland, USA," [//imagej.nih.gov/ij/](http://imagej.nih.gov/ij/) (2012).
- 36 M. Welvaert and Y. Rosseel, "On the definition of signal-to-noise ratio and contrast-to-noise ratio for fMRI data," *PLoS One* 8, (2013).
- 37 K. Yasaka, M. Katsura, M. Akahane, J. Sato, I. Matsuda, and K. Ohtomo, "Model-based iterative reconstruction for reduction of radiation dose in abdominopelvic CT: comparison to adaptive statistical iterative reconstruction," *Springerplus* 2, 209 (2013).
- 38 W. Chang, J.M. Lee, K. Lee, J.H. Yoon, M.H. Yu, J.K. Han, and B.I. Choi, "Assessment of a model-based, iterative reconstruction algorithm (MBIR) regarding image quality and dose reduction in liver computed tomography," *Invest. Radiol.* 48, 598–606 (2013).
- 39 S. Park, M.A. Kupinski, E. Clarkson, and H.H. Barrett, "Ideal-observer performance under signal and background uncertainty.," *Inf. Process. Med. Imaging* 18, 342–53 (2003).
- 40 F.O. Bochud, C.K. Abbey, and M.P. Eckstein, "Visual signal detection in structured backgrounds. III. Calculation of figures of merit for model observers in statistically nonstationary backgrounds.," *J. Opt. Soc. Am. A. Opt. Image Sci. Vis.* 17, 193–205 (2000).
- 41 H.H. Barrett, J. Yao, J.P. Rolland, and K.J. Myers, "Model observers for assessment of image quality.," *Proc. Natl. Acad. Sci. U. S. A.* 90, 9758–9765 (1993).
- 42 H.C. Gifford, "A visual-search model observer for multislice-multiview SPECT images.," *Med. Phys.* 40, 092505 (2013).
- 43 S. V. Beiden, R.F. Wagner, G. Campbell, C.E. Metz, Y. Jiang, and H.-P. Chan, "Multiple-reader studies, digital mammography, computer-aided diagnosis, and the Holy Grail of imaging physics: II," *SPIE Proc. Med. Imaging* 4320, 619–626 (2001).
- 44 S.H. Lee, M.-J. Kim, C.-S. Yoon, and M.-J. Lee, "Radiation dose reduction with the adaptive statistical iterative reconstruction (ASIR) technique for chest CT in children: An intra-individual comparison," *Eur. J. Radiol.* 81, e938–e943 (2012).
- 45 L.P. Qi, Y. Li, L. Tang, Y.L. Li, X.T. Li, Y. Cui, Y.S. Sun, and X.P. Zhang, "Evaluation of dose reduction and image quality in chest CT using adaptive statistical iterative reconstruction with the same group of patients," *Br. J. Radiol.* 85, 906–911 (2012).

- 46 J.H. Chen, E.H. Jin, W. He, and L.Q. Zhao, "Combining automatic tube current modulation with adaptive statistical iterative reconstruction for low-dose chest CT screening," *PLoS One* 9, 1–7 (2014).
- 47 C. McCollough, A. Primak N., N. Braun, J. Kofler, L. Yu, and J. Cristner, "Strategies for Reducing Radiation Dose," *Radiol Clin North* 47, 27–40 (2009).
- 48 A.E. Burgess, "The Rose model, revisited," *J. Opt. Soc. Am. A* 16, 633–646 (1999).
- 49 J.M. Bland and D.G. Altman, "Multiple significance tests: the Bonferroni method," *BMJ* 310, 170 (1995).
- 50 T. V Perneger, "What's wrong with Bonferroni adjustments.," *BMJ* 316, 1236–1238 (1998).
- 51 S.L. Hillis, "A comparison of denominator degrees of freedom methods for multiple observer ROC analysis," *Stat. Med.* 26, 596–619 (2007).

#### Appendix A: Bonferroni Correction

Under null hypothesis (NH) true conditions, a valid significance testing procedure maintains the probability of a Type I error (incorrect rejection of the NH) at the chosen value of alpha, i.e., 5% in our study. The Bonferroni correction falls under the subject of multiple significance tests. To quote Bland and Altman [49]: "Many published paper include large numbers of significance tests. These may be difficult to interpret because if we go on testing long enough we will inevitably find something that is significant. We must beware of attaching too much importance to a lone significant result among a mass of non-significant ones".

In the current context there are two significance tests, the first for the mAs effect (with 6-levels) and the second for the reconstruction effect (with 2-levels). For the mAs-effect the DBMH procedure accounts for the 6 pairings and maintains the NH rejection rate at 5%. In other words, if the study were repeated 2000 times independently under NH true conditions (obviously this is only possible using a data simulator) there would be about 100 incorrect rejections of the NH for the mAs-effect. However, one is also attempting to draw conclusions about the effect of the two reconstruction algorithms, i.e., applying a second significance testing procedure. Again, the DBMH procedure maintains the Type I error rate at 5% for this comparison, so for 2000 simulations one expects about 100 incorrect NH rejections for the reconstruction effect. The question arises: to what extent the set of specific simulations where the NH was rejected for the mAs comparison (e.g., the 23<sup>rd</sup>, 30<sup>th</sup>, ..., 1940<sup>th</sup>, etc. simulations, for a total of about 100) are common or distinct from the set of specific simulations that incorrectly rejected the algorithm effect. If the two sets are identical, then one still has a total of 100 NH rejections and the overall NH rejection rate is 5% and no correction is needed, which is the best-case scenario. The worst-case scenario is that the two sets are completely different, in which case the total number of NH rejections is 200. The only way to control for this is to set a more stringent criterion for rejecting the NH. For example, if the criterion were set to reject 2.5% of the time for each type of comparison, there would be 50 NH rejections for the mAs comparison study, and 50 different rejections for the algorithm comparison study, for a total of 100 NH rejections. To summarize, the Bonferroni correction involves using a smaller value of alpha, equal to the desired value divided by the number of significance tests. It is a conservative correction that, depending on the correlations between the two significance test results, tends to yield an effective alpha of less than 5%. A conservative correction is not always desirable because it leads to loss of statistical power and more sophisticated procedures are available [50].

## Appendix B: JAFROC Statistics and Degrees of Freedom

JAFROC software reports the results of an overall F-test of the  $H_0$  that all modalities being tested have identical FOMs. The analysis obtains two estimates of variance, the first due to the differences between modalities and the second due to other causes. If the observed ratio of the first variance to the second variance is large enough, the FOMs are expected to be significantly different. The ratio follows the F-distribution, which is characterized by two quantities called the numerator and denominator degrees of freedom,  $ndf$  and  $ddf$  respectively. In general, if the ratio of the two variances is large and the degrees of freedom are large, the study tends to be more significant (smaller p-value) [51].

## PAPER 6

### A PHANTOM-BASED JAFROC OBSERVER STUDY OF TWO CT RECONSTRUCTION METHODS: THE SEARCH FOR OPTIMISATION OF LESION DETECTION AND EFFECTIVE DOSE

Thompson, J. D., Chakraborty, D. P., Szczepura, K., Vamvakas, I., Tootell, A., Manning, D. J., & Hogg, P. (2015). Paper presented at the Proc. SPIE 9416, Medical Imaging 2015: Image Perception, Observer Performance, and Technology Assessment, Orlando, Florida.

#### ABSTRACT

**Purpose:** To investigate the dose saving potential of iterative reconstruction (IR) in a computed tomography (CT) examination of the thorax.

**Materials and Methods:** An anthropomorphic chest phantom containing various configurations of simulated lesions (5, 8, 10 and 12mm; +100, -630 and -800 Hounsfield Units, HU) was imaged on a modern CT system over a tube current range (20, 40, 60 and 80mA). Images were reconstructed with (IR) and filtered back projection (FBP). An ATOM 701D (CIRS, Norfolk, VA) dosimetry phantom was used to measure organ dose. Effective dose was calculated. Eleven observers (15.11±8.75 years of experience) completed a free response study, localizing lesions in 544 single CT image slices. A modified jackknife alternative free-response receiver operating characteristic (JAFROC) analysis was completed to look for a significant effect of two factors: reconstruction method and tube current. Alpha was set at 0.05 to control the Type I error in this study.

**Results:** For modified JAFROC analysis of reconstruction method there was no statistically significant difference in lesion detection performance between FBP and IR when figures-of-merit were averaged over tube current ( $F(1,10)=0.08$ ,  $p = 0.789$ ). For tube current analysis, significant differences were revealed between multiple pairs of tube current settings ( $F(3,10) = 16.96$ ,  $p<0.001$ ) when averaged over image reconstruction method.

**Conclusion:** The free-response study suggests that lesion detection can be optimized at 40mA in this phantom model, a measured effective dose of 0.97mSv. In high-contrast regions the diagnostic value of IR, compared to FBP, is less clear.

**Keywords:** Free-response, modified JAFROC, iterative reconstruction, CT, effective dose, dose optimization, lesion detection

## **Introduction**

### **Background**

The increasing popularity of computed tomography (CT) as a diagnostic imaging modality raises concerns in regard of radiation dose.<sup>1</sup> In the UK the use of CT is increasing at a higher rate annually than any other modality.<sup>2</sup> Since the inception of CT in the 1970's, filtered back projection (FBP) has been the mainstay of image reconstruction methods. Image production with FBP does not tolerate a large reduction in tube current (mA), while all other acquisition parameters remain constant, due to the associated increase in image noise.<sup>3</sup> This can make dose optimization problematic, where it is preferable to have low noise and high spatial resolution images for interpretation. Iterative reconstruction (IR) has recently gained acceptance in the clinical setting due to improvements in computation power; previously this had not been practicable due to the length of time it had taken to reconstruct a series of images. The impact of this development may have a welcome impact in dose and image optimization; specifically because there is less dependence of spatial resolution on image noise with IR.<sup>3</sup> The innovation associated with IR has allowed improved image quality for the same radiation dose, with recent studies comparing FBP and IR suggesting dose saving over the range of 23-76%.<sup>4</sup> In this study we seek to assess the diagnostic value of a relatively new IR image reconstruction algorithm for lesion detection in an anthropomorphic chest phantom.

### **Methodology**

#### **Image Acquisition**

CT images were acquired on the Toshiba Aquilion ONE 320-slice multi-detector CT (MDCT) scanner (Toshiba Medical Systems, Minato-Ku, Japan). A range of tube current (20, 40, 60 and 80mA) was used while all other acquisition parameters remained constant: 120 kilovolt potential (kVp), 0.5-second rotation time, pitch 1, 64x0.5mm detector configuration and a 320mm scan field of view (FOV). Images were reconstructed at 1mm thickness using a 320mm reconstructed FOV on a matrix size of 512x512 for a pixel size of 0.625mm.

An anthropomorphic chest phantom (Lungman N1 Multipurpose Chest Phantom, Kyoto Kagaku Company, Japan) representing a 70Kg male was loaded with several different configurations of spherical simulated lesions from a pool of fifteen different sizes and density (5, 8, 10, 12mm; +100, -630 and -800 Hounsfield Units, HU). The higher density (+100HU) lesions are composed of polyurethane, hydroxyapatite and a urethane resin; the lower density (-630 and -800HU) lesions are composed of urethane. The phantom was scanned on each tube current setting, and reconstructed with FBP and IR for all lesion configurations. Lesion positions were recorded at the time of placement and acquisition, to provide a 'truth' reference map.

From the acquired data, the same 34 normal and 34 abnormal transaxial image slices were selected from each acquisition-reconstruction combination were chosen for the observer study. Table position and image slice number were used to ensure the same transaxial slice was selected on each occasion. No physical movement of the phantom occurred between acquisitions; this ensured continuity and precise replication of lesion positions for all CT acquisitions. The result was eight sets of precisely matched image data for four variations of tube current and the two image reconstruction methods, Figure 1.

## **Dose Measurement**

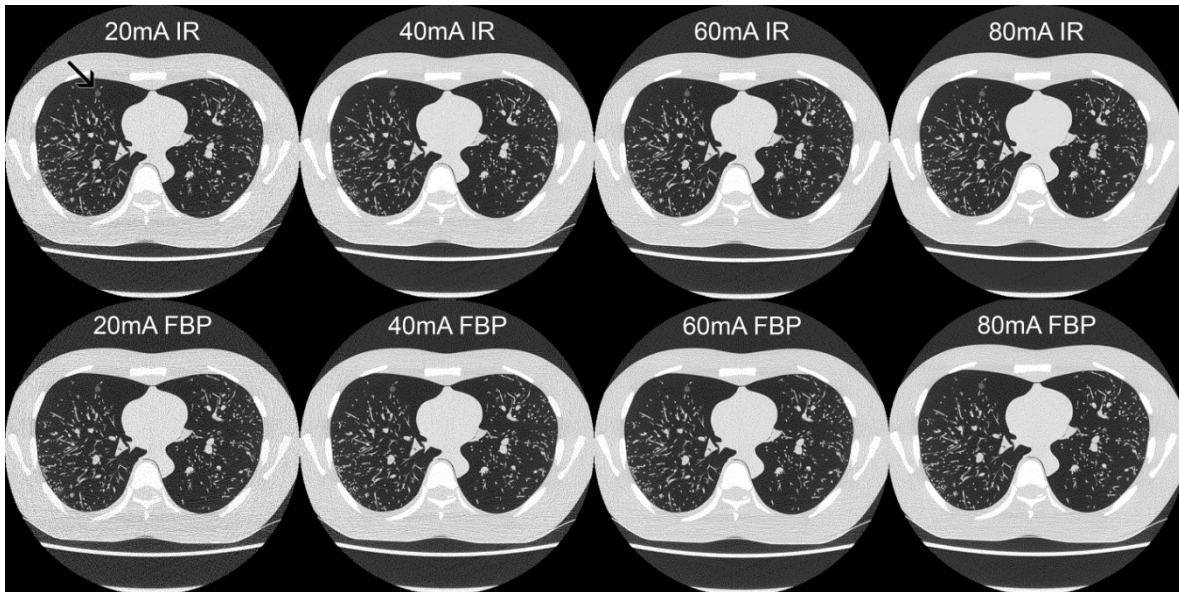
An ATOM 701D (*CIRS, Norfolk, VA*) whole-body dosimetry verification phantom was used to measure organ dose. Annealed thermoluminescent dosimeters (*TLD100H LiF:Mg,Cu,P, Thermo Scientific, Waltham, MA*) were positioned in clinically relevant places for each of the four conditions and effective dose calculated.<sup>5</sup>

## **Observer Study**

Eleven observers (15.11±8.75 years of experience) completed the observer study. Observers were introduced to the appearances of the phantom and simulated lesions, and they were instructed that all the lesions were spherical and that no other pathological mimics that may have been caused by the phantom were of interest in this study. Each observer evaluated 544 single CT images for simulated lesions. They were informed that half of the images being evaluated would contain simulated lesions and that there were 1-3 simulated lesions (mean 1.35±0.54) in each abnormal image, the remaining images contained no simulated lesions. A single transaxial CT image was treated as an individual case. Observers completed the image evaluation in two separate sessions in order to reduce the effects of fatigue. Images were presented in a different randomized order for each observer.

ROCView<sup>6</sup> was run on the same monitor (PG21HQX, Wide, 20", LCD, Wide Corporation, Korea; 1536x2080 pixels, 3.2 megapixel resolution) to collect free-response data for all evaluations. Observers localized lesions with mouse clicks; localizations were classified as lesion localization (LL) or non-lesion localization (NL) by a 20-pixel acceptance radius. Observers were instructed to mark the center of each suspected lesion. This prompted an unmarked (no graduations) slider-bar rating scale to appear; moving the slider to the right demonstrated an increasing level of confidence. The slider bar collected ratings over a 10-point scale. Images were viewed on a fixed lung window (1500, -500) to maximize lesion visibility and reduce this source of variability due to the observer.

**Figure 1: A single transaxial slice showing a solitary simulated lesion (black arrow, top left). Images reconstructed with IR are shown on the top row for all tube current values and the corresponding images reconstructed with FBP are on the bottom row. The simulated soft tissue of the anthropomorphic chest phantom illustrates the difference in image noise.**



### Statistical Analysis – Crossed-modality JAFROC analysis

In the analysis of ROC type studies the modality is generally regarded as a *single factor* with  $I$  levels, where  $I$  is usually small (e.g.,  $I = 2, 3$  or  $4$ ). The figure of merit, for example the area under the ROC curve, for modality  $i$  ( $i = 1, 2, \dots, I$ ) and reader  $j$  ( $j = 1, 2, \dots, J$ , where  $J$  is the number of readers), is denoted  $q_{ij}$ . The analysis compares the observed difference in reader-averaged figures of merit between modalities  $i$  and  $i'$  ( $i \neq i'$ ) to the estimated variability of the difference. The reader-averaged difference in figures of merit is  $q_i - q_{i'}$ , where the dot symbol represents an average over the corresponding index. The variability of the difference is estimated using the modified Obuchowski-Rockette (OR) method,<sup>7,8</sup> with resampling (e.g., jackknifing) used to determine the two covariances needed for the OR method. In the study the equally weighted JAFROC figure of merit was used for  $q$ . The JAFROC figure of merit is the weighted empirical probability that a lesion rating is higher than any rating on a normal case. In this study all lesions on a case were assigned the same weight. The weighting gives equal importance to each case, independent of the number of true lesions in it. For consistency checking, inferred-ROC analysis was also performed using the highest rating on a case to define the inferred-ROC rating of the case.

With  $I$  levels, the number of possible  $i$  vs.  $i'$  comparisons is  $I(I-1)/2$ . For example, if  $I = 2$ , the number of comparisons is 1 and if  $I = 3$ , the number of comparisons is 3. If this study were analyzed in this manner, then the number of modalities  $I = 8$  (4 levels of mA for each of two reconstruction methods) would imply 28 comparisons. Besides decreasing statistical power, the results of such comparisons would not be particularly informative regarding the two questions of main interest: (i) whether performance depends on mA and (ii) whether performance depends on the reconstruction method.

In this study each image is actually defined by *two factors*. The first factor is tube current, which had 4 levels: 20, 40, 60 and 80 mA. The second factor is reconstruction method which had two levels: FBP and IR. Since each level of the first factor occurs in combination with each level of the second factor, the factors are crossed. The figure of merit is represented by  $q_{i_1 i_2 j}$  where  $i_1$  ( $i_1 = 1, 2, \dots, I_1$ ) represents the levels of the first factor and  $i_2$  ( $i_2 = 1, 2, \dots, I_2$ ) represents the levels of the second factor. In this study  $I_1 = 4$ , corresponding to the four levels of the mA factor, and  $I_2 = 2$ , corresponding to the two levels of the reconstruction method factor. The approach followed was to conduct two sequential analyses: (i) in the first, termed *mA analysis*, the figure of merit was averaged over the  $i_2$ , or reconstruction index, and (ii) in the second, termed *reconstruction analysis*, the figure of merit was averaged over the  $i_1$ , or *mA index*. For example, in mA-analysis the difference figure of merit was  $q_{i_1 \cdot \cdot} - q_{i_1' \cdot \cdot}$ , where the first dot on the figure of merit represents an average over the  $i_2$  index and the second dot represents an average over readers. In either analyses the resulting figure of merit depends on a *single* modality factor and reader, to which the standard OR method was applied. The mA analysis addresses the question of whether there is a mA effect and in this analysis the number of possible comparisons is six. The reconstruction analysis addressed the question of whether there is a reconstruction method effect and in this analysis the number of possible comparisons is one. To control for the increased probability of a Type I error due to multiple testing on the same dataset, the Bonferroni correction was applied by setting the threshold for declaring significance at 0.025; this is expected to conservatively maintain the overall probability of a Type I error at  $\alpha = 0.05$ . We use the term *crossed-modality analysis* to describe this type of modified analysis of ROC-type data.

Since the phantom is unique, and conclusions are only possible that are specific to this one phantom, the case (or image) factor was regarded as fixed. For this reason only results of random-reader fixed-case analyses are reported. Software for crossed-modality JAFROC analysis was implemented in the R programming language, and is freely available on request from DPC.

## Results

### Crossed-modality JAFROC analysis

For the *crossed-modality* modified JAFROC analysis of reconstruction method where the data was averaged over tube current,  $i_1$ , there was no statistically significant difference in lesion detection performance between FBP and IR ( $F(1,10) = 0.08$ ,  $p = 0.789$ ). For the *crossed-modality* modified JAFROC analysis of tube current (mA) where data was averaged over reconstruction method,  $i_2$ , significant differences were revealed between several pairs of tube current settings ( $F(3,10) = 16.96$ ,  $p < 0.001$ ). The figures of merit for all modalities can be found in Table 1. The corresponding highest-rating inferred ROC figures of merit can be found in Table 2. Statistical differences were observed between 20mA and 40mA, 20mA and 60mA and 20mA and 80mA. Additionally, a statistical difference was also observed between 40mA and 80mA, but 40mA and 60mA were statistically similar, as was the final pair of 60mA and 80mA; these differences are summarized in Figure 2.

### Effective dose

The effective dose (mSv) was 0.49mSv, 0.97mSv, 1.64mSv and 2.11mSv for CT acquisitions at 20mA, 40mA, 60mA and 80mA respectively, while all other acquisition parameters were kept constant.

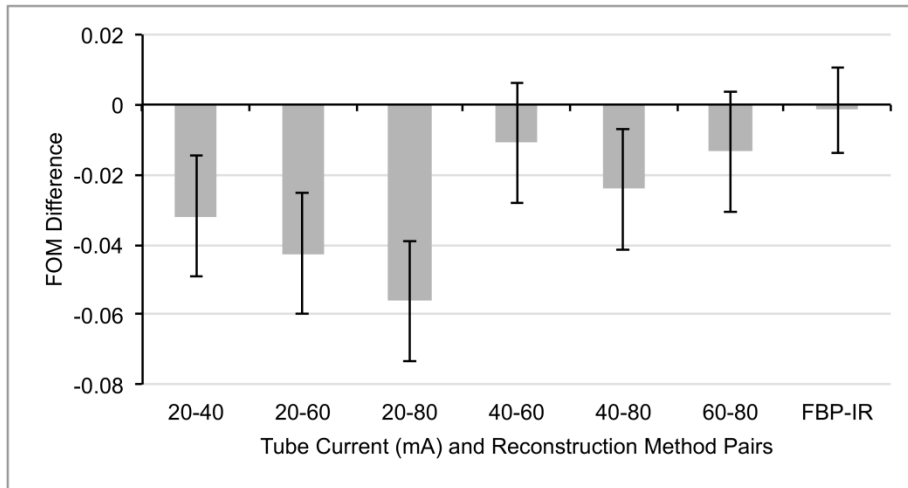
**Table 1. : Modified JAFROC analysis results showing figures-of-merit and 95% confidence intervals (CI) for modalities averaged over the  $i_1$  (mA) and  $i_2$  (reconstruction method) indexes.**

Crossed Modality Analysis	Reconstruction Method & Tube Current setting	Modified JAFROC FOM (95% CI)
<i>Averaged over <math>i_1</math></i>	FBP	0.867 (0.832,0.903)
	IR	0.869 (0.833,0.904)
<i>Averaged over <math>i_2</math></i>	20mA	0.835 (0.769,0.875)
	40mA	0.867 (0.827,0.908)
	60mA	0.878 (0.864,0.910)
	80mA	0.891 (0.858,0.925)

**Table 2. : Highest-rating inferred ROC analysis results showing figures-of-merit and 95% confidence intervals (CI) for modalities averaged over the  $i_1$  (mA) and  $i_2$  (reconstruction method) indexes.**

Crossed Modality Analysis	Reconstruction Method & Tube Current setting	Highest-rating inferred ROC FOM (95% CI)
<i>Averaged over <math>i_1</math></i>	FBP	0.918 (0.894,0.941)
	IR	0.915 (0.891,0.938)
<i>Averaged over <math>i_2</math></i>	20mA	0.892 (0.865,0.919)
	40mA	0.910 (0.884,0.937)
	60mA	0.925 (0.904,0.945)
	80mA	0.938 (0.916,0.960)

**Figure 2: The treatment pairs for analyses averaged over  $i_1$  and  $i_2$ , displaying the magnitude of difference and 95% confidence intervals for the *crossed-modality* JAFROC analysis. For a difference in performance to be declared significant the 95% confidence interval must not include zero. Therefore, statistical differences are observed between 20mA and 40mA, 20mA and 60mA, 20mA and 80mA and 80mA and also between 40mA and 80mA.**



## Conclusions

For this phantom simulation there was no significant difference in lesion detection performance when IR was used in place of FBP. This is in great contrast to previous claims of large percentage dose saving with iterative reconstruction techniques. In this phantom, tube current was optimized at 40mA, an effective dose of 0.97mSv, with clear evidence that lesion detection performance was not maintained at 20mA. This suggests dose saving potential of 50%, on the basis of the tube current range investigated in this work. The quoted figure of dose saving must always be evaluated in consideration of the starting point.

Future work would seek to assess the value of iterative reconstruction in low-contrast body areas, such as the abdomen.

The *crossed-modality* JAFROC analysis method described in this paper has relevance for situations where co-existing factors exist and contribute to observer performance. In the current work, the individual comparisons of all tube current and reconstruction method options would have been inconclusive.

1. Brenner DJ, Hall EJ. "Computed tomography: an increasing source of radiation exposure," *N Engl J Med* 357, 2277–84 (2007).
2. Care Quality Commission, "IR(ME)R Annual Report 2012," Care Quality Commission, 05 February 2013, [http://www.cqc.org.uk/sites/default/files/documents/20130205\\_irmer\\_annual\\_report\\_2012\\_\\_final.pdf](http://www.cqc.org.uk/sites/default/files/documents/20130205_irmer_annual_report_2012__final.pdf) (10 August 2014).
3. Korn A, Fenchel M, Bender B, Danz S, Hauser TK, Ketelsen D, Flohr T, Claussen CD, Heuschmid M, Ernemann U, Brodoefel H. "Iterative reconstruction in head CT: image quality of routine and low-dose protocols in comparison with standard filtered back-projection," *Am J Neuro Radiol* 33, 218-224 (2012).
4. Willemink MJ, Leiner T, de Jong PA, de Heer LM, Nievelstein RA, Schilham AM, Budde RP. "Iterative reconstruction techniques for computed tomography part 2: initial results in dose reduction and image quality," *Eur Radiol* 23, 1632-42 (2013).
5. International Commission on Radiological Protection. "The 2007 Recommendations of the International Commission on Radiological Protection: ICRP Publication 103," *Ann ICRP* 37, 2-4 (2007).
6. Thompson J, Hogg P, Thompson S, Manning D, Szczepura K. "ROCView: prototype software for data collection in jackknife alternative free-response receiver operating characteristic analysis," *Br J Radiol* 85, 1320-1326 (2012).
7. Obuchowski NA, Rockette HE, "Hypothesis testing of the diagnostic accuracy for multiple diagnostic tests: an ANOVA approach with dependant observations," *Commun Stat Simul Comput* 24:285-308 (1995).
8. Obuchowski NA, "Multi-reader multi-modality ROC studies: hypothesis testing and sample size estimation using an ANOVA approach with dependent observations," *Acad Radiol* 2, 522-529 (1995).

## PAPER 7

### EFFECTIVE DOSE AND EFFECTIVE RISK FROM POST–SINGLE PHOTON EMISSION COMPUTED TOMOGRAPHY IMAGING OF THE LUMBAR SPINE

Tootell, A., McEntee, M., Szczepura, K., & Hogg, P. (2016). *Journal of Medical Imaging and Radiation Sciences*, 47(3), 267-275. doi: <http://dx.doi.org/10.1016/j.jmir.2016.04.012>

#### **Abstract**

##### Purpose

Planar bone scans play an important role in the staging and monitoring of malignancy and metastases. Metastases in the lumbar spine are associated with significant morbidity, therefore accurate diagnosis is essential. Supplementary imaging after planar bone scans is often, required to characterise lesions, however, this is associated with additional radiation dose. This paper provides information on the comparative effective dose and effective risk from supplementary lumbar spine radiographs, low-dose CT (LDCT) and diagnostic CT (DCT).

##### Method

Organ dose was measured in a phantom using thermo-luminescent dosimeters. Effective dose and effective risk were calculated for radiographs, LDCT, and DCT imaging of the lumbar spine.

##### Results

Radiation dose was 0.56mSv for the antero-posterior and lateral lumbar spine radiographs, 0.80mSv for LDCT, and 3.78mSv for DCT. Additional imaging resulted in an increase in effective dose of 12.28%, 17.54% and 82.89% for radiographs, LDCT and DCT respectively. Risk of cancer induction decreased as age increased. The difference in risk between the modalities also decreased. Males had a statistically significant higher risk than female patients ( $p=0.023$ ) attributed to the sensitive organs being closer to the exposed area.

##### Conclusion

Effective Dose for LDCT is comparable to radiographs of the lumbar spine. Due to the known benefits image fusion brings it is recommended that LDCT replace radiographs imaging for characterisation of lumbar spine lesions identified on planar bone scan. DCT is associated with significantly higher effective dose than LDCT. Effective risk is also higher and the difference is more marked in younger female patients.

## Introduction

Planar whole-body bone scintigraphy (BS) using Technetium 99m phosphates or phosphonates [1] and a gamma camera continues to play an important role in the staging and monitoring of malignant disease due to its ability to demonstrate lesions earlier than conventional radiographic methods [1, 2]. The lumbar spine is a common site for bony metastases arising from primary tumour sites in the prostate and breast due to venous drainage into the vertebral plexus [3]. Metastases in the spine are associated with significant morbidity, therefore accurate and early diagnosis is important for effective patient management [3-5]. Multiple lesions in the spine detected using BS does not provide a definitive diagnosis but are suggestive of metastatic disease [6]. When solitary spinal lesions are discovered a definitive diagnosis is challenging due to the spectrum of potential pathological processes. These cases are often referred for additional imaging to localise and/or characterise them.

Over a decade ago research lead to a significant change in scanning technique [1]. BS evolved to include single photon emission computed tomography (SPECT) and later computed tomography (CT), with SPECT-CT now regarded as an essential tool in diagnosing and assessing metastatic bone disease [7]. Prior to tomographic imaging, patients were referred for supplementary imaging to help localise or characterise a lesion: typically using conventional plain radiography, CT or MRI. Hybrid imaging systems now allow fusion of CT and SPECT images, providing the clinician with physiological data overlaid on anatomical information. This removes the necessity for side-by-side comparison.

The benefits of image fusion in nuclear medicine imaging are covered extensively in literature, which reports an increase in the accuracy, sensitivity, specificity and diagnostic confidence [8-11]. These benefits are associated with additional risk, since supplementary imaging requires additional radiation dose to the patient. Research has shown that the additional dose from CT acquisitions acquired as part of a SPECT-CT study are not insignificant and on occasions can exceed the dose from the administration of the radiopharmaceutical. Increases in effective dose of between 2% and 600% are reported [12].

The early use of CT in combination with SPECT was aimed at attenuation correction (AC) and consisted of a CT component with fixed acquisition parameters. These scanner types are frequently referred to as low-dose with an effective dose 80-85% lower than diagnostic quality CT scans [12-15]. Diagnostic CT (DCT) can be used to aid diagnosis rather than correcting the emission data alone [16] and also provide localisation data [17]. Regardless of the modality the additional dose has to be taken into account in the justification of the exposure [18, 19]. Justification should ensure that the benefit of the exposure outweighs the potential risk from the additional exposure.

The additional dose from the CT component of SPECT-CT has been investigated [12-15]. Larkin et al [14], Sharma et al [12] and Montes et al [15] use the dose length product and conversion ( $k$ ) factors to calculate effective dose. Hara et al [13] measured organ dose with thermoluminescent dosimeters (TLD) however only organs within the primary beam were measured. The paper does not recreate the clinical situation where organs outside the primary beam would be subject to scatter radiation.

The aims of our research are to calculate effective dose and effective risk from imaging of the lumbar spine using radiographs, LDCT and DCT. From this data the additional dose over BS alone are calculated. Male and female effective risk will be compared to figures from SPECT alone and SPECT plus supplementary imaging.

## Method

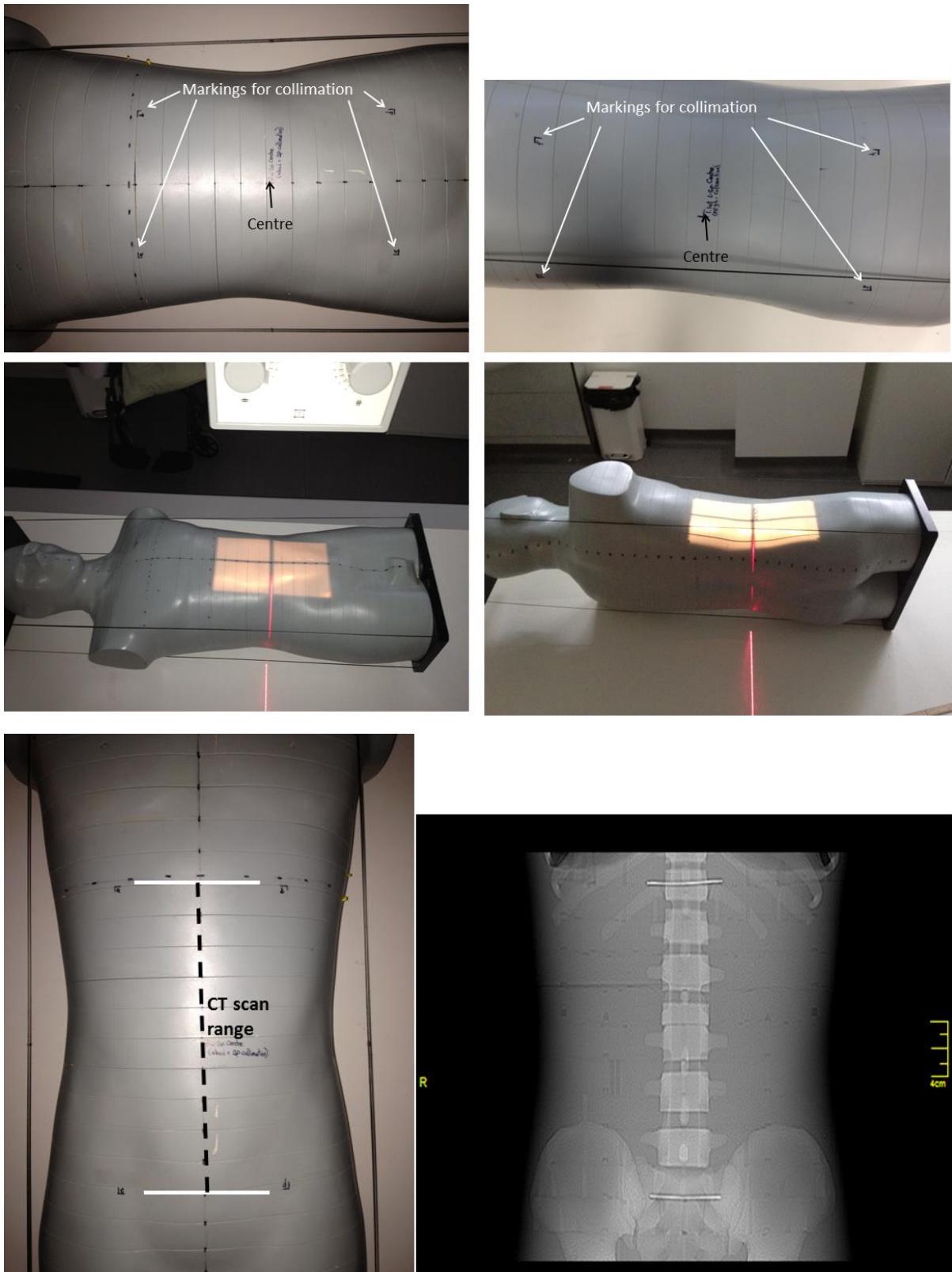
Using an adult dosimetry phantom (ATOM 701D (CIRS Inc, Virginia USA)), organ dose was measured using thermo-luminescent dosimeters (TLD100H (Thermo Fisher Scientific Massachusetts, USA)) . Effective dose and effective risk were calculated as described below. Three imaging systems were used in this study. The first was radiographs using a Wolverson Acroma General X-ray system (Willenhall, UK) with an Agfa computed radiography system (Agfa Health Care, Mortsel, Belgium). The second was multi-detector diagnostic CT (DCT) (Toshiba Aquillion 16, Toshiba Medical Systems Corporation, Tochigi-ken, Japan). The third was a low-specification CT component from a hybrid SPECT-CT system (low-dose CT (LDCT)) (GE Infinia Hawkeye 4, GE Healthcare, Little Chalfont, UK). Imaging equipment quality control for tube output and automatic exposure devices met the required standards and manufacturer guidelines [20-22]. Air-calibrations for the two CT systems were performed as part of the warm-up procedures. The imaging parameters were based on those used in the clinical environment and had undergone an optimisation process through audits of image quality and diagnostic reference levels. The automatic exposure control for radiographs and the mA modulation function for the DCT were used. For LDCT exposure factors for an average sized patient were used (Table 2).

### The Phantom

The anthropomorphic dosimetry phantom consists of 39 contiguous sections of differing density epoxy resin (representing bone, lung and soft tissue) that when put together make up the head and torso of an adult male. TLD locations were positioned for precise dosimetry of specific internal organs. Whole body effective dose calculation was completed using the ATOM 701-D configuration that utilises a total of 271 TLDs over 22 organs [23, 24].

For AP and lateral lumbar spine, the area of interest adhered to criteria set out in a standard radiography technique book [25]. The medial-sagittal and medial-coronal planes, the field of view and the centre for antero-posterior and left lateral projections of the lumbar spine were marked onto the phantom's surface with permanent marker pen and radiolucent markers were used to aid positioning of the CT acquisitions (Figure 1).

**FIGURE 1 MARKING THE PHANTOM FOR AP AND LEFT LATERAL LUMBAR SPINE PROJECTIONS AND CT LUMBAR SPINE.**



Positioning the phantom for the LDCT acquisition on the SPECT-CT hybrid system involved the use of external positioning aids. Commercially available laser spirit levels allowed the phantom to be centrally positioned on the table and parallel to its long axis. A scout view is not routinely acquired as planning of the CT range is performed on patients using the emission data. To ensure close replication of clinical practice the scan range was determined by setting a zero refresh rate on the positioning monitor and placing a  $^{57}\text{Co}$  source on the markings on the phantom until it was visible on the scanner's positioning monitor. These two points corresponded to the upper and lower limit of the CT acquisition. To ensure the use of the unsealed source in this manner did not contribute to the dose recorded by the TLDs, the dose recorded in 5 seconds at a distance of 1 cm in air was calculated. Using the reference activity of 3.7 MBq for the Cobalt source resulted in  $6.53 \times 10^{-4}$  mGy. This value is below the sensitivity of the TLDs and so was considered negligible when calculating the dose from the TLDs in the phantom.

#### Thermoluminescent dosimeters

The TLDs were read using a Harshaw 3500 manual TLD reader one day after their exposure. To ensure accuracy and reproducibility the TLDs were subjected to quality control checks. The TLDs were annealed by heating to 240°C for 10 minutes. They were then exposed to a uniform field of X-radiation using a general x-ray unit, processed and grouped together into batches of similar response. To ensure repeatability the batches were annealed and exposed to the same uniform field and their responses compared. A paired student t-test was performed and there was no significant difference in the responses of the two exposures ( $p > 0.1$ ). The inter batch coefficient of variance was calculated and was less than 2.0%. Calibration was performed on each batch using a general x-ray unit at energies of 120kV and 80kV to correspond with settings used in the imaging protocols [26]

The TLDs were positioned in the phantom at locations of the organs identified in ICRP 103 (Table 1) at the organ positions specified by the manufacturer [23, 24, 27]. Five TLDs remained with the phantom at all times apart from during image acquisition for background correction.

**TABLE 1 NUMBER OF TLDs USED IN CRITICAL ORGANS**

Organ	Number of TLD	Organ	Number of TLD
Adrenals	2	Liver	30
Bladder	16	Lungs	36
Brain	11	Oesophagus	3
Breast	2	Pancreas	5
Active bone Marrow	85 Clavicle 20, Cranium 4 Cervical Spine <sup>†</sup> 2 Femora 4 Mandible <sup>◇×</sup> 6 Pelvis 18 Ribs 18 Sternum 4 Thoraco-lumbar Spine 9	Prostate	3
Eyes*	2	Spleen	14
Gall Bladder	5	Stomach	11
Heart	2	Testes	2
Intestine (Small and large)	16 Colon 11 Small intestine 5	Thyroid	10
Kidneys	16	Thymus	4
<p>* Not included in effective dose calculations</p> <p>† TLDs located in the anterior of C2 and upper oesophagus were used to calculate extra thoracic organ dose</p> <p>◇ TLDs located in the left and right lingula of the mandible and to the left and right of the sublingual fossa were used to calculate salivary gland organ dose</p> <p>× TLDs located in the left and right lingula of the mandible were used to calculate oral mucosa organ dose</p>			

To increase the signal to noise ratio of the TLD readings three complete exposures were performed using the acquisition parameters shown in Table 2. This resulted in a cumulative dose being recorded on the TLDs which was divided by three to give a dose per exposure. Effective dose for the three modalities was calculated using tissue weighting factors listed in ICRP report 103 [27] (see Table 3). Statistical analysis was performed using two-way ANOVA with post hoc testing with Bonferroni correction.

**TABLE 2 PARAMETERS USED FOR IMAGING THE LUMBAR SPINE IN CR, DIAGNOSTIC CT AND LOW DOSE CT**

<b>Radiographs</b>			
	kV	AED chamber	Post mAs
AP	75	Central	Mean 60 (SD=0)
Left lateral	80	Central	Mean 72 (SD=0)

<b>Diagnostic CT</b>			
Scan Projection Radiograph			
	kV	mAs	Scan range
AP	120	150	250 mm
Left Lateral	120	45	250 mm

<b>Axial scan</b>						
Mode	kV	mA	Rotation (s)	Pitch	Detector range	Scan range
Helical	120	Auto Lower: 100  Upper: 450  SD: 7.5	0.75	0.938	16 mm 16x1 mm	245 mm Upper- Mid T12 Lower- Upper S3

<b>Low Dose CT</b>						
Mode	kV	mA	Rotation (rotations per minute)	Pitch (distance per rotation) (mm)	Detector range	Scan range
Helical	120	2.5	2	1.9	20 mm 4 x 5 mm	245 mm Upper- Mid T12 Lower- Upper S3

**TABLE 3 TISSUE WEIGHTING FACTORS FROM ICRP REPORT 103 [18]**

Tissue	$W_T$	$\sum w_T$
Bone Marrow, Colon, Lung, Stomach, Breast, Remainder tissues*	0.12	0.72
Gonads	0.08	0.08
Bladder, Oesophagus, Liver, Thyroid	0.04	0.16
Bone Surface <sup>x</sup> , Brain, Salivary glands, Skin <sup>x</sup>	0.01	0.04
*adrenals, extrathoracic region, gallbladder, heart, kidneys, lymphatic nodes <sup>x</sup> , oral mucosa, pancreas, prostate, small intestine, spleen, thymus		
<sup>x</sup> excluded in this study.		

Risk calculations were carried out following a method described by Brenner [28, 29]. Lifetime risk of cancer incidence figures were obtained from Wall et al [30]. The sum of the product of the measured organ dose (mGy) and the life time risk of cancer incidence for that organ (percentage per mGy) gave the effective risk. Resources dictated that the phantom used within this study was male, however by using TLD readings from locations that correspond with the gonads and uterus and excluding the male testes and prostate it was possible to calculate an effective risk for females.

Organ and effective dose from the administration of 800 MBq <sup>99m</sup>Tc labelled phosphate or phosphonates was calculated using dose per unit activity (mSv/MBq) from Bombardieri et al [1]. Comparisons were made between the dose from additional imaging and the initial bone scan acquisition.

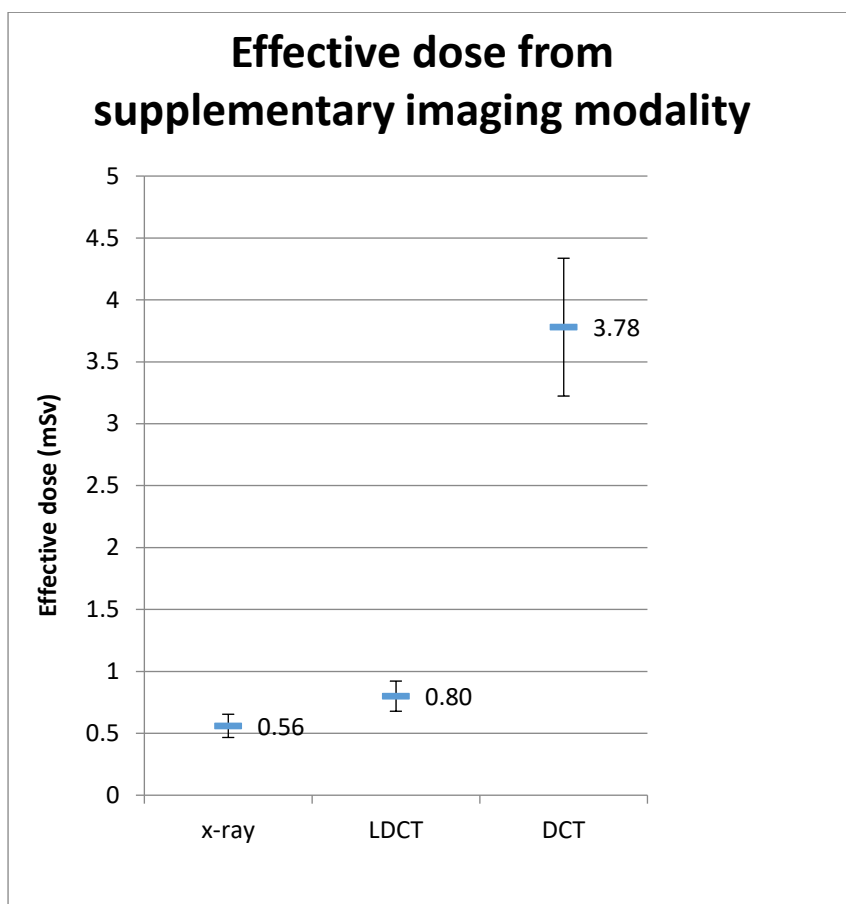
## Results

A comparison of dose data as displayed by the modalities is shown in Table 4. DLP and CTDi are significantly higher for DCT compared to LDCT. This supports the findings of the dosimetry data that DCT will result in a higher dose. Comparison of the effective dose from the three supplementary imaging techniques is shown in Figure 2. Imaging using DCT results in a higher effective dose compared to radiographs and LDCT. The error bar for DCT is larger due to the 2% error in the TLDs being applied to a larger dose reading.

**TABLE 4 COMPARISON OF DAP/DLP AND CTDI**

	Radiographs	LDCT	DCT
DAP (mGy.cm <sup>2</sup> )	2873	--	--
DLP (mGy.cm)	--	96.0	349.6
CTDi (mGy)	--	3.97	20.0

FIGURE 2 EFFECTIVE DOSE FROM THE SUPPLEMENTARY IMAGING MODALITIES<sup>3</sup>



Effective dose is calculated from the sum of the weighted organ doses and does not indicate the difference to individual organs. Table 5 and Table 6 illustrate the organ dose from and increase due to the supplementary imaging modality compared to the calculated organ dose from the administration of the radiopharmaceutical. Certain organs, for example the colon, liver and stomach, exhibit a large increase due to the low uptake of radiopharmaceutical but are situated within the scan range. There is a consistent difference in organ dose between DCT and LDCT and DCT and radiographs showing the distribution of the organ dose is consistent for the supplementary imaging modality.

<sup>3</sup> The error bars displayed in this figure were calculated through the propagation of the 2% error of the TLDs. The error of each TLD was applied to the recorded dose and the potential upper (+2%) and lower (-2%) values of the TLDs were calculated. These values (upper, measured and lower) were used in effective dose calculations and displayed in Figure 2.

**TABLE 5 COMPARISON OF ORGAN DOSE FROM THE THREE SUPPLEMENTARY MODALITIES COMPARED TO THE BONE SCAN (800MBQ PHOSPHATE OR PHOSPHONATE).**

Organ	Absorbed dose (mGy)			
	BS	Radiographs	LDCT	DCT
Active bone marrow	7.36	0.15	0.33	1.75
Bladder	38.40	0.55	0.59	3.83
Brain	1.36	0.00	0.00	0.01
Breast	0.57	0.04	0.07	0.44
Colon	2.16	1.58	2.12	9.00
Liver	0.96	1.42	1.42	7.23
Lungs	1.04	0.11	0.15	1.16
Oesophagus	0.80	0.06	0.11	0.72
Stomach	0.96	1.29	2.14	9.86
Thyroid	1.04	0.01	0.02	0.09
Remainder organ	1.52	0.79	1.10	5.21

**TABLE 6 INCREASE IN ORGAN DOSE FOR THE ORGANS**

Organ	Absorbed dose (mGy)						
	BS only	BS & Radiographs		BS & LDCT		BS & DCT	
		mGy	% increase	mGy	% increase	mGy	% increase
Active bone marrow	7.36	7.51	2.09	7.69	4.49	9.11	23.76
Bladder	38.40	38.95	1.43	38.99	1.55	42.23	9.97
Brain	1.36	1.36	0.04	1.36	0.02	1.37	0.73
Breast	0.57	0.61	7.72	0.64	12.39	1.01	77.86
Colon	2.16	3.74	73.26	4.28	98.2	11.16	16.54
Liver	0.96	2.38	147.58	2.38	147.73	8.19	753.27
Lungs	1.04	1.15	10.14	1.19	14.83	2.20	111.76
Oesophagus	0.80	0.86	7.87	0.91	13.93	1.52	89.4
Stomach	0.96	2.25	134.74	3.10	222.95	10.82	1027.35
Thyroid	1.04	1.05	0.83	1.06	2.23	1.13	8.81
Remainder	1.52	2.31	52.04	2.62	72.41	6.73	342.47

Using data published by Wall et al[30], life time cancer risk for all cancers and cancers of the organs identified in Table 6 were calculated. Comparison of risk between bone scan (BS) only, BS with conventional radiography, BS with low dose CT, and BS with diagnostic CT from 40 to 89 years are shown in Figure 3, Figure 4 and Figure 5.

**FIGURE 3 EFFECTIVE RISK FROM EXPOSURE FOR ALL CANCERS FOR A EURO-AMERICAN POPULATION**

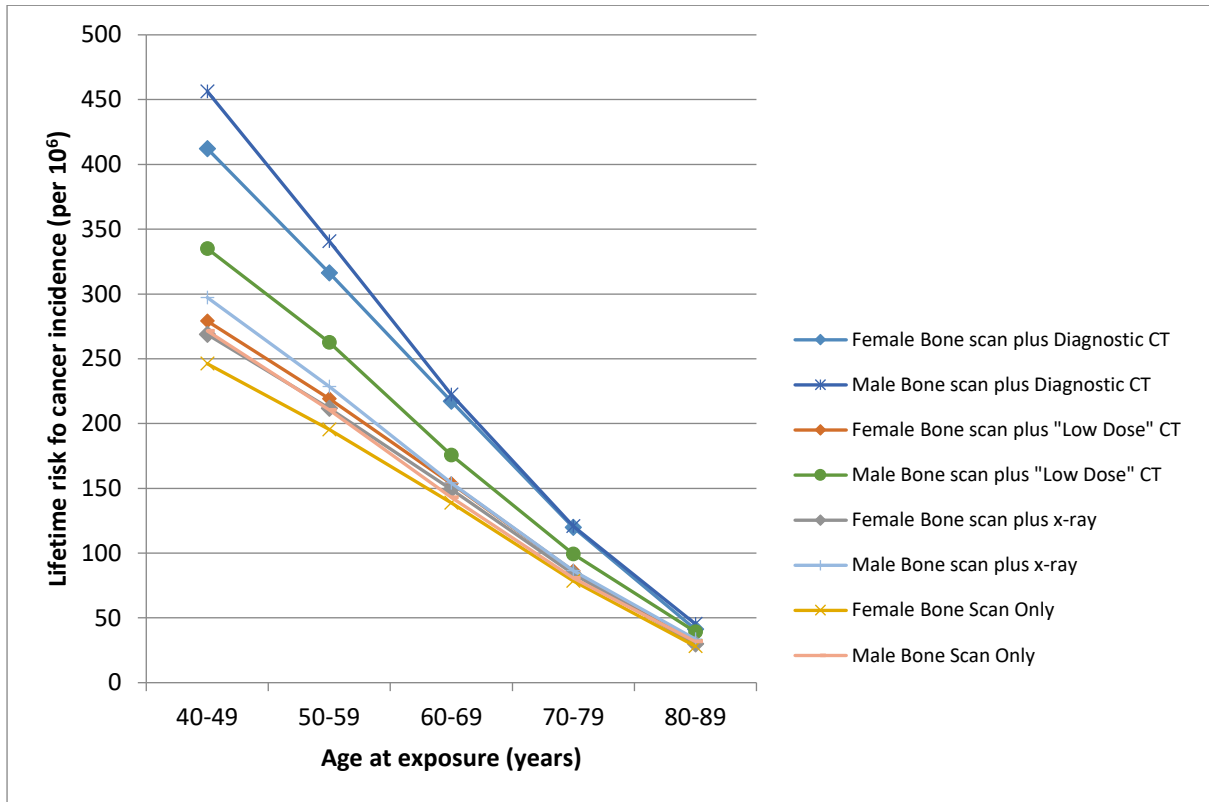


**FIGURE 4 EFFECTIVE RISK FROM EXPOSURE FOR ALL CANCERS FOR A FEMALE EURO-AMERICAN POPULATION**

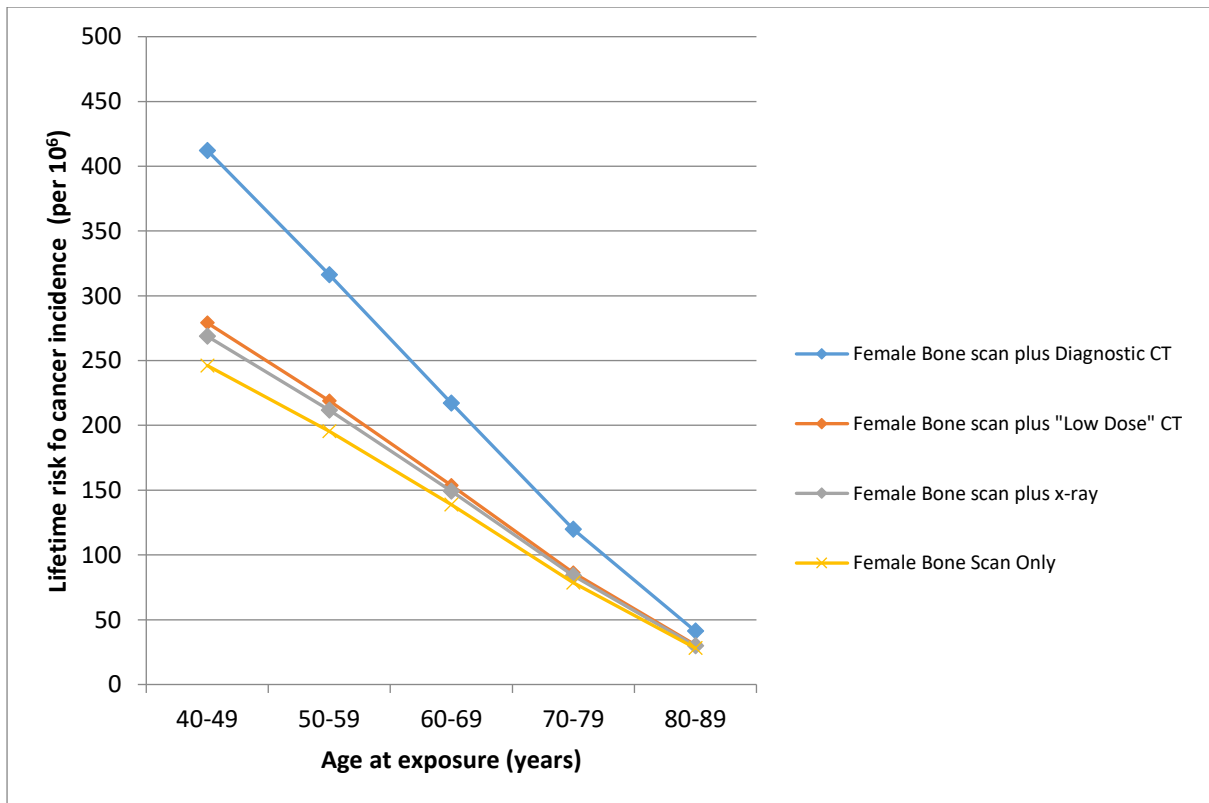
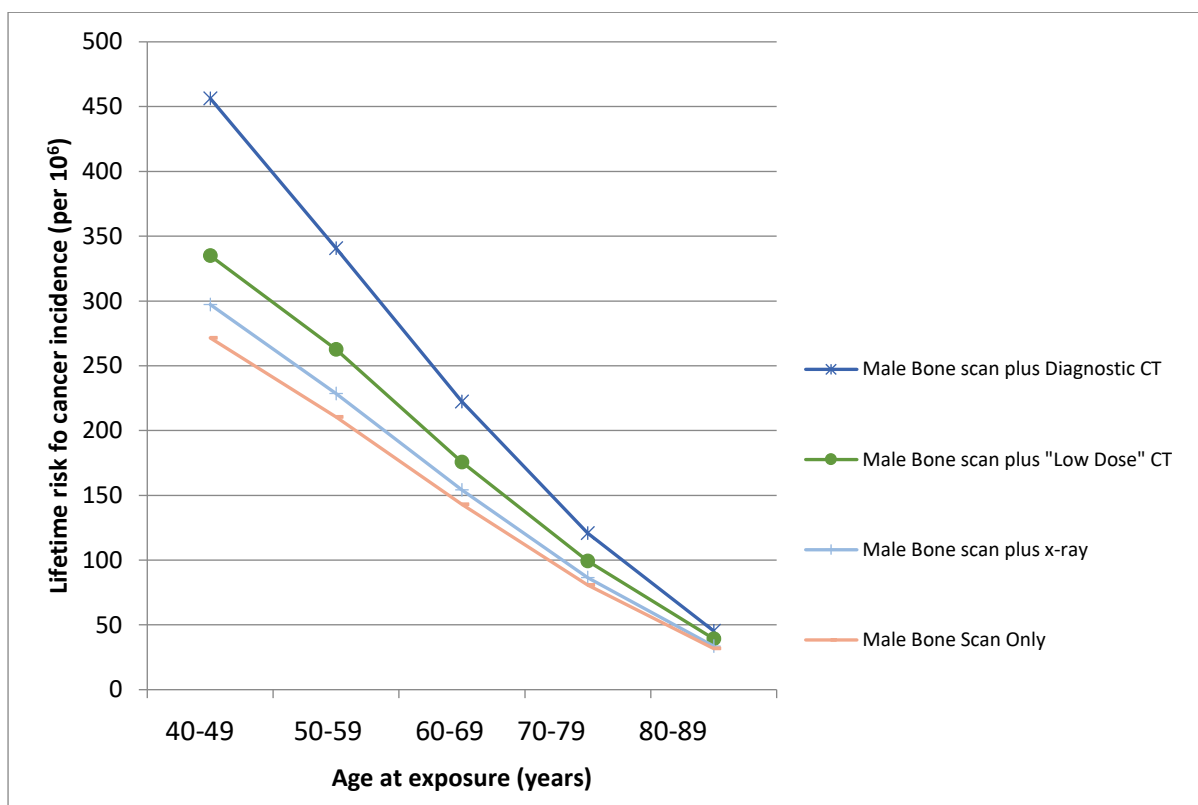


**FIGURE 5 EFFECTIVE RISK FROM EXPOSURE FOR ALL CANCERS FOR A MALE EURO-AMERICAN POPULATION**



## Discussion

Image fusion has been shown to increase accuracy and reporter confidence [8-11]. It has been suggested that DCT that can further aid diagnostic decisions due to its ability to acquire and display submillimetre structures thus showing the accurate location and internal architecture of a lesion [31-35]. To date little data directly comparing the additional organ and effective dose and effective risk for all available supplementary imaging options has been published. Results show that the effective dose from lumbar spine imaging using radiographs was 0.56 mSv ( $\pm 0.09$ ), LDCT 0.80 mSv ( $\pm 0.12$ ) and DCT was 3.78 mSv ( $\pm 0.56$ ), The calculated effective dose from the administration of 800 MBq of  $^{99m}\text{Tc}$  labelled phosphate or phosphonate is 4.56 mSv. Thus the additional effective dose from supplementary imaging is 12.3% for radiographs, 17.5% for LDCT and 82.9% for DCT.

This increase in effective dose was hypothesised and this result is in agreement with other research [12-14, 36]. However consideration of effective dose does not provide the narrative as it is not apparent which organs contribute to this increase. Table 6 shows there are increases in organ dose from the supplementary imaging techniques. Comparison of organ doses using two way ANOVA showed that there was a statistically significant difference between the three options ( $p=0.001$ ). Post hoc testing with Bonferroni correction showed that there was a statistically significant difference between BS & DCT and BS & LDCT ( $p=0.001$ ) and BS & DCT and BS & radiographs ( $p=0.001$ ). There was no statistical difference between BS & LDCT and BS & radiographs ( $p=0.810$ ). On this basis there is a strong rationale for the use of LDCT over radiographs for imaging the lumbar spine. There is no statistically significant increase in organ dose and literature suggests that accuracy and clinician confidence is increased when using LDCT compared with radiographs.

There is no change to the urinary bladder dose and there is a relatively small increase in dose (from 38.4 mGy to 42.23 mGy (9.91%) for BS & DCT, 38.99 (1.55%) for LDCT and 38.95 mGy (1.43%) for BS & radiographs). The stomach receives one of the lowest doses from the radiopharmaceutical (0.96 mGy). Following supplementary imaging this figure increases to 10.82 mGy (+1027.35%) for BS+DCT, 3.10 mGy (+222.95%) for BS & LDCT and 2.25 mGy (+134.74%) for BS & radiographs. These results are due to the organ being directly in the field of view when imaging the lumbar spine. While these results are specific to lumbar spine imaging they have shown that the supplementary imaging can significantly increase organ dose.

Effective dose is commonly used in medical imaging to compare the risks from different modalities or techniques. Effective dose should not be used to calculate risk to an individual patient or patient types as it does not consider the age of the patient. Effective risk is a method described by Brenner [28, 29, 37] and Wall [30] in which tissue weighting factors are replaced with organ-specific radiation-induced cancer risk, such as those published by The Nuclear and Radiation Studies board [38], and Wall [30]. Discussion about the use of effective dose and effective risk are beyond the remit of this article but are reported widely in literature [28-30, 37, 39-42].

Figure 4 and Figure 5 illustrate the difference in the lifetime risk of radiation induced cancer between the supplementary modalities with increasing age. The difference between these values does decrease with age and when comparison is made between the effective risk for patients over 70 the difference is very small. The higher organ doses for BS & DCT is reflected in the higher risks for these ages with an incidence of 217 per million exposures for females and 154 per million examinations for males.

A limitation of this study is that the whole of the lumbar spine was imaged by the three modalities. In clinical practice a localised CT scan based on the planar and SPECT bone scan could be performed as opposed to the whole lumbar spine. This would limit the exposure to the area of interest meaning that organ doses would be less. This is likely not to be the case for radiographs where the full lumbar spine would be imaged. In other words, LDCT would likely be lower than radiographs.

This study uses the standard adult male phantom for dosimetry measurements. External validity of the research could be improved with the use of a female anthropomorphic phantom. However initial comparison of risk between male and female shows that the figures for male patients are higher. The reason for the difference is due to differences in the sensitivities of the tissues. Sensitive organs in the female patient such as the breast tissue receive very little additional dose in imaging the lumbar spine as these are outside the field of view. Also, the specific focus of this work is the lumbar spine; a lesion requiring further clarification in the thoracic spine would result in breast tissue receiving a higher dose and would affect effect risk. Further research into supplementary imaging of other common sites of bony pathology is therefore warranted.

In older patients there is little additional risk however, in younger patients, risk is greater. In patients over 70 the difference in risk from the additional imaging decreases to the point where performing a DCT instead of LDCT could be justified. DCT can provide diagnostic image quality and afford good diagnostic value in the characterisation of a lesion.

Even-Sapir et al [31] suggest that referral for and justification of DCT over LDCT should be taken on a case-by-case basis and the benefits of the higher image quality and therefore high dose balanced against the risks [31]. There are likely to be instances when higher resolution images are required and in these cases the higher dose and associated risk from DCT is justified. The diagnostic value of the supplementary imaging options is beyond this work but research has shown the benefit of

supplementing SPECT with CT [8, 31, 43, 44]. Further research in the usefulness of higher dose/higher quality CT acquisitions compared to low dose would facilitate the risk/benefit discussion.

Accepted practice is to use CT as a supplementary imaging modality over radiographs due to the benefits image fusion brings [45-47]. Recent papers consider the use of 16 slice or higher CT scanners and they note that the improved image quality allows reporters to comment upon the internal structure of a lesion as well as identifying its location [8, 9, 31, 43, 44, 48]. The current work has shown acquisitions using DCT result in a statistically significant higher dose.

### **Conclusion**

Our work demonstrates that a DCT acquisition result in an effective dose and effective risk that is significantly higher than a LDCT acquisition. The LDCT system used in our work has demonstrated a small increase in dose and risk compared with radiographs. However LDCT brings the benefits of improved diagnostic confidence and thus are recommended as the preferred choice of bone scan supplemental imaging for bony metastases.

1. Bombardieri E, Aktolun C, Baum RP, Bishof-Delaloye A, Buscombe J, Chatal JF, et al., *Bone scintigraphy: procedure guidelines for tumour imaging*. Eur J Nucl Med Mol Imaging, 2003. **30**(12): p. BP99-106.
2. Nathan M, Gnanasegaran G, Adamson K, and Fogelman I, *Bone Scintigraphy: Patterns, Variants, Limitations and Artefacts*, in *Radionuclide and Hybrid Bone Imaging*, I. Fogelman, G. Gnanasegaran, and H. Wall, Editors. 2012, Springer Berlin Heidelberg. p. 377-408.
3. Davies AM, Sundaram M, and James SJ, *Imaging of Bone Tumors and Tumor-Like Lesions: Techniques and Applications*. 2009: Springer-Verlag.
4. Abdel Razek AA and Castillo M, *Imaging appearance of primary bony tumors and pseudo-tumors of the spine*. J Neuroradiol, 2010. **37**(1): p. 37-50.
5. Rodallec MH, Feydy A, Larousserie F, Anract P, Campagna R, Babinet A, et al., *Diagnostic imaging of solitary tumors of the spine: what to do and say*. Radiographics, 2008. **28**(4): p. 1019-41.
6. Rodallec MH, Feydy A, Larousserie F, Anract P, Campagna R, Babinet A, et al., *Diagnostic Imaging of Solitary Tumors of the Spine: What to Do and Say*. RadioGraphics, 2008. **28**(4): p. 1019-1041.
7. International Atomic Energy Agency, *Clinical Applications of SPECT/CT: New Hybrid Nuclear Medicine Imaging System (IAEA-TECDOC-1597)*. 2008: Vienna, Austria.
8. Helyar V, Mohan HK, Barwick T, Livieratos L, Gnanasegaran G, Clarke SE, et al., *The added value of multislice SPECT/CT in patients with equivocal bony metastasis from carcinoma of the prostate*. Eur J Nucl Med Mol Imaging, 2010. **37**(4): p. 706-13.
9. Jiang L, Han L, Tan H, Hu P, Zhang Y, and Shi H, *Diagnostic value of (9)(9)mTc-MDP SPECT/spiral CT in assessing indeterminate spinal solitary lesion of patients without malignant history*. Ann Nucl Med, 2013. **27**(5): p. 460-7.
10. Patel CN, Chowdhury FU, and Scarsbrook AF, *Hybrid SPECT/CT: the end of "unclear" medicine*. Postgrad Med J, 2009. **85**(1009): p. 606-13.
11. Utsunomiya D, Shiraishi S, Imuta M, Tomiguchi S, Kawanaka K, Morishita S, et al., *Added Value of SPECT/CT Fusion in Assessing Suspected Bone Metastasis: Comparison with Scintigraphy Alone and Nonfused Scintigraphy and CT1*. Radiology, 2006. **238**(1): p. 264-271.
12. Sharma P, Sharma S, Ballal S, Bal C, Malhotra A, and Kumar R, *SPECT-CT in routine clinical practice: increase in patient radiation dose compared with SPECT alone*. Nucl Med Commun, 2012. **33**(9): p. 926-32.
13. Hara N, Onoguchi M, Takenaka K, Matsubara K, Ujita H, and Kenko Y, *Assessment of Patient Exposure to X-Radiation from SPECT/CT Scanners*. Journal of Nuclear Medicine Technology, 2010. **38**(3): p. 138-148.
14. Larkin AM, Serulle Y, Wagner S, Noz ME, and Friedman K, *Quantifying the Increase in Radiation Exposure Associated with SPECT/CT Compared to SPECT Alone for Routine Nuclear Medicine Examinations*. International Journal of Molecular Imaging, 2011. **2011**.
15. Montes C, Tamayo P, Hernandez J, Gomez-Caminero F, Garcia S, Martin C, et al., *Estimation of the total effective dose from low-dose CT scans and radiopharmaceutical administrations delivered to patients undergoing SPECT/CT explorations*. Ann Nucl Med, 2013. **27**(7): p. 610-7.
16. Griffiths M, Thompson J, Tootell A, Driver J, Kane T, Mountain V, et al., *SPECT-CT and its role in imaging and oncology*. Imaging in Oncology, Society of Radiographers, 2009.
17. Sharma P, Singh H, Kumar R, Bal C, Thulkar S, Seenu V, et al., *Bone scintigraphy in breast cancer: added value of hybrid SPECT-CT and its impact on patient management*. Nuclear Medicine Communications, 2012. **33**(2): p. 139-147.
18. International Commission on Radiological Protection, *ICRP Publication 103: Recommendations of the ICRP*. 2013: SAGE Publications.
19. International Commission on Radiological Protection, *1990 Recommendations of the International Commission on Radiological Protection: User's Edition*. 1992: International Commission on Radiological Protection.

20. GE Healthcare, *Infinifa + Hawkeye 4 User's Guide*. 2006, Buckinghamshire, UK: GE Healthcare.
21. Hiles PA, Mackenzie A, Scally A, and Wall B, *Recommended Standards for the Routine Performance Testing of Diagnostic X-ray Imaging Systems*. 2005: Institute of Physics and Engineering in Medicine.
22. Toshiba Medical Systems Corporation, *Operation Manual for Toshiba Scanner Aquillion TSX-101A Reference Volume*. 2008, Tochigi-Ken, Japan: Toshiba Medical Systems Corporation.
23. CIRS Tissue Simulation and Phantom Technology, *Adult Male Phantom Model Number 701-D Appendix 5*. 2010, CIRS, Inc: Virginia, USA.
24. CIRS Tissue Simulation and Phantom Technology. *Dosimetry Verification Phantoms Model 701-706 Data Sheet*. 2012 [cited 2012 19th January]; Available from: [http://www.cirsinc.com/file/Products/701\\_706/701\\_706\\_DS.pdf](http://www.cirsinc.com/file/Products/701_706/701_706_DS.pdf).
25. Clark KC, Whitley AS, Sloane C, and Hoadley G, *Clark's Positioning In Radiography*. 2005: Arnold Publishers.
26. Tootell A, Szczepura K, and Hogg P. *e090: Effective Dose from Computed Tomography Attenuation Correction for Myocardial Perfusion Imaging: A comparison of Four Commonly Used systems*. United Kingdom Radiographic Congress 2013; Available from: <http://ukrc2013.profile-e posters.co.uk/eposter/action/view/layout/2/id/3351>.
27. ICRP, *The 2007 Recommendations of the ICRP*, in *ICRP Publication 103*. 2007, Ann. ICRP. p. 2-4.
28. Brenner DJ, *Effective dose: a flawed concept that could and should be replaced*. *British Journal of Radiology*, 2008. **81**(967): p. 521-523.
29. Brenner DJ, *Effective Dose- A Flawed Concept that Could and Should be Replaced*, in *International Commission on Radiological Protection*. 2011: Washington DC.
30. Wall BF, Haylock R, Jansen JTM, Hillier MC, Hart D, and Shrimpton PC, *Radiation Risks from Medical X-ray Examinations as a Function of the Age and Sex of the Patient. Report HPA-CRCE-028*. 2011, Health Protection Agency: Chilton.
31. Even-Sapir E, Flusser G, Lerman H, Lievshitz G, and Metser U, *SPECT/Multislice Low-Dose CT: A Clinically Relevant Constituent in the Imaging Algorithm of Nononcologic Patients Referred for Bone Scintigraphy*. *Journal of Nuclear Medicine*, 2007. **48**(2): p. 319-324.
32. Even-Sapir E, Keidar Z, and Bar-Shalom R, *Hybrid Imaging (SPECT/CT and PET/CT)—Improving the Diagnostic Accuracy of Functional/Metabolic and Anatomic Imaging*. *Seminars in Nuclear Medicine*, 2009. **39**(4): p. 264-275.
33. Thompson J, Hogg P, Higham S, and Manning D, *Accurate localization of incidental findings on the computed tomography attenuation correction image: the influence of tube current variation*. *Nucl Med Commun*, 2013. **34**(2): p. 180-4.
34. Thompson J, Hogg P, Manning D, and Szczepura K. *Lesion detection in the CT attenuation correction image of 5 different low resolution SPECT/CT systems: a multi-centre study*. in *British Nuclear Medicine Society*. 2012. Harrogate: Lippincott Williams Wilkins.
35. Thompson JD, Hogg P, Manning DJ, Szczepura K, and Chakraborty DP, *A Free-response Evaluation Determining Value in the Computed Tomography Attenuation Correction Image for Revealing Pulmonary Incidental Findings: A Phantom Study*. *Academic Radiology*, 2014. **21**(4): p. 538-545.
36. Horger M, Eschmann SM, Pfannenbergl C, Vonthein R, Besenfelder H, Claussen CD, et al., *Evaluation of Combined Transmission and Emission Tomography for Classification of Skeletal Lesions*. *American Journal of Roentgenology*, 2004. **183**(3): p. 655-661.
37. Brenner DJ, *We can do better than effective dose for estimating or comparing low-dose radiation risks*. *Annals of the ICRP*, 2012. **41**(3-4): p. 124-128.
38. Committee to Assess Health Risks from Exposure to Low Levels of Ionizing Radiation, Nuclear and Radiation Studies Board Division on Earth and Life Studies, and National Research Council of the National Academies, *Health Risks From Exposure to Low Levels of Ionizing Radiation: BEIR VII Phase 2*. 2006: Washington, DC.

39. Dietze G, Harrison JD, and Menzel HG, *Effective dose: a flawed concept that could and should be replaced. Comments on a paper by D J Brenner (Br J Radiol 2008;81:521–3)*. British Journal of Radiology, 2009. **82**(976): p. 348-351.
40. Martin CJ, *Effective dose: how should it be applied to medical exposures?* British Journal of Radiology, 2007. **80**(956): p. 639-647.
41. Ortiz P, *The use of Effective Dose in Medicine in The 2nd International Symposium on the System of Radiological Protection*. 2013, ICRP: United Arab Emirates.
42. Tootell A, Szczepura K, and Hogg P, *An overview of measuring and modelling dose and risk from ionising radiation for medical exposures*. Radiography, 2014. **20**(4): p. 323-332.
43. Even-Sapir E, *Imaging of Malignant Bone Involvement by Morphologic, Scintigraphic, and Hybrid Modalities\**. Journal of Nuclear Medicine, 2005. **46**(8): p. 1356-1367.
44. Ndlovu X, George R, Ellmann A, and Warwick J, *Should SPECT-CT replace SPECT for the evaluation of equivocal bone scan lesions in patients with underlying malignancies?* Nuclear Medicine Communications, 2010. **31**(7): p. 659-665.
45. Palmedo H, Marx C, Ebert A, Kreft B, Ko Y, Türler A, et al., *Whole-body SPECT/CT for bone scintigraphy: diagnostic value and effect on patient management in oncological patients*. European Journal of Nuclear Medicine and Molecular Imaging, 2014. **41**(1): p. 59-67.
46. British Nuclear Medicine Society. *Clinical Guideline for Bone Scintigraphy*. 2014 [cited 2015 4th March]; Available from: [http://www.bnms.org.uk/images/stories/Procedures\\_and\\_Guidelines/BNMS\\_Bone\\_Scintigraphy\\_Guideline\\_v1.pdf](http://www.bnms.org.uk/images/stories/Procedures_and_Guidelines/BNMS_Bone_Scintigraphy_Guideline_v1.pdf).
47. Zhang Y, Shi H, Cheng D, jiang L, Xiu Y, Li B, et al., *Added value of SPECT/spiral CT versus SPECT in diagnosing solitary spinal lesions in patients with extraskkeletal malignancies*. Nuclear Medicine Communications, 2013. **34**(5): p. 451-458.
48. Palmedo H, Marx C, Ebert A, Kreft B, Ko Y, Turler A, et al., *Whole-body SPECT/CT for bone scintigraphy: diagnostic value and effect on patient management in oncological patients*. Eur J Nucl Med Mol Imaging, 2014. **41**(1): p. 59-67.

## PAPER 8

### ANALYSIS OF EFFECTIVE AND ORGAN DOSE ESTIMATION IN CT WHEN USING mA MODULATION: A SINGLE SCANNER PILOT STUDY

Tootell, A., Szczepura, K., & Hogg, P. (2017). *Radiography*, 37(0), 842–847. doi: <https://doi.org/10.1016/j.radi.2017.02.006>

#### **Abstract**

Effective dose (ED) estimation in CT examinations can be obtained by combining dose length product (DLP) with published ED per DLP coefficients or performed using software. These methods do not account for tube current (mA) modulation which is influenced by patient size.

#### **Aim**

To compare different methods of organ and ED estimation to measured values when using mA modulation in CT chest, abdomen and pelvis examinations.

#### **Method**

Organ doses from CT of the chest, abdomen and pelvis were measured using digital dosimeters and a dosimetry phantom. ED was calculated. Six methods of estimating ED accounting for mA modulation were performed using ImPACT CTDosimetry and Dose Length Product to ED coefficients. Corrections for the phantom mass were applied resulting in 12 estimation methods. Estimated organ doses from ImPACT CTDosimetry were compared to measured values.

#### **Results**

Calculated EDs were; chest 12.35 mSv ( $\pm 1.48$  mSv); abdomen 8.74 mSv ( $\pm 1.36$  mSv) and pelvis 4.68 mSv ( $\pm 0.75$  mSv). There was over estimation in all three anatomical regions. Correcting for phantom mass improved agreement between measured and estimated ED. Organ doses showed overestimation of dose inside the scan range and underestimation outside the scan range.

#### **Conclusion**

Reasonable estimation of effective dose for CT of the chest and abdomen can be obtained using ImPACT CTDosimetry software or k-coefficients. Further work is required to improve the accuracy of ED estimation from CT of the pelvis. Accuracy of organ dose estimation has been shown to depend on the inclusion or exclusion of the organ from the scan range.

## Introduction

Advances in technology have facilitated Computed Tomography's (CT) expansion in providing rapid complex submillimetre imaging allowing more accurate diagnoses to be made [1-3]. In many instances CT is the first line investigation, however this has resulted in it becoming the dominant source of radiation risk/dose in medical imaging [3]. As with any medical imaging procedure involving radiation, there is a need for all involved to be aware of and monitor dose to patients; this is achieved by dose estimation as direct measurement of organ dose is not possible in the clinical environment.

Effective dose is often calculated by combining dose length product [DLP], (the product of the CT dose index volume ( $CTDi_{vol}$ ) and scan length) with published coefficients ( $k$ -coefficient) [4-7]. This approach uses data published by the American Association of Physicists in Medicine (AAPM) [4]. Critics of this method state that the use of tissue weighting factors from ICRP 60 and scanner data from as early as 1990 means that the coefficients lack relevance to modern multidetector scanners in use today [7]. Updated figures have been published and used by Elbakri and Kirkpatrick [5] and Huda et al [6]. Both these articles argued that due to the updated tissue weighting factors published by the ICRP the conversion factors require updating too. Huda et al [6] provide figures that are independent of the make and model of scanner whilst Elbakri and Kirkpatrick [5] argued that accuracy can be improved further by taking into account scanner-specific results. In Elbakri and Kirkpatrick's paper figures for a range of scanner types are provided [5].

An alternative method of effective dose estimation can be performed by combining  $CTDi_{vol}$  with data produced using Monte Carlo mathematical simulation. Data provided by the UK's National Radiological Protection Board (NRPB) can be used to calculate effective dose by utilising ImPACT's CT dosimetry tool (CTDosimetry V1.0.4) [8]. Although convenient, the data used in the Monte Carlo simulation was generated from early CT systems (not multidetector) therefore effective dose estimation has to be performed by fitting the characteristics of newer scanners to older designs [9]. This has the potential to introduce error [10].

Tube current modulation (mA modulation) is not taken into account when dose estimations are performed using the software or  $k$ -coefficients. mA modulation is standard on modern CT imaging equipment and it has the ability to manipulate the exposure and therefore dose as the patient is imaged. The ability to accurately estimate dose using fixed tube current has been shown but organ dose generally decreases with the use of tube current-modulated acquisition and this should be taken into account in any estimation method, but patient size can directly affect the dose reduction achieved [11].

The Medical Internal Radiation Dose (MIRD) mathematical phantom used in the development of the  $k$ -coefficients by the AAPM, Elbakri and Kirkpatrick and Huda et al and the stylised/mathematical phantom used in ImPACT's dosimetry tool represents a patient mass of 70 kg which is regarded as a low in comparison to modern demographics [4-6, 8, 12]. Research by Castellano stated that there is a change in effective dose for a change in mass with effective dose lower in larger patients for the same imaging parameters [13]. Castellano provides ratios for scaling effective dose using 70 kg as the reference value. The scaling factors indicate a 13% decrease in effective dose per 20 kg increase in mass for chest and abdomen CT acquisitions and a 9% decrease in effective dose per 20 kg increase in mass for pelvis acquisitions. For fixed exposure parameters, effective dose decreases as patient mass increases suggesting that dose is likely to be overestimated [13].

This initial work utilised a single scanner type and phantom size and with a focuses on organ and effective dose calculation accuracy using mA modulation in CT of the chest, abdomen and pelvis. This paper examines different methods of dose estimation and compares these to direct measurements of organ doses made using an anthropomorphic phantom and MOSFET dosimeters. Effective dose calculations were compared against values generated using k-coefficients and ImPACT software. To account for mA modulation mass weighted corrections were applied in an attempt to improve accuracy for effective dose calculations.

## Method

For CT of the chest, abdomen and pelvis twelve methods of estimating effective dose were used (Table 1). CT dosimetry software published by the ImPACT CT scanner evaluation group (ImPACT CTDosimetry spreadsheet v 1.0.4, ImPACT, London, UK) was used to estimate organ and effective dose. For each anatomical region, the DLP was recorded. Dose per DLP figures published by the American Association of Physicists in Medicine (AAPM) [4], Huda et al [6] and Elbakri and Kirkpatrick [5] were used to calculate effective dose (Table 2). One method of calculating effective dose from directly measured organ doses using MOSFETs was undertaken for CT of the chest, abdomen and pelvis using MOSFET dosimeters (Best Medical Canada, Kanata, Canada) and a male ATOM dosimetry phantom model 701-D (CIRS Inc. Virginia, USA). In all cases a Toshiba Aquillion 16 Multidetector CT scanner was used (Toshiba medical systems, Otawara-Shi, Japan). This system utilises filtered back projection reconstruction and for the purpose of the data collection manufacturer recommended reconstruction algorithms and a mA standard deviation of 5. The CT system uses Toshiba’s SUREExposure3D method of tube current modulation during exposure. This uses the anterior-posterior and lateral scan plan radiograph to ascertain the optimum exposure. The system modulates the tube current in the z-axis and during rotation [14].

Direct dose measurements (MOSFET) were taken as the gold standard against which estimation methods were compared [15, 16].

**TABLE 1 METHODS OF DOSE ESTIMATION**

1. ImPACT effective mA
2. ImPACT average mA
3. ImPACT mA modulation
4. AAPM k-coefficient
5. Huda et al k-coefficient
6. Elbakri and Kirkpatrick k-coefficient
7. Mass corrected ImPACT effective mA
8. Mass corrected ImPACT average mA
9. Mass corrected ImPACT mA modulation
10. Mass corrected AAPM k-coefficient
11. Mass corrected Huda et al k-coefficient
12. Mass corrected Elbakri and Kirkpatrick k-coefficient

**TABLE 2 COEFFICIENTS FOR CALCULATION OF EFFECTIVE DOSE FROM DLP**

	k-coefficient mSv/mGy.cm		
	AAPM [4]	Huda et al [6]	Elbakri and Kirkpatrick [5]
Chest	0.014	0.017	0.020
Abdomen	0.015	0.016	0.017
Pelvis	0.015	0.018	0.017

**Dose measurement**

MOSFET dosimeters provide an accurate and reproducible method of collecting organ dosimetry data [17]. In this work four banks of five dosimeters were used (n=20). Calibration was performed as per manufacturer instructions at a tube voltage of 120 kV using the supplied calibration jig and a calibrated RaySafe X2 with R/F sensor (Unfors RaySafe AB, Bildal, Sweden). The error of these was 2.01%.

Indelible ink and radiopaque markers were used on an adult ATOM dosimetry phantom to ensure reproducible and accurate positioning and scanning of the phantom. MOSFET detectors were located within the phantom in the positions corresponding to the critical organs required for effective dose calculations [18-20] (see Table 3). Dose measurement was performed in 20 locations at a time as we had total of 20 MOSFET sensors (Figure 1). In total 269 locations were used to measure organ dose and compute effective dose. For each MOSFET position, three exposures were made and a mean and standard deviation calculated to minimise random error.

**FIGURE 1 FLOW DIAGRAM ILLUSTRATING THE DATA COLLECTION PROCESS FOR DOSE MEASUREMENT**

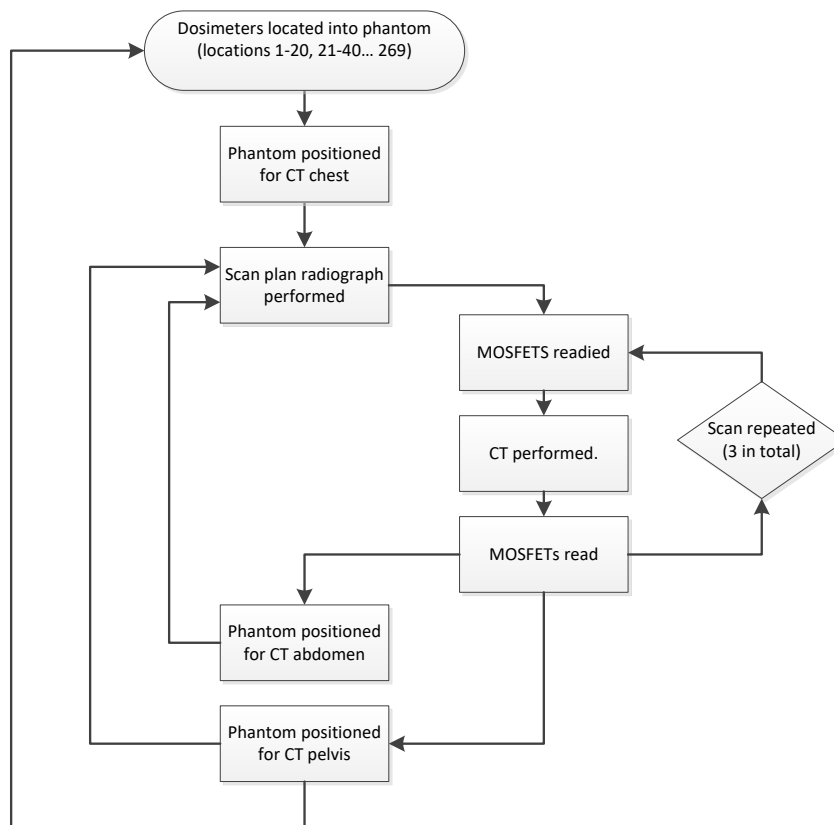


**TABLE 3 TABLE STATING THE NUMBER OF MOSFET LOCATIONS USED FOR ORGAN DOSE MEASUREMENT**

Organ	Number of dosimeter locations
Adrenals	2
Bladder	16
Brain	11
Breast	2
Active bone Marrow	85 Clavicle 20, Cranium 4 Cervical Spine <sup>†</sup> 2 Femora 4 Mandible <sup>◇×</sup> 6 Pelvis 18 Ribs 18 Scapula <sup>°</sup> 9 Sternum 4 Thoraco-lumbar Spine 9
Gall Bladder	5
Heart	2
Intestine (Small and large)	16 Colon 11 Small intestine 5
Kidneys	16
Liver	30
Lungs	36
Oesophagus	3
Pancreas	5
Prostate	3
Spleen	14
Stomach	11
Testes	2
Thyroid	10
Thymus	4
<sup>†</sup> locations in the anterior of C2 and upper oesophagus were used to calculate extra thoracic organ dose  <sup>◇</sup> locations in the left and right lingula of the mandible and to the left and right of the sublingual fossa were used to calculate salivary gland organ dose  <sup>×</sup> locations in the left and right lingula of the mandible were used to calculate oral mucosa organ dose  <sup>°</sup> locations in close proximity to the left and right glenoid fossa were used for dose to the upper humeri	

For each scan, the dose length product (DLP) and the recorded effective mAs were noted. The mean DLP was calculated. Axial images were reconstructed at 1 mm slices to match the acquisition's collimation. The mAs values for each axial image were recorded and an average mAs was calculated (Table 4).

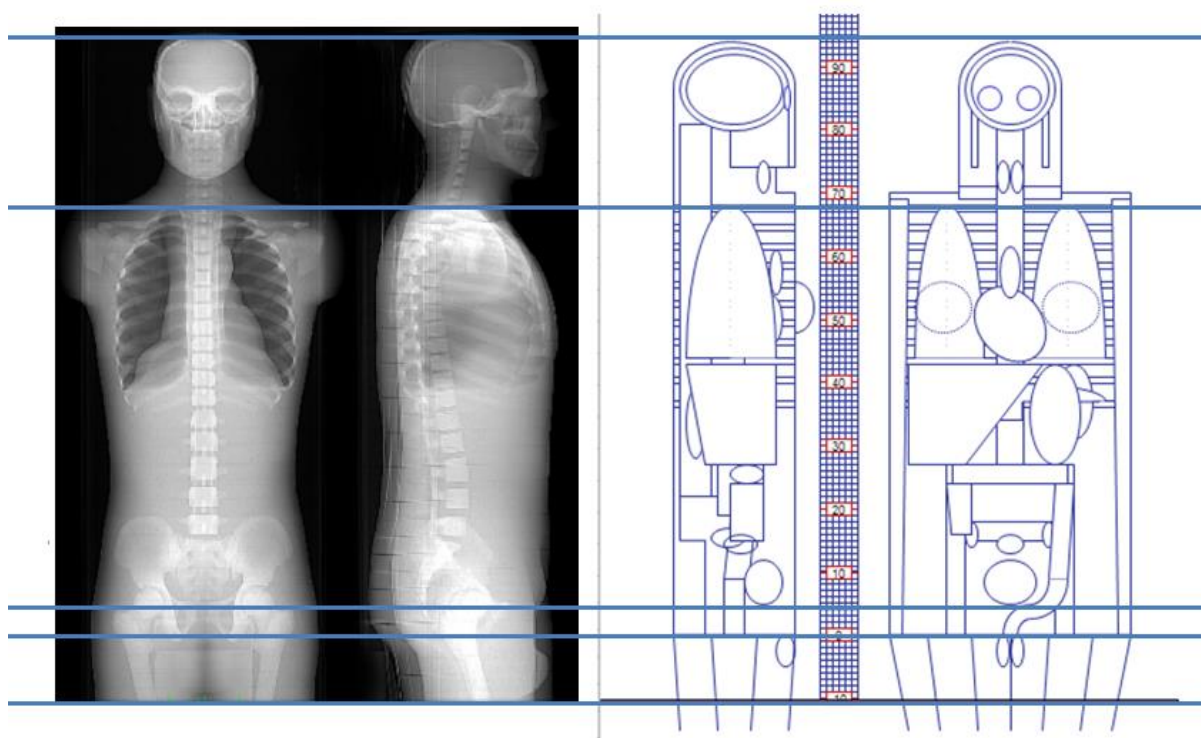
**TABLE 4 IMAGING PARAMETERS**

	Chest	Abdomen	Pelvis
kV	120	120	120
Auto $mA$ standard deviation	5	5	5
Rotation time (s)	0.5	0.5	0.5
$mAs_{eff}$	235	235	235
$mAs_{\bar{x}}$	203.21	201.41	211.34
Acquired slice thickness (detector length in z-axis)	16 x 1 mm	16 x 1 mm	16 x 1 mm
Pitch	0.938	0.938	0.938
$DLP_{\bar{x}}$	904.49	792.72	791.76
$CTDI_{\bar{x}}$	33.2	33.2	33.2

#### Comparison of ATOM and ImPACT standard phantoms

The ATOM phantom and the standard phantom within the ImPACT CT dosimetry software are of different dimensions. To compensate, scaling of the ImPACT phantom was performed. The ATOM phantom from the apex of the skull to the upper border of the symphysis pubis was measured at 830 mm. The length of the ImPACT standard phantom between the same reference points was 890 mm. Therefore a 1 mm slice in the ATOM phantom equated to a 1.07 mm slice in the standard phantom ImPACT CT dosimetry software. The proportions of the chest, abdomen and pelvis were compared to ensure that accurate comparisons were being made; Figure 2 illustrates good agreement between the two phantoms' proportions for these.

**FIGURE 2 COMPARISON OF THE PROPORTIONS OF THE CHEST, ABDOMEN AND PELVIS OF THE TWO PHANTOMS. THE DOSIMETRY PHANTOM (LEFT) HAS BEEN SCALED BY A FACTOR OF 1.07 RELATIVE TO THE SOFTWARE PHANTOM**



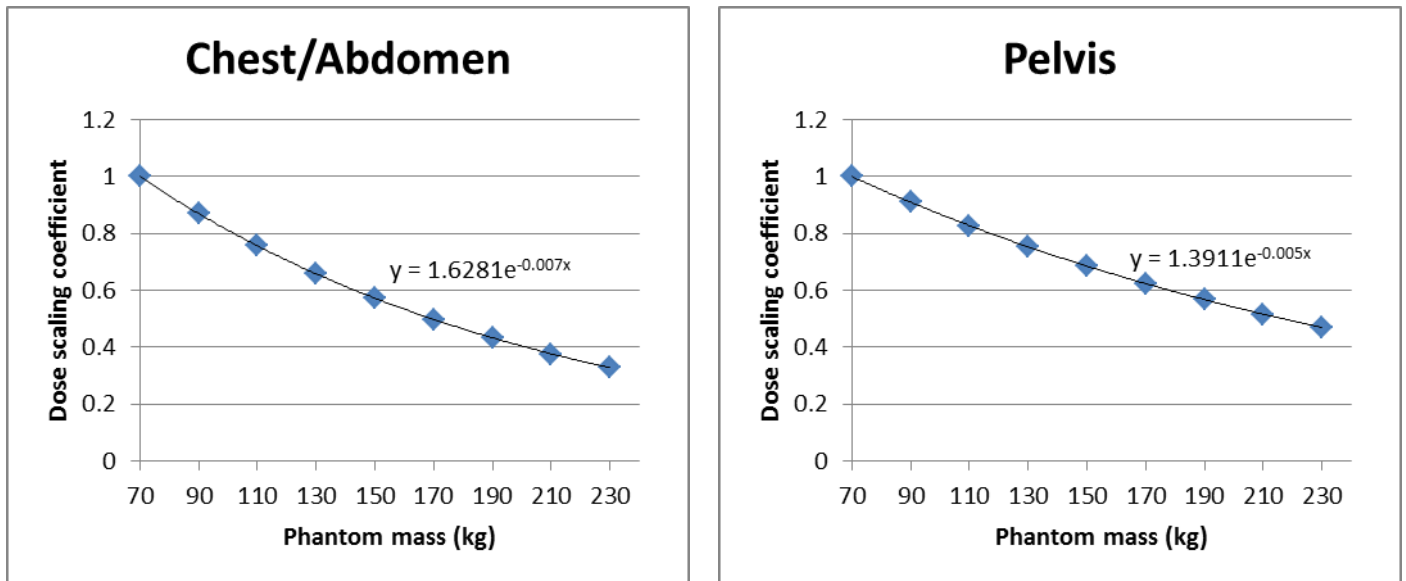
The phantom used in ImPACT’s CT dosimetry software that was used in the development of the DLP for effective dose calculations is based on a whole body mass of 70 kg [5, 6, 8, 21]. The ATOM phantom has a mass of 73 kg and consists of the head and torso only. According to Tozeren this accounts for only 55.4 % of total body mass [22] (Table 5).

**TABLE 5 RELATIVE WEIGHT OF BODY SEGMENTS FOR AN ADULT MALE [22]**

Region/limb	Percentage contribution to total body mass (%)
Torso	48.3
Head and Neck	7.1
Upper legs	21.0
Lower legs	9.0
Feet	3.0
Upper arms	6.6
Lower arms	3.8
Hands	1.2
TOTAL	100

Using the data, a total body mass of the ATOM phantom was calculated. The resulting mass was much greater at 131.8 kg; an increase in mass of 88.29%. Using the work of Castellano [13] Figure 3 was created to calculate the correction factor for mass. An assumption was made that this relationship remained constant ( $R^2=1$ ).

**FIGURE 13 GRAPHS SHOWING EFFECTIVE DOSE SCALING COEFFICIENT CALCULATIONS FOR THE CHEST/ABDOMEN AND PELVIS.**



Dose calculations using ImpACT CT Dosimetry software was performed in three ways;

- (i) Using the effective mAs quoted by the scanner for the full range of the acquisition,
- (ii) Using the average mAs for the full range of the acquisition,
- (iii) Using the mAs for each axial slice and summing the organ and effective doses to give final figures.

For method 3 in Table 1 a macro was created to be used within the ImpACT Excel spreadsheet that calculated the start and finish position for each slice and the corresponding mAs to calculate the effective dose per slice, which was then summated for the whole scan. The Toshiba Aquillion 16 has an overbeaming requirement of 2 rotations (1 at each end of the scan) [23]. With a collimation of 16x1 mm and a pitch of 0.938 an additional 15.0 mm at each end of the scan is required. When scaled, this is equivalent to 16.05 mm at the start and end of the acquisition in the simulation. The mA for the first and last slices was used as the mA for the respective upper and lower overbeamed sections of the scan for the mA modulation calculation. Comparisons between mass corrected and non-corrected figures using data from Table 5 were made.

#### Comparison of Organ doses

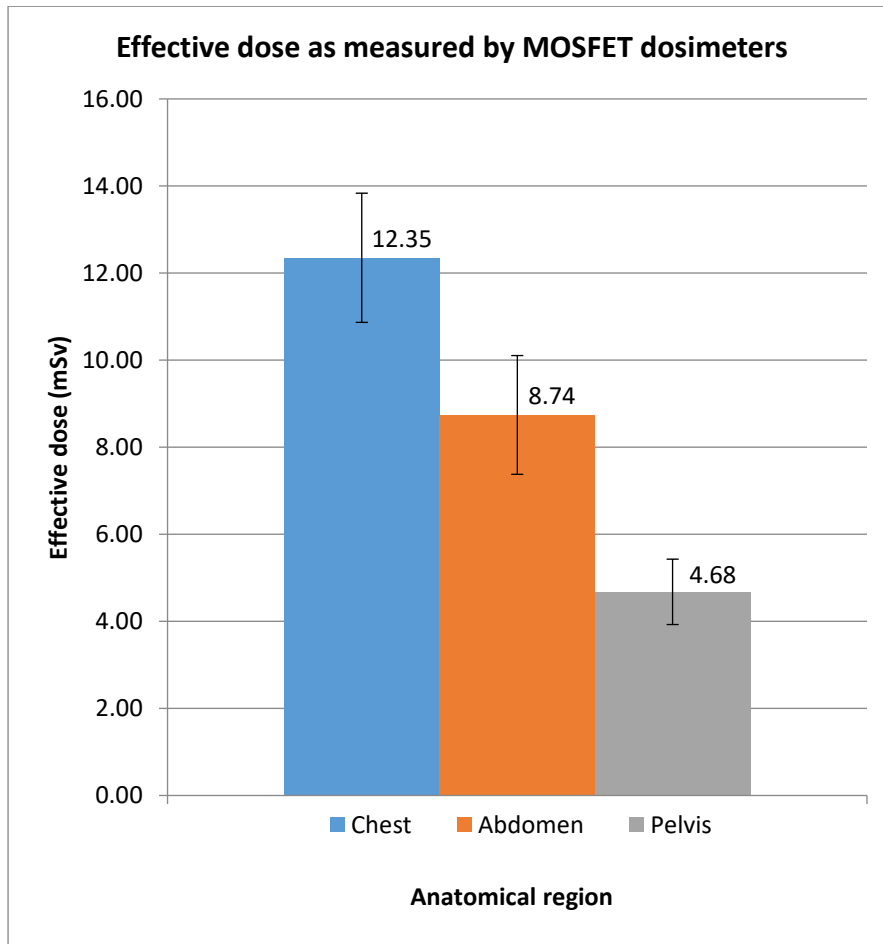
Effective dose is calculated by summing the weighted equivalent organ doses. Any difference in measured and estimated organ doses would be carried through into the final effective dose estimations. Comparison of estimated and measured organ doses was carried out to establish any sources of error. Unlike methods using DLP and conversion factors, dose estimation using ImpACT CT Dosimetry software allows figures for organ dose to be collated so this comparison could only analyse dose estimations using ImpACT CT Dosimetry software. It was also not feasible to correct for mass as accurate estimation of the distribution of intrathoracic and visceral fat was not possible. The difference between simulated and measured organ doses was calculated for each method (i. ImpACT

effective mA. ii. ImPACT average mA. iii. ImPACT mA modulation). These values were compared statistically using a single factor ANOVA.

## Results

Effective doses calculated from the MOSFET organ dose measurements (Figure 4) were 12.35 mSv ( $\pm 1.48$  mSv) for CT of the chest; 8.74 mSv ( $\pm 1.36$  mSv) for CT of the abdomen and 4.68 mSv ( $\pm 0.75$  mSv) for CT of the pelvis.

FIGURE 4 CALCULATED EFFECTIVE DOSE<sup>4</sup>



<sup>4</sup> The error bars displayed in Figure 4 are a combined standard deviation of the MOSFET readings. The mean and standard deviation of the three repeated measures was calculated for each dosimeter location. To calculate organ dose, the mean of the organs dosimeter data was calculated and the organ's standard deviation calculated by combining the individual standard deviations using the equation

$SD_{org} = \sqrt{(SD_1)^2 + \dots + (SD_n)^2}$ . Tissue weighting factors were applied to the organ dose and standard deviation. The sum of the weighted organ provided the effective dose and the square root of the summed squared standard deviations provided the error in the effective dose.

Table 6 and Figure 5 illustrate the comparison of effective dose between measured and calculated values, with and without correction of phantom mass. Figure 5 demonstrates that using mass corrected values leads to greater accuracy for the calculated effective dose in comparison to the measured values.

**TABLE 6 EFFECTIVE DOSE MEASUREMENT AND CALCULATION METHODS.**

Method	Effective Dose (mSv)		
	Chest	Abdomen	Pelvis
<b>Calculated (MOSFET)</b>	12.35 (±1.48)	8.74 (±1.36)	4.68 (±0.75)
<b>Estimated (Uncorrected for mass)</b>			
ImPACT effective mA	19.00	15.00	10.00
ImPACT average mA	17.00	14.00	9.90
ImPACT mA modulation	17.08	13.86	9.93
AAPM conversion factors [4]	12.66	11.89	11.88
Huda et al conversion factors [6]	15.38	12.68	14.25
Elbakri and Kirkpatrick conversion factors [5]	17.91	13.24	13.22
<b>Estimated (Corrected for mass)</b>			
Mass corrected ImPACT effective mA	12.30	9.71	7.20
Mass corrected ImPACT average mA	11.00	9.06	7.13
Mass corrected ImPACT mA modulation	11.05	8.97	7.15
Mass corrected AAPM conversion factors [4]	8.19	7.69	8.55
Mass corrected Huda et al conversion factor [6]	9.95	8.21	10.26
Mass corrected Elbakri and Kirkpatrick conversion factors [5]	11.59	8.57	9.51

FIGURE 5 COMPARISON OF CORRECTED AND UNCORRECTED EFFECTIVE DOSE ESTIMATIONS OF THE (A) CHEST (B) ABDOMEN AND (C) PELVIS TO CALCULATED EFFECTIVE DOSE

FIGURE 5A

### Comparison of corrected and uncorrected estimations to calculated effective dose for the chest

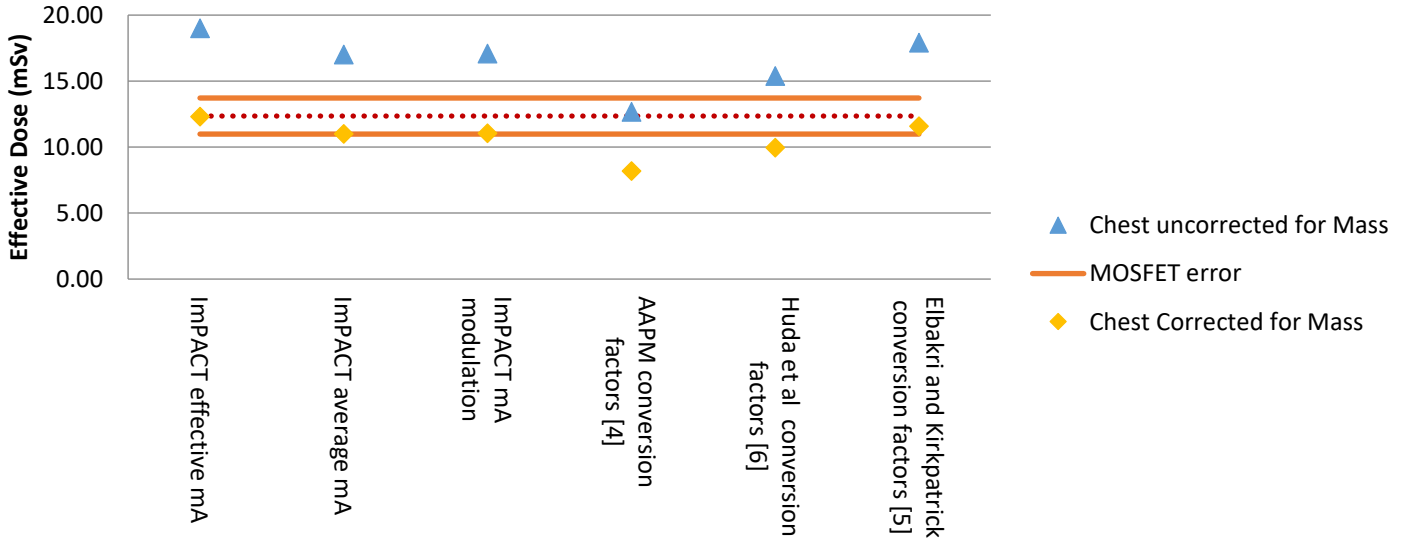


FIGURE 5B

### Comparison of corrected and uncorrected estimations to calculated effective dose for the abdomen

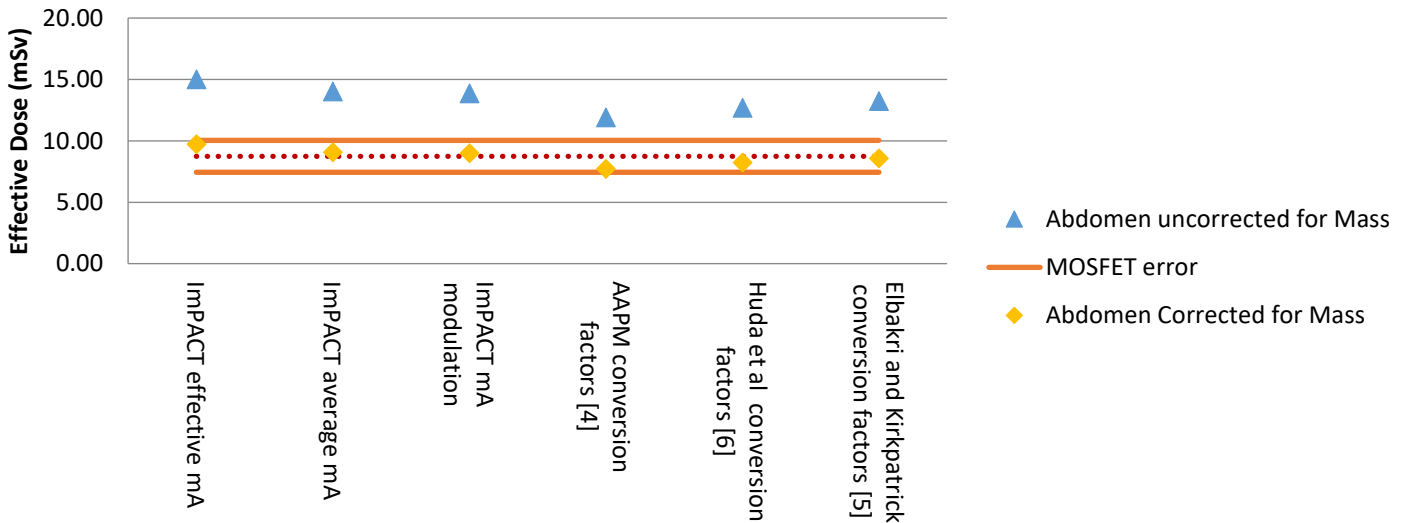
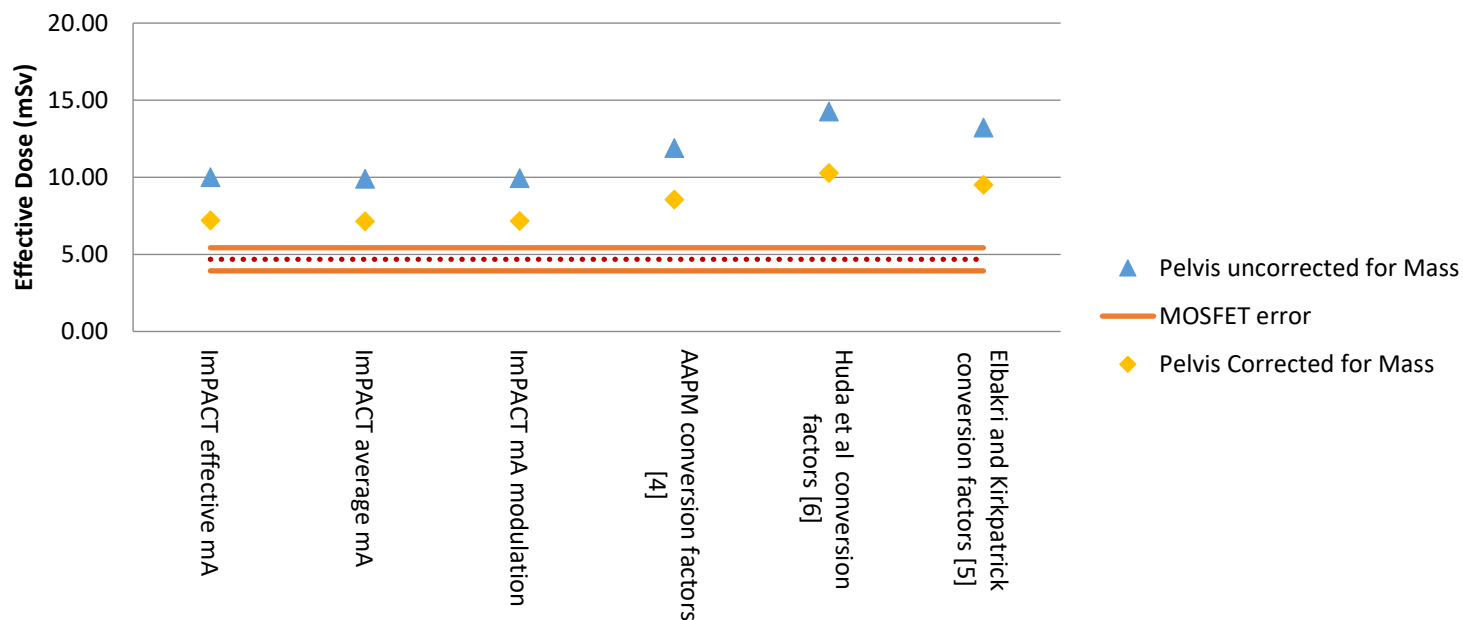


FIGURE 5c

### Comparison of corrected and uncorrected estimations to calculated effective dose for the pelvis



Comparison of estimated organ for CT of the chest, abdomen and pelvis is shown in Table 7. A very strong positive correlation between the three estimation methods ( $r > 0.99$ ) and no significantly statistical difference is shown (Single Factor ANOVA,  $p > 0.9$ ).

**TABLE 7 COMPARISON OF ESTIMATED ORGAN DOSES USING MEAN, EFFECTIVE AND MODULATED MAs FOR CT OF THE CHEST, ABDOMEN AND PELVIS.**

Organ	Organ dose (mGy)											
	Chest				Abdomen				Pelvis			
	Measured	ImPACT CT Dosimetry			Measured	ImPACT CT Dosimetry			Measured	ImPACT CT Dosimetry		
$mAs_{\bar{x}}$		$mAs_{eff}$	$mAs_{mod}$	$mAs_{\bar{x}}$		$mAs_{eff}$	$mAs_{mod}$	$mAs_{\bar{x}}$		$mAs_{eff}$	$mAs_{mod}$	
Gonads	0.04	0.00	0.00	0.00	0.16	0.07	0.07	0.07	5.58	37.00	39.00	36.00
Bone Marrow	8.10	12.00	14.00	12.22	4.55	8.50	9.30	8.59	5.45	10.00	10.00	10.01
Colon	0.51	0.35	0.40	0.32	14.3	19.00	20.00	18.76	16.6	23.00	24.00	22.81
Lung	24.7	45.00	52.00	45.27	5.48	9.50	10.00	9.44	0.16	0.04	0.05	0.04
Stomach	11.3	8.80	10.00	7.87	26.0	41.00	45.00	40.78	2.02	1.00	1.10	1.04
Bladder	0.09	0.02	0.02	0.02	1.93	1.10	1.20	1.16	19.8	47.00	49.00	47.93
Breast	27.7	35.00	40.00	36.79	1.47	1.80	2.00	1.79	0.08	0.04	0.04	0.04
Liver	18.9	14.00	17.00	12.71	22.4	38.00	41.00	37.70	0.71	0.62	0.65	0.62
Oesophagus	22.7	53.00	61.00	53.35	3.02	1.40	1.60	1.43	0.07	0.01	0.01	0.01
Thyroid	16.3	8.00	9.30	8.39	0.37	0.14	0.16	0.14	0.05	0.01	0.01	0.01
Brain	0.32	0.30	0.35	0.31	0.01	0.01	0.01	0.01	0.03	0.00	0.00	0.00
Salivary Glands	2.41	0.30	0.35	0.31	0.39	0.01	0.01	0.01	0.07	0.00	0.00	0.00
Remainder	11.0	13.00	15.00	12.84	11.7	19.00	21.00	19.27	4.09	6.90	7.20	7.00

## Discussion

The options of mA value that are used within the ImPACT CT Dosimetry software values (effective, average or modulated) has an insignificant effect on the estimated effective dose with the coefficient of variation of 6.4%, 4.4% and 0.5% for the chest, abdomen and pelvis respectively. Establishing the mAs per slice is a time consuming process and for convenience, the effective mAs can be used when estimating effective dose using ImPACT CT Dosimetry software. This value is easily obtained from CT imaging equipment.

With the exception of the AAPM k-coefficient, uncorrected effective dose was over estimated (Figure 5). There was closer agreement for the CT of the chest (Figure 5a) with over estimation ranging from 2.48% to 42.4% (0.31 mSv to 6.65 mSv). There was poorer agreement in the abdomen (Figure 5b) and pelvis (Figure 5c) with over estimation of 30.54% to 52.74% (3.15 mSv to 6.26 mSv) and 72.48% to 101% (6.26 mSv to 9.57 mSv) respectively.

Tube current modulation takes into account patient size within set parameters. The phantom used in this study is larger than the phantom used within ImPACT's software and in the development of the k-coefficients therefore effective dose should be lower [4-6, 13]. Correcting for mass improved agreement between the effective dose estimations and calculations. Differences were -40.51% to -0.41% (-4.16 mSv to 0.05 mSv) in the chest, -12.78% to 3.60% (-1.05 mSv to 0.32 mSv) in the abdomen. It can be seen from Figure 5a,b and c that the majority of the mass corrected values fall within the error of the MOSFET dosimeters indicating no significant differences between the calculated and estimated values. Effective dose for the pelvis (figure 5c) showed the greatest disagreement after correcting for mass with differences to MOSFET ranging from 41.76% to 74.70% (2.47 mSv to 5.58 mSv). The disagreement between effective dose of the pelvis suggests that the correction factor used requires further research utilising phantoms of different sizes.

ANOVA showed no statistical difference in the estimation of organ dose using the average, effective or modulated mA ( $p=0.9$ ). Using the mean of these three methods a comparison of estimated and measured organ doses shown in Table 7 highlights a pattern. It is apparent that organs within the scan range have an average estimate that is higher than measured values and those organs outside the scan range i.e. those organs whose dose comes from scattered radiation, have estimates that are lower than the measured values. To explore the effect this would have on effective dose estimations and calculations the tissue weighting factors were applied and the percentage contribution to effective dose of organs within and outside the scan range was calculated (Table 8). It is recognised that certain organs would be part in and part out of the scan range but for the purpose of this analysis, organs that were mostly in the scan range were classified as 'in' and vice versa.

**TABLE 8 PERCENTAGE CONTRIBUTION OF ORGANS INSIDE AND OUTSIDE THE SCAN RANGE TO EFFECTIVE DOSE CALCULATIONS**

	Percentage contribution to calculated effective dose (%)	
	Inside	outside
Chest	71.5	28.5
Abdomen	58.5	41.5
Pelvis	91.4	8.6

The chest and abdomen show better balance between contributions of organs inside and outside the scan range which would explain why these estimations are in closer agreement when compared to the chest and pelvis. The pelvis, however, has an imbalance with the greatest contribution to the effective dose calculation coming from organs inside the scan range- specifically the bladder, gonads and colon. With the suggested tendency of ImPACT dosimetry software to over-estimate organ dose inside the primary beam the reason for the large difference in calculated effective dose using measured organ dose to estimated effective dose is apparent. Reasons for these errors require further investigation and should focus on the suitability of the Monte Carlo data sets used in ImPACT's CTDosimetry software, the "best-fitting" of newer scanners to data in the ImPACT CTDosimetry software.

It is recognised that this work is not without limitations. Only one scanner type and phantom was used. The tube current modulation parameters remained constant through the data collection. Only filtered back projection reconstruction was used. To validate the mass correction of effective dose estimations further validation of mass correction is required using phantoms of different sizes. Investigation into the mass correction for CT of the pelvis is required as our work has shown that over estimation occurs even after correction for mass. Should accurate organ dose estimations be required, clinicians should be aware of the under and over estimation of dose for organs inside and outside the scan range.

### **Conclusion**

Our work has shown that for this scanner type and exposure parameters a reasonable estimation of effective dose for CT of the chest and abdomen can be obtained using ImPACT CTDosimetry software or the k-coefficients referenced. The use of the k-coefficients is the quicker method compared to using ImPACT software but these do not give an indication of organ doses. Our work has shown that there is a pattern for overestimation of organ dose inside the scan range and underestimation outside the scan range. Additional investigations using other scanners are required to establish if this is a consistent pattern. Further work is required to improve the accuracy of the mass correction factor for the pelvis and to test the external validity of the method varying the mass of the phantom and across different makes and models of CT scanner.

1. Lowe AS and Kay CL, *Recent developments in CT: a review of the clinical applications and advantages of multidetector computed tomography*. Imaging, 2006. **18**(2): p. 62-67.
2. Golding SJ, *Multi-slice computed tomography (MSCT): the dose challenge of the new revolution*. Radiation Protection Dosimetry, 2005. **114**(1-3): p. 303-307.
3. Shrimpton P, Hillier MC, S M, and SJ G, *Doses from Computed Tomography (CT) Examinations in the UK – 2011 Review*. 2014, Public Health England: Oxfordshire.
4. *Diagnostic Imaging Council CT Committee*. 2007: Maryland, USA.
5. Elbakri IA and Kirkpatrick IDC, *Dose-Length Product to Effective Dose Conversion Factors for Common Computed Tomography Examinations Based on Canadian Clinical Experience*. Canadian Association of Radiologists Journal, 2013. **64**(1): p. 15-17.
6. Huda W, Ogden KM, and Khorasani MR, *Converting Dose-Length Product to Effective Dose at CT*. Radiology, 2008. **248**(3): p. 995-1003.
7. McNitt-Gray M, *Assessing Radiation Dose: How to Do It Right, in 2011 AAPM CT Dose Summit*. 2011: Denver.
8. ImPACT, *CT Patient Dosimetry Calculator*. 2003, Medical Devices Agency: London.
9. Tootell A, Szczepura K, and Hogg P, *An overview of measuring and modelling dose and risk from ionising radiation for medical exposures*. Radiography, 2014. **20**(4): p. 323-332.
10. Groves AM, Owen KE, Courtney HM, Yates SJ, Goldstone KE, Blake GM, et al., *16-detector multislice CT: dosimetry estimation by TLD measurement compared with Monte Carlo simulation*. Br J Radiol, 2004. **77**(920): p. 662-5.
11. Angel E, Yaghmai N, Jude CM, DeMarco JJ, Cagnon CH, Goldin JG, et al., *Dose to Radiosensitive Organs During Routine Chest CT: Effects of Tube Current Modulation*. AJR. American journal of roentgenology, 2009. **193**(5): p. 1340-1345.
12. McCollough CH, Leng S, Yu L, Cody DD, Boone JM, and McNitt-Gray MF, *CT Dose Index and Patient Dose: They Are Not the Same Thing*. Radiology, 2011. **259**(2): p. 311-316.
13. Castellano E, *CT Dose calculations for individual patients - what you should know, in 12th CT Users Group*. 2010: London.
14. Centre for Evidence-based Purchasing (CEP), *Comparative Specifications 16 slice CT scanners*. March 2009: NHS/PASA, London.
15. Hintenlang D, *TH-C-301-03: Utilization of MOSFET Dosimeters for Clinical Measurements in Radiology*. Medical Physics, 2011. **38**(6): p. 3861-3861.
16. Chida K, Inaba Y, Masuyama H, Yanagawa I, Mori I, Saito H, et al., *Evaluating the performance of a MOSFET dosimeter at diagnostic X-ray energies for interventional radiology*. Radiological Physics and Technology, 2009. **2**(1): p. 58-61.
17. D H, *The Utilization of MOSFET Dosimeters for Clinical Measurements in Radiology*, in *Joint Programme The American Association of Physicists in Medicine (AAPM) and the Canadian Organization of Medical Physicists (COMP)*. 2011: British Columbia.
18. CIRS Tissue Simulation and Phantom Technology, *Adult Male Phantom Model Number 701-D Appendix 5*. 2010, CIRS, Inc: Virginia, USA.
19. CIRS Tissue Simulation and Phantom Technology. *Dosimetry Verification Phantoms Model 701-706 Data Sheet*. 2012 [cited 2012 19th January]; Available from: [http://www.cirsinc.com/file/Products/701\\_706/701\\_706\\_DS.pdf](http://www.cirsinc.com/file/Products/701_706/701_706_DS.pdf).
20. ICRP, *The 2007 Recommendations of the ICRP*, in *ICRP Publication 103*. 2007, Ann. ICRP. p. 2-4.
21. Huda W, Sterzik A, Tipnis S, and Schoepf UJ, *Organ doses to adult patients for chest CT*. Medical Physics, 2010. **37**(2): p. 842-847.
22. Tozeren A, *Human Body Dynamics*. 2014, New York: Springer.
23. The ImPACT Group, *Comparative Specifications: 16 Slice CT Scanners*, in *CEP08025*. 2009, NHS Purchasing and Supply Agency, Centre for Evidence-based Purchasing: London.

# APPENDIX

## NUCLEAR MEDICINE SCANNING PROTOCOLS

### ISOTOPE BONE SCAN

#### REFERRAL CRITERIA

All Consultants and Junior Medical staff can refer in accordance with R.C.R. guidelines

GPs, if known malignancy and pain or after discussion with Consultant Radiologist

#### JUSTIFICATION CRITERIA

Metastatic bone disease Arthralgia Paget's disease Perthes disease/ irritable hip Osteomyelitis Bone pain Infected/loose prostheses or other metalwork ↑Alk Phos ↑PSA	? Fracture e.g scaphoid, N.o.F. Stress fracture Shin splints Back pain Infection Primary bone tumour Vascularity – AVN, R.S.D Sacro-iliitis Mandibular condyle hyperplasia
---	--

#### PROTOCOL

Booking method	On receipt of a signed request form request on Order Comms or if urgent, by phone if confirmed by fax
Patient preparation	None
Radiopharmaceutical	500Mbq 99TcmMDP (supplied by RLUH)
Personnel competent to administer	Isotope scan dept. staff with prior authorisation

Method of administration	Intravenously, following flush with normal saline if venflon or butterfly needle used
Paediatric patients	Activity scaled down in accordance with the ARSAC guidelines.(weight of child required)
Advice after administration	Drink plenty of fluids and empty bladder Frequently
Time delay before scan	3 hours preferably, minimum 2.5hrs
Equipment	GE Discovery 670Pro with LEHR collimator
Scanning procedure	<p>The bladder should be emptied immediately before any view of the pelvis</p> <p>Select patient on acquisition workstation , acquire study and select parameters for imaging</p> <p>Whole body imaging either with W.B facility or statics (patient dependant)</p> <p>Static images of affected area</p> <p>Posterior and Anterior views may be obtained simultaneously</p> <p>Dynamic studies may be necessary for some referrals e.g ? R.S.D</p> <p>Dynamic acquisition – flow images 15 frames @ 8 seconds per frame (delay may be required, 5secs for wrists &amp; knees, . 10secs for feet) then blood pool image 5 mins. 128x128 matrix</p>
Patient position	Supine or erect
Analysis and display	No analysis required unless SI joint profiles are necessary Display all acceptable images with annotation
Supplements	<p>When the clinical question is for suspected loosening or infection of a KNEE prosthesis, a 3-phase scan should be performed as routine.</p> <p>SPECT for mandibular condyle hyperplasia.</p>

	<p>SPECT/CT may be required according to protocol (see end of Bone imaging protocol)</p> <p>Request of supplementary imaging for any isolated hot spots (see protocol and authorisation)</p>
--	--

## REPORTING

When the scan is complete the images are processed on Xeleris workstation and a screen capture of final image sent to Carestream. Consultant to select relevant SPECT CT images to send to PACS where indicated.

Radiologist to report on to CRIS and secretarial staff to type report and send out to appropriate Consultant or Ward

## SPECT/CT PROTOCOL FOLLOWING BONE SCANS

The Radiographers in Nuclear Medicine are authorised to perform SPECT/CT on any patients that have a known malignant disease and present with a single “hot” spot on the Bone scan.

This “hot” spot should be in the Thoracic or Lumbar spine or in the Pelvis (except degenerative disease in the hips).

SPECT CT may be indicated in targeted bone scans for Orthopaedics as vetted by Radiologist.

For initial staging of Breast / Prostate malignancy, any uptake in spine should ideally proceed to SPECT CT rather than plain films (if unsure ask Radiologist to review).

For patient with a history of malignancy and symptoms specific to one area, SPECT CT if abnormal on bone scan.

Pre-planned Orthopaedic SPECT CT of feet / ankles to be booked for Whiston where possible.

Electronic vetting allows for the Radiologist to comment if SPECT CT is indicated or should be considered of a specific area usually described as symptomatic if it does not fall within any of the above criteria. If in doubt, try to contact Dr Howes / Dr Patel to review the images.